

C. F. Kollbrunner · K. Basler

Torsion in Structures

Springer-Verlag Berlin Heidelberg GmbH

C. F. Kollbrunner · K. Basler

Torsion in Structures

An Engineering Approach

Translated from the German Edition by E. C. Glauser

With Annotations and
an Appendix by B. G. Johnston



Springer-Verlag Berlin Heidelberg GmbH 1969

CURT F. KOLLBRUNNER

Senator h.c., Dr. h. c., Dr. sc. techn.
Dipl. Bau-Ing. ETH, SIA
Zollikon/Zurich, Switzerland
President of the
Institute for Engineering Research
Zurich, Switzerland

KONRAD BASLER

Dr. Ing. (Ph. D.)
Dipl. Bau-Ing. ETH, SIA, M. ASCE
Partner, Basler & Hofmann
Consulting Engineers, Zurich, Switzerland

ERNST C. GLAUSER

Dr. Ing. (Ph. D.)
Dipl. Bau-Ing. ETH, SIA, A.M. ASCE
Project Engineer in
Basler & Hofmann, Consulting Engineers
Zurich, Switzerland

BRUCE G. JOHNSTON

Ph.D., M.S., F. ASCE
Professor of Civil Engineering
University of Arizona,
Tucson, Arizona, U.S.A.

Title of the Original Edition:
Torsion (1966)

ISBN 978-3-662-22559-2
DOI 10.1007/978-3-662-22557-8

ISBN 978-3-662-22557-8 (eBook)

With 112 figures and 22 tables

This work is subject to copyright. All rights are reserved, whether the whole or part of the material is concerned, specifically those of translation, reprinting, re-use of illustrations, broadcasting, reproduction by photocopying machine or similar means, and storage in data banks.

Under § 54 of the German Copyright Law where copies are made for other than private use, a fee is payable to the publisher, the amount of the fee to be determined by agreement with the publisher.

© by Springer-Verlag Berlin Heidelberg 1969.
Originally published by Springer-Verlag Berlin/Heidelberg in 1969
Softcover reprint of the hardcover 1st edition 1969

Library of Congress Catalog Card Number: 79-88817

The reproduction of registered trade-marks in this book does not warrant the assumption, even without any special marking, that such names are to be considered free under the trade-mark law and may be used by anyone

Title No. 01599

Preface of the Authors

This English edition has been translated from the German edition by Dr. E. GLAUSER, Dipl. Ing. ETH, in the office of Basler & Hofmann, Consulting Engineers, Zurich, Switzerland. The translator made a large number of minor improvements and alterations.

Dr. E. GLAUSER received his Ph. D. from the University of Michigan, Ann Arbor, under the supervision of Professor BRUCE G. JOHNSTON, then Professor of Structural Engineering at that university. Dr. JOHNSTON kindly reviewed the draft of this translation and made annotations and corrections. He also enriched the book by the appendix which gives a precise evaluation of the torsion constants of standard rolled shapes and offers information on stress concentration factors.

Our special thanks are due to both Drs. E. GLAUSER and B. G. JOHNSTON for their careful translation and editing.

Zollikon and Zurich,
July 1969

Curt F. Kollrunner Konrad Basler

Preface of the Translator

This textbook represents a translation of the corresponding German version which was published by the same publishing company in 1966. The good reception of the German edition induced the authors to make this fundamentally new and comprehensive treatment of torsion accessible to a larger group of interested engineers. The translator did not follow the original version literally. He tried to eliminate the few mistakes in the original and made other changes and modifications which promised to facilitate the understanding of the text.

It is the aim of this book to devise methods for the analysis of torsion in structures using tools familiar to most structural engineers. The methods yield the stress distribution in twisted single-span or continuous members with solid, thin-walled, open or closed cross sections resting on either regular or skew supports.

A prismatic member exhibits two ways to resist twist. The first results in a circulatory shear flow in the cross section while the second yields shear stresses resulting from the change in axial stresses. The first contribution is denoted by Saint-Venant torsion, the second by warping torsion.

The discussion of each of these effects may be divided up into a structural mechanics section and into a structural analysis section. While the first is concerned with the analysis of stresses in a given cross section taking into account only the conditions of the considered cross section, the second deals with the structure as a whole and determines the distribution of the torsional moments for a given load.

The sum of the Saint-Venant torsional moment T_s and the warping torsional moment T_ω is in equilibrium with the total torsional moment T . It is a further task of the structural analysis to determine the decomposition of the torsional moment T into the two components T_s and T_ω . Mixed torsion is said to occur if neither of the components T_s and T_ω predominate.

A number of advantages result from the introduction and discussion of these two components separately, i. e., relatively unknown terms such as the sectorial coordinate ω or the warping moment M_ω may be explained within a closed context. A much better justification, however, is given by the practical applications themselves. Chapter 10 provides a demonstration that for most practical cases, the effect of one component may be neglected as compared to the effect of the other. Warping torsion is usually negligible or may at best be considered by local corrections in slender members with compact solid or hollow cross sections. Saint-Venant torsion, on the other hand, may be neglected in thin-walled open cross sections such as in cold formed profiles or open orthotropic plate bridges. The structural mechanics aspect of the analysis, however, is independent of

whether the Saint-Venant torsional moment T_s or the warping torsional moment T_ω occur separately or together.

It was for those reasons that it was decided to present the subject of torsion in structures in the following 13 chapters:

Parts	Structural Mechanics	Structural Analysis
I Saint-Venant torsion	Chapter 1 and 2	Chapters 3 and 4
II Warping torsion	Chapters 5 and 6	Chapters 7 and 8
III Mixed torsion		Chapters 9 and 10
IV Folded Plates	Chapters 11, 12 and 13	

Both the theories of bending and warping torsion assume that the cross sections of a loaded member maintain their shape. There are of course structural members which do not satisfy this condition.

Chapter IV demonstrates for a certain class of structures (folded plates) what happens if the condition of constant shape is completely dropped. The methods presented therein, however, assume that the plates are hinged to each other. The result of this folded plate theory together with the result of the ordinary bending and warping torsion theory represent therefore bounds for the true behaviour of a plate member whose cross sections are only partially maintained. Chapter 13 shows that these two bounds are for most practical applications close to each other so as to provide a powerful tool for the designer. The application of more sophisticated methods (applying Fourier Series, finite differences, finite elements, etc.) does not seem to be necessary as long as the distribution of the plate stresses remains linear.

If not otherwise mentioned, all chapters assume prismatic members of an elastic material whose shear deformations may be neglected as compared to those caused by axial stresses. The internal forces are calculated for the undeformed state of the structure and thus do not permit conclusions as to its stability.

There is hardly any subject in the theory of structural mechanics in which the sign conventions, the definition of coordinate systems and the presentation of the theory is of as great importance as in the theory of warping torsion. The systematology and clearness of presentation is lost if, just to name a few examples, the x-axis is for some discussions in the plane of the cross sections and for others pointing along the length of the member, if the y-axis points upwards for discussions of cross sections and downwards for the calculation of deflections, if loads are positive when pointing in the direction of a positive axis and equally directed stresses negative, etc. In order to arrive at a consistent system of definitions, the authors were forced to introduce notations and sign conventions which may not be very familiar to some readers. The system is defined before its first use, i. e. with respect to coordinates in Section 5.1.

Up to the turn of the last century, the torsion phenomenon was thought to be completely covered by the theory developed by DE SAINT-VENANT [1]. It was not realized at that time that the shear stresses in the cross sections may not be solely a part of a closed shear flow but may also be caused by a change in the axial stresses (warping torsion).

Important contributions to the application of de Saint-Venant's theory were made by R. BREDT [2] to whom we owe formula (2.5), by L. PRANDTL [3] who discovered the analogy between the torsion and the membrane problem, by A. FÖPPL because of his contributions to the evaluation of the torsion constants of rolled sections [4, 5] and finally by C. WEBER and W. GÜNTHER [6].

A general problem of mixed torsion seems to have been solved for the first time by S. TIMOSHENKO. After L. PRANDTL treated in his dissertation the lateral buckling of beams with rectangular cross section, S. TIMOSHENKO investigated the same problem for the case of I-sections. This investigation led TIMOSHENKO to the discovery of what he called "torsion with flange bending." His famous results, the solutions of an eigenvalue problem, were first published in Russian in 1905 and in German in 1910.

In 1909, C. VON BACH [8] reported the results of experiments conducted on beams with [-type cross section which clearly showed a nonplanar strain distribution (since the strain gages indicated the sum of the bending and warping strains). It was more than 10 years until R. MAILLART [9] and A. EGGENSCHWYLER [10] gave a correct interpretation to this suspected contradiction of the Bernoulli-Navier hypothesis. They introduced the shear center of the cross section as a point common to all shear forces causing bending without torsion.

The general theory for warping torsion of open, thin-walled cross sections was initiated by H. WAGNER [11] and R. KAPPUS [12]. As aircraft engineers, they were concerned with the torsional buckling of thin-walled members. More than 20 years later, these fundamental ideas appeared in the structural engineering literature as well. F. W. BORNSCHEUER [13] contributed a systematology of cross-sectional quantities for both bending and warping. The application of these theories to the design of steel structures was outstandingly described by F. WANSLEBEN [14]. R. HEILIG [15] investigated the influence of shear deformations which turned out to be negligible in most cases.

J. N. GOODIER [16], S. TIMOSHENKO [17] and F. BLEICH [18] presented excellent summaries of the theories for open, thin-walled members with special emphasis on stability problems. Aspects applicable to aircraft engineering were presented by P. KUHN [19].

Very recently, the German and English translations of a book by V. Z. VLASOV [20] appeared. This book must have existed in Russia since 1940. It presents the subject of mixed torsion in a most outstanding manner and it seems that its author applied the term "sectorial coordinate" for the first time.

Without special mention, the authors of this book utilized the results of many other scientists and engineers which contributed to the present knowledge of torsion, e. g. [21].

This book represents a condensation of the research which was carried out from 1961 to 1965. A part of this work was published by the Swiss Association of Steel Manufacturers [22, 23, 24, 25] and by the Swiss construction magazine [26].

Zurich, July 1969

Ernst Glauser

References to the Preface

- [1] SAINT-VENANT, B. DE: Mémoires des savants étrangers, Vol. 14, 1855.
- [2] BREDT, R.: Kritische Bemerkungen zur Drehungselastizität. Z. VDI 40 (1968) 785.
- [3] PRANDTL, L.: Zur Torsion von prismatischen Stäben. Phys. Z. 4 (1903) 758.
- [4] FÖPPL, A.: Der Drillingswiderstand von Walzeisenträgern. Z. VDI 61 (1917) 694.
- [5] FÖPPL, A., and L. FÖPPL: Drang und Zwang, München/Berlin: R. Oldenbourg 1928.
- [6] WEBER, C., and W. GÜNTHER: Torsionstheorie, Braunschweig: Vieweg 1958.
- [7] TIMOSHENKO, S.: Einige Stabilitätsprobleme der Elastizitätstheorie. Z. Math. Phys. 58 (1910).
- [8] BACH, C. VON: Versuche über die tatsächliche Widerstandsfähigkeit von Balken mit [-förmigem Querschnitt. Z. VDI 1909, 1910.
- [9] MAILLART, R.: Zur Frage der Biegung. Schweiz. Bauztg. 77 (1921) 195.
- [10] EGGENSCHWYLER, A.: Über die Festigkeitsberechnung von Schiebetoren und ähnlichen Bauwerken. Diss. E. T. H., 1921, Borna bei Leipzig: Robert Noske
- [11] WAGNER, H.: Verdrehung und Knickung von offenen Profilen. Festschrift 25 Jahre T. H. Danzig, 1929, or Luftf.-Forschg. 11 (1934) 329.
- [12] KAPPUS, R.: Drillknicken zentrisch gedrückter Stäbe mit offenem Profil im elastischen Bereich. Luftf.-Forschg. 13 (1937) 444.
- [13] BORNSCHEUER, F. W.: Systematische Darstellung des Biege- und Verdrehvorganges unter besonderer Berücksichtigung der Wölbkrafttorsion. Stahlbau 21 (1952) 1.
- [14] WANSLEBEN, F.: Die Theorie der Drillfestigkeit von Stahlbauteilen, Köln: Stahlbau-Verlag 1956.
- [15] HEILIG, R.: Der Schubverformungseinfluß auf die Wölbkrafttorsion von Stäben mit offenem Profil. Stahlbau 30 (1961) 67.
- [16] GOODIER, J. N.: The Buckling of Compressed Bars by Torsion and Flexure. Cornell University, Engineering Experiment Station, Bulletin 27, 1941.
- [17] TIMOSHENKO, S.: Theory of Bending, Torsion and Buckling of Thin-Walled Members of Open Cross-Section. J. Franklin Inst. 239 (1945).
- [18] BLEICH, F.: Buckling Strength of Metal Structures, New York: McGraw-Hill 1952.
- [19] KUHN, P.: Stresses in Aircraft and Shell Structures, New York: McGraw-Hill 1956.
- [20] VLASOV, V. Z.: Thin-Walled Elastic Beams. English Translation, National Science Foundation, Washington D. C., U.S. Dept. Commerce 1961, also, London: Oldbourne Press 1961.
- [21] THÜRLIMANN, B.: Lecture Notes C. E. 453 and C. E. 411. Lehigh University, Bethlehem, Pa., U.S.A., 1958, 1959.
- [22] KOLLMRUNNER, C. F., and K. BASLER: Torsionskonstanten und Schubspannungen bei Saint-Venantscher Torsion. Mitt. TKSSV., Vol. 23, Verlag Schweizer Stahlbau-Vereinigung, July 1962.
- [23] KOLLMRUNNER, C. F., and K. BASLER: Torsionsmomente und Stabverdrehung bei Saint-Venantscher Torsion. Mitt. TKSSV., Vol. 27, Verlag Schweizer Stahlbau-Vereinigung, Oktober 1963.
- [24] KOLLMRUNNER, C. F., and K. BASLER: Sektorielle Größen und Spannungen bei offenen, dünnwandigen Querschnitten. Mitt. TKSSV., Vol. 28, Verlag Schweizer Stahlbau-Vereinigung, January 1964.
- [25] KOLLMRUNNER, C. F., and K. BASLER: Statik der Wölbkrafttorsion und der gemischten Torsion. Mitt. TKSSV., Vol. 31, Verlag Schweizer Stahlbau-Vereinigung, May 1965.
- [26] BASLER, K.: Zur Statik schief gelagerter Träger. Schweiz. Bauztg. 82 (1964) 269.

Contents

Nomenclature	XIV
I. Saint-Venant Torsion	1
1 Solid Cross Sections	1
1.1 Introduction	1
a) Rotation of the Shaft	1
b) Shear Stress Distribution	2
1.2 Applications	3
a) Circular Cross Section	3
b) Narrow Rectangular Cross Section	4
c) Equilateral Triangular Cross Section	5
1.3 Saint-Venant's Approximation for the Torsion Constant	7
1.4 Built-Up Solid Cross Sections	9
2 Closed, Thin-Walled Cross Sections	10
2.1 Introduction	10
a) Prandtl's Analogy	11
b) Bredt's Formula	12
2.2 Applications	13
a) Radially Symmetric Hollow Cross Sections	13
b) Validity of the Assumption "Thin-Walled"	15
c) Mixed Open-Closed Cross Sections	16
d) Composite Cross Sections	17
e) Lattice Walls	19
2.3 Multicellular Box Section Members	21
a) General Remarks	21
b) Representation of the Resulting Shear Flows (Differences in Elevation)	23
c) Evaluation of the Shear Flows q_i (Lid Elevations)	24
d) Computational Scheme	27
e) Examples	29
2.4 Special Cases and Limiting Values	31
a) Separated Cells	31
b) Limiting Values for the Torsion Constant	32
c) Several Cells in Two-Dimensional Configuration	34
2.5 Cells Connected by a Common Base Cell	35
a) Introduction	35
b) Analysis	36
c) Interpretation of the Results	38
d) Special Cases	40
2.6 Shear Stresses Caused by a Resultant Shearing Force Acting on the Closed, Hollow Cross Section	42
a) Problem	42
b) Shear Stresses Caused by a Shearing Force	43
c) Shear Center	44

3 Torsional Moments and Member Rotation for Saint-Venant Torsion	46
3.1 Introduction	46
a) Saint-Venant Torsion	46
b) Differential Equation	46
c) Notations	47
3.2 The Single Member	47
a) Statically Determinate Support	47
b) Member With No End-Rotations	48
3.3 The Continuous Rod on Elastically Rotating Supports	50
a) The “Three-Rotation Equations”	50
b) The “Three-Torsional-Moment Equations”	52
3.4 Examples	53
a) Systems	53
b) Selection of the Method	55
c) Influence Lines	57
4 Skew Supported Members With Saint-Venant Torsion	58
4.1 Introduction	58
a) Assumptions	58
b) Notations and Abbreviations	58
c) Torsional Moments and their Side-Effects	62
d) Example: Iterative Procedure	63
4.2 Analytical Solution	65
a) Slope at Skew Supports	65
b) Three-Moment Equations	66
c) Forces and Deformations	68
d) Example: Three-Span Continuous Beam	71
4.3 Eccentric Loads	75
a) Decomposition of Loads	75
b) System Acted Upon by a Concentrated Moment	76
c) System Acted Upon by a General Eccentric Load	79
d) Example: Influence Surfaces	81
4.4 General Considerations	85
a) Member Constant C	85
b) Conditions at the Supports	86
c) Maximum Shearing Stresses Caused by Skewed Supports	93
d) Summary	94
II. Warping Torsion	96
5 Stress Analysis	96
5.1 Notation	96
a) Sign Convention	96
b) Coordinate System	96
c) Quantities Depending on the Coordinates x and y	96
d) Correlation of Signs for Quantities Depending on the Coordinate z . .	97
$\alpha)$ Bending in y -Direction	97
$\beta)$ Pure Twist	98
$\gamma)$ Bending in x -Direction	99
$\delta)$ Axial Forces	99
5.2 Characteristic Behavior of Thin-Walled Cross Sections	100
a) Equilibrium Condition for the Wall Element	101
b) Compatibility Condition	101

c) The Tangential Displacement in Terms of ξ, η, φ	101
d) Assumptions	102
e) The Six Equilibrium Conditions Written for a Cross Section	102
5.3 Bending without Twist	103
a) Longitudinal Displacement w	103
b) Axial Stress σ	104
c) Shear Stresses τ	105
d) Shear Center	106
5.4 Twist	107
a) Basic Requirements and the Warping Function w	107
b) Warping Stresses	108
c) Center of Twist	109
5.5 Miscellaneous Considerations	110
a) Properties of the Area Integrals	110
b) Identity of Shear Center and Center of Twist	111
c) The Equilibrium Conditions for the Shearing Forces	112
6 Numerical Calculation of the Cross-Sectional Constants	112
6.1 Computation Scheme	112
a) Geometrical Approximation	112
b) Required Quantities	113
c) Finite Difference Relations	113
d) The Set-Up of the Table	117
6.2 Example	118
a) Cross-Sectional Quantities	118
b) Stresses	118
6.3 Built-Up Open Cross Sections	123
a) Sign Conventions	123
b) Branchings	124
c) Symmetries	124
d) Concentrated Areas	125
e) Composite Cross Sections	125
f) Example	125
7 Analysis of Warping Structures	131
7.1 Introduction	131
a) Concept	131
b) Usual Ways of Support	131
c) Influence Lines	132
7.2 Transverse Influence Lines	133
a) Meaning and Importance	133
b) The Calculation of Transverse Influence Lines	134
7.3 The Continuous, Prismatic Bar	138
a) Warping of the Member	138
b) The Forces in the Bar	140
c) Three-Warping-Moment Equations	141
d) Influence Surfaces	141
7.4 Axial Forces	143
a) Relations	143
b) Example	144

	Contents	XI
8 Warping Torsion in Skew Supported Members	145	
8.1 Introduction	145	
a) Assumptions	145	
b) Notation	145	
8.2 Analysis	147	
a) Base System	147	
b) Deformations	149	
c) Member Forces	150	
d) Equal Skew Angles	151	
8.3 Examples	152	
a) Single-Span Beam on Skewed and Parallel Supports	152	
b) Two-Span Beam on Skewed Supports	155	
III. Mixed Torsion	158	
9 Internal Forces	158	
9.1 Elements of the Analysis	158	
a) Differential Equation	158	
b) Solution for an Infinitely Long Bar	159	
c) Solution for the Bar of Finite Length l	161	
d) Particular Solutions	162	
e) Boundary Conditions	163	
9.2 Examples of the Simply Supported Member	164	
a) Warping Moment at the End of the Member	164	
b) Twisted Supports	165	
c) Uniformly Distributed Torsional Load	165	
d) Concentrated Torsional Load	167	
9.3 Continuous Beams	170	
a) Three-Warping-Moment Equations	170	
b) Deformations and Forces	172	
c) Examples	173	
α) Symmetric, Three-Span Continuous Beam	173	
β) The Fixed-End Member Under Uniformly Distributed Torsional Load	175	
10 Miscellaneous Problems	176	
10.1 Stress Analysis of Rolled Sections	176	
a) General Considerations	176	
b) I -Sections	178	
c) L -Sections	180	
d) T -Sections	186	
10.2 Approximate Solutions	187	
a) The Parameter κ as an Index for the Torsional Behavior	187	
b) Shear Deformation	188	
c) Large κ -Values, Limiting Case and Approximation for $\max M_\omega$	190	
d) Small κ -Values, Limiting Case and Approximation	191	
e) The Accuracy of Approximate Solutions	194	
10.3 The Skew Supported Bar with Mixed Torsion	198	
a) Introduction	198	
b) Base System and Compatibility Conditions	199	
c) Internal Forces	201	
IV. Folded Plates	202	
Introduction	202	
11 General Analysis of Folded Plates	203	
11.1 Systems of Equations	203	
a) Three-Shear Equations	203	

b) Three-Stress Equations	205
c) Example	206
11.2 Equivalent Load System	208
a) Components in the Plane of the Plates	208
b) Separation of Variables	208
c) Affinitive Loads	209
11.3 Shear Stresses	210
a) General Analysis	210
b) Example	213
11.4 General Formulation	213
a) Plates of Variable Thickness and with Protruding Portions	213
b) Axial Forces	214
c) Formulation of Expressions for the Axial Stresses and Shear Stresses .	214
d) Three-Shear and Three-Stress Equations	216
e) Example	217
f) Deformations	219
12 Core Point Method	221
12.1 Introduction	221
a) Different Methods of Solution	221
b) Introductory Example	222
12.2 Plates Connected at their Boundaries	223
a) Recurrence Relations	223
b) Application of the Recurrence Relations	224
12.3 General Folded Plate	225
a) Recurrence Relations	225
b) Example	225
12.4 Miscellaneous Considerations	228
a) Derivation of the Recurrence Relations	228
b) Bracketing	230
c) The Substitute Two-Plate Structure	231
d) Closed Cross Sections	232
13 Relations Between the Folded-Plate Theory and the Theory of Slender Members	236
13.1 Folded-Plate Theory Not Applicable	237
a) Several Plates Meeting at One Common Hinge	237
b) Coinciding Planes of the Plates	237
c) Large Changes in the Geometry of the Cross Section	238
13.2 Equivalence of Both Theories	243
a) The Two-Plate Profile	243
b) The Three-Plate Profile	245
13.3 The Essential Difference Between the Two Theories	252
a) General Remarks	252
α) Deformations	252
β) Stresses	252
b) The Roof Cross Section	253
c) T-Beam Cross Sections	255
α) Load On the Central Girder	256
β) Load on an Outer Plate Girder	256
γ) Residual Stresses	256

13.4 The Approximation to the Actual Structural Behavior	258
a) The Influence of a Cross Beam	258
b) Diaphragms as Infinitely Rigid Cross Girders	261
c) The Number of Diaphragms	263
d) Summary	266
Dimensions of a Few Newly Introduced Quantities	266
Appendix: Rolled Structural Shapes	267
A. 1 Introduction	267
A. 2 The Rectangular and Trapezoidal Sections	268
A. 3 Torsion Constants for Structural Shapes	268
A. 4 Maximum Shear Stress due to Saint-Venant Torsion	273
A. 5 Acknowledgement	274
A. 6 Notation for Appendix	275
Author Index	276
Subject Index	277

Nomenclature¹

Only the most important notations are explained below. For terms related to skew supported rods refer to Section 4.1 b.

a	Rotation of the left member end: $\varphi'(z = 0)$
A	Enclosed area (of hollow cross sections)
b	Rotation of the right member end: $-\varphi'(z = l)$
c	Width of plate
C	Center of gravity
d	Characteristic length = $\sqrt{EI_{\omega\omega}/GK}$
D	Center of rotation, shear center, $D = I_{xx}I_{yy} - I_{xy}^2$
E	Modulus of elasticity
F	Area of cross section
F_f	Area of flange
G	Shear modulus
h	Distance, height of triangle
I_{xz}	$\int_F x^2 dF$ = Moment of inertia
I_{yy}	$\int_F y^2 dF$ = Moment of inertia
I_{xy}	$\int_F xy dF$ = Product of inertia
$I_{\omega\omega}$	$\int_F \omega^2 dF$ = Sectorial moment of inertia
$I_{\omega x}$	$\int_F \omega x dF$ = Sectorial product of inertia
$I_{\omega y}$	$\int_F \omega y dF$ = Sectorial product of inertia
K	Torsion constant
l	Length of member
m_D	Distributed torsional moment acting on member
M_D	Concentrated torsional moment acting on member
M_x	$\int_F \sigma x dF$ = Bending moment
M_y	$\int_F \sigma y dF$ = Bending moment
M_ω	$\int_F \sigma \omega dF$ = Warping moment
N	Axial force
O	Origin of coordinate system

¹ The reader of the English edition will be repaid by a careful preliminary study of the nomenclature. In the interest of providing an English translation with minimum cost and maximum accuracy, the notations in the German edition have been retained. Note, for example, that for I_{xz} and I_{yy} , the subscripts indicate the variable coordinate rather than the reference axis.

p	Distributed load
P	Concentrated load
q	τt = Shear flow
Q	Shearing force
r	Radius
s	Arc length, curvilinear coordinate
S	Statical moment, membrane tension
\tilde{S}_x	$\int_0^s x \, dF$ = Statical moment of the cut-off portion
\tilde{S}_y	$\int_0^s y \, dF$ = Statical moment of the cut-off portion
\tilde{S}_ω	$\int_0^s \omega \, dF$ = Sectorial statical moment of the cut-off portion
t	Wall thickness
T	Total torsional moment due to acting loads
T_s	Saint-Venant torsional moment
T_ω	Warping torsional moment
U	Strain energy
v	Displacement in s -direction
w	Displacement in z -direction
X	Redundant quantities
x, y	Coordinates in the plane of the cross section
X, Y	Non-normalized coordinates parallel to x, y
z	Coordinate coinciding with the member axis
α	Angular displacement at the left end
β	Angular displacement at the right end
γ	Shear deformation $\left(= \frac{\tau}{G}\right)$
Γ	Contour line of the membrane
ε	Strain $\left(= \frac{\sigma}{E}\right)$
ζ	z/l = Normalized z -coordinate
η	Notation for $\int \frac{ds}{t}$
η_{ii}	integrated along the entire circumference of cell i
η_{ik}	integrated along the wall common to cell i and k
χ	$\sqrt{l^2 G K / EI_{\omega\omega}}$, notation, constant of proportionality
ξ, η	Displacement in x - resp. y -direction
σ	Normal stress
τ	Shear stress
φ	Rotation of the member (angle)
φ'	Rotation per unit length $\left(= \frac{d\varphi}{dz}\right)$
Φ	Stress function
ω	Normalized sectorial coordinate, v. Eq. (5.27)
Ω	Non-normalized sectorial coordinate, v. Eq. (5.25)

Superscripts:

(f) Quantity of a member whose ends are fixed against rotation

Subscripts for Continuous Rods: i Designation of spans, even numbers k Designation of supports, odd numbers

I. Saint-Venant Torsion

1 Solid Cross Sections

1.1 Introduction

This first part deals with solid prismatic shafts with cross-sectional area F which transmit a given torsional moment T . The rotation of the shaft and the shear stresses are to be determined. The exact solution of this problem for non-circular sections was first provided by SAINT-VENANT.¹

a) Rotation of the Shaft

The rotation of the shaft is measured by the angle Φ which indicates the amount of rotation of the cross section at a distance z along the shaft from the origin (Fig. 1.1). Since this angle depends on the position of the origin, one is interested in the unit rotation $d\varphi/dz = \varphi'$ of the shaft, which at every cross section z is uniquely determined by the torsional moment $T(z)$.

Initially, the material will be assumed to be elastic, with properties described by Hooke's law. The unit rotation is therefore proportional to the torsional moment T and inversely proportional to the shear modulus G .

$$\varphi' = \varkappa \frac{T}{G}.$$

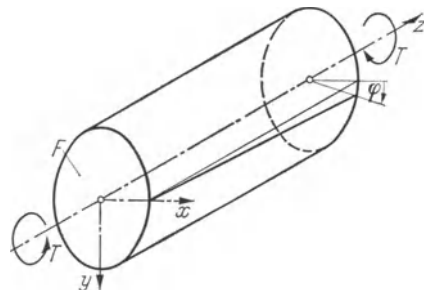


Fig. 1.1. Shaft Rotation φ due to a Torsional Moment T .

The constant of proportionality \varkappa will not only adjust the dimension of this equation but will furthermore give an indication as to the suitability of the cross section with respect to torsion. The left side of this equation has the dimension [length]⁻¹, the quotient to the right [length]⁻³. The constant of proportionality \varkappa will therefore have the dimension [length]⁻⁴. Hence it seems more appropriate to work with the reciprocal value of \varkappa which then will have the dimension of an area moment of inertia. The above relation may now be written:

$$\varphi' = \frac{T}{GK}. \quad (1.1)$$

K is called the *torsion constant* and the product GK is designated as the *torsional rigidity*. The torsion constant is equal to the polar moment of inertia

¹ NAVIER: Résumé des leçons sur l'application de la mécanique, 3rd ed., edited by SAINT-VENANT, Paris: Dunod 1864.

only in the case of a circular cross section. K may be defined as the constant of proportionality with the dimension [length]⁴ that makes an equality out of the differential relation (1.1) which is essentially Hooke's law.

Before giving its determination, the evaluation of the shear stress due to torsion will be explained briefly.

b) Shear Stress Distribution

The distribution of shear stress due to torsion in solid cross sections can be visualized with the help of Prandtl's analogy¹.

A membrane is assumed to be stretched across an opening which has the same shape as the cross section of the shaft. The membrane is under uniform tension S (force per unit length). The effect of a torsional moment corresponds to the effect of a uniformly distributed pressure p acting perpendicular to the plane of the membrane.

The resulting membrane deflection is designated by $\Phi(x, y)$ and is supposed to be small (Fig. 1.2). $\Phi(x, y)$ is also mathematically equivalent to the torsion stress function, which will here be designated by the same symbol.

PRANDTL showed that the following analogies between the membrane and the torsion problems exist:

The torsional moment T is represented by twice the volume V between the membrane and the plane of the cross section,

$$T = 2V. \quad (1.2)$$

The resultant shear stresses are tangential to the contour lines of the membrane, have an absolute value which is equal to the slope of the membrane normal to the contour lines. Shear stress components in the x and y coordinate directions are:

$$\tau_{zx} = \frac{\partial \Phi}{\partial y}, \quad \tau_{zy} = -\frac{\partial \Phi}{\partial x}. \quad (1.3)$$

The product $2G\varphi'$ of the torsion problem corresponds to the ratio p/S of the membrane problem. Thus

$$\frac{p}{S} = 2G\varphi'. \quad (1.4a)$$

This statement, (1.4a), leads together with (1.3) to a relation which is valuable for the calculation of the torsion constant. Consider for this purpose the membrane sector which is cut off along the contour line Γ (Fig. 1.2). The resultant of the membrane pressure which acts on the enclosed area A is equal to pA . But this has to be equal to the sum of the vertical components of the membrane tension which acts along the contour line Γ .

Considering further that the horizontal component of the membrane tension is everywhere equal to S and that the slope of the membrane according to

¹ PRANDTL, L.: Zur Torsion von prismatischen Stäben. Phys. Z. 4 (1903) 758.

(1.3) is equal to the shear stress, the equilibrium condition can be written in the form:

$$pA = \oint_{\Gamma} S\tau ds;$$

since $S = \text{constant}$:

$$\frac{p}{S} A = \oint_{\Gamma} \tau ds$$

and due to (1.4 a)

$$2G\varphi' A = \oint_{\Gamma} \tau ds. \quad (1.4b)$$

If Eq. (1.4 b) is given the form of Eq. (1.1), then a comparison of the two equations yields immediately the following torsion constant:

$$K = \frac{2AT}{\oint_{\Gamma} \tau ds}. \quad (1.5)$$

The symbols in this equation have the meaning:

- $\oint_{\Gamma} \tau ds$: Line integral of the shear stresses along an arbitrary shear stress trajectory (contour line of the membrane) [force/length];
- A : Area enclosed by the closed line Γ [length]²;
- T : Torsional moment producing the shear stresses [force · length];
- K : Torsion constant [length]⁴.

A procedure for the approximate calculation of the shear stresses and the torsion constant will now be summarized. The shape of the membrane may be visualized and for this purpose soap film experiments, real or hypothetical, are helpful. The volume between the membrane and the plane of the cross section has to be determined in order to use Eq. (1.2). The distribution of the shear stresses may be sketched on the basis of Eqs. (1.3), and Eq. (1.5) yields finally the torsion constant K . The following few examples will illustrate the procedure.

1.2 Applications

a) Circular Cross Section

Fig. 1.2 shows the membrane which corresponds to the circular cross section. In applying Prandtl's analogy, the slope of the membrane is assumed to be very small (similar to the slope of a deflected beam, which has to be small to satisfy the assumption that the curvature is equal to the second derivative of the deflection).

A paraboloid of revolution should be a good first approximation for the shape of the membrane. It is given with respect to polar coordinates ϱ, φ by the following expression:

$$\Phi(\varrho, \varphi) = \Phi_0 \left[1 - \left(\frac{\varrho}{r} \right)^2 \right].$$

The constant φ_0 stands for the deflection of the membrane in the centre of the circular cross section. It is determined by Eq. (1.2) which states that twice the volume of this paraboloid of revolution is equal to the torsional moment:

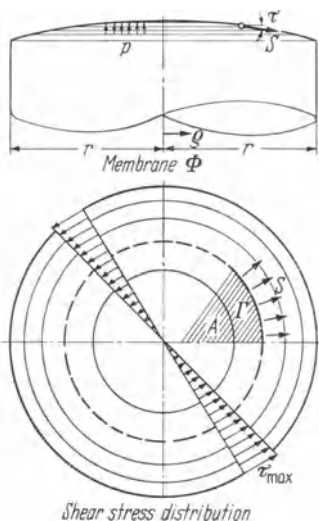


Fig. 1.2 Prandtl's Analogy for the Circular Cross Section.

$$T = 2 \int_0^r \Phi_0 \left[1 - \left(\frac{\varrho}{r} \right)^2 \right] 2\pi\varrho d\varrho,$$

$$\Phi_0 = \frac{T}{\pi r^2}$$

and therefore

$$\Phi = \frac{T}{\pi r^2} \left[1 - \left(\frac{\varrho}{r} \right)^2 \right].$$

From Eq. (1.3) it follows:

$$|\tau| = \frac{d\Phi}{d\varrho} = \frac{2T}{\pi r^4} \varrho.$$

The distribution of the shear stress is plotted in Fig. 1.2. The maximum shear stress occurs at the boundary of the cross section and equals:

$$\tau_{\max} = \frac{2T}{\pi r^3}. \quad (1.6)$$

For this constant value of τ , the line integral along the boundary of length $2\pi r$ becomes:

$$\oint_r \tau ds = \frac{2T}{\pi r^3} 2\pi r = \frac{4T}{r^2}.$$

Eq. (1.5) leads now to the following value for the torsion constant:

$$K = \frac{\pi}{2} r^4. \quad (1.7)$$

b) Narrow Rectangular Cross Section

For narrow rectangular cross sections whose width b exceeds by far its thickness t , the short sides may influence the shape of the membrane only over a distance from the edges which is of the order of magnitude of the thickness.

Aside from these end zones, the membrane may be assumed to be parabolic, cylindrical and stretched from one long side to the other as shown in Fig. 1.3:

$$\Phi(x, y) = \Phi_0 \left[1 - \left(\frac{2x}{t} \right)^2 \right].$$

Eq. (1.2) leads to:

$$T = 2 \frac{2}{3} \Phi_0 tb.$$

This yields:

$$\Phi_0 = \frac{3}{4} \frac{T}{bt}$$

and

$$\Phi = \frac{3}{4} \frac{T}{bt} \left[1 - \left(\frac{2x}{t} \right)^2 \right].$$

The shear stresses are obtained from Eqs. (1.3):

$$|\tau_{xy}| = \frac{d\Phi}{dx} = 6 \frac{T}{bt^3} x.$$

They are a maximum at the boundary:

$$\tau_{\max} = 3 \frac{T}{bt^2}. \quad (1.8)$$

According to Eq. (1.5)

$$K = \frac{2AT}{\oint r ds} = \frac{2btT}{2b\tau_{\max}},$$

the torsion constant becomes: $K = \frac{1}{3} bt^3$.

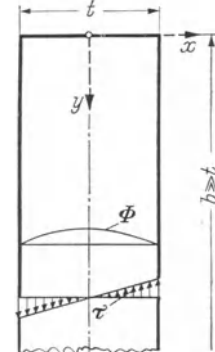


Fig. 1.3. The Narrow Rectangular Cross Section.

Excercise 1.1. *Narrow Cross Section.* Prove the following relations for the narrow cross section (thickness $t \ll$ width b) with only slight variation in the thickness t :

$$K = \frac{1}{3} \int_0^b r^3 ds, \quad \tau_{\max} = \frac{T}{K} t.$$

c) Equilateral Triangular Cross Section

The cross section together with an explanation of the applied notation are given in Fig. 1.4a. The membrane will have a horizontal tangent plane at the corners of the triangle. This fact is made quite obvious by a visualization of the stretched membrane, and it finds its more realistic proof through the consideration of the equilibrium of a small corner element. If the surface of the prismatic shaft is free of stress, the resultant shear stress can only be parallel to the boundaries of the cross section. Since a nonzero shear stress cannot be at the same time parallel to two different directions, the slope of the membrane at the corners must be equal to zero.

In order to define the height of the membrane along the axis of symmetry $y = 0$ which satisfies the boundary conditions, a polynomial of at least third order has to be selected. The requirement of a zero height at the boundary $x = -a$ and a zero slope at the corner $x = 2a$ (Fig. 1.4a) leads to the following assumption for the polynomial:

$$\Phi(x, y=0) = c \left(\frac{x}{a} + 1 \right) \left(\frac{x}{2a} - 1 \right)^2.$$

Vertical sections through the membrane which are parallel to the y -direction will result in curves which are symmetric with respect to the x -axis and of zero

height at the boundaries. The simplest curve with these properties is again a parabola. The shape of the membrane is now completely determined. The width of a volume element dV in y -direction is according to Fig. 1.4a $2(2a - x)/\sqrt{3}$, the height $\Phi(x, y = 0)$ as stated above and the thickness dx .

The volume of the element of parabolic shape is two thirds of the product of these three dimensions. The total volume enclosed by the membrane is therefore:

$$V = \frac{8ac}{3\sqrt{3}} \int_{2a}^{-a} \left(\frac{x}{a} + 1\right) \left(\frac{x}{2a} - 1\right)^3 dx = \frac{27\sqrt{3}}{20} a^2 c,$$

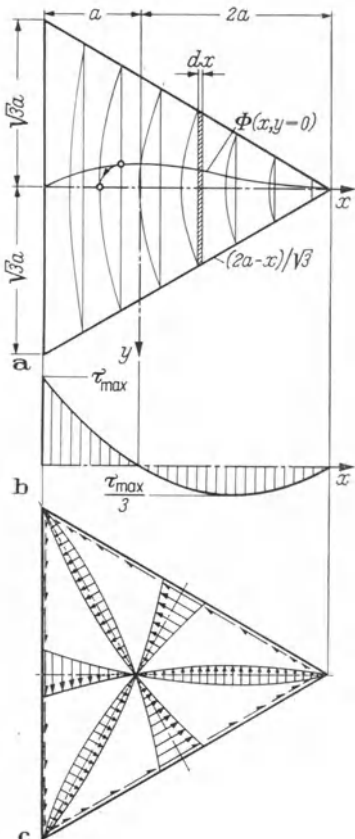


Fig. 1.4. The Equilateral Triangular Cross Section.

which with Eq. (1.2) leads to the height c of the membrane:

$$T = \frac{27\sqrt{3}}{10} a^2 c,$$

$$c = \frac{10}{27\sqrt{3}} \frac{T}{a^2}.$$

This determines:

$$\Phi(x, y = 0) = \frac{10}{27\sqrt{3}} \frac{T}{a^2} \left(\frac{x}{a} + 1\right) \left(\frac{x}{2a} - 1\right)^2$$

and, as a consequence of Eq. (1.3):

$$\begin{aligned} |\tau_{zy}|_{y=0} &= \frac{d\Phi(x, y=0)}{dx} \\ &= \frac{5}{3\sqrt{3}} \frac{T}{a^3} \frac{x}{a} \left(\frac{x}{2a} - 1\right). \end{aligned}$$

This distribution of the shear stresses is plotted in Fig. 1.4b. The maximum occurs at the boundary and has the value:

$$\tau_{\max} = \frac{5}{6\sqrt{3}} \frac{T}{a^3}. \quad (1.10)$$

Since the boundary of the cross section $x = -a$ is a contour line of the membrane and since the membrane cross sections parallel to this boundary are parabolas, the slopes of the membrane and therefore the shear stresses along this side will show a parabolic distribution.

Note that due to symmetry the same derivation is valid if the cross section is turned by $\pm 120^\circ$. This leads to the shear stress distribution which is plotted in Fig. 1.4c.

Eq. (1.5) determines again the torsion constant. It is:

$$K = \frac{2AT}{\oint_{\Gamma} \tau ds} = \frac{2 \cdot 3 \sqrt{3} a^2 T}{\frac{2}{3} \tau_{\max} 2a \sqrt{3} \cdot 3} = \frac{aT}{\frac{2}{3} \tau_{\max}},$$

and therefore:

$$K^* = \frac{9\sqrt{3}}{5} a^4. \quad (1.11)$$

1.3 Saint-Venant's Approximation for the Torsion Constant

Up to this point the torsion constant has been computed on the basis of assumed shear stresses along at least one shear stress trajectory. It occurs quite often, however, e.g. when setting up the defining equations of structures or in stability investigations, that one is not interested in the shear stresses but in the torsional rigidity of the members. The following formula will allow a quick estimate of the torsion constant for arbitrarily shaped solid cross sections.

The torsion constant characterizes the suitability of a cross section with respect to torsion in much the same way as I_{xx}^{**} and I_{yy}^{**} describe the flexural properties of the cross section in the x - and y -directions respectively or to the way the cross-sectional area is related to the axial forces in the member. One might well ask whether it would be possible to give an approximate functional relation between the torsion constant K and the already known characteristic values I_{xx} , I_{yy} and F of the cross section. This relation might be assumed in the form:

$$K = f(F, I_{xx}, I_{yy}).$$

The arguments of such a function must not depend on the selection of a particular coordinate system. This requirement is satisfied for the area F of the cross section, but the area moments of inertia would have to appear at least as the sum $I_{xx} + I_{yy} = I_{rr}$, since only the polar moment of inertia I_{rr} does not depend on a rotation of the coordinate system. A better assumption might therefore be:

$$K = f[F, (I_{xx} + I_{yy})] = f[F, I_{rr}].$$

It can be observed from the expression for the torsion constant of a narrow rectangular cross section that K appears in the form of the moment of inertia, the product of one dimension with the third power of the other. In this case, where $I_{xx} \cong 0$ and $I_{yy} \cong I_{rr}$, the product $I_{rr} K$ is proportional to F^4 , $\left(\frac{1}{12} b^3 t \frac{1}{3} b t^3 = \frac{1}{36} b^4 t^4\right)$.

Introducing the constant α , which for a narrow rectangular cross section is equal to 36, the functional relation can be given in the following form:

$$K = \frac{F^4}{\alpha I_{rr}}.$$

* This is identical with the exact solution obtained by SAINT-VENANT in 1864.

** Editor's note: Contrary to usual usage in the U.S.A., I_{xx} and I_{yy} are, respectively, the area moments of inertia about the y and x axes.

While this simple expression was derived from the consideration of a case where one dimension is much longer than the other, the constant κ should be determined from a cross section which has about the same extension in every direction.

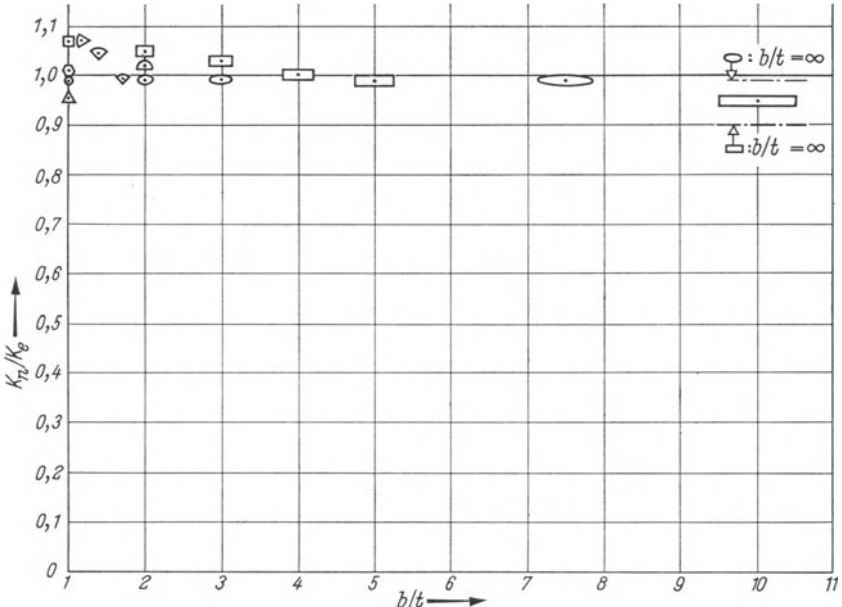
If the properties of a circular cross section are introduced ($F = \pi r^2$, $I_{rr} = \frac{\pi}{2} r^4$, $K = \frac{\pi}{2} r^4$), then $\kappa = 4\pi^2 \approx 40$ and therefore:

$$K = \frac{F^4}{40 I_{rr}}. \quad (1.12)$$

This approximate formula was developed by SAINT-VENANT¹. It is surprising how varied the shape of the cross section may be. The formula is valid not only for cross sections with about equal extension in two mutually perpendicular directions but also for cases where these two distances are drastically different. The cross section, however, is not supposed to have reentrant corners. It will be shown in the next section how these cases have to be treated.

Exercise 1.2. Saint-Venant's Approximate Formula. Search in the literature for precise values for the torsion constant of different solid cross sections. Apply Saint-Venant's approximate formula to these sections to verify their accuracy.

The following figure contains a collection of results. The ordinate represents the ratio between approximate and precise value while the abscissa shows the ratio between the maximum and minimum dimensions of the cross section.



Results of Exercise 1.2: Accuracy of Saint-Venant's Approximate Formula for the Torsion Constant K . Ratio Between Approximate and Precise Value, K_n/K_e , as a Function of the Ratio Between Maximum and Minimum Extension of the Cross Section, b/t .

¹ SAINT-VENANT: De la torsion des prismes. Tome XIV de l'Académie des Sciences, Paris 1855.

1.4 Built-Up Solid Cross Sections

Cross sections of structural members are very frequently of complicated shape like the one shown in Fig. 1.5. In these cases, the cross section is thought as being built up of different, simply shaped elements with areas (F_1, F_2, \dots, F_n) as shown in Fig. 1.5.

If it is assumed that the shape of the member cross section remains unchanged during rotation, with each element undergoing the same unit rotation φ' as the whole cross section:

$$\varphi'_i = \varphi' \quad (i = 1, 2, \dots, n)$$

and according to Eq. (1.1) $\frac{T_i}{G K_i} = \frac{T}{G K}$ ($i = 1, 2, \dots, n$),

$$\text{therefore } T_i = \frac{K_i}{K} T \quad (i = 1, 2, \dots, n), \quad (1.13)$$

where T is the torsional moment which acts on the whole cross section with torsion constant K , while T_i and K_i are the corresponding values of the element i . The equilibrium condition for the torsional moments is:

$$\sum_{i=1}^n T_i = T.$$

Eq. (1.13) replaces the unknown torsional moment T_i :

$$\frac{T}{K} \sum_{i=1}^n K_i = T,$$

which leads to

$$K = \sum_{i=1}^n K_i. \quad (1.14)$$

If the approximate formula (1.12) is used to compute the torsion constant K_i of the element i , then the following relation for the torsion constant of a composite cross section built up of arbitrarily shaped elements is obtained:

$$K \cong \frac{1}{40} \sum_{i=1}^n \frac{F_i^4}{I_{rr,i}}. \quad (1.15)$$

Herein are:

F_i : Cross-sectional area of the i -th element.

$I_{rr,i}$: Polar moment of inertia, $I_{rr} = I_{xx} + I_{yy}$, of the i -th element;

For the special case, when all the elements are narrow rectangles, formula (1.14) can according to Eq. (1.9) be written in the form:

$$K = \frac{1}{3} \sum_{i=1}^n b_i t_i^3. \quad (1.16)$$

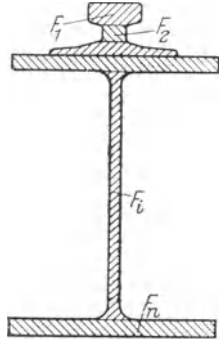


Fig. 1.5. Solid Cross Section
Built-Up of n Different
Elements.

Herein are:

- b_i : Width (large extension) of the i -th rectangle;
 t_i : Thickness of the i -th rectangle.

To the best of our knowledge, Eq. (1.16) has been postulated for the first time by A. FÖPPL¹.

The approximate formulas (1.15) and (1.16) are not quite exact for the following two reasons: Firstly, there is a certain mistake in each term of the sum since they consider the torsion constant of the i -th element only approximately, and secondly, the fillets which usually occur in the connection between two different elements are neglected.

Reference may be made to the Appendix of this english edition for procedures suitable to the calculation of more precise values for the torsion constant of rolled sections².

The elements³ of riveted or welded plate girders may be built up of different cover plates as shown in Fig. 1.6. The question is, whether the cover plates have to be considered independently of one another or whether the element of which

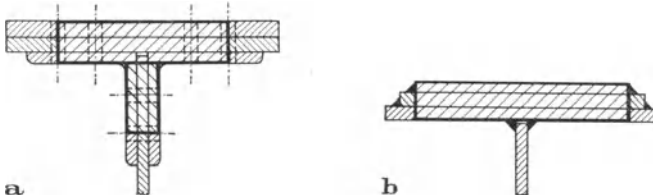


Fig. 1.6. The Decomposition of the Cross Section of Riveted (a) and Welded (b) Plate Girders with Cover Plates.

they are a part may be treated as a whole. The Lehigh University in Bethlehem, Pennsylvania, conducted extensive experiments to answer this question⁴. Fig. 1.6 visualizes the result of this investigation. The portion limited by the most outward line of rivets or the most inward weld may be treated as a whole while the portion of the cover plates outside this boundary has to be considered independently.

2 Closed, Thin-Walled Cross Sections

2.1 Introduction

To be consistent with the heading of the first chapter, "Solid Cross Sections", the second chapter should have been titled "Hollow Cross Sections". Since in most practical applications the walls are thin compared with the dimensions of the

¹ FÖPPL, A.: Der Drillungswiderstand von Walzeisenträgern. Z. VDI, 61 (1917) 694. — FÖPPL, A., and L. FÖPPL: Drang und Zwang, München and Berlin: R. Oldenbourg 1928.

² Editor's Note: In the case of rolled WF, Tee, Zee, and channel sections as rolled in the U.S.A., the major steel companies make available tables that list the torsion constants of standard shapes to an accuracy better than $\pm 0,5$ percent. These tables were developed on the basis of procedures presented herein in the Appendix.

³ Editor's Note: Currently riveted girders have been replaced quite generally by welded girders. Current practice in welded girders usually calls for a single flange plate of required thickness rather than the use of welded flange reinforcing plates.

⁴ CHANG, F. K., and B. G. JOHNSTON: Torsion of Plate Girders. Trans. Am. Soc. of Civ. Eng. 118 A (1953) 337

cross section, this chapter will deal with this special case with only few exceptions. A criterion as to what may be considered to be a thin-walled cross section is given in Section 2.2b.

a) Prandtl's Analogy

Prandtl's Analogy, which has been applied to solid cross sections in the previous chapter, also may be used for hollow cross sections in the same form with the condition, however, that the inner boundary has to correspond to a contour line of the membrane. This condition calls for a zero slope in the direction tangential to the inner boundary corresponding to a zero component of the shear stress perpendicular to this line. This is an immediate consequence of a stress-free inner wall of the hollow prismatic shaft.

The membrane across the hollow space may be thought as being replaced by a horizontal, plane lid. Though the true membrane is only stretched across the effective area of the cross section, the uniformly distributed pressure p acts nevertheless on the membrane as well as on the plane lid, e.g. on everything inside the periphery of the cross section (Fig. 2.1).

Prandtl's analogy applies to the whole region which is contained by the plane of the cross section, the membrane and the lid. It can be described by the stress functions $\Phi(x, y)$, whose gradient, however, is no longer a continuous vector function.

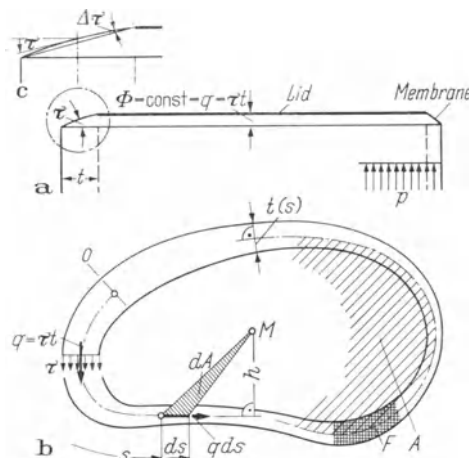


Fig. 2.1. Prandtl's Analogy for the Thin-Walled Hollow Cross Section.

If the thickness of the walls is small compared to the dimensions of the cross section, e.g. if the cross section is thin-walled, then the analysis may be considerably simplified for the following two reasons:

Firstly, it is admissible to deal with the average slope of the membrane which is equal to the slope of a parabolic membrane cross section at the center line of the wall (Fig. 2.1c). The assumption of an average slope is equivalent to a constant shear stress distribution across the wall. The condition that the lid is parallel to the

plane of the cross section (Fig. 2.1 a) can be expressed by:

$$\tau t = \text{const.} = q. \quad (2.1)$$

Secondly, the average direction of the contour lines, which are identical to the shear stress trajectories, is assumed to be equal to the direction of the center line of the wall, even if the wall thickness is variable with respect to the arc length s (Fig. 2.1 b). This means that the shear force per unit length q , Eq. (2.1), is tangential to the center line of the wall.

The constant q which is the product of the average shear stress and the wall thickness and has the dimension [force/length] is usually designated as the "shear flow". This name originates from the hydrodynamic analogy which is another of the many models that have been constructed for the torsion problem.

The *hydrodynamic analogy* relates the shear stress distribution to the velocity field for an ideal, incompressible fluid circulating with uniform vorticity in a constant depth channel of the same cross section as the twisted bar. The flow in the channel is equal to the product of average velocity and channel width t , thus equal to q .

The membrane model permits one to visualize that where τ is greatest, the wall thickness is smallest. The corresponding statement in the hydrodynamic analogy is that where the flow velocity is greatest, the channel width is smallest.

This analogy permits one to see that in a branching point the sum of in- and outflows is zero, $\sum q_i = 0$. The corresponding interpretation for the membrane analogy is that in going completely around a branching point the total difference of height is zero, thus again $\sum q_i = 0$.

b) Bredt's Formula

The evaluation of the shear stresses τ and the torsion constant K for thin-walled, hollow cross sections is made in the same way as for solid cross sections.

The volume V covered by the membrane and the lid is approximately the product of the height $\Phi_0 = q$ and the area A enclosed by the center line of the walls (Fig. 2.1), thus $V = qA$. The torsional moment T is, according to Eq. (1.2) equal to twice the volume V :

$$T = 2qA \quad (2.2)$$

or

$$q = \frac{T}{2A}. \quad (2.3)$$

This demonstrates that the shear flow q depends on the enclosed area but not on the shape of the hollow cross section.

The relation between shear flow and torsional moment (2.2) follows directly from an equilibrium consideration. The contribution of the wall element of length ds to the torsional moment with respect to the point M is $dT = hq ds = 2q dA$.

Integration yields immediately Eq. (2.2) which is independent of the selected reference point M .

The shear flow can be calculated with formula (2.3) and the shear stresses finally with Eq. (2.1).

The explicit expression for the *shear stresses* is:

$$\tau(s) = \frac{T}{2At(s)}. \quad (2.4)$$

If this value is introduced into Eq. (1.5), then the following expression for the *torsion constant* of a thin-walled hollow cross section is obtained:

$$K = \frac{4A^2}{\oint \frac{ds}{t(s)}}. \quad (2.5)$$

Herein are:

$\oint \frac{ds}{t(s)}$: Contour integral along the center line s of the reciprocal value of the wall thickness $t(s)$. If the hollow cross section is built up of n parts, each with the constant wall thickness t_i , then the integral may be replaced by the sum:

$$\oint \frac{ds}{t} = \sum_{i=1}^n \frac{s_i}{t_i}.$$

For the case of a constant wall thickness t all along the circumference of length u , the value of the integral becomes:

$$\oint \frac{ds}{t} = \frac{u}{t}.$$

A : Area enclosed by the center line of the walls (Fig. 2.1 b). (Not to be confused with the effective area of the cross section F).

The expression (2.5) was given for the first time by R. BREDT¹ and is known as Bredt's formula.

2.2 Applications

a) Radially Symmetric Hollow Cross Sections (Fig. 2.2)

If t is the wall thickness and r_m the radius of the wall center line, then expressions for the average shear stress τ and the torsion constant K can be derived from Eqs. (2.4) and (2.5):

$$\tau = \frac{T}{2\pi r_m^3 t}, \quad (2.6)$$

$$K = \frac{\frac{1}{t} \cdot 2\pi r_m}{\frac{4\pi^2 r_m^4}{t}} = 2\pi r_m^3 t. \quad (2.7)$$

This simple example is now used to demonstrate the drastic difference in the torsional properties of open and closed hollow cross sections.

Suppose that a circular tube is fabricated from a bent strip of a steel plate. The cross section of the tube is thin-walled and open before the weld is applied and closed afterwards. The open cross section will resist torsion like a narrow rectangle. The shear stresses and the torsion constant may be determined from the results (1.8) and (1.9) width the width "b" of the rectangle replaced by the length of the wall center line $2\pi r_m$.

These results are given in the lower left hand corner of Fig. 2.2. The sketches on the left side show the stress distribution and the membrane analogy for this

¹ BREDT, R.: Kritische Bemerkungen zur Drehungselastizität. Z. VDI (1896) 815.

case. The left side of the cross section represents a completely elastic state and the right side a completely plastic state. The corresponding presentation for the

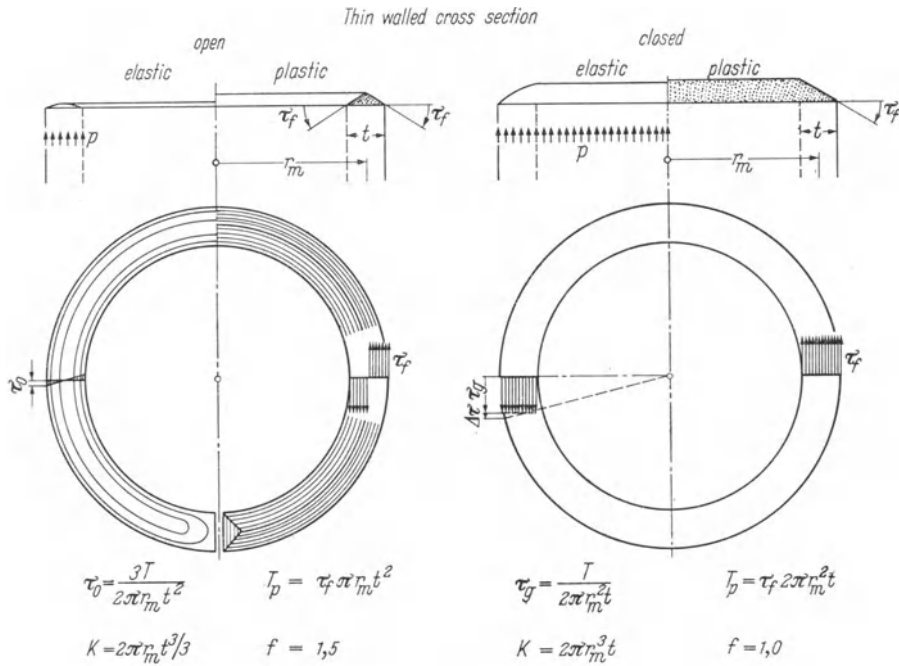


Fig. 2.2. Comparison Between Open and Closed Hollow Cross Sections.

closed, hollow cross section is made on the right side of this figure. The drastic difference in the torsional properties of these two cases arises from the drastically different lever arms available for carrying the torsional moment.

Ratios comparing the torsional properties of these two cases from different viewpoints are given in Table 2.1. In this table, values corresponding to the open cross section are temporarily characterized by the letter "o" and those corresponding to the closed cross section by the letter "g".

Table 2.1. Comparison of the Shear Stresses τ , Torsional Moments T and Unit Rotations ϕ' in Open (Subscript o) and Closed (Subscript g), Circular, Hollow Cross Sections with Wall Thickness t and Radius of the Wall Center Line r_m

	In case of equality between:		
	Shear stresses $\tau_o = \tau_g$	Torsional moment $T_o = T_g$	Unit rotation $\phi'_o = \phi'_g$
The ratios between the values in the open and in the closed cross section of the			
Shear stresses $\frac{\tau_o}{\tau_g}$ are:	1	$3 \frac{r_m}{t}$	$\frac{t}{r_m}$
Torsional moments $\frac{T_o}{T_g}$ are:	$\frac{1}{3} \frac{t}{r_m}$	1	$\frac{1}{3} \left(\frac{t}{r_m}\right)^2$
Specific rotations $\frac{\phi'_o}{\phi'_g}$ are:	$\frac{r_m}{t}$	$3 \left(\frac{r_m}{t}\right)^2$	1

The first column in this table shows for example that with equal maximum shear stresses the open cross section will carry only the $t/3r_m$ -th part of the torsional moment in the closed cross section though it will have a deformation which is r_m/t -times greater. An open tube with a ratio of average radius to wall thickness of ten carries only one thirtieth of the torsional moment and has a deformation which is ten times greater than in a closed tube even though both cases are for equal maximum shear stress and the same area of cross section. If, on the other hand, both cases are required to have the same deformations, then the ratio between the torsional moments would have to be 1:300.

It should be noted that the above derivations are only valid when the torsional moment causes only shear stresses in the cross sections (Saint-Venant torsion). The open cross section, however, will in general resist torsional moments in a more complex manner, which will be described in parts II and III.

b) Validity of the Assumption “Thin-Walled”

The assumption of a constant shear stress τ across the wall of a hollow cross section is only an approximation. There is a difference $\Delta\tau$ between the maximum and the average shear stress (Fig. 2.2).

This fact is visualized by the additional deflection of the membrane as shown in Fig. 2.1 c. The slope of the membrane is always smaller at the inner boundary of the walls than at the periphery. The corresponding difference in shear stresses forces the wall elements to undergo the same unit rotation as the whole cross section. $\Delta\tau$ may therefore be considered to be the maximum shear stress in the open cross section having the same specific rotation as the corresponding closed cross section with the average shear stress τ .

If an element out of the wall of an open, thin-walled cross section is considered to be a segment of a narrow rectangle, then the unit rotation of the open profile is given by $\varphi' = \Delta\tau/tG$. This leads to the following relation when set equal to the specific rotation of the closed cross section:

$$\Delta\tau = t \frac{T}{K}. \quad (2.8)$$

K is given by Eq. (2.5).

The ratio between the difference and the average value of the shear stress is obtained from Eq. (2.4):

$$\frac{\Delta\tau}{\tau} = \frac{t^2}{2A} \oint \frac{ds}{t}. \quad (2.9a)$$

For the special case of constant wall thickness along the circumference of the hollow cross section, this equation reduces to:

$$\frac{\Delta\tau}{\tau} = \frac{F}{2A}. \quad (2.9b)$$

The additional shear stresses with the maximum $\Delta\tau$ result in an additional torsional moment ΔT which, strictly speaking, should be added to the torsional

moment given by expression (2.2). The relative correction is given by:

$$\frac{\Delta T}{T} = \frac{1}{3K} \oint t^3 ds \quad (2.10a)$$

for the general case and by

$$\frac{\Delta T}{T} = \frac{1}{3} \left(\frac{F}{2A} \right)^2 \quad (2.10b)$$

for the case of constant wall thickness.

The error in Eq. (2.2) can therefore be neglected simply because the lever arm belonging to ΔT corresponds to the wall thickness while the lever arm belonging to T is of a higher order of magnitude pertaining to the cross section dimensions.

The question as to whether or not a cross section may be considered to be thin-walled in order to obtain a result of a certain prescribed accuracy may now be answered with the help of Eqs. (2.9) and (2.10). The requirement of less than 10% error in calculating the shear stresses for a hollow cross section with constant wall thickness is satisfied when the effective area of the cross section is less than one fifth of the area enclosed by the wall center line. The condition of less than 10% error in the torsional moment is, on the other hand, already satisfied when the effective area of the cross section does not exceed the area enclosed by the wall center line. Many cross sections occurring in structural engineering practice may therefore be analyzed with the theory developed for thin-walled hollow cross sections and do not need the refinement in the analysis represented by Eqs. (2.9) and (2.10).

c) Mixed Open-Closed Cross Sections

The closed cross sections used in steel constructions often have added outstanding profiles as shown in Fig. 2.3a.

In accordance with Section 2.2b, this type of cross section may be analyzed in the following way: As illustrated in Fig. 2.3, segments which do not contribute to the closure of a cross-section make but a very small contribution to the torsional

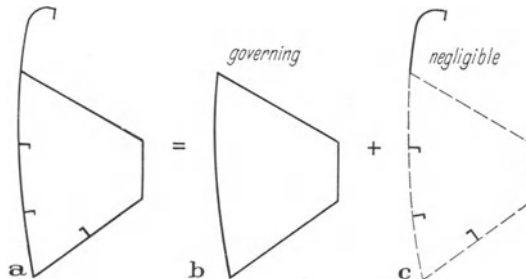


Fig. 2.3. Mixed Open-Closed Cross Section Subjected to Saint-Venant Torsion.

properties of the closed cross section (Fig. 2.3b) and may therefore be neglected. Since the theory assumes that all parts of the cross section rotate by the same amount, the investigation of the shear stress difference $\Delta\tau$, Eq. (2.9), is valid for

the attached open ribs as well. The shear stresses in these parts are small compared to those in the closed region in the same proportion as the cross sectional areas of the ribs are small compared to area of the totally enclosed region.

d) Composite Cross Sections

The torsion analysis of box-type cross sections consisting of different materials, may be reduced to the analysis of a homogeneous cross section with modified wall thicknesses for portions not consisting of the reference material. This approach (as used for the flexural analysis of composite steel-concrete members) may be justified for the case of torsion in the following manner:

The work done by the external forces acting on a member is equal to the stored strain energy or work done by the internal forces.

If Hooke's law describes the elasticity of the material, this work is simply "one half of the force times the displacement". The torsional moment T acting on the cross section represents the external force acting through the angle $d\varphi = \varphi' dz$. The force τdF acting on one volume element and thus moving by the amount γdz represents the elemental work done by the internal forces. The total internal strain energy is the integrated sum of the contributions, and is equal to the work done by the external force T :

$$\frac{1}{2} T \varphi' dz = \frac{1}{2} dz \int_F \tau \gamma dF.$$

With $\gamma = \frac{\tau}{G}$ this relation becomes:

$$T \varphi' = \int_F \frac{\tau^2}{G} dF.$$

The shear stress in a thin-walled closed cross section is given by Eq. (2.4) and the area dF of one element is $t(s) ds$. Thus:

$$\varphi' = \frac{T}{4 A^2} \oint \frac{ds}{Gt}.$$

In this integrand both the shear modulus G and the wall thickness t may be functions of the arc length s . If one introduces a reference material with the shear modulus G_0 , then the above equation may be rewritten in the form:

$$\varphi' = \frac{T}{G_0 K}, \quad \text{where } K = \frac{4 A^2}{\oint \frac{G_0 ds}{G t}}. \quad (2.11)$$

The expression for K in Eq. (2.11) is made equivalent to formula (2.5) if the transformed thickness t^* of the walls is introduced:

$$t^* = \frac{G}{G_0} t. \quad (2.12)$$

Since the shear flow q is independent of the thickness of the walls, Eqs. (2.3) and (2.4) remain unchanged and yield the shear flow q and the shear stress τ . The additional stresses $\Delta\tau$, however, depend on the relative shear flexibility of the different materials and the result obtained from Eq. (2.8) has therefore to be multiplied by $n = G/G_0$.

Consider as an example the composite cross section of a highway bridge as shown in Fig. 2.4. It presents a quadrangular closed cross section with steel

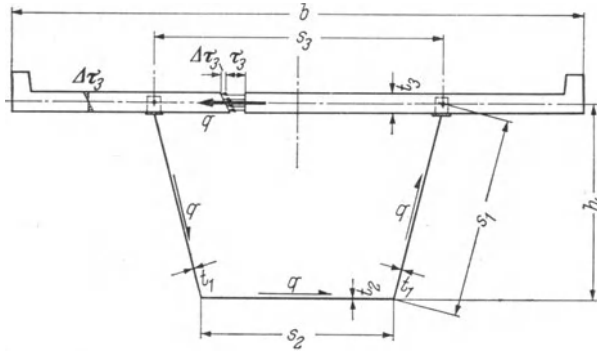


Fig. 2.4. Composite Cross Section.

plates on three sides topped by a concrete floor slab. The torsion constant of this cross section is:

$$K = \frac{h^2(s_2 + s_3)^2}{2\frac{s_1}{t_1} + \frac{s_2}{t_2} + \frac{s_3}{nt_3}},$$

where $n = G_{\text{concrete}}/G_{\text{steel}}$ (e.g. $n = 1/5$).

The shear flow in all four sides of the closed box is:

$$q = \frac{T}{h(s_2 + s_3)},$$

which immediately leads to the shear stresses in the three different sides:

$$\tau_1 = \frac{T}{t_1 h(s_2 + s_3)}, \quad \tau_2 = \frac{T}{t_2 h(s_2 + s_3)}, \quad \tau_3 = \frac{T}{t_3 h(s_2 + s_3)}.$$

The cantilever portion of the floor slab has shear stresses which are, according to Saint-Venant torsion, linearly distributed across the thickness of the slab. They have a maximum value of:

$$\Delta\tau_3 = nt_3 \frac{T}{K}$$

or, expressed relative to the shear stress τ_3 :

$$\frac{\Delta\tau_3}{\tau_3} = n \frac{2\frac{s_1}{t_1} + \frac{s_2}{t_2} + \frac{s_3}{nt_3}}{h(s_2 + s_3)} t_3^2.$$

Since the concrete slab is much thicker than the steel plates and has lower permissible stresses, the additional stresses $\Delta\tau$ might influence the design. Additionally, they usually need to be added to the contribution of shear and warping torsion (if the latter has to be considered, see Section 10.2).

e) Lattice Walls

A truss, a framework or some other lattice structure may occasionally constitute one or more wall elements of a thin-walled, closed box member. Such a framework may be replaced in the analysis by an equivalent wall element of constant thickness t^* which, as in the previous example, may be obtained from strain energy consideration.

Consider the shaft shown in Fig. 2.5a. The wall elements consist of three plates and one lattice truss system. The strain energy U of the shaft of length a is:

$$\begin{aligned} U &= \frac{1}{2} \sum_{i=1}^4 a \int_{F_i} \tau_i \gamma_i dF_i \\ &= \frac{a}{2G} \sum_{i=1}^4 \int_{F_i} \tau_i^2 dF_i. \end{aligned}$$

If each of the wall elements is of constant thickness t_i and of width b_i , then $\tau_i = q/t_i$ and $F_i = b_i t_i$ and thus:

$$U = \frac{aq^2}{2G} \sum_{i=1}^4 \frac{b_i}{t_i}.$$

The contribution of the fictitious wall element to the strain energy is therefore:

$$\Delta U = \frac{aq^2}{2G} \frac{b}{t^*}.$$

The fictitious wall thickness t^* will now be determined from the condition that the contribution ΔU has to be equal to the strain energy in the truss element of length a .

The shear flow q results in a total shear force Q in the plane of the truss of $Q = qb$.

The shear Q causes the force $D = Q/\sin \alpha$ in the diagonal of length d . Since $\sin \alpha = b/d$, it is simply $D = qd$.

Fig. 2.5b shows the upper chord separated from the adjacent wall element. The shear flow q acts along the line of separation. It is introduced by the diagonals into the gusset plates in the form of concentrated forces. These concentrated forces cause axial forces in the chords which may be assumed to vary linearly within the distance a , from zero up to the maximum value of $\Delta F = qa$, $|\Delta F_0| = |\Delta F_u| = |q|a$.

The strain energy in a chord of length l and area of cross section F subjected to the axial load P is $P^2 l / 2 E F$ and for the case where the axial force varies

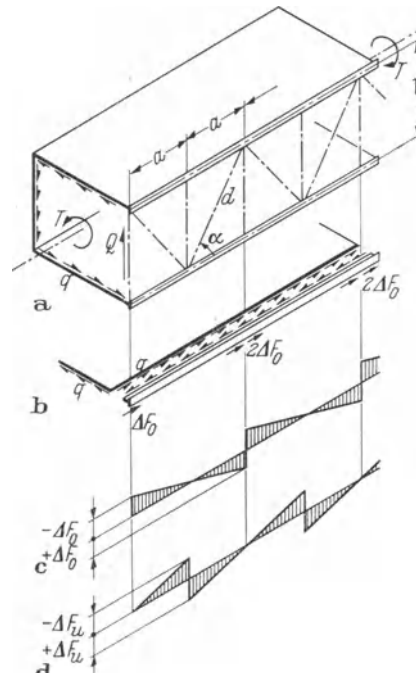


Fig. 2.5. Closed Box Member with one Wall Element in the Form of a Truss.

linearly within the distance l from zero to P , $P^2 l / 6 E F$. Using these results, the strain energy of a truss element of length a may be written down as follows:

$$\text{Contribution of the upper chord: } \frac{1}{2E} \left(\frac{qa}{F_o} \right)^2 \frac{a}{3} F_o = \frac{q^2}{2E} \frac{a^3}{3F_o}.$$

$$\text{Contribution of the diagonal: } \frac{1}{2E} \left(\frac{qd}{F_d} \right)^2 dF_d = \frac{q^2}{2E} \frac{d^3}{F_d}.$$

Contribution of the post: free of stress

$$\text{Contribution of the lower chord: } \frac{1}{2E} \left(\frac{qa}{F_u} \right)^2 \frac{a}{3} F_u = \frac{q^2}{2E} \frac{a^3}{3F_u}.$$

$$\text{Total for truss of length } a: \quad = \frac{q^2}{2E} \left(\frac{d^3}{F_d} + \frac{a^3}{3} \left(\frac{1}{F_o} + \frac{1}{F_u} \right) \right).$$

The thickness t^* of the fictitious wall element is obtained when this sum is set equal to the expression for ΔU obtained above:

$$t^* = \frac{E}{G} \frac{ab}{\frac{d^3}{F_d} + \frac{a^3}{3} \left(\frac{1}{F_o} + \frac{1}{F_u} \right)}. \quad (2.13)$$

The following remarks are made with respect to the determination of the chord cross sections F_o and F_u : The wall S adjacent to the chord G will assist in carrying the force ΔF . This may be considered by including a portion of the wall area F_S with the chord area F_G to yield the equivalent chord area F^* . An estimate of the contribution of the wall S may be obtained from a consideration of the two limiting cases presented in Fig. 2.6:

- a) The wall element which is connected to the wall S on the opposite side of the chord G has an area F which is much smaller than F_S , i.e. $F \ll F_S$.
- b) The area F of the wall element exceeds by far the area F_S , i.e. $F \gg F_S$.

If the wall S is assumed to have a rectangular cross section, then in case a the neutral axis goes through the outermost point of the core and in case b it goes through the opposite boundary of the section.

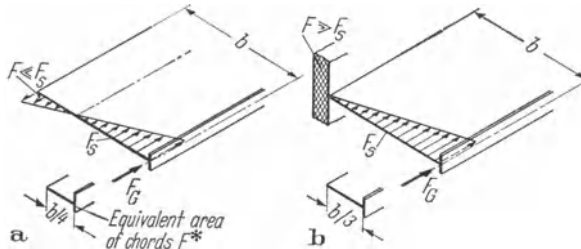


Fig. 2.6. Limiting Cases for the Equivalent Area of the Chords.

In the stress determination, the portion of the wall S which should be added to the area of the chords in the first case (a) is $F_S/4$ and in the second case (b) $F_S/3$ [see inequalities (12.18a)]. These are limiting cases and the true equivalent area of

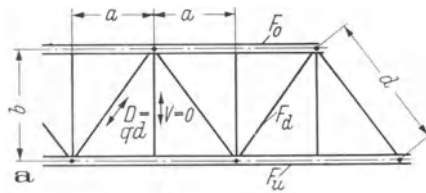
the chords is likely to be somewhere in between. Furthermore, the force F_G changes over a length which is of the order of magnitude of the width of the wall S . It is therefore possible that the classical beam theory overestimates the contribution of the wall S . Consequently, it is better to base the computation of F_o and F_u in Eq. (2.13) on the lower limiting value as sketched in Fig. 2.6a, e.g.:

$$F^* = F_G + \frac{1}{4}F_S. \quad (2.14)$$

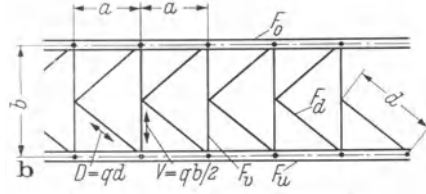
Exercise 2.1. *Lattice Walls.* Compute the fictitious wall thicknesses t^* of the lattice walls shown below.

Results to Exercise 2.1

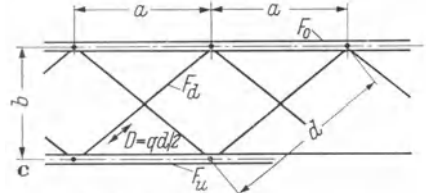
Case a):
$$t^* = \frac{E}{G} \frac{ab}{\frac{d^3}{F_d} + \frac{a^3}{3} \left(\frac{1}{F_0} + \frac{1}{F_u} \right)}$$



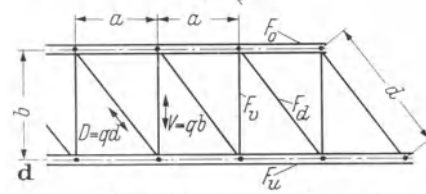
Case b):
$$t^* = \frac{E}{G} \frac{ab}{\frac{2d^3}{F_d} + \frac{b^3}{4F_v} + \frac{a^3}{12} \left(\frac{1}{F_0} + \frac{1}{F_u} \right)}$$



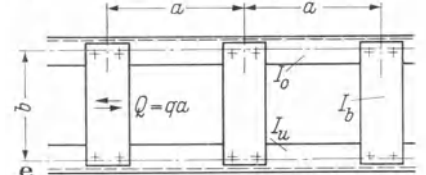
Case c):
$$t^* = \frac{E}{G} \frac{ab}{\frac{d^3}{2F_d} + \frac{a^3}{12} \left(\frac{1}{F_0} + \frac{1}{F_u} \right)}$$



Case d):
$$t^* = \frac{E}{G} \frac{ab}{\frac{d^3}{F_d} + \frac{b^3}{F_v} + \frac{a^3}{12} \left(\frac{1}{F_0} + \frac{1}{F_u} \right)}$$



Case e):
$$t^* = \frac{E}{G} \frac{1}{\frac{ab^2}{12I_b} + \frac{a^2b}{48} \left(\frac{1}{I_0} + \frac{1}{I_u} \right)}.$$



2.3 Multicellular Box Section Members

a) General Remarks

The problem is the analysis of a closed box section consisting of more than one longitudinal cell. The problem involves essentially the superposition of individual closed box member solutions.

Fig. 2.7a shows schematically a cross section consisting of n cells. Two cells at the left end are redrawn to a larger scale (Fig. 2.7c) together with a cross section through the corresponding membrane (Fig. 2.7b). The membrane analogy as stated in Section 1.1 and 2.1 may be used for this case as well. It requires in particular that all regions inside the outer periphery of the cross section are subjected to the uniformly distributed pressure p and that the hollow spaces of the different cells are covered by horizontal, plane lids.

The arrangement of the cells does not necessarily need to lead to the band-shaped cross section shown in Fig. 2.7a. Cells may be interconnected in any

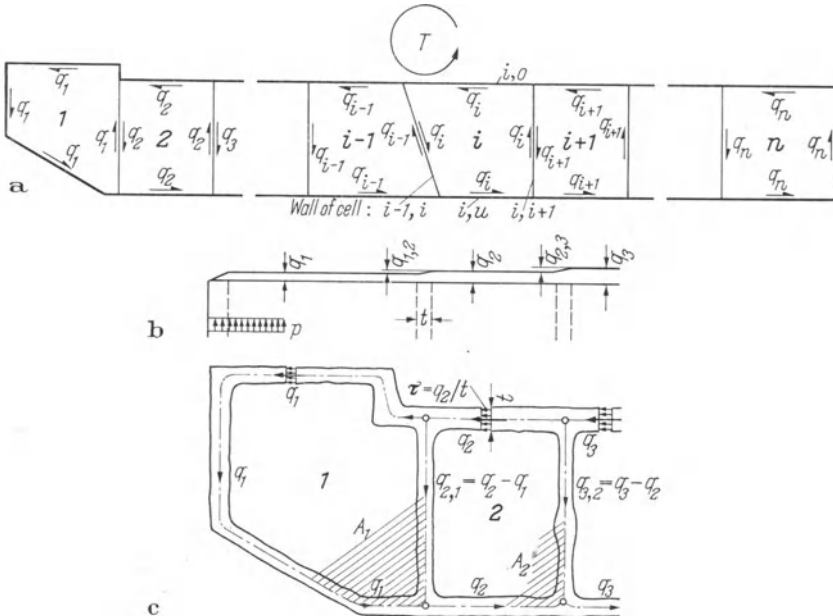


Fig. 2.7. Hollow Cross Section with n Cells.

a) Cell Configuration, b) Cross Section of the Membrane Belonging to c) Two Cells at the Left End.

manner. Fig. 2.8a shows an example of such a two-dimensional arrangement and Fig. 2.8b demonstrates how one may visualize the membrane analogy for this case

The fundamental problem is again the evaluation of the shear stresses and the torsion constant for Saint-Venant torsion. The shear stresses, however, are usually given in terms of shear flow i.e. shear stress times the wall thickness.

A possible shear flow distribution in the cross section in Fig. 2.8a is sketched in Fig. 2.8c. The problem is therefore to determine the magnitude of shear flow in each wall of the cross section.

Note that a change in the direction of a wall — even as much as 90° or more — does not constitute a new wall in the sense of the torsion theory as long as the wall does not pass an intersection with another cell. The example in Fig. 2.8 exhibits therefore 20 unknown shear flows among which some may be equal for reasons of symmetry.

This does not mean that the cross section is as many times statically indeterminate as there are unknown shear flows. A part of the unknowns may always be eliminated with the help of the “continuity conditions” at the branching points. An algorithm, however, may be developed only in relation to a specific problem.

The computational scheme should be clear and very generally valid so as to be easily adaptable for automatic computation (Table 2.2). It may again be derived with the help of the membrane analogy.

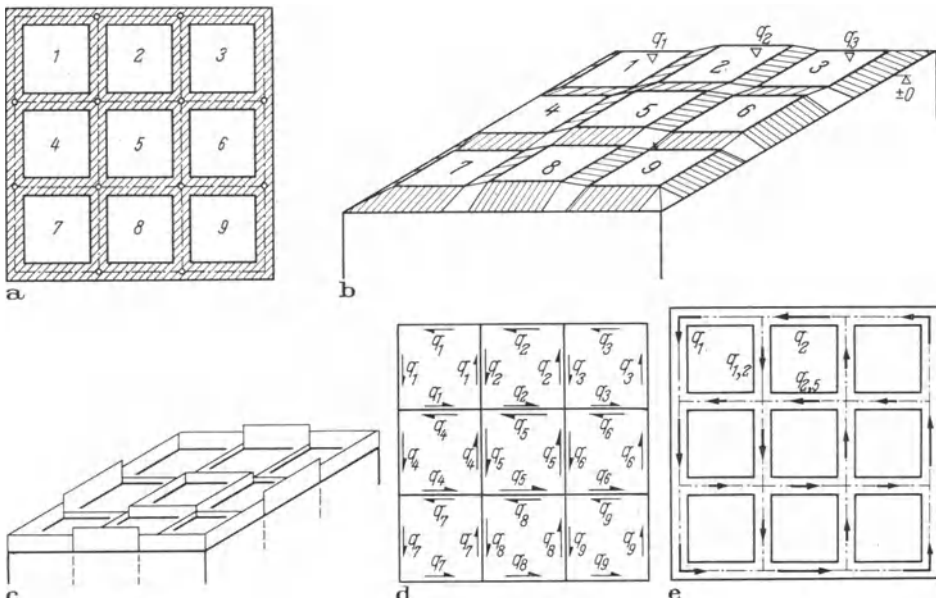


Fig. 2.8. Example of a Multicellular Cross Section.

a) Cell Configuration, b) Membrane Analogy, c) Shear Flow Distribution, d) Lid Levels Translated into Shear Flow Vectors, e) Resulting Shear Flow in Vector Presentation.

The membrane which corresponds to a multicellular, hollow cross section has as many plane lids as there are hollow spaces or cells. The shape of the membrane is completely determined, when the elevations of all lids are given.

The questions therefore are: How are the elevations of the lids computed and how do they lead to the shear flows in the walls in a systematic manner? The second question will be answered first.

b) Representation of the Resulting Shear Flows (Differences in Elevation)

It has been explained in relation to Fig. 2.1 and shown in Fig. 2.1a that the elevation of the lid corresponds to the shear flow in a monocellular cross section. The shear flow in a wall separating two cells of a multicellular cross section is equal to the difference in elevation of the lids in these two cells as can be seen from Fig. 2.8b.

One still needs a convention for the sign of the shear flow. The axes of a Cartesian coordinate system cannot be used as reference directions since a change

in the direction of a wall does not constitute a change in the shear flow direction. The only basis for the sign is the sense of rotation, e.g. the sense of rotation of the shear flow around one cell. The shear flow in a wall which separates two cells will of course have different signs depending on which cell one thinks the wall is a part of. But after this has been decided, the following statements uniquely determine the sign of the shear flow:

1. If the shear flow q_i in the wall between the cells i and k flows around the cell i in a sense which is equal to the reference sense of rotation, then the shear flow q_i is positive.
2. The reference sense of rotation is equal to the sense of rotation of a positive torsional moment acting on the cross section.
3. The shear flow q_{ik} in the wall of the cell i which is at the same time wall of the cell k is therefore computed as follows:

$$q_{ik} = q_i - q_k, \begin{cases} (i = 1, 2, \dots, n), \\ (k = \text{adjacent to cell } i), \end{cases} \quad (2.15)$$

which means in other words “elevation of reference lid (i) minus elevation of adjacent lid (k)”. If the wall of the cell i coincides with the periphery of the cross section, then cell k is missing and q_i is already equal to the resulting shear flow.

This determines both value and sign of the shear flow in the walls. A better visualization of the acting forces may be obtained by considering the superposition of shear flows around individual cells.

The elevation of each lid of the membrane corresponds to a constant shear flow in the wall of that particular cell. This shear flow is best represented in the form of a vector. If this is done for the whole cross section, then every interior wall will show two vectors. If they are superposed, they complete the vectorial picture of the shear flows, which is correct both with respect to direction and magnitude of the individual vectors.

The presentation of lid elevations in the form of constant shear flows around the corresponding cells was used in Fig. 2.7c and 2.8d. Fig. 2.8e finally shows the resulting shear flow distribution obtained from a superposition of the vectors in Fig. 2.8d.

c) Evaluation of the Shear Flows q_i (Lid Elevations)

The lid elevations q_i are determined from an equilibrium consideration of the membrane. The pressure acting on a lid is counteracted by the vertical component of the membrane forces. The condition for their equilibrium has already been utilized for the derivation of Eq. (1.5). This equation may be written for each cell as follows:

$$\oint_i \tau ds = \frac{2T}{K} A_i \quad (i = 1, 2, \dots, n). \quad (2.16)$$

T represents the torsional moment acting on the whole cross section, A_i the area enclosed by the periphery of any cell i and the left side of this equation is the contour integral of the shear stress along this line. The shear stress corresponds to

the slope of the membrane in the membrane analogy which is equal to the difference in lid elevation divided by the wall thickness, $\tau = q/t$.

If the path of integration is further divided into parts which either separate two cells or coincide with the periphery, then the contour integral may be written as a sum of the corresponding integrals.

The shear flow q_{ik} remains constant in everyone of these regions. One may therefore write for $i = 1, 2, \dots, n$ and $k = \text{cell adjacent to cell } i$:

$$\oint_i \tau ds = \oint_i \frac{q}{t} ds \\ = \sum_{\text{Cell } i} q_{ik} \int_{ik} \frac{ds}{t}$$

and according to definition (2.15)

$$= \sum_{\text{Cell } i} q_i \oint_i \frac{ds}{t} - \sum_k q_k \int_{ik} \frac{ds}{t}.$$

Since q_i is the same in all walls of the cell i (elevation of lid i) and may therefore be extracted from the sum, Eq. (2.16) becomes:

$$q_i \oint_i \frac{ds}{t} - \sum_k q_k \int_{ik} \frac{ds}{t} = \frac{2T}{K} A_i \quad (2.17)$$

($i = \text{Cell } 1, 2, \dots, n$ of the cross section)

($k = \text{Cell adjacent to cell } i$).

Expression (2.17) represents a system of n linear equations for the unknown shear flows q_i . It takes the following form when written down for the cross section sketched in Fig. 2.7

$$q_1 \oint_1 \frac{ds}{t} - q_2 \int_{1,2} \frac{ds}{t} = \frac{2T}{K} A_1, \\ -q_1 \int_{1,2} \frac{ds}{t} + q_2 \oint_2 \frac{ds}{t} - q_3 \int_{2,3} \frac{ds}{t} = \frac{2T}{K} A_2, \\ -q_2 \int_{2,3} \frac{ds}{t} + q_3 \oint_3 \frac{ds}{t} - q_4 \int_{3,4} \frac{ds}{t} = \frac{2T}{K} A_3, \\ \dots \quad \dots \quad \dots = \dots$$

The elements in this matrix are nondimensional line integrals which will be denoted by η . They are all integrals of the reciprocal value of the wall thickness along the wall center line. Only the regions of integration are different which,

however, may be directly expressed by the subscripts of the matrix elements:

$$\eta_{ik} = \int_{i,k} \frac{ds}{t} : \text{Integral along the wall separating cell } i \text{ and cell } k, \quad (2.18a)$$

$$\eta_{ii} = \oint_i \frac{ds}{t} : \text{Contour integral along the circumference of cell } i.$$

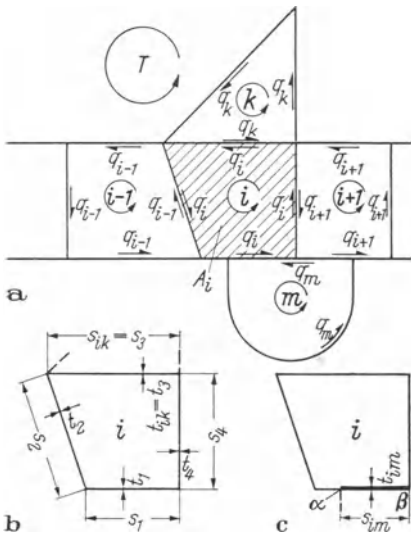


Fig. 2.9. Notation.

If the wall thickness is piecewise constant, then these matrix elements may be given in the following form for the arrangement and notation shown in Fig. 2.9a and 2.9b.

$$\eta_{ik} = \frac{s_{ik}}{t_{ik}} = \frac{s_3}{t_3}, \quad (2.18b)$$

$$\eta_{ii} = \sum_{i=1}^4 \frac{s_i}{t_i} = \frac{s_1}{t_1} + \frac{s_2}{t_2} + \frac{s_3}{t_3} + \frac{s_4}{t_4}.$$

The defining equation for the element η_{ik} (2.18a) shows that the matrix is symmetric, $\eta_{ik} = \eta_{ki}$. The arrangement of the elements in the matrix does not, however, need to be band-shaped. This is a consequence of the band-shaped arrangement of the cells in the cross section of Fig. 2.7. If cells k and m were added to

this cross section in the manner shown in Fig. 2.9a, then cell i would make the following contribution to the system of equations:

$$q_i \eta_{ii} - q_{i-1} \eta_{i-1,i} - q_k \eta_{ki} - q_{i+1} \eta_{i,i+1} - q_m \eta_{im} = \frac{2T}{K} A_i.$$

The formula for the computation of the element η_{im} will be given as another illustration for the application of Eqs. (2.18a) and (2.18b). When the notation given in Fig. 2.9c is used, these equations may be rewritten in the form:

for variable wall thickness: $\eta_{im} = \int_{\alpha}^{\beta} \frac{ds}{t(s)},$

for constant wall thickness: $\eta_{im} = \frac{s_{im}}{t_{im}}.$

The right side of the system of equations shows the torsion constant K which is not as yet determined. K is a part of the factor $2T/K$ which is the same in every equation and which may therefore temporarily be put equal to 1.

If the solution of the system with A_i on the right side only is denoted by \bar{q}_i , then the solution of the actual system is given by:

$$q_i = \bar{q}_i \frac{2T}{K}. \quad (2.19)$$

This merely determines the proportion of the lid elevation with respect to each other. It requires one more relation to evaluate their magnitudes. According to Eq. (1.2) the torsional moment is equal to twice the volume between the membrane and the plane of the cross section, thus

$$2 \sum_{i=1}^n q_i A_i = T.$$

Eq. (2.19) transforms this equation into:

$$\frac{4T}{K} \sum_{i=1}^n \bar{q}_i A_i = T,$$

from which there finally follows:

$$K = 4 \sum_{i=1}^n A_i \bar{q}_i. \quad (2.20)$$

This solves the two main problems for the multicellular, hollow cross section, (a) the evaluation of the torsion constant and (b) the determination of the shear stresses for the case of Saint-Venant torsion.

d) Computational Scheme

Table 2.2 summarizes the analysis of an arbitrary, multicellular cross section for Saint-Venant torsion.

Initially the line and contour integrals (2.18) along common walls or along the circumference of the cells are calculated. Then the areas A_i of the cells i which are enclosed by the center line of the walls are determined. This defines all of the elements in the system of equations. The integrals η represent the matrix elements and the areas A_i the “generalized displacements”.

The solutions \bar{q}_i of this system of equations are the basis to compute the torsion constant K from Eq. (2.20) and the shear flows q_i from Eq. (2.19). The superposition of q_i leads to the shear flows acting in the walls of the cross section and they again lead to the shear stresses when divided by the thickness of the walls [v. Eq. (2.1)].

Table 2.2 shows further a method to compute an upper and a lower bound for the torsion constant K without having to solve the system of equations. The derivation of this method is given in Section 2.4 b.

Table 2.2. Computational Scheme for the Determination of the Torsion Constant K and the Shear Flow q of a Multicellular Hollow Cross Section (Saint-Venant Torsion)

Notation

The cross section consists of n cells consecutively numbered from 1 to n .
 s = Peripheral length along the center line of the walls,
 $t(s) =$ Wall thickness (may vary with s). } v. Fig. 2.7

Matrix Elements

Diagonal elements: (always appear positive in the system of equations)	$\eta_{ii} = \oint_i \frac{ds}{t}$: Contour integral along the center line of the walls which enclose cell i	v. Eq. (2.18)
Off-diagonal elements: (always appear negative in the system of equations)	$\eta_{ik} = \int_{i,k} \frac{ds}{t}$: Line integral along the center line of the wall which separates cell i and cell k	
“Generalized displacements” (always positive when to the right of the = sign)	A_i : Area enclosed by the wall center line of cell i	v. Fig. (2.7)

System of Equations for the Unknowns \bar{q}_i (with the dimension of A_i)

\bar{q}_1	\bar{q}_2	\bar{q}_3	\dots	\bar{q}_n	“gen. displ.”	to the upper bound for K :
$+ \eta_{11} - \eta_{12} \dots \dots$				$= A_1$	$\rightarrow \frac{A_1^2}{\eta_{11} - \eta_{12} - \dots}$	
$- \eta_{21} + \eta_{22} - \eta_{23} \dots$				$= A_2$	$\rightarrow \frac{A_2^2}{-\eta_{21} + \eta_{22} - \eta_{23} - \dots}$	
$\dots - \eta_{32} + \eta_{33} \dots$				$= A_3$	$\rightarrow \frac{A_3^2}{\dots + \eta_{33} - \dots}$	
				... neg.		
				pos.		
				neg. $\eta_{nn} = A_n$	$\rightarrow \frac{A_n^2}{\dots + \eta_{nn}}$	
<hr/>						
to the lower bound for K :				Σ matrix elements	Σ gen. displ.	$\Sigma \frac{A_i^2}{\Sigma \text{elements in row } i}$

Upper and Lower Bounds for the Torsion Constant (v. Section 2.4 b)

in words: $4 \frac{(\Sigma \text{ gen. displ.})^2}{\Sigma \text{ matrix elements}} < K < 4 \sum_i \frac{(\text{gen. displ. } i)^2}{\Sigma \text{ elements in row } i}$,

in symbols: $4 \frac{\left(\sum_{i=1}^n A_i \right)^2}{\sum_{i=1}^n \sum_{k=1}^n \eta_{ik}} < K < 4 \sum_{i=1}^n \frac{A_i^2}{\sum_{k=1}^n \eta_{ik}}$. v. Eq. (2.26)

Torsion Constant $K = 4 \sum_{i=1}^n A_i \bar{q}_i$, (\bar{q}_i = solution to the system of equations). v. Eq. (2.20)
(precise value)

Shear Flows $q_i = \bar{q}_i \frac{2T}{K}$. (i = 1, 2, ..., n). v. Eq. (2.19)

The *sense of rotation* of the shear flow q_i around the cell i is equal to the sense of rotation of the torsional moment T (reference sense of rotation).

The *resulting shear flow* q in the whole cross section is graphically obtained by a superposition of the n shear flows q_i . This process is analytically expressed in the form

$$q_{ik} = q_i - q_k, \quad v. \text{ Eq. (2.15)}$$

where a positive sign for q_{ik} means that it flows with a positive sense of rotation around cell i .

The *shear stresses* are obtained when the shear flow is divided by the wall thickness, $\tau = q/t$.

e) Examples

As a first example, a simple, hollow cross section consisting of two cells will be analyzed. The results may still be given in an explicit manner.

The system of equations is:

$$\begin{aligned} \eta_{11}\bar{q}_1 - \eta_{12}\bar{q}_2 &= A_1, \\ -\eta_{12}\bar{q}_1 + \eta_{22}\bar{q}_2 &= A_2. \end{aligned}$$

It has the solutions:

$$\begin{aligned} \bar{q}_1 &= (A_1\eta_{22} + A_2\eta_{12}) / (\eta_{11}\eta_{22} - \eta_{12}^2), \\ \bar{q}_2 &= (A_2\eta_{11} + A_1\eta_{12}) / (\eta_{11}\eta_{22} - \eta_{12}^2), \end{aligned}$$

which immediately lead to the torsion constant K [Eq. (2.20)] and to the resulting shear flows [Eqs. (2.19) and (2.15)]:

$$\begin{aligned} K &= 4 \frac{A_1^2\eta_{22} + 2A_1A_2\eta_{12} + A_2^2\eta_{11}}{\eta_{11}\eta_{22} - \eta_{12}^2}, \\ q_1 &= \frac{T}{2} \frac{A_1\eta_{22} + A_2\eta_{12}}{A_1^2\eta_{22} + 2A_1A_2\eta_{12} + A_2^2\eta_{11}}, \\ q_2 &= \frac{T}{2} \frac{A_2\eta_{11} + A_1\eta_{12}}{A_1^2\eta_{22} + 2A_1A_2\eta_{12} + A_2^2\eta_{11}}, \\ q_{12} &= \frac{T}{2} \frac{A_1(\eta_{22} - \eta_{12}) - A_2(\eta_{11} - \eta_{12})}{A_1^2\eta_{22} + 2A_1A_2\eta_{12} + A_2^2\eta_{11}}. \end{aligned} \quad (2.21)$$

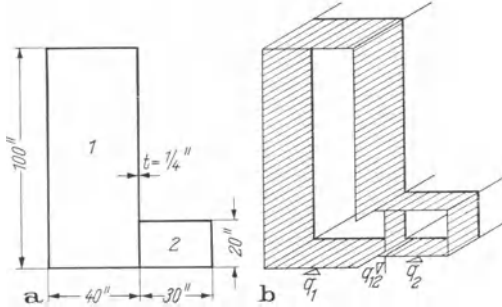


Fig. 2.10. Example of a Bicellular Cross Section.

The numerical results for the bicellular cross section shown in Fig. 2.10a are as follows:

$$\begin{aligned} \eta_{11} &= \frac{1}{1/4} (40 + 100 + 40 + 100) = 1120, \\ \eta_{12} &= \frac{1}{1/4} 20 = 80, \\ \eta_{22} &= \frac{1}{1/4} (30 + 20 + 30 + 20) = 400, \\ A_1 &= 40 \cdot 100 = 4000 \text{ in}^2, \\ A_2 &= 30 \cdot 20 = 600 \text{ in}^2. \end{aligned} \quad (2.22 \text{ a})$$

and introduced into formula (2.21):

$$\begin{aligned}
 K &= 6,51 \cdot 10^4, & [\text{in}^4], \\
 q_1 &= 1,15 \cdot 10^{-4} T^{(\text{in}\cdot\text{lb})}, & \left[\frac{\text{lb}}{\text{in}} \right], \\
 q_2 &= 0,69 \cdot 10^{-4} T^{(\text{in}\cdot\text{lb})}, & \left[\frac{\text{lb}}{\text{in}} \right], \\
 q_{12} &= 0,46 \cdot 10^{-4} T^{(\text{in}\cdot\text{lb})}, & \left[\frac{\text{lb}}{\text{in}} \right].
 \end{aligned} \tag{2.22 b}$$

The distribution of the shear flows is plotted in Fig. 2.10b.

The second example deals with the multicellular cross section shown in Fig. 2.8a. If the symmetries and the regularities in the dimensions of the cross section are ignored, the following system of equations expresses the configuration of the cells with respect to each other:

\bar{q}_1	\bar{q}_2	\bar{q}_3	\bar{q}_4	\bar{q}_5	\bar{q}_6	\bar{q}_7	\bar{q}_8	\bar{q}_9	
$+\eta_{11}$	$-\eta_{12}$		$-\eta_{14}$						$= A_1$
$-\eta_{21}$	$+\eta_{22}$	$-\eta_{23}$		$-\eta_{25}$					$= A_2$
	$-\eta_{32}$	$+\eta_{33}$			$-\eta_{36}$				$= A_3$
$-\eta_{41}$		$+\eta_{44}$	$-\eta_{45}$		$-\eta_{47}$				$= A_4$
$-\eta_{52}$		$-\eta_{54}$	$+\eta_{55}$	$-\eta_{56}$		$-\eta_{58}$			$= A_5$
	$-\eta_{63}$		$-\eta_{65}$	$+\eta_{66}$			$-\eta_{69}$		$= A_6$
		$-\eta_{74}$			$+\eta_{77}$	$-\eta_{78}$			$= A_7$
			$-\eta_{85}$		$-\eta_{87}$	$+\eta_{88}$	$-\eta_{89}$		$= A_8$
				$-\eta_{96}$		$-\eta_{98}$	$+\eta_{99}$		$= A_9$

In order to present numerical results, it is assumed that all cells are square, have equal lateral lengths a and equal wall thicknesses t . All diagonal elements of the matrix are therefore $\eta_{ii} = 4a/t$, the off-diagonal elements $\eta_{ik} = a/t$ and the “generalized displacements” $A_i = a^2$. Making further use of the two-fold symmetry of the cross section, the reduced system of equations becomes:

\bar{q}_1	\bar{q}_2	\bar{q}_5	
4	-2		$= at$
-2	4	-1	$= at$
	-4	4	$= at$

which leads to:

$$\left. \begin{array}{l} \bar{q}_1 = \frac{11}{16} a t \\ \bar{q}_2 = \frac{14}{16} a t \\ \bar{q}_5 = \frac{18}{16} a t \end{array} \right\} (2.20) \rightarrow K = 4a^3 t \frac{118}{16}, \quad (2.19) \rightarrow \left\{ \begin{array}{l} q_1 = \frac{T}{2a^2} \frac{11}{118}, \\ q_2 = \frac{T}{2a^2} \frac{14}{118}, \\ q_5 = \frac{T}{2a^2} \frac{18}{118}, \end{array} \right. \quad (2.23)$$

and according to (2.15): $\left\{ \begin{array}{l} q_{12} = -\frac{T}{2a^2} \frac{3}{118}, \\ q_{25} = -\frac{T}{2a^2} \frac{4}{118}. \end{array} \right.$

(The sketches in Fig. 2.8 were drawn on the basis of these results.)

2.4 Special Cases and Limiting Values

a) Separated Cells

Completely separated cells which are constructed and connected so as to be part of a multicellular cross section constitute a special case. This may occur in bridges whose box-type main girders are transversely connected by rigid floor beams in order to maintain the shape of the entire cross section. There are no walls which are common to two cells. The line integrals η_{ik} vanish therefore leaving only the diagonal elements η_{ii} in the matrix. The equations become independent of each other and the solutions can be given immediately:

$$\bar{q}_i = \frac{A_i}{\eta_{ii}} \quad (i = 1, 2, \dots, n).$$

According to Eq. (2.20) the torsion constant is:

$$K = 4 \sum_{i=1}^n \frac{A_i^2}{\eta_{ii}} \quad (2.24a)$$

or according to the definition (2.18a)

$$K = \sum_{i=1}^n \frac{4A_i^2}{\oint_i \frac{ds}{t}}, \quad (2.24b)$$

which by means of formula (2.5) states that:

$$K = \sum_{i=1}^n K_i, \quad (2.24c)$$

i.e. the torsion constant of the entire cross section is equal to the sum of the torsion constants of the separated hollow cross sections.

Eq. (2.19) leads to the shear flow in the walls of cell i :

$$q_i = \frac{A_i}{\eta_{ii}} \frac{2T}{K} \quad (i = 1, 2, \dots, n), \quad (2.25a)$$

which may be rewritten in the form:

$$q_i = \frac{\frac{4A_i^2}{\oint \frac{ds}{t}}}{2A_i K} \frac{T}{2A_i K}, \quad (2.25b)$$

which simplifies by means of formula (2.5) to:

$$q_i = \frac{K_i}{K} \frac{T}{2A_i} \quad (i = 1, 2, \dots, n). \quad (2.25c)$$

b) Limiting Values for the Torsion Constant¹

One may think of different reasons for the off-diagonal elements η_{ik} to vanish or to become negligible. One reason, the disappearance of the region of integration due to the lack of common walls, has already been given above. The elements η_{ik} may, on the other hand, become negligible when the corresponding common walls are supposed to have a shear modulus G which exceeds by far the shear modulus G_0 of the remaining walls [Eq. (2.12)]. This interpretation shows that the computation of the torsion constant assuming common walls to have no shear flexibility will invariably overestimate and therefore provide an upper bound for the torsion constant.

Eq. (2.24b) may be used to evaluate this upper bound. The contour integrals, however, have to be reduced by the contribution of the common walls. This may be accomplished by subtracting the integrals η_{ik} of the walls common to cell i and k from the complete contour integral η_{ii} of cell i . This is exactly the sum of the elements in row i of the matrix. The upper bound for the torsion constant of a multicellular cross section may therefore be derived from the system of equations for the shear flow distribution. The quotient, square of the "generalized displacement" A_i divided by the sum of all elements in row i of the matrix, is calculated for each equation. The upper bound for K is now equal to four times the sum of these quotients. The computational scheme is given in Table 2.2.

A lower bound for the torsion constant is readily determined. The outer periphery of a multicellular cross section is treated as the wall of a single cell. The partitioning into several cells is neglected. Formula (2.5) for a monocellular cross section may be applied with A the area of the entire cross section, thus:

$$A = \sum_{i=1}^n A_i.$$

The contour integral along the periphery of the cross section may either be newly evaluated or it may again be derived from the matrix defining the shear

¹ The possibility of bracketing is mentioned in P. KUHN: Stresses in Aircraft and Shell Structures, New York: McGraw-Hill 1956.

flow distribution in the multicellular cross section. It is equal to this sum of all elements in this matrix.

$$\oint_{\text{(total cross section)}} \frac{ds}{t} = \sum_{i=1}^n \sum_{k=1}^n \eta_{ik}.$$

Table 2.2 provides a scheme for the computation of the lower bound.

It is thus possible to give an upper and a lower bound for the torsion constant K without having to solve first the system of equations for the shear flow distribution.

$$4 \frac{\left(\sum_{i=1}^n A_i \right)^2}{\sum_{i=1}^n \sum_{k=1}^n \eta_{ik}} < K < 4 \sum_{i=1}^n \frac{A_i^2}{\sum_{k=1}^n \eta_{ik}}. \quad (2.26)$$

The bracketing of the torsion constant K will be demonstrated for the cross section shown in Fig. 2.10. The numerical values for the elements of the system of equations (2.22a) are used.

$$\begin{array}{ccc} \bar{q}_1 & \bar{q}_2 & A (\text{in}^2) \\ \hline 1120 & - 80 = 4000 & \left| \frac{4000^2}{1120 - 80} = 1,538 \cdot 10^4 \right. \\ - 80 & 400 = \frac{600}{\hline} & \left| \frac{600^2}{400 - 80} = 0,113 \cdot 10^4 \right. \\ \hline 1360 & 4600 & 1,651 \cdot 10^4 \\ \hline \end{array}$$

$$4 \cdot \frac{4600^2}{1360} < K < 4 \cdot 1,651 \cdot 10^4,$$

$$6,22 \cdot 10^4 \text{ in}^4 < K < 6,60 \cdot 10^4 \text{ in}^4.$$

The exact solution of the system of equations results in a value $K = 6,51 \cdot 10^4 \text{ in}^4$ [solutions (2.22b)].

Exercise 2.2. Bicellular Hollow Cross Section. To get an idea on how narrow the inequalities (2.26) set the limits for the torsion constant K , the hollow cross section consisting of a square and a rectangular cell of variable shape shall be investigated.

a) The cross section with constant wall thickness t consists of two quadratic cells with lateral lengths a and $\varkappa a$. A variation of the parameter \varkappa from zero to one covers all possible shapes of this bicellular, hollow cross section.

Results:

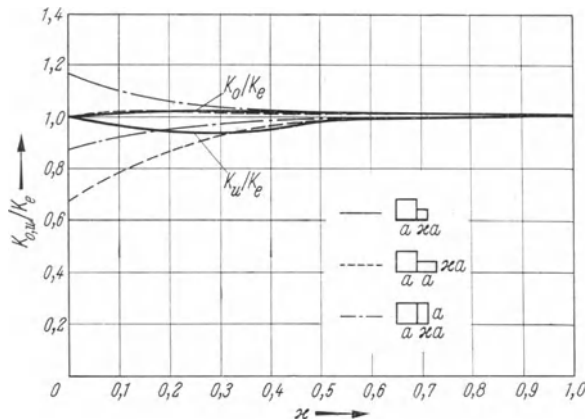
$$\text{Upper bound for } K: \quad K_o = \frac{1 + \frac{4}{3}\varkappa^3 - \frac{1}{3}\varkappa^4}{1 - \frac{1}{4}\varkappa} a^3 t,$$

$$\text{Exact value for } K: \quad K_e = \frac{1 + \frac{1}{2}\varkappa^2 + \varkappa^3}{1 - \frac{1}{16}\varkappa} a^3 t,$$

$$\text{Lower bound for } K: \quad K_u = \frac{1 + 2\varkappa^2 + \varkappa^4}{1 + \frac{1}{2}\varkappa} a^3 t.$$

b) One cell is a rectangle with the lateral lengths a and $\varkappa a$. Calculate the ratios K_o/K_e and K_u/K_e as functions of the parameter \varkappa .

The results from part a) and part b) are summarized in the following figure:



Results to Exercise 2.2: Upper and Lower Bound of the Torsion Constant With Respect to the Exact Value, K_o/K_e and K_u/K_e , for a Cross Section with Two Rectangular Cells of Different Size and Shape.

Exercise 2.3. Several Cells in a One-Dimensional Configuration. N quadratic cells with lateral length a and wall thickness t are lined up in order to form a rectangular cross section of length Na and width a .

Compute for a finite number of cells N the exact value K_e for the torsion constant together with its upper and lower bound K_o and K_u and present them as ratios K_u/K_e und K_o/K_e . For a large number of cells N give at least the ratio between the upper and lower bound K_u/K_o .

The results are presented in the table below:

Number of Cells N	$\frac{K_u}{K_e}$	$\frac{K_o}{K_e}$
2	1,00	1,00
3	0,988	1,021
4	0,975	1,015
5	0,978	1,014
		$\frac{K_u}{K_o}$
10		0,97
100		0,99
N		$\frac{1}{1 + \frac{N-2}{3N^2}}$

c) Several Cells in Two-Dimensional Configuration

The previous examples show that the inequality (2.26) sets surprisingly close limits for the torsion constant K when the cells are lined up in one direction only. The upper bound, however, may present a poor approximation for K whenever a multicellular cross section extends in different directions. It even becomes in-

finite when at least one cell is completely enclosed by neighbouring cells. Such cells correspond to rows in the matrix whose sum of the elements is zero. According to inequality (2.26) this sum is the denominator of a fraction.

In order to avoid this fact, remember again the considerations which led to the formula for the upper bound for K . All interior walls were considered to be without flexibility. These walls are pointed out in the cross section shown in Fig. 2.11 a. Cell No. 5 is completely enclosed by infinitely rigid walls thus leading to $K_0 = \infty$. The most obvious correction of this situation is shown in Fig. 2.11 b. The infinite torsional rigidity of an interior cell is destroyed if at least one of its walls remains flexible. The assumption shown in Fig. 2.11 c even preserves the symmetries of the original cross section.

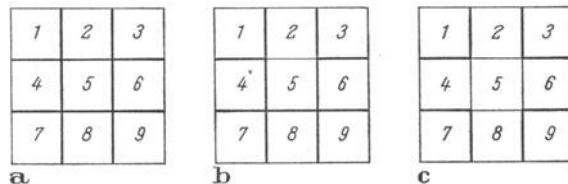


Fig. 2.11. Improvement of the Upper Bound for K for a Two-Dimensional Configuration of the Cells.

The resulting equations are no longer independent but as many matrix elements become zero as there are assumed to be rigid walls.

2.5 Cells Connected by a Common Base Cell

a) Introduction

Frequently small cells of arbitrary shape and size have walls in common with a large cell but not with each other. The large cell is designated as the zero cell,

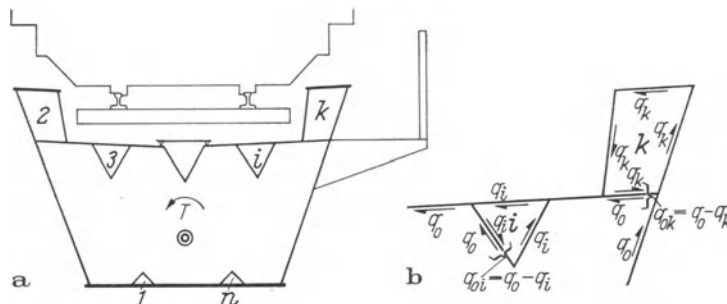


Fig. 2.12. Multicellular, Hollow Cross Section Consisting of n Separated Cells which are Connected by a Common Base Cell.

Fig. 2.12a¹. The torsion constant and the shear flows for this special case of a multicellular, hollow cross section may be derived in an explicit form.

¹ This cross section is taken from the following paper: ZUCKER, O.: Bau der Eisenbahnbrücke über die Autobahn bei Wuppertal-Ost. Stahlbau 29 (1960) 344.

According to the methods applied in Section 2.4, the cross section is divided up into cells which are joined together but do not enclose each other. The base cell is designated by the number 0 and the others are consecutively numbered from 1 to n . These $n + 1$ cells present an equal number of unknown shear flows (lid elevations in the membrane) which by superposition lead to the resulting shear flow distribution. The shear flow q_0 is already equal to the resulting shear flow in those portions of the walls of cell 0 which are not common to any other cell. The resulting shear flow in the common parts of the wall is obtained by superposition. This is demonstrated for a small part of the cross section shown in Fig. 2.12a in Fig. 2.12 b.

The resulting shear flows for this special case of a multicellular hollow cross section may be divided up into the following three groups:

q_0 , in the wall belonging entirely to cell 0;

q_i , in the wall belonging entirely to cell i ($i = 1, 2, \dots, n$);

q_{0i} , in the wall common to cell 0 and cell i ($i = 1, 2, \dots, n$).

The conditions for a “common wall” may be derived from the statement that the individual cells have to be joined together and thus do not enclose each other. In order to clarify this statement, the walls defining the area of the cells (generalized displacements) and entering into the computation of the different matrix elements are separately sketched in Fig. 2.13. For the case of constant wall thickness, values for the elements η_{0i} and η_{ii} may be read directly from this figure.

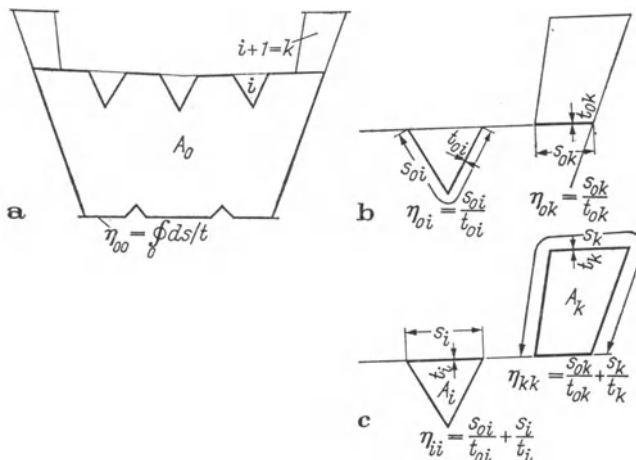


Fig. 2.13. Computation of the Elements η_{00} , η_{0i} , η_{ii} , A_0 and A_i .

b) Analysis

The peculiarity of this cross section in which independent cells are connected by a common base cell is reflected in the system of equations for the shear flow distribution. This system takes the following form:

\bar{q}_0	\bar{q}_1	\bar{q}_2	q_i	\bar{q}_n	
η_{00}	$-\eta_{01}$	$-\eta_{02}$	\dots	$-\eta_{0i}$	\dots
$-\eta_{10}$	η_{11}				$= A_1$
$-\eta_{20}$		η_{22}			$= A_2$
\dots			\dots		$= \dots$
$-\eta_{i0}$			η_{ii}		$= A_i$
\dots				\dots	$= \dots$
$-\eta_{n0}$				η_{nn}	$= A_n$

All equations except the first may be written in the following general form:

$$-\eta_{i0}\bar{q}_0 + \eta_{ii}\bar{q}_i = A_i \quad (i = 1, 2, \dots, n),$$

thus:
$$\bar{q}_i = \frac{A_i}{\eta_{ii}} + \frac{\eta_{i0}}{\eta_{ii}}\bar{q}_0 \quad (i = 1, 2, \dots, n). \quad (2.27a)$$

If these equations (2.27a) are introduced into the first equation of system (2.27) considering the symmetry of the matrix elements, one obtains:

$$\bar{q}_0\eta_{00} - \sum_{i=1}^n \eta_{0i} \left(\frac{A_i}{\eta_{ii}} + \frac{\eta_{i0}}{\eta_{ii}}\bar{q}_0 \right) = A_0,$$

or
$$\bar{q}_0 \left(\eta_{00} - \sum_{i=1}^n \frac{\eta_{0i}^2}{\eta_{ii}} \right) = A_0 + \sum_{i=1}^n A_i \frac{\eta_{i0}}{\eta_{ii}}. \quad (2.27b)$$

With the substitution

$$\begin{aligned} A &= A_0 + \sum_{i=1}^n A_i \frac{\eta_{i0}}{\eta_{ii}}, \\ B &= \eta_{00} - \sum_{i=1}^n \frac{\eta_{0i}^2}{\eta_{ii}}, \\ C &= \sum_{i=1}^n \frac{A_i^2}{\eta_{ii}}, \end{aligned} \quad (2.28)$$

there follows from Eq. (2.27b):

$$\bar{q}_0 = \frac{A}{B}$$

and from Eqs. (2.27a)

$$\bar{q}_i = \frac{A_i}{\eta_{ii}} + \frac{\eta_{i0}}{\eta_{ii}} \frac{A}{B} \quad (i = 1, 2, \dots, n).$$

If these values are introduced into the equation for the torsion constant, Eq. (2.20), one finally arrives at the following expression:

$$\begin{aligned}
 K &= 4 \left[A_0 \bar{q}_0 + \sum_{i=1}^n A_i \bar{q}_i \right], \\
 &= 4 \left[A_0 \frac{A}{B} + \sum_{i=1}^n \frac{A_i^2}{\eta_{ii}} + \frac{A}{B} \sum_{i=1}^n A_i \frac{\eta_{0i}}{\eta_{ii}} \right], \\
 &= 4 \left[A_0 \frac{A}{B} + C + \frac{A}{B} (A - A_0) \right], \\
 K &= 4 \frac{A^2 + BC}{B}.
 \end{aligned} \tag{2.29}$$

The torsion constant K determines the values of the resulting shear flows according to Eq. (2.19).

$$q_0 = \frac{2T}{K} \bar{q}_0 = \frac{T}{2} \frac{A}{A^2 + BC}, \tag{2.30}$$

$$q_i = \frac{2T}{K} \bar{q}_i = \frac{T}{2} \frac{\eta_{0i} A + A_i B}{\eta_{ii} (A^2 + BC)} \quad (i = 1, 2, \dots, n), \tag{2.31 a}$$

$$q_{0i} = q_0 - q_i = \frac{T}{2} \frac{(\eta_{ii} - \eta_{0i}) A - A_i B}{\eta_{ii} (A^2 + BC)} \quad (i = 1, 2, \dots, n). \tag{2.32 a}$$

It is sometimes more appropriate to express the two groups of shear flows q_i and q_{0i} , Eqs. (2.31 a) and (2.32 a), in terms of the shear flow q_0 in the walls of the base cell:

$$q_i = q_0 \left(\frac{\eta_{0i}}{\eta_{ii}} + \frac{A_i}{\eta_{ii}} \frac{B}{A} \right) \quad (i = 1, 2, \dots, n), \tag{2.31 b}$$

$$q_{0i} = q_0 \left(\frac{\eta_{ii} - \eta_{0i}}{\eta_{ii}} - \frac{A_i}{\eta_{ii}} \frac{B}{A} \right) \quad (i = 1, 2, \dots, n). \tag{2.32 b}$$

The sign of the shear flows q_0 and q_i depends only on the sign of the torsional moment T . Positive shear flows around the corresponding cell have the same sense of rotation as a positive torsional moment on the cross section. Positive shear flows q_{0i} act in the direction of a positive q_0 .

This completes the solution of the torsion problem for this special case. The torsion constant as well as the shear flows are presented explicitly in Eqs. (2.29) to (2.32).

c) Interpretation of the Results

Formulas (2.31 b) and (2.32 b) indicate that both q_i and q_{0i} may be considered to be the superposition of two shear flows since each is given by a sum of two elements. It will be shown below that the first element in each case represents the part of q_0 flowing through the corresponding wall of cell i when this cell itself carries nothing of the torsional moment T while the second element is the correction necessary to make the cell a part of the entire cross section.

Consider the portion of the wall which includes cell i as shown in Fig. 2.14. The shear flow q_0 is branched into the parts q_{0i} and q_i in the walls of cell i . These parts have to satisfy the equilibrium condition

$$q_0 = q_{0i} + q_i$$

and the compatibility condition which calls for equal¹ shear deformations of the walls s_{0i} and s_i :

$$\int_{s_{0i}} \gamma \, ds = \int_{s_i} \gamma \, ds.$$

Since $\gamma = \frac{q}{tG}$, this condition becomes:

$$q_{0i} \int_{s_{0i}} \frac{ds}{t} = q_i \int_{s_i} \frac{ds}{t}.$$

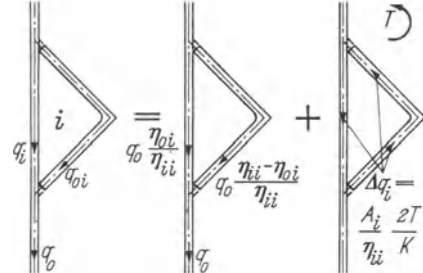


Fig. 2.14. Interpretation of Formulas (2.31 b) and (2.32 b).

According to the definition (2.18a) these two integrals are designated by η_{0i} and $\eta_{ii} - \eta_{0i}$ respectively, thus leading to the following compatibility condition:

$$q_{0i} \eta_{0i} = q_i (\eta_{ii} - \eta_{0i}).$$

This relation together with the equilibrium condition divide the shear flow q_0 into the following two parts:

$$\begin{aligned} q_i &= \frac{\eta_{0i}}{\eta_{ii}} q_0 && (i = 1, 2, \dots, n), \\ q_{0i} &= \frac{\eta_{ii} - \eta_{0i}}{\eta_{ii}} q_0 && (i = 1, 2, \dots, n), \end{aligned} \quad (2.33)$$

which are in fact the first elements in the sums of expressions (2.31 b) and (2.32 b).

The correction term shall now be determined which introduces the fact that the cell i undergoes the same rotation as the entire cross section.

The second element in the sums of expressions (2.31 b) and (2.32 b) may be transformed in the following way by means of Eqs. (2.30) and (2.29):

$$\begin{aligned} q_0 \frac{A_i}{\eta_{ii}} \frac{B}{A} &= \frac{T}{2} \frac{A}{A^2 + BC} \frac{A_i}{\eta_{ii}} \frac{B}{A} && (i = 1, 2, \dots, n), \\ &= 2T \frac{B}{4(A^2 + BC)} \frac{A_i}{\eta_{ii}} && (i = 1, 2, \dots, n), \\ &= \frac{A_i 2T}{\eta_{ii} K} && (i = 1, 2, \dots, n), \end{aligned}$$

This correction to be respectively added to and subtracted from q_i and q_{0i} in Eq. (2.33) would be the shear flow acting in the walls of cell i if this cell rotated independently by the same amount as the entire cross section [v. Eq. (2.25a)].

¹ Effectively a result of the assumption that $A_i = 0$ prior to making the correction.

d) Special Cases

The n cells which are attached to a common base cell are quite often completely equivalent (Fig. 2.15). Formulas (2.29) to (2.32) may be simplified for this special case. If the common base cell is denoted by the number 0 and the n equivalent cells by the number 1, then the substitutions (2.28) become:

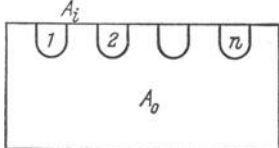


Fig. 2.15. n Equivalent Cells
Added to One Common Base Cell.

$$A = A_0 + n A_1 \frac{\eta_{01}}{\eta_{11}},$$

$$B = \eta_{00} - n \frac{\eta_{01}^2}{\eta_{11}},$$

$$C = n \frac{A_1^2}{\eta_{11}}.$$

These expressions are now simple enough to permit replacement of A , B and C in Eqs. (2.29) to (2.32), whence

$$\begin{aligned} K &= 4 \frac{A_0^2 \eta_{11} + 2n A_0 A_1 \eta_{01} + n A_1^2 \eta_{00}}{\eta_{00} \eta_{11} - n \eta_{10}^2}, \\ q_0 &= \frac{T}{2} \frac{A_0 \eta_{11} + n A_1 \eta_{01}}{A_0^2 \eta_{11} + 2n A_0 A_1 \eta_{01} + n A_1^2 \eta_{00}}, \\ q_1 &= \frac{T}{2} \frac{A_0 \eta_{01} + A_1 \eta_{00}}{A_0^2 \eta_{11} + 2n A_0 A_1 \eta_{01} + n A_1^2 \eta_{00}}, \\ q_{01} &= \frac{T}{2} \frac{A_0(\eta_{11} - \eta_{01}) - A_1(\eta_{00} - n \eta_{01})}{A_0^2 \eta_{11} + 2n A_0 A_1 \eta_{01} + n A_1^2 \eta_{00}}. \end{aligned} \quad (2.34)$$

The coefficients η_{00} , η_{01} , η_{11} , A_0 and A_1 may be read from Fig. 2.13 in which i and k are thought to be replaced by 1. For $n = 1$, formulas (2.34) have to become identical to those given for a bicellular cross section, Eqs. (2.21).

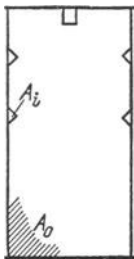


Fig. 2.16. Base Cell With Arbitrary
but Small Secondary Cells.

The expressions given above are exact within the framework of thin wall member theory for the analysis of multicellular hollow cross sections. If, however, in another special case the areas A_i enclosed by the secondary cells are much smaller than the area A_0 of the base cell (Fig. 2.16), then a simplification of the given relations is justified.

The smaller the area A_i is to the area A_0 , the smaller is the contribution of the secondary cells in carrying the torsional moment. In the limit, the wall branches in the region of the attached cell, but the enclosed area A_i vanishes.

An approximation for the torsion constant K can thus be obtained if in Eq. (2.29) [and Eqs. (2.28)] all terms are neglected which have A_i as factor. This leads to:

$$K = \frac{4 A_0^2}{\eta_{00} - \sum_{i=1}^n \frac{\eta_{0i}^2}{\eta_{ii}}}.$$

A comparison of this expression with Bredt's formula (2.5) shows that only the evaluation of the integral in the region of the attached cell requires a change. Based on the notation explained in Fig. 2.17, the integration across the branched part of the wall should be performed as follows:

$$\begin{aligned} \left[\int \frac{ds}{t} - \frac{\eta_{0i}^2}{\eta_{ii}} s_\beta \right] s_\alpha &= \frac{s_{0i}}{t_{0i}} - \frac{\left(\frac{s_{0i}}{t_{0i}} \right)^2}{\frac{s_{0i}}{t_{0i}} + \frac{s_i}{t_i}}, \\ &= \frac{s_i}{t_i + \frac{s_i t_{0i}}{s_{0i}}}, \\ &= \frac{s_i}{t^*}. \end{aligned}$$

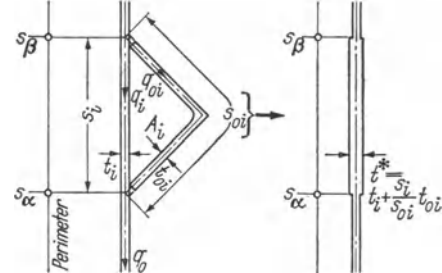


Fig. 2.17. Equivalent Wall Thickness t^* for Branched Parts of the Wall.

The introduction of a fictitious wall thickness

$$t^* = t_i + \frac{s_i}{s_{0i}} t_{0i} \quad (2.35)$$

makes it possible to compute the torsion constant as if one dealt with a simple monocellular cross section.

According to expression (2.2) the shear flow q_0 in the base cell is:

$$q_0 = \frac{T}{2A_0}. \quad (2.36a)$$

According to Eqs. (2.33) it is divided into two parts which, with the notation of Fig. 2.17, are as follows:

$$q_i = \frac{q_0}{1 + \frac{s_i t_{0i}}{s_{0i} t_i}}, \quad (2.36b)$$

$$q_{0i} = \frac{q_0}{1 + \frac{s_{0i} t_i}{s_i t_{0i}}}. \quad (2.36c)$$

The suppression of the areas A_i as opposed to A_0 , which led to the simple formulas (2.35) and (2.36), has a smaller influence on the computation of the torsion constant and the shear flow q_0 than it has on the branch flows q_i and q_{0i} . A correction may readily be evaluated.

The rotation of cell i together with the entire cross section causes a correction shear flow Δq_i which is restricted to the walls enclosing cell i . This correction may, according to the considerations made in Section 2.5c (sketch to the right of Fig. 2.14), be given by the formula:

$$|\Delta q_i| = \frac{A_i}{\eta_{ii}} \frac{2T}{K} \quad (2.37a)$$

which, with the notation of Fig. 2.17, may be rewritten as:

$$|\Delta q_i| = \frac{A_i}{\frac{s_{0i}}{t_{0i}} + \frac{s_i}{t_i}} \frac{2T}{K}. \quad (2.37b)$$

This local shear flow q_i flows around cell i in the same sense as q_0 flows around the base cell.

Exercise 2.4. *Several Cells in Two-Dimensional Configuration.* Calculate the torsion constant K and the maximum shear flow q_{\max} in the following quadratic, multicellular, hollow cross sections with lateral length a and constant wall thickness t :

Number of cells:	4	Length of one division:	$a/2$
	9		$a/3$
	16		$a/4$

Results:

Remarks. Procedures for the approximate torsion analysis of multicellular hollow cross sections are presented above. It turns out that the method which yields a lower bound for the torsion constant by neglecting the interior walls is normally very appropriate. The table below suggests the accuracy which might be expected for different cell configurations. The torsion constant K and the maximum shear flow q_{\max} are tabulated for the two-dimensional arrangement of 1, 4, 9 and 16 square cells. They have constant wall thicknesses t and are arranged in order so as to fill a square cross-section of overall breadth a . All four cases are identical with respect to the lower bound approximation. The observed deviations from this approximation, however, are surprisingly small if the crudeness of the procedure is kept in mind.

Cross-section	K	q_{\max}
	$1,00a^3t$	$1,00 \frac{T}{2a^2}$
	$1,00a^3t$	$1,00 \frac{T}{2a^2}$
	$1,09a^3t$	$1,068 \frac{T}{2a^2}$
	$1,21a^3t$	$0,964 \frac{T}{2a^2}$

The torsion constant K and the maximum shear flow q_{\max} are tabulated for the two-dimensional arrangement of 1, 4, 9 and 16 square cells. They have constant wall thicknesses t and are arranged in order so as to fill a square cross-section of overall breadth a . All four cases are identical with respect to the lower bound approximation. The observed deviations from this approximation, however, are surprisingly small if the crudeness of the procedure is kept in mind.

2.6 Shear Stresses Caused by a Resultant Shearing Force Acting on a Closed, Hollow Cross Section

a) Problem

Although the essential purpose of this book is the torsion analysis of structural members, flexural stresses constitute a related problem that should be considered.

One reason for this is the close relationship between the computational procedures for the evaluation of the shear flows caused by a torsional moment for either Saint-Venant torsion or for warping torsion. A second reason is the fact that behavior under external loads cannot be separated into a torsion part and a flexural part without knowing the position of the shear center.

The evaluation of the shear flows in thin-walled, hollow cross sections faces the difficulty that no initial value q_1 is known to begin with. It will be shown later,

Eq. (5.17), that this initial value q_1 should serve as a constant of integration for the calculation of the shear flow distribution.

An initial value of $q_1 = 0$ may be given for open profiles due to the absence of shear stresses in the surface.

In order to determine these initial values for the shear flows, every closed, hollow cross section may be transformed into an open cross section if the walls of all cells i are cut open. The actual continuity of the shear flows in the walls of closed cells is reestablished by means of redundant shear flows q_i . They are introduced along the cutting lines and are assumed to show the same distribution along the length of the member as the shear force Q .

The shear flows q_i represent n unknowns in the case of a hollow cross section with n cells. They are completely determined by the n conditions prescribing vanishing shear deformations around all cells:

$$\oint_i \gamma \, ds = 0 \quad (i = 1, 2, \dots, n). \quad (2.38)$$

Herein $\gamma = \tau/G$ which, with the definition of the shear flow as shear stress τ times wall thickness t , $q = \tau \cdot t$, may be written as $\gamma = q/Gt$.

$$\oint_i \frac{q}{Gt} \, ds = 0 \quad (i = 1, 2, \dots, n). \quad (2.39)$$

These ideas were first applied by W. J. GOODEY¹ for the computation of shear stresses in closed, hollow cross sections. The process was later simplified by A. PFLÜGER² and H. EBNER³.

b) Shear Stresses Caused by a Shearing Force

The following method is valid for arbitrarily shaped, multicellular, hollow cross sections which, however, must not have cells which are completely enclosed by others. All cells may therefore be opened in the boundary of the entire cross section, such that the redundant shear flow q_i is restricted to the walls of cell i only. The shear flow q_i is of constant magnitude and flows in the walls of cell i from one side of the incision to the other.

All shear flows q_i are introduced with the same sense of rotation as a positive torsional moment acting on the cross section (v. Fig. 1.1).

The resulting shear flow q is now a superposition of the shear flows q_0 in the open profile and the influence of the redundants. The latter is equal to q_i in the walls which coincide with the boundary of the cross section and according to the sign convention [Eq. (2.15)] equal to $q_{ik} = q_i - q_k$ in the others.

¹ GOODEY, W. J.: Shear Stresses in Hollow Sections. Aircraft Engng., No. 86, April 1936.

² PFLÜGER, A.: Beitrag zur Ermittlung der Schubspannungen in mehrzelligen Hohlquerschnitten. Ing.-Arch. 8 (1937).

³ EBNER, H.: Zur Festigkeit von Schalen- und Rohrholmflügeln. Luftfahrtforschung, 14 (1937).

If again i stands for the cells 1 to n and k for the cell adjacent to cell i , then condition (2.39) may be written as follows:

$$\oint_i \frac{q_0}{Gt} ds + q_i \oint_i \frac{ds}{Gt} - \sum_k q_k \int_{i,k} \frac{ds}{Gt} = 0 \quad (2.40)$$

(i = cell 1, 2, ..., n of the cross section),

(k = cell adjacent to cell i).

A variable shear modulus G may again be considered by introducing a fictitious wall thickness $t^* = Gt/G_0$ according to Eq. (2.12). If in addition the element of Eq. (2.40) which represents the shear deformation of an open cross section, the "generalized displacement", is put on the right side of the equation, one arrives at a system of equations which is very similar to the system (2.17):

$$q_i \oint_i \frac{ds}{t^*} - \sum_k q_k \int_{i,k} \frac{ds}{t^*} = - \oint_i q_0 \frac{ds}{t^*} \quad (2.41)$$

(i = cell 1, 2, ..., n of the cross section),

(k = cell adjacent to cell i).

The matrix is identical for the systems (2.17) and (2.41), except that the "generalized displacement" $2TA_i/K$ is replaced by:

$$- \oint_i q_0 \frac{ds}{t^*}. \quad (2.42)$$

The fictitious wall thickness t^* is equal to the actual wall thickness t when the shear modulus G is constant.

The resulting shear flow q is the superposition of the shear flow q_0 in the open cross section and that of the redundants:

$$q = q_0 + q_i \quad (2.43)$$

(i = cell 1, 2, ..., n of the cross section).

Since positive shear flows q_i have the same sense of rotation with respect to cell i , their superposition in a common wall leads by itself to the difference $q_i - q_k$.

c) Shear Center

If a general system of forces acting on a member is resolved into torsional and bending components with respect to the shear center, these cause respectively pure rotation and pure bending of the member. The position of the shear center (D) depends on the properties of the cross section only. It is therefore constant with respect to the cross section for prismatic members and may be given by the coordinates x_D and y_D . x and y are arbitrary cartesian coordinates with the

center of gravity of the cross section as origin. They constitute together with the axis of the member (the z -axis) a right-handed coordinate system.

The resultant of the shear flows has to be equal to the shearing force acting on the cross section. This condition may be formulated separately for the two components Q_x and Q_y of the shearing force. The product of the component Q_y and its distance x from the center of gravity has to be equal to the integral over the product of the shear flow caused by Q_y and its distance h_c from the center of gravity. A similar relation holds for the component Q_x .

$$\begin{aligned} Q_y x &= \int_s q(Q_y) h_c ds, \\ -Q_x y &= \int_s q(Q_x) h_c ds. \end{aligned} \quad (2.44)$$

If both Q_x and Q_y are assumed to be unity, then the left sides of expressions (2.44) represent already the coordinates x_D and y_D of the shear center.

The shear flows in a closed, hollow cross section are according to Eq. (2.43) obtained from a superposition of the shear flows q_0 in the open base cross section and the influence of the redundants. This is considered in the following expressions:

$$\begin{aligned} x_D &= \int_s q_0(Q_y = 1) h_c ds + \sum_{i=1}^n q_i(Q_y = 1) \oint_i h_c ds, \\ y_D &= - \int_s q_0(Q_x = 1) h_c ds - \sum_{i=1}^n q_i(Q_x = 1) \oint_i h_c ds. \end{aligned} \quad (2.45)$$

The first element in each sum of Eqs. (2.45) represents a coordinate of the shear center in the open cross section. It shall be denoted by x_{D0} and y_{D0} respectively. The second elements represent the displacement (Δx_D , Δy_D) of the shear center when the cross section is closed.

Eqs. (2.45) may thus be written more compactly as follows:

$$\begin{aligned} x_D &= x_{D0} + \Delta x_D, \\ y_D &= y_{D0} + \Delta y_D. \end{aligned} \quad (2.46)$$

Eqs. (5.22) represent expressions for the coordinates x_{D0} and y_{D0} based on arbitrary axis through the center of gravity while Eqs. (5.23) refer to principal centroidal axis. They are identical to Eqs. (5.39) and (5.40) respectively. A sign consistent algorithm for the application of these expressions is developed in Chapter 6. The corrections Δx_D and Δy_D have to be calculated only for closed, hollow cross sections and they are nothing but the torsional moment corresponding to the redundant shear flows. This becomes clear when the contour integral in the expressions for Δx_D and Δy_D is replaced by twice the area A_i of cell i :

$$\begin{aligned} \Delta x_D &= 2 \sum_{i=1}^n A_i q_i(Q_y = 1), \\ \Delta y_D &= -2 \sum_{i=1}^n A_i q_i(Q_x = 1). \end{aligned} \quad (2.47)$$

All basic relations for the determination of the shear center for thin-walled, hollow cross sections are thus given. It is remarkable that the same system of equations (2.17) serves for the torsional analysis as well as for the computation of the shear flows due to a shearing force and the determination of the shear center.

3 Torsional Moments and Member Rotation for Saint-Venant Torsion

3.1 Introduction

a) Saint-Venant Torsion

In the previous two chapters, the torsional moment T acting on a cross section was assumed to be known. The determination of this torsional moment T along the length of a member, however, is a problem of structural analysis to which various chapters of this book will be devoted. This and the next chapter will be concerned with the evaluation of the torsional moment T_s for pure Saint-Venant torsion while Chapters 7 and 8 will deal with pure warping torsion T_ω . Chapter 9, finally, will consider a combination of Saint-Venant and warping torsion, $T = T_s + T_\omega$. Chapter 10 summarizes the relative degree by which either Saint-Venant torsion or warping torsion dominate behavior, giving consideration to shape of cross-section, type of load, and slenderness of the member.

This chapter and the next chapter deal with pure Saint-Venant torsion, hence the subscript s in T_s designating Saint-Venant torsion as opposed to ω for warping torsion will be dropped for the time being. If the total torsional moment T is carried by Saint-Venant torsion only, $T = T_s$.

b) Differential Equation

The differential equation for Saint-Venant torsion is of a very simple and linear nature [v. Eq. (1.1)]. It is a special case of Hooke's law and expresses that unit rotation φ' is directly proportional to the torsional moment T and inversely proportional to the torsional rigidity GK . The integration of the differential equation (1.1) leads to:

$$\varphi(a) = \int_0^a \frac{T(z)}{GK(z)} dz. \quad (3.1)$$

Herein are:

- φ Member rotation, indicating the angle of rotation of the cross section at position $z = a$ with respect to the original cross section at position $z = 0$.
- T Torsional moment acting at the position z of the member. It is positive (in accordance with the familiar right hand rule) when acting counter clockwise with respect to an outward normal pointing in either the direction of the positive z -axis on the positive end or in the direction of the negative z -axis at the negative end of the member.
- G Shear modulus.
- K Torsion constant.

c) Notations

Although the application of the simple linear differential equation (1.1) may seem to be quite elementary, the torsional analysis of continuous members is not necessarily trivial. The simple beam, which is statically determinate for a flexural analysis, usually has one redundant support when used to carry torsional moments: The rotation of the member has to be zero at each support, thus yielding the required additional condition for the forces in the member.

Since the simple beam will be used as the base system for the analysis of continuous members, one must distinguish between two different types of support. The superscript (*f*) will be used to designate the forces in the member whose ends are fixed against torsional rotation while the subscript 0—"due to acting loads"—suffices to characterize the member forces in the statically determinate case.

The forces in continuous members need a characterization both with respect to the point of action and the cause. This is done by double-subscripts. The spans are designated by the even integers *i* and the supports by the odd integers *k*.

In order to show whether the torsional moment T_k at the support *k* acts immediately to the left (in the span *i* - 1) or to the right (in the span *i*) of the support, the number of the adjacent span is added as subscript, e.g. $T_{k,i-1}$ or $T_{k,i}$ (v. Fig. 3.1).

The following particular notations will be used:

$$\varphi_{ii} = \int_0^{l_i} \frac{dz}{GK(z)}, \quad \text{for prismatic members} = \frac{l_i}{GK_i} \quad (3.2a)$$

= Member rotation caused by the unit torsional moment $T = 1$; its reciprocal value is the moment caused by a unit rotation $\varphi = 1$.

μ_k = Moment necessary for a unit rotation $\varphi_k = 1$ of the support *k* (= spring constant). (3.2b)

Double-subscripts added to the rotations φ characterize influence coefficients for the base system.

The first subscript signifies the position of the influence coefficient while the second stands for the cause, a unit force. The cause subscript 0 always means: "due to acting loads". (3.2c)

3.2 The Single Member

a) Statically Determinate Support

The torsional support forces are statically determinate if the supports prevent a torsional rotation at only one point of the member. The distribution of the torsional moment is then a consequence of the equilibrium conditions alone. The solution of the linear differential equation $\varphi' = T/GK$ has to satisfy the boundary condition $\varphi = 0$ at the fixed point of the member. If this point is further chosen to be the origin of the coordinate system, then the member rotation due to a localized torsional moment M_D or due to the uniformly distributed torsional

moment m_D may be obtained from Eq. (3.1). The results are summarized for the prismatic member i in Figs. 3.1 a and 3.1 b.

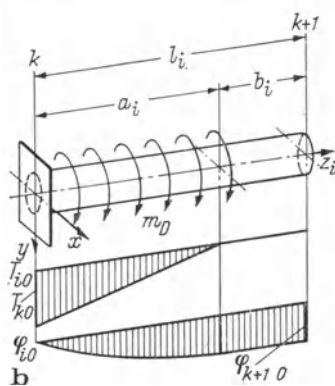
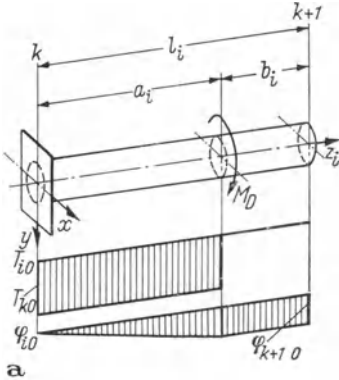


Table 3.1 a

	$0 < z_i < a_i$	$a_i < z_i < l_i$
T_{i0}	M_D	0
φ_{i0}	$\frac{M_D}{G K_i} z_i$	$\frac{M_D}{G K_i} a_i$

a) Concentrated Torsional Moment M_D

Table 3.1 b

	$0 < z_i < a_i$	$a_i < z_i < l_i$
T_{i0}	$m_D a_i \left(1 - \frac{z_i}{a_i}\right)$	0
φ_{i0}	$\frac{m_D a_i}{G K_i} z_i \left(1 - \frac{z_i}{2a_i}\right)$	$\frac{m_D a_i}{G K_i} \frac{a_i}{2}$

b) Uniformly Distributed Torsional Moment m_D Fig. 3.1. a and b. Torsional Moment T and Rotation φ of the Statically Determinant Member i Subjected to Two Different Load Arrangements.

b) Member With No End-Rotations

If both the supports k and $k + 1$ prevent the member i from rotating, then the member is statically indeterminate (Fig. 3.2). The fixed-end moment $T_{k+1,i}^{(f)}$ at $k + 1, i$ may be considered to be the redundant quantity. This leads to the following compatibility condition:

$$\varphi_{k+1,0} + T_{k+1,i}^{(f)} \varphi_{ii} = 0. \quad (3.3)$$

$$T_{k+1,i}^{(f)} = -\frac{\varphi_{k+1,0}}{\varphi_{ii}}. \quad (3.3)$$

The torsional moment and the member rotation at each location z_i is the superposition of the effect of the applied loads and the redundant force on the statically determinate base-system:

$$T_{i0}^{(f)} = T_{i0} + T_{k+1,i}^{(f)}, \quad (3.4a)$$

$$\varphi_{i0}^{(f)} = \varphi_{i0} + \varphi_{i,k+1} T_{k+1,i}^{(f)}. \quad (3.4b)$$

The influence coefficient $\varphi_{i,k+1}$ is (according to the definition 3.2 c) the member rotation at location z_i caused by a unit torsional moment acting at the member-end $k+1$. Thus:

$$\varphi_{i,k+1} = \int_0^{z_i} \frac{dz}{GK(z)},$$

which for a prismatic member becomes $\varphi_{i,k+1} = z_i/GK_i$. Figs. 3.2 and Tables 3.2 were worked out for the constant torsional rigidity GK_i .

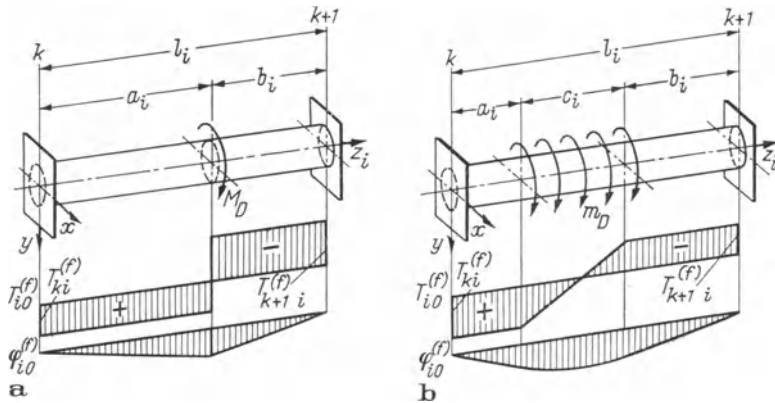


Fig. 3.2. a and b. Torsional Moment T and Rotation φ of the Fixed-End Member i Subjected to Two Different Load Arrangements.

a) Concentrated Torsional Moment M_D , b) Piecewise Uniformly Distributed Torsional Moment m_D .

Table 3.2a

	$0 < z_i < a_i$	$a_i < z_i < l_i$
$T_{i0}^{(f)}$	$M_D \frac{b_i}{l_i}$	$-M_D \frac{a_i}{l_i}$
$\varphi_{i0}^{(f)}$	$\frac{M_D}{GK_i} \frac{b_i}{l_i} z_i$	$\frac{M_D}{GK_i} \frac{a_i}{l_i} (l_i - z_i)$

Table 3.2b

	$0 < z_i < a_i$	$a_i < z_i < a_i + c_i$	$a_i + c_i < z_i < l_i$
$T_{i0}^{(f)}$	$+ m_D c_i \frac{b_i + \frac{c_i}{2}}{l_i}$	$m_D c_i \left(\frac{b_i + \frac{c_i}{2}}{l_i} - \frac{z_i - a_i}{c_i} \right)$	$- m_D c_i \frac{a_i + \frac{c_i}{2}}{l_i}$
$\varphi_{i0}^{(f)}$	$\frac{m_D c_i}{GK_i} \frac{b_i + \frac{c_i}{2}}{l_i} z_i$	$\frac{m_D}{2GK_i} \left[-a_i^2 + z_i \left(2a_i + 2c_i - 2\frac{a_i c_i}{l_i} - \frac{c_i^2}{l_i} \right) - z_i^2 \right]$	$\frac{m_D c_i}{GK_i} \frac{a_i + \frac{c_i}{2}}{l_i} (l_i - z_i)$

Exercise 3.1. Uniformly Distributed Applied Torsional Moment. Compute the torsional moments T_{i0} and the member rotation φ_{i0} for the member i which is subjected to a uniformly distributed torsional moment m_D along the entire length of the member. Calculate equivalent results by means of the following three methods:

Procedure presented in Section 3.2b,

Using table 3.2b for $a_i = b_i = 0$ and $c_i = l_i$,

Procedure presented in Section 3.2a considering the symmetries in system and load.

Results:

$$T_{i0}^{(f)} = m_D l_i \left(\frac{1}{2} - \frac{z_i}{l_i} \right),$$

$$\varphi_{i0}^{(f)} = \frac{m_D}{2GK_i} z_i (l_i - z_i).$$

3.3 The Continuous Rod on Elastically Rotating Supports

In the analysis of bending moments in continuous beams, one distinguishes between supports which are fixed, free to rotate, or elastically yielding. Only elastically rotating supports are of interest for a member which is subjected to Saint-Venant torsion. If a support rotation were completely prevented, then there would be no continuity effects and the support would counteract the entire torsional moment. If, on the other hand, the support showed no resistance against torsional rotation, then the support could be neglected in a torsional analysis.

Similar to the flexural analysis of a continuous beam, it should be possible to devise a linear system of equations whose solutions would either be the torsional moments or the torsional rotations at the supports. The first case corresponds to the force method and the second to the deformation method. These two systems of equations will be derived hereinafter. The notation will again be explained briefly:

The subscripts i denote the spans and the subscripts k denote the supports. Even numbers are used for i and odd ones for k .

The member rotations $\varphi_k, \varphi_{k+1}, \dots$ occur at the supports $k, k+1, \dots$. In order to distinguish between the torsional moments occurring in cross sections immediately to the left or to right of the supports k and $k+1$, the number of the adjacent span is shown as follows: $T_{k,i-1}, T_{ki}$ and $T_{k+1,i}, T_{k+1,i+1}$, resp. If $k=3$ (and thus $i=4$, v. Fig. 3.3), then the four torsion moments at the ends of span $i=4$ would be T_{32}, T_{34} and T_{54}, T_{56} , resp.

The elastically rotating support k is described by the relation between the support reaction M_{Dk} and the rotation φ_k which are always opposite to each other:

$$M_{Dk} = -\mu_k \varphi_k. \quad (3.5)$$

The support is thus characterized by the “spring constant” μ_k which is equal to the moment necessary to cause a support rotation of $\varphi_k = 1$.

a) The “Three-Rotation Equations”

If all supports are initially assumed to be completely rigid with respect to rotation, then the moments at the supports are equal to the fixed-end moments $T_{ki}^{(f)}$ and $T_{k+1,i}^{(f)}$ for which examples were given in Fig. 3.2. If the fixed supports

are unlocked, moments are released by the adjacent and opposite member-ends. These two influences may be expressed as the product of the moment caused by a unit end-rotation $\varphi = 1 [= 1/\varphi_{ii}, v. \text{Eq. (3.2)}]$ and the actual rotation:

$$T_{ki} = T_{ki}^{(j)} - \frac{\varphi_k}{\varphi_{ii}} + \frac{\varphi_{k+1}}{\varphi_{ii}}, \quad (3.6a)$$

$$T_{k,i-1} = T_{k,i-1}^{(j)} - \frac{\varphi_{k-1}}{\varphi_{i-1,i-1}} + \frac{\varphi_k}{\varphi_{i-1,i-1}}. \quad (3.6b)$$

A system of equations for the unknown support rotations φ_k is obtained when the *equilibrium condition* is formulated for each support. According to the support detail in Fig. 3.3 b which shows the acting forces in a positive direction, the equilibrium condition for the support k is as follows:

$$-T_{k,i-1} + M_{Dk} + T_{ki} = 0 \quad (k = 1, 3, 5, \dots). \quad (3.7)$$

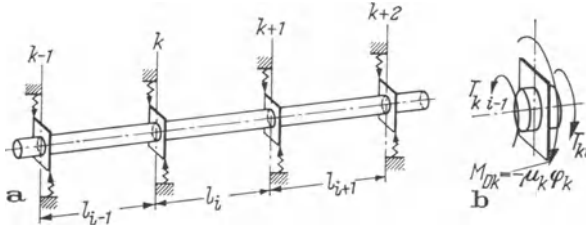


Fig. 3.3. The Continuous, Elastically Supported Rod (a) and Torsional Moments Acting at Support k (b).

If Eqs. (3.5), (3.6a) and (3.6b) are used to replace the torsional moments in Eq. (3.7), then the contribution of support k to the system of equations may be written in the following form:

$$\begin{aligned} \frac{1}{\varphi_{i-1,i-1}} \varphi_{k-1} - \left(\frac{1}{\varphi_{i-1,i-1}} + \mu_k + \frac{1}{\varphi_{ii}} \right) \varphi_k + \frac{1}{\varphi_{ii}} \varphi_{k+1} &= T_{k,i-1}^{(j)} - T_{ki}^{(j)} \\ (k = 1, 3, 5, \dots \text{ supports}), \quad (i = 2, 4, 6, \dots \text{ spans}). \end{aligned} \quad (3.8a)$$

If the torsional rigidity GK is constant within any one span, then these equations may, according to Eq. (3.2a), be written more explicitly:

$$\begin{aligned} \frac{GK_{i-1}}{l_{i-1}} \varphi_{k-1} - \left(\frac{GK_{i-1}}{l_{i-1}} + \mu_k + \frac{GK_i}{l_i} \right) \varphi_k + \frac{GK_i}{l_i} \varphi_{k+1} &= T_{k,i-1}^{(j)} - T_{ki}^{(j)} \\ (k = 1, 3, 5, \dots \text{ supports}), \quad (i = 2, 4, 6, \dots \text{ spans}). \end{aligned} \quad (3.8b)$$

Herein are:

K_{i-1}, K_i Torsion constants within spans $i-1$ and i , resp.

G Shear modulus.

l_{i-1}, l_i Length of span $i-1$ resp. i .

- μ_k “Spring constant” of the support k , e.g. the moment which causes a rotation of the support k by the angle $\varphi = 1$.
- $\varphi_{k-1}, \varphi_k, \varphi_{k+1}$ Unknowns of the system of equations, e.g. rotations of the continuous rod at the supports $k - 1$, k and $k + 1$ respectively.
- $T_{k,i-1}^{(j)}, T_{ki}^{(j)}$ Torsional moments respectively to the left and to the right of support k if all supports are fixed with respect to torsion.

The member-end moments may be computed from Eqs. (3.6).

The law of superposition applies at any location z_i of the member i .

$$T(z_i) = T_{i0}^{(j)} + \frac{\varphi_{k+1} - \varphi_k}{\varphi_{ii}}. \quad (3.9a)$$

The member rotation for the case of a constant torsional rigidity of the member i is:

$$\varphi(z_i) = \varphi_{i0}^{(j)} + \varphi_k \left(1 - \frac{z_i}{l_i}\right) + \varphi_{k+1} \frac{z_i}{l_i}. \quad (3.9b)$$

The quotient z_i/l_i must be replaced by $\varphi_{i,k+1}/\varphi_{ii}$ when the torsional rigidity is variable.

The support reactions are finally determined by means of Eq. (3.5).

b) The “Three-Torsional-Moment Equations”

In the force method a statically determinate base system is introduced. This may be pictured as composed of the statically determinate elements which, aside from the elastic supports, are sketched in Fig. 3.1. The originally continuous rod is cut apart immediately to the left of the supports.

The total torsional moment in element i is caused by the applied loads (T_{k0}) and the two unknown redundant end-moments $T_{k,i-1}$ and $T_{k+1,i}$. The resultant of these moments is carried by the support k . The support reaction M_{Dk} is thus given by the expression:

$$M_{Dk} = -T_{k,i-1} + T_{k0} + T_{k+1,i}. \quad (3.10)$$

Eq. (3.5) relates the support reaction M_{Dk} with the support rotation φ_{ki} . This rotation has to be compatible with the rotation of the end k of the preceding element $i - 1$ which is the sum of the support rotation $\varphi_{k-1,i-1}$ and the rotation of member $i - 1$, $\varphi_{k0} + T_{k,i-1} \varphi_{i-1,i-1}$.

The *compatibility condition* requires equal rotation of the elements i and $i - 1$ at the support k . This condition may be formulated for all supports except the first:

$$\varphi_{k,i-1} - \varphi_{ki} = 0 \quad (3.11)$$

or in terms of torsional moments:

$$\frac{-T_{k-1,i-2} + T_{k-1,0} + T_{k,i-1}}{\mu_{k-1}} + \varphi_{k0} + \varphi_{i-1,i-1} T_{k,i-1} - \frac{-T_{k,i-1} + T_{k0} + T_{k+1,i}}{\mu_k} = 0$$

which, when rearranged, becomes the required three-moment equation. The three unknown moments are the torsional moments immediately to the left of three consecutive supports.

$$\begin{aligned} -\frac{1}{\mu_{k-1}} T_{k-1, i-2} + \left(\frac{1}{\mu_{k-1}} + \varphi_{i-1, i-1} + \frac{1}{\mu_k} \right) T_{k, i-1} - \frac{1}{\mu_k} T_{k+1, i} \\ = -\frac{T_{k-1, 0}}{\mu_{k-1}} + \frac{T_{k0}}{\mu_k} - \varphi_{k0} \\ (k = 3, 5, \dots \text{ supports}), \\ (i = 2, 4, 6, \dots \text{ spans}). \end{aligned} \quad (3.12)$$

Herein are:

$T_{k-1, i-2}, T_{k, i-1}, T_{k+1, i}$	Torsional moments immediately to the left of three consecutive supports and unknowns of the system of equations.
μ_{k-1}, μ_k	“Spring constant” of the support $k-1$ and k resp. as defined in (3.2 b).
$\varphi_{i-1, i-1}$	Member rotation caused by a unit torsional moment, v. Eq. (3.2 a).
$T_{k-1, 0}, T_{k0}, \varphi_{k0}$	“Generalized displacements” as defined in (3.2 c), for which some examples are given in Fig. 3.1.

The solutions of the system of equations are the basis for the computation of the torsional moment and the rotation in any position z_i of the element i .

$$T(z_i) = T_{i0} + T_{k+1, i}, \quad (3.13 \text{ a})$$

$$\varphi(z_i) = \varphi_{i0} + \varphi_{i, k+1} T_{k+1, i} + \frac{-T_{k, i-1} + T_{k0} + T_{k+1, i}}{\mu_k}. \quad (3.13 \text{ b})$$

The reaction M_{Dk} of the support k is given by Eq. (3.10).

3.4 Examples

a) Systems

The systems of equations (3.8) and (3.12) developed in the preceding section may be applied whenever the design of a structure calls for the torsion analysis of a continuous, elastically supported bar for which Saint-Venant torsion provides an adequate description of the behavior.

A bridge with box-type main girders, for instance, may be treated according to formula (2.25c) only when the main girders are forced by very rigid cross girders to undergo negligible or nearly equal torsional rotations. Otherwise, the cross girders offer only an elastic torsional support to the main girders whereby both the torsional moments in the main girders and the reactions on the cross girders have to be determined by means of the theory developed above.

Crane girders are quite often carried by flexible frames and columns which thus offer elastic support restraint in torsion. Such a crane girder is investigated below. The girder is supposed to be a part of the portal crane shown in Fig. 3.4.

In order to facilitate the numerical computation, the flexural rigidity of the frames and end cross-bars is taken to be EI , the torsional rigidity of the crane girders GK and the length of all members a . The crane bridge, which carries the trolley at its center, may be positioned anywhere between the two end cross-bars. The two parallel crane girders are thus equally loaded by the wheel loads

of the crane which in general cause both flexure and torsion. The crane girder will have to carry a torsional moment M_D whenever the line of application of the wheel loads does not coincide with the shear center of the box girders.

The crane girder enters the torsion analysis as a continuous bar which is elastically supported at the points 1 and 7 by the cross bars and at the points 3 and 5 by the frames (Fig. 3.4 b).

The “spring constants” μ_1 and μ_3 are according to the definition (3.2 b) equal to the moments which cause a unit rotation of the corresponding supports. In

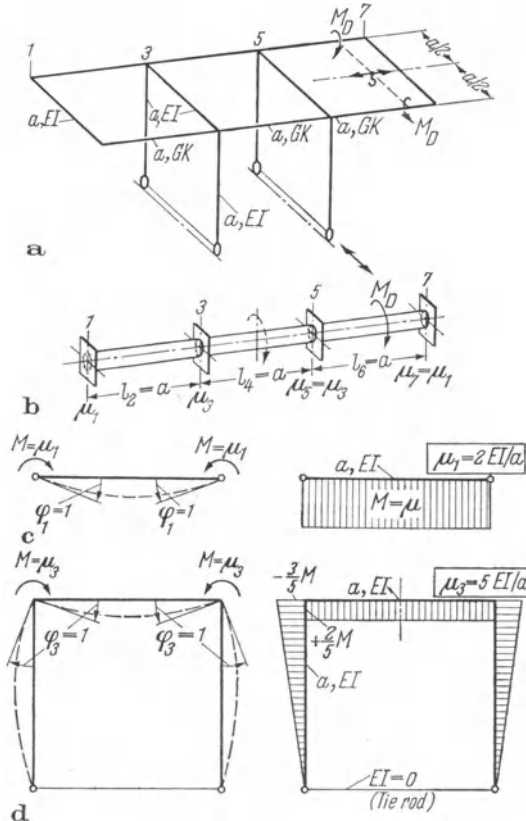


Fig. 3.4. Example: Portal Crane Structure.

this case, the flexibility of the supports is determined by the flexibility of structural systems, a simple beam for μ_1 and a two-hinged, rectangular frame for μ_3 . These systems together with the moments caused by the “spring-constants” are shown in Figs. 3.4c and 3.4d. Moreover, the member constants φ_{ii} are obtained from Eq. (3.2a):

$$\begin{aligned}\mu_1 &= \mu_7 = 2 \frac{EI}{a}, \\ \mu_3 &= \mu_5 = 5 \frac{EI}{a},\end{aligned}\quad (3.14)$$

$$\varphi_{22} = \varphi_{44} = \varphi_{66} = \frac{a}{GK}.$$

b) Selection of the Method

The selection of a particular three-element equation, (3.8) or (3.12), depends primarily on the question of whether the member rotations φ or the torsional moments T are of main interest.

The system of equations (3.8) is written in terms of unknown support rotations while the system (3.12) is based on the unknown torsional moments immediately to the left of the supports. This difference does not have severe consequences in a particular problem since the principle of superposition is used in both cases to calculate the rotations and the torsional moments along the bar.

The three-rotation equations have to be formulated for each support and the three-moment equations for each span. Since there is usually one support more than there are spans, the first system has usually one unknown more than the second. Symmetries in a particular system may, on the other hand, be more immediately considered in terms of support rotations. Hence, there is no reason which might justify a definite preference for one of these two methods.

First, the three-rotation equations (3.8) will be applied to the crane girder shown in Fig. 3.4b with the torsional moment M_D acting at the center of the span l_4 . This leads to the following general form of the system of equations:

$$\begin{aligned}
 \varphi_1 & & \varphi_3 & & \varphi_5 & & \varphi_7 \quad \text{generalized} \\
 & -\left(2 \frac{EI}{a} + \frac{GK}{a}\right) & + \frac{GK}{a} & & & & \text{displacements} \\
 & + \frac{GK}{a} & -\left(\frac{GK}{a} + 5 \frac{EI}{a} + \frac{GK}{a}\right) & + \frac{GK}{a} & & = -\frac{M_D}{2} \\
 & + \frac{GK}{a} & -\left(\frac{GK}{a} + 5 \frac{EI}{a} + \frac{GK}{a}\right) & + \frac{GK}{a} & & = -\frac{M_D}{2} \\
 & + \frac{GK}{a} & -\left(\frac{GK}{a} + 2 \frac{EI}{a}\right) & = 0
 \end{aligned}$$

The symmetry in the structure and the load ($\varphi_1 = \varphi_7$, $\varphi_3 = \varphi_5$) and a multiplication of both sides by a/GK reduce the general system to:

$$\begin{aligned}
 -\left(1 + 2 \frac{EI}{GK}\right) \varphi_1 & + \varphi_3 & = 0 \\
 \varphi_1 & -\left(1 + 5 \frac{EI}{GK}\right) \varphi_3 & = -\frac{M_D}{2} \frac{a}{GK}.
 \end{aligned}$$

The solutions are:

$$\begin{aligned}
 \varphi_1 = \varphi_7 & = \frac{\frac{M_D}{2} \frac{a}{GK}}{\frac{EI}{GK} \left(7 + 10 \frac{EI}{GK}\right)}, \\
 \varphi_3 = \varphi_5 & = \left(1 + 2 \frac{EI}{GK}\right) \varphi_1.
 \end{aligned} \tag{3.15a}$$

Eq. (3.9a) yields the torsional moments:

$$T_2 = -T_6 = \frac{M_D}{7 + 10 \frac{EI}{GK}}, \quad |T_4| = \frac{M_D}{2}. \quad (3.15 \text{ b})$$

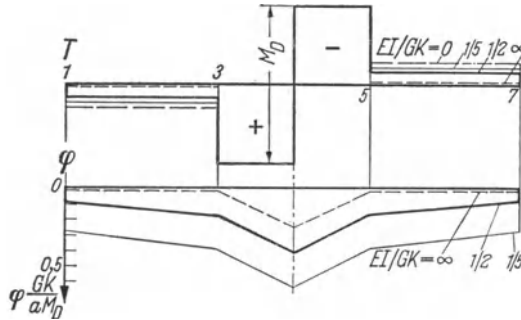


Fig. 3.5. Torsional Moments T and Member Rotations φ in the Crane Girder of Fig. 3.4 (M_D Acting at the Center of Span l_4).

These results together with the member rotations following from Eq. (3.9b) are plotted in Fig. 3.5 for different ratios EI/GK which represent a nondimensional measure for the torsional rigidity of the supports.

The same crane girder (Fig. 3.4b) will now be analyzed by means of Eqs. 3.12 which lead to a system of equations with the torsional moments immediately to the left of the supports as unknowns:

generalized displ.	generalized displ.	generalized displ.	generalized displ.
T_{32}	T_{54}	T_{76}	= $-\frac{T_{10}}{\mu_1} + \frac{T_{30}}{\mu_3} - \varphi_{30}$
$\left(\frac{1}{\mu_1} + \varphi_{22} + \frac{1}{\mu_3}\right)$	$-\frac{1}{\mu_3}$	$-\frac{1}{\mu_5}$	= $-\frac{T_{30}}{\mu_3} + \frac{T_{50}}{\mu_5} - \varphi_{50}$
$-\frac{1}{\mu_3}$	$+ \left(\frac{1}{\mu_3} + \varphi_{44} + \frac{1}{\mu_5}\right)$	$- \frac{1}{\mu_5}$	= $-\frac{T_{50}}{\mu_5} + \frac{T_{70}}{\mu_7} - \varphi_{70}$
	$- \frac{1}{\mu_5}$	$+ \left(\frac{1}{\mu_5} + \varphi_{66} + \frac{1}{\mu_7}\right)$	

The torsional moment M_D acting at the center of span 4, a case which was investigated by means of the three-rotation equations, leads to the following generalized displacements:

$$T_{10} = T_{50} = 0, \quad T_{30} = M_D,$$

$$\varphi_{30} = \varphi_{70} = 0, \quad \varphi_{50} = \frac{M_D}{GK} \frac{a}{2}.$$

If further the elements (3.14) are introduced and both sides of the equations are multiplied by $10EI/a$, one arrives at the following simplified system:

T_{32}	T_{54}	T_{76}	generalized displ.
$+ 7 + 10 \frac{EI}{GK}$	-2	-2	$= +2M_D$
-2	$+4 + 10 \frac{EI}{GK}$	-2	$= -2M_D - 5M_D \frac{EI}{GK}$
	-2	$+7 + 10 \frac{EI}{GK}$	$= 0.$

The solution of this system, with the help of Eqs. (3.13), leads to the force and rotations given in Eqs. (3.15) which were calculated by the alternative method.

e) Influence Lines

Since the systems (3.8) and (3.12) represent an analytic formulation of the problem, the evaluation of influence lines is readily accomplished. It is quite interesting to observe, however, that prismatic members will have piecewise linear influence lines though the corresponding structural system may be statically indeterminate. This is a consequence of the simplicity of the differential equation $\varphi' = T/GK$ which for a constant torsional rigidity GK yields a linear relation between the member rotation φ and a concentrated torsional moment $T = 1$.

Influence lines for the torsional moments in the bar of Fig. 3.4b based on a support rigidity ratio $EI/GK = 1/2$ are plotted for the cross sections immediately to the right of the first support (Fig. 3.6a), at the center of the first span (Fig. 3.6b), to the left and to the right of the second support (Figs. 3.6c and 3.6d) and at the center of the entire bar (Fig. 3.6e). The difference between the influence lines c) and d) is the influence line for the reaction in support 3 (Fig. 3.6f) and, aside from a constant factor [Eq. (3.5)], the influence line for the rotation of support 3.

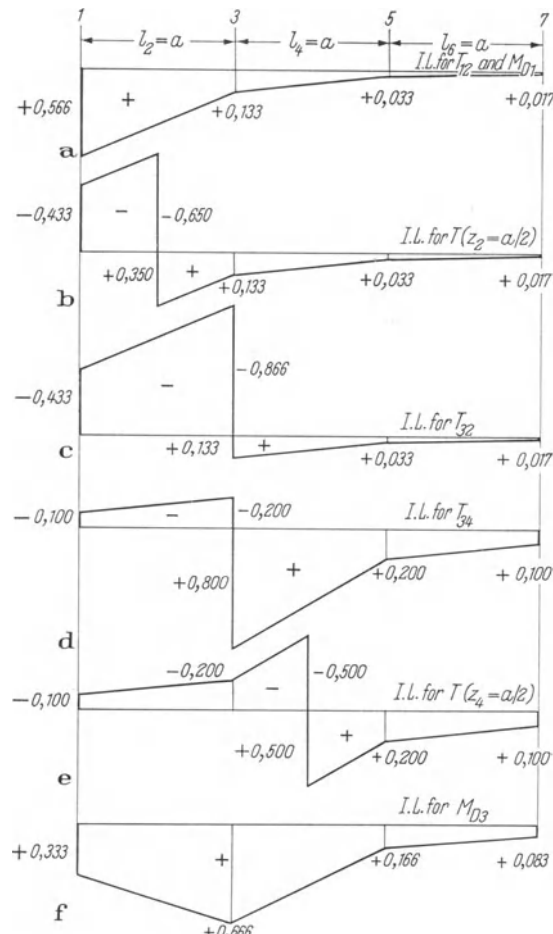


Fig. 3.6. Influence Lines for the Torsional Moments (a to e) and the Support Reactions (a and f) of the Crane Girder Shown in Fig. 3.4b. Assumption: $GK = \text{const}$, $\mu_1 = \mu_7 = 2EI/a$, $\mu_3 = \mu_5 = 5EI/a$, $EI/GK = 1/2$.

4 Skew Supported Members with Saint-Venant Torsion

4.1 Introduction

a) Assumptions

The two usual assumptions are made. The members are slender, e.g. the spans exceed by far the largest extension of the cross sections, and Saint-Venant torsion alone provides a suitable basis for analysis. The torsional property of a member is thus described completely by its torsional rigidity GK which is again given in Fig. 4.1 for a rectangular and a monocellular, hollow cross section [v. Eqs. (1.9) and (2.5)].

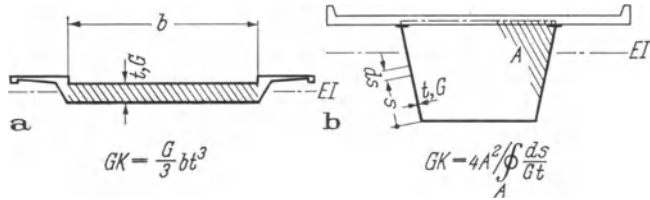


Fig. 4.1. Torsional Rigidity GK of a Plate Bridge (a) and a Monocellular Box Girder (b).

The analysis will be developed for straight members and cross sections which are symmetric with respect to the vertical axis. The cross sections as such and the obliqueness of the supports may be variable. The notation is of great importance and will therefore be explained first. The characteristic interlinkage between torsional moments and bending moments is then analytically derived. It is illustrated in the last part of this section by means of the iterative solution to a specific, simple example. A general method of analysis for centric loads is derived in Section 4.2 and supplemented for eccentric loads in Section 4.3. The closing Section 4.4 presents some general considerations and the solution to different problems.

b) Notations and Abbreviations

The spans of continuous beams are designated by i for which the even numbers $i = 2, 4, 6, \dots$ are used in numerical computations. The supports are identified by k and numbered consecutively by odd numbers. The subscripts $k+1, i-1$

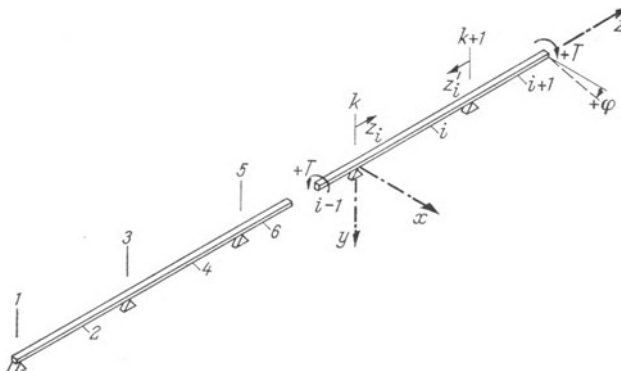


Fig. 4.2. Designation of Spans and Supports for a Continuous Beam.

mean one step forward or one step backward, respectively, in the corresponding group of numbers (v. Fig. 4.2).

Fig. 4.2 also shows the position and orientation of the coordinate system and the direction of positive member rotations and torsional moments. The abscissa which measures the member axis in the opposite direction is designated by a prime, z' . The same characterization is applied to the nondimensional coordinate parameters $\zeta = z/l$, $\zeta' = z'/l$.

The angular displacement and reactions at the left support and distances from this support are denoted by α , A and a respectively. The corresponding notation belonging to the support on the right is β , B and b .

If an influence coefficient requires double-subscripts, then the first stands for its position and the second for its cause. The cause subscript 0 means always "due to applied loads".

Since this chapter does not use any moments of inertia other than I_{yy} , the double-subscript yy shall be dropped within Chapter 4

List of the Notations Used in Chapter 4

- a Distance from the left support
- A Support reaction to the left of the simple beam
- b Distance from the right support
- B Support reaction to the right of the simple beam
- C Member constant $\frac{GK}{EI} \frac{\operatorname{tg}^2 \delta}{2}$, with subscripts: v. Table 4.2
- d Width of the member
- D Determinant defined in Table 4.2
- e Longitudinal Distance between two obliquely placed support points
- E Modulus of elasticity
- F Resulting support reaction
- G Shear modulus = $E/2(1 + \nu)$
- I Moment of inertia (with respect to x -axis, v. Fig. 4.1)
- K Torsion constant (v. Fig. 4.1)
- l Span
- M Bending moment
- M_D Moment with respect to member axis
- p Distributed load
- P Single load
- Q Shearing force
- T Torsional moment
- x Coordinate (Fig. 4.2), eccentricity of a load
- y Coordinate (Fig. 4.2), vertical displacement
- z Coordinate (Fig. 4.2), distance from the left support
- z' Opposite to coordinate z , distance from the right support
- α Angular displacement at the left support (v. Table 4.1)
- β Angular displacement at the right support (v. Table 4.1)
- γ Displacement coefficient: $\frac{dz}{GK}$ (v. Table 4.1)
- δ Skew angle of the support with respect to rectangular case
- $\zeta = z/l$, nondimensional coordinate parameter for z
- $\zeta' = z'/l$, nondimensional coordinate parameter for z'
- λ Length ratio between end span and intermediate span
- ν Poisson's ratio (e.g. 1/3 for steel, 1/6 for concrete)
- $\xi = x/l$, nondimensional coordinate parameter for x
- σ Normal stress

- τ Shear Stress
 φ Torsional rotation of the member

Subscripts

- i Even numbers assigned to spans (v. Fig. 4.2)
 k Odd numbers assigned to supports (v. Fig. 4.2)
 0 "due to applied load"
 D "due to the moment M_D acting as load"

Superscripts

- (f) Base system with prevented torsional rotation at both ends

Table 4.1.

Displacement Coefficients and Generalized Displacements for the Simple Beam of Span i

Displacement Coefficients	for Variable Cross Section	for Prismatic Bar
$\alpha_{ik}:$	$\frac{1}{l_i^2} \int_0^{l_i} \frac{z' z'}{EI} dz'$	$\frac{l_i}{3EI_i}$
$\alpha_{i,k+1} = \beta_{ik}:$	$\frac{1}{l_i^2} \int_0^{l_i} \frac{zz'}{EI} dz$	$-\frac{l_i}{6EI_i}$
$\beta_{i,k+1}:$	$\frac{1}{l_i^2} \int_0^{l_i} \frac{zz}{EI} dz$	$\frac{l_i}{3EI_i}$
$\gamma_i:$	$\int_0^{l_i} \frac{dz}{GK}$	$\frac{l_i}{GK}$
Generalized Displacements for Single Load P		
$\alpha_{i0}:$	$\frac{1}{l_i} \int_0^{l_i} \frac{M_0 z'}{EI} dz'$	$\frac{Pl_i^2}{6EI_i} (\zeta'_i - \zeta'^3_i)$
$\beta_{i0}:$	$\frac{1}{l_i} \int_0^{l_i} \frac{M_0 z}{EI} dz$	$\frac{Pl_i^2}{6EI_i} (\zeta_i - \zeta^3_i)$
Generalized Displacements for Equally Distributed. Load p		
$\alpha_{i0}:$	$\frac{p}{2l_i} \int_0^{l_i} \frac{zz'^2}{EI} dz'$	$\frac{pl_i^3}{24EI_i}$
$\beta_{i0}:$	$\frac{p}{2l_i} \int_0^{l_i} \frac{z' z^2}{EI} dz$	$\frac{pl_i^3}{24EI_i}$

Table 4.2. List of Member Constants C and D

Cross Section	Variable	EI and GK Constant Within One Span	
		Different from Support to Support	Same angle (δ) for each support
$C_{i,k} =$	$\frac{\operatorname{tg} \delta_k (\alpha_{ik} \operatorname{tg} \delta_k + \alpha_{i,k+1} \operatorname{tg} \delta_{k+1})}{\gamma_i}$	$\frac{GK_i}{EI_i} \frac{\operatorname{tg} \delta_k}{6} (2 \operatorname{tg} \delta_k + \operatorname{tg} \delta_{k+1})$	
$C_{i,k+1} =$	$\frac{\operatorname{tg} \delta_{k+1} (\alpha_{ik} \operatorname{tg} \delta_k + \alpha_{i,k+1} \operatorname{tg} \delta_{k+1})}{\gamma_i}$	$\frac{GK_i}{EI_i} \frac{\operatorname{tg} \delta_{k+1}}{6} (2 \operatorname{tg} \delta_k + \operatorname{tg} \delta_{k+1})$	$= C_i = \frac{GK_i}{EI_i} \frac{\operatorname{tg}^2 \delta}{2}$
$C_{i\beta k} =$	$\frac{\operatorname{tg} \delta_k (\beta_{ik} \operatorname{tg} \delta_k + \beta_{i,k+1} \operatorname{tg} \delta_{k+1})}{\gamma_i}$	$\frac{GK_i}{EI_i} \frac{\operatorname{tg} \delta_k}{6} (\operatorname{tg} \delta_k + 2 \operatorname{tg} \delta_{k+1})$	
$C_{i\beta k+1} =$	$\frac{\operatorname{tg} \delta_{k+1} (\beta_{ik} \operatorname{tg} \delta_k + \beta_{i,k+1} \operatorname{tg} \delta_{k+1})}{\gamma_i}$	$\frac{GK_i}{EI_i} \frac{\operatorname{tg} \delta_{k+1}}{6} (\operatorname{tg} \delta_k + 2 \operatorname{tg} \delta_{k+1})$	
$D_i =$	$1 + C_{i,k} + C_{i\beta k+1}$	$1 + \frac{GK_i}{EI_i} \frac{\operatorname{tg}^2 \delta_k + \operatorname{tg} \delta_k \operatorname{tg} \delta_{k+1} + \operatorname{tg}^2 \delta_{k+1}}{3}$	$1 + 2C_i = 1 + \frac{GK_i}{EI_i} \operatorname{tg}^2 \delta$

c) Torsional Moments and Their Side-Effects

Skewness of supports causes torsional moments in the members even for vertical, centric loads. These torsional moments in turn have an influence on the bending moments. In order to derive this connection, the span i between the supports k and $k + 1$ will be considered (Fig. 4.3a).

The member is acted upon by the loads p and P as well as by the support moments M_k and M_{k+1} which all act in the vertical plane through the member axis. The member shall temporarily be considered to be supported at the two end points of its axis only. Since there is no reason for a torsional rotation of the member, the vertical deflection of its neutral plane may be sketched as in Fig. 4.3 b. The deflected plane shows a difference in height of $\alpha_i \cdot e_k$ at the support k and a difference of $\beta_i e_{k+1}$ at the support $k + 1$.

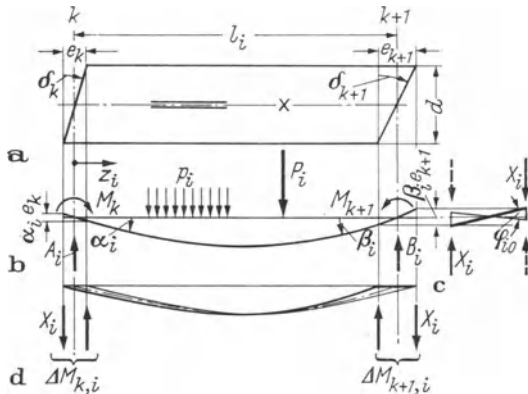


Fig. 4.3. Connection Between Deflection and Rotation.

The view in the direction of the member axis (Fig. 4.3 c) shows the rotation φ_{i0} necessary to put the member ends back on the skewed supports:

$$\varphi_{i0} = -\left(\frac{\alpha_i e_k}{d} + \frac{\beta_i e_{k+1}}{d}\right).$$

Introduction of the skew angle δ of the supports in the form $e_k/d = \tan \delta_k$ and $e_{k+1}/d = \tan \delta_{k+1}$ yields the following compatibility condition:

$$\alpha_i \tan \delta_k + \varphi_i + \beta_i \tan \delta_{k+1} = 0. \quad (4.1)$$

This condition has to be satisfied for each span of the continuous member.

The rotation of the member of length l_i and of torsional rigidity GK by the angle φ_i requires the torsional moment $T_i = \varphi_i/\gamma_i$, where the displacement coefficient γ_i was defined in table 4.1. The compatibility condition 4.1 may thus be written as:

$$T_i = -\frac{\alpha_i \tan \delta_k + \beta_i \tan \delta_{k+1}}{\gamma_i}. \quad (4.2)$$

One may think of this torsional moment as being a force couple X_i acting at the end points of support k . It is counteracted by the opposite force couple X_{i0} at support $k + 1$. The assumption that the lever arm of the two couples shall be

equal to the width d of the member is convenient in view of the following considerations, but not at all necessary.

It is apparent from Fig. 4.3d that the forces X_i influence the bending moments in the member i , causing the following changes in the support moments M_{ki} and $M_{k+1,i}$:

$$\left. \begin{aligned} \Delta M_{ki} &= X_i e_k = \frac{T_i}{d} e_k = T_i \operatorname{tg} \delta_k \\ \Delta M_{k+1,i} &= X_i e_{k+1} = \frac{T_i}{d} e_{k+1} = T_i \operatorname{tg} \delta_{k+1} \end{aligned} \right\}. \quad (4.3)$$

Positive angular displacements α_i and β_i and positive angles δ_k and δ_{k+1} , according to Eq. (4.2), always lead to a negative value for the torsional moment T_i . Thus the changes in the support moments (4.3) are also negative. If the skew angle δ of the supports were negative, then the torsional moment T_i would become positive but expressions (4.3) would still yield negative values because of negative values for the tangents. Skewed supports thus act as end-restraints of the member, introducing support moments, but increasing maximum moments in the span.

d) Example: Iterative Procedure

The foregoing may be used to obtain an estimate on the effects of skewed supports. They may even be used as the basis of an iterative procedure which in many cases will converge to the solution of the problem. As an illustration, the system shown in Fig. 4.4 shall be analyzed. A small, rectangular plate spans between a simple support at the left end to a support at the right which is oblique by the angle δ . The member is acted upon by the uniformly distributed load p .

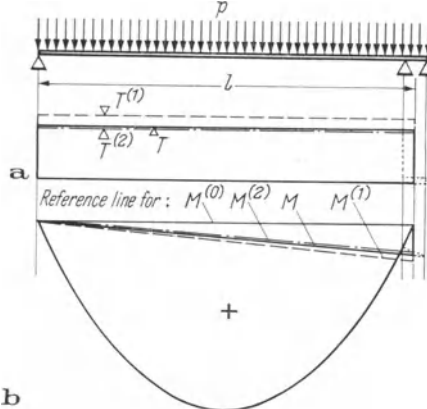


Fig. 4.4. An Example for the Iterative Procedure with Diagrams of the Torsional Moments (a) and Bending Moments (b).

The torsional moment and the associated corrections in the support moments are according to formulas (4.2) and (4.3):

$$\left. \begin{aligned} T &= -\beta \frac{GK}{l} \operatorname{tg} \delta \\ \Delta M_A &= 0 \\ \Delta M_B &= -\beta \frac{GK}{l} \operatorname{tg}^2 \delta. \end{aligned} \right\} \quad (4.4a)$$

The angular displacements at the supports may as a first step be calculated for simple supports. The angle β_0 which is of interest in this example may be taken from Table 4.1:

$$\beta^{(1)} = \frac{pl^3}{24EI},$$

thus

$$\left. \begin{aligned} T^{(1)} &= -\frac{pl^2}{8} \frac{GK}{EI} \frac{\operatorname{tg} \delta}{3}, \\ \Delta M_B^{(1)} &= -\frac{pl^2}{8} \frac{GK}{EI} \frac{\operatorname{tg}^2 \delta}{3}. \end{aligned} \right\} \quad (4.4 \text{ b})$$

and

The correction $\Delta M_B^{(1)}$ is slightly too big since it reduces the angular displacements β by the amount $\Delta\beta^{(1)} = \beta_2 |\Delta M_B^{(1)}|$, where β_2 is again listed in Table 4.1:

$$\Delta\beta^{(1)} = \frac{l}{3EI} \frac{pl^2}{8} \frac{GK}{EI} \frac{\operatorname{tg}^2 \delta}{3}.$$

This yields a second, better approximation for the angular displacement:

$$\beta^{(2)} = \beta^{(1)} - \Delta\beta^{(1)} = \frac{pl^3}{24EI} \left(1 - \frac{GK}{EI} \frac{\operatorname{tg}^2 \delta}{3} \right),$$

which, because of the overestimated correction, is now slightly too small. The absolute values of the following second approximations for T and ΔM_B represent therefore lower bounds for the absolute values of the exact solutions:

$$\left. \begin{aligned} T^{(2)} &= -\frac{pl^2}{8} \left(1 - \frac{GK}{EI} \frac{\operatorname{tg}^2 \delta}{3} \right) \frac{GK}{EI} \frac{\operatorname{tg} \delta}{3}, \\ \Delta M_B^{(2)} &= -\frac{pl^2}{8} \left(1 - \frac{GK}{EI} \frac{\operatorname{tg}^2 \delta}{3} \right) \frac{GK}{EI} \frac{\operatorname{tg}^2 \delta}{3}. \end{aligned} \right\} \quad (4.4 \text{ c})$$

Suppose now that the torsional stiffness GK is equal to $\sqrt{3}$ times the flexural stiffness EI [which is approximately true for concrete beams of rectangular cross section (v. Section 4.4a)] and the skew angle $\delta = 30^\circ$, then:

$$\frac{GK}{EI} \frac{\operatorname{tg}^2 \delta}{3} = \frac{\sqrt{3}}{9}.$$

Under these assumptions, Eqs. (4.4b) and (4.4c) determine the following bounds for the torsional moment T and the support moment ΔM_B :

$$\left. \begin{aligned} 1 &> 24 \frac{|T|}{pl^2} > 0,807, \\ 1 &> 24\sqrt{3} \frac{|\Delta M_B|}{pl^2} > 0,807. \end{aligned} \right\} \quad (4.4 \text{ d})$$

If the iteration were continued, one would arrive at a geometric series for the angular displacement β :

$$\beta = \frac{pl^3}{24EI} \left[1 - \frac{GK}{EI} \frac{\operatorname{tg}^2 \delta}{3} + \left(\frac{GK}{EI} \frac{\operatorname{tg}^2 \delta}{3} \right)^2 - \dots + \dots \right],$$

which has the sum:

$$\beta = \frac{pl^3}{24EI} \frac{1}{1 + \frac{GK}{EI} \frac{\operatorname{tg}^2 \delta}{3}}.$$

This angle determines again the torsional moment T and the support moment ΔM_B :

$$\left. \begin{aligned} T &= -\frac{pl^2}{8} \frac{\frac{GK}{EI} \frac{\operatorname{tg} \delta}{3}}{1 + \frac{GK}{EI} \frac{\operatorname{tg}^2 \delta}{3}} \\ \Delta M_B &= -\frac{pl^2}{8} \frac{\frac{GK}{EI} \frac{\operatorname{tg}^2 \delta}{3}}{1 + \frac{GK}{EI} \frac{\operatorname{tg}^2 \delta}{3}} \end{aligned} \right\} \quad (4.4e)$$

The solution of this numerical example, previously determined to be limited by the upper bound 1 and the lower bound 0.807 in Eqs. (4.4d), now can be calculated by means of Eqs. (4.4e) to be 0.838. The moment diagrams which correspond to the upper and lower bound as well as the exact value are plotted in Fig. 4.4.

WANSLEBEN¹ was, to our knowledge, the first to point out the simple relation between angular displacements and rotations and thus indicate the possibility of such an iterative procedure. K. BASLER tried for some time to apply these ideas to a continuous member in order to arrive at a convergent iterative procedure. It turned out that an iterative procedure for the continuous case usually does not converge uniformly (e.g. no upper and lower bounds for the solution may be given) and it may even not converge at all. Convergence criteria, on the other hand, may only be given for the most simple cases. The procedure for the single span member, as developed above, does not converge whenever the member constant

$$C_{\beta, B} = \frac{GK}{EI} \frac{\operatorname{tg}^2 \delta}{3}$$

is equal to or greater than one.

The rigorous analytical procedure in the following section was developed to test the quality of the iteration. It turned out to be so surprisingly simple that an iteration will offer no advantage in many cases.

4.2 Analytical Solution

a) Slope at Skew Supports

The determination of the slope at the supports must include the correction necessary for horizontal but skewed supports:

$$\left. \begin{aligned} \alpha_i &= \alpha_{i0} + M_k \alpha_{ik} + M_{k+1} \alpha_{ik+1} + \Delta M_{ki} \alpha_{ik} + \Delta M_{k+1i} \alpha_{ik+1} \\ \beta_i &= \beta_{i0} + M_k \beta_{ik} + M_{k+1} \beta_{ik+1} + \Delta M_{ki} \beta_{ik} + \Delta M_{k+1i} \beta_{ik+1}. \end{aligned} \right\} \quad (4.5)$$

Introducing the corrections as expressed by Eqs. (4.3).

$$\alpha_i = \alpha_{i0} + M_k \alpha_{ik} + M_{k+1} \alpha_{ik+1} + T_i (\alpha_{ik} \operatorname{tg} \delta_k + \alpha_{ik+1} \operatorname{tg} \delta_{k+1}),$$

$$\beta_i = \beta_{i0} + M_k \beta_{ik} + M_{k+1} \beta_{ik+1} + T_i (\beta_{ik} \operatorname{tg} \delta_k + \beta_{ik+1} \operatorname{tg} \delta_{k+1}).$$

¹ WANSLEBEN, F.: Beitrag zur Berechnung schiefer, drillsteifer Brücken. Stahlbau 24 (1955) 224.

The torsional moment T_i is given by Eq. (4.2) and the resulting expression may be simplified by means of the member constants defined in Table 4.2.

$$\alpha_i = \alpha_{i0} + M_k \alpha_{ik} + M_{k+1} \alpha_{ik+1} - \alpha_i C_{iak} - \beta_i C_{iak+1}$$

$$\beta_i = \beta_{i0} + M_k \beta_{ik} + M_{k+1} \beta_{ik+1} - \alpha_i C_{i\beta k} - \beta_i C_{i\beta k+1}.$$

These equations take the following form when arranged in terms of member and load dependent elements:

$$\left. \begin{aligned} \alpha_i(1 + C_{iak}) + \beta_i C_{iak+1} &= \alpha_{i0} + M_k \alpha_{ik} + M_{k+1} \alpha_{ik+1} \\ \alpha_i C_{i\beta k} &+ \beta_i(1 + C_{i\beta k+1}) = \beta_{i0} + M_k \beta_{ik} + M_{k+1} \beta_{ik+1}. \end{aligned} \right\} \quad (4.6)$$

Since $C_{iak} C_{i\beta k+1} = C_{i\beta k} C_{iak+1}$, the determinant of the matrix elements takes the simple form:

$$D_i = 1 + C_{iak} + C_{i\beta k+1}.$$

The solutions of the system of equations (4.6) are therefore as follows:

$$\left. \begin{aligned} \alpha_i &= \frac{1}{D_i} [M_k(\alpha_{ik} + \alpha_{ik} C_{i\beta k+1} - \beta_{ik} C_{iak+1}) + \\ &\quad + M_{k+1}(\alpha_{ik+1} + \alpha_{ik+1} C_{i\beta k+1} - \beta_{ik+1} C_{iak+1}) + \\ &\quad + \alpha_{i0} + \alpha_{i0} C_{i\beta k+1} - \beta_{i0} C_{iak+1}] \\ \beta_i &= \frac{1}{D_i} [M_k(\beta_{ik} + \beta_{ik} C_{iak} - \alpha_{ik} C_{i\beta k}) + \\ &\quad + M_{k+1}(\beta_{ik+1} + \beta_{ik+1} C_{iak} - \alpha_{ik+1} C_{i\beta k}) + \\ &\quad + \beta_{i0} + \beta_{i0} C_{iak} - \alpha_{i0} C_{i\beta k}]. \end{aligned} \right\} \quad (4.7)$$

b) Three-Moment Equations

The single spans investigated so far satisfy the support conditions inasmuch as their skewed boundaries are horizontal. A continuous beam, because of continuity in the longitudinal direction, introduces a second compatibility condition of equal and opposite angular displacements of the adjacent members at the supports:

$$\beta_{i-1} + \alpha_i = 0. \quad (4.8)$$

The first of the Eqs. (4.7) provides an expression for the angle α_i , while a reduction of the subscripts i and k by one in the second equation yields the angle β_{i+1} . As in the case of the well known three-moment equations for continuous beams on freely rotating supports, the relation resulting from condition (4.8) may be arranged in various ways. Both the load and member properties may either appear in the factors of the unknown support moments M_{k-1} , M_k and M_{k+1} or the load dependent elements may be put separately on the right side of the

equal sign. The relations given hereinafter utilize the second way of presenting the three-moment equations for the skew supported, continuous member. The three-moment equations will be given four times in order of increasing system regularity. The general case is followed by the case which assumes constant flexural and torsional rigidity within any one span (Special Case 1), the case assuming in addition constant skew angle of the supports is Special Case 2 and finally the case with both constant rigidities and constant skew angle of supports over the entire system is Special Case 3.

$$\text{General case} \quad \begin{cases} \text{Variable cross section: } EI(z), GK(z), \\ \text{Different skew angles of supports: } \delta_{k-1} \neq \delta_k \neq \delta_{k+1}. \end{cases}$$

$$\begin{aligned} & M_{k-1} (\beta_{i-1k-1} + \beta_{i-1k-1} C_{i-1\alpha k-1} - \alpha_{i-1k-1} C_{i-1\beta k-1}) D_i + \\ & + M_k [(\beta_{i-1k} + \beta_{i-1k} C_{i-1\alpha k-1} - \alpha_{i-1k} C_{i-1\beta k-1}) D_i + \\ & + (\alpha_{ik} + \alpha_{ik} C_{i\beta k+1} - \beta_{ik} C_{i\alpha k+1}) D_{i-1}] + \\ & + M_{k+1} (\alpha_{ik+1} + \alpha_{ik+1} C_{i\beta k+1} - \beta_{ik+1} C_{i\alpha k+1}) D_{i-1} = \\ & = - [(\beta_{i-10} + \beta_{i-10} C_{i+1\alpha k-1} - \alpha_{i-10} C_{i-1\beta k-1}) D_i + \\ & + (\alpha_{i0} + \alpha_{i0} C_{i\beta k+1} - \beta_{i0} C_{i\alpha k+1}) D_{i-1}], \end{aligned} \quad (4.9)$$

for displacements α, β : v. Table 4.1, first column,
member constants C, D : v. Table 4.2, first column,

subscripts k, i : v. Fig. 4.2 ($k = 1, 3, 5, \dots$,
 $i = 2, 4, 6, \dots$).

$$\text{Special Case 1} \quad \begin{cases} \text{Cross section constant within one span: } EI_i, GK_i, \\ \text{Different skew angles of supports: } \delta_{k-1} \neq \delta_k \neq \delta_{k+1}. \end{cases}$$

The values from the second column of table 4.1 and 4.2 are introduced into formula (4.9).

$$\begin{aligned} & M_{k-1} \frac{l_{i-1}}{6EI_{i-1}} \left(1 - \frac{GK_{i-1}}{EI_{i-1}} \frac{\operatorname{tg} \delta_{k-1} \operatorname{tg} \delta_k}{2} \right) D_i + \\ & + M_k \left[\frac{l_{i-1}}{6EI_{i-1}} \left(2 + \frac{GK_{i-1}}{EI_{i-1}} \frac{\operatorname{tg}^2 \delta_{k-1}}{2} \right) D_i + \frac{l_i}{6EI_i} \left(2 + \frac{GK_i}{EI_i} \frac{\operatorname{tg}^2 \delta_{k+1}}{2} \right) D_{i-1} \right] + \\ & + M_{k+1} \frac{l_i}{6EI_i} \left(1 - \frac{GK_i}{EI_i} \frac{\operatorname{tg} \delta_k \operatorname{tg} \delta_{k+1}}{2} \right) D_{i-1} = \\ & = \left[\alpha_{i-10} \frac{GK_{i-1} \operatorname{tg} \delta_{k-1} + 2 \operatorname{tg} \delta_k \operatorname{tg} \delta_{k-1}}{6} - \beta_{i-10} \left(1 + \frac{GK_{i-1} 2 \operatorname{tg} \delta_{k-1} + \operatorname{tg} \delta_k \operatorname{tg} \delta_{k-1}}{6} \right) \right] D_i + \\ & + \left[\beta_{i0} \frac{GK_i 2 \operatorname{tg} \delta_k + \operatorname{tg} \delta_{k+1} \operatorname{tg} \delta_{k+1}}{6} - \alpha_{i0} \left(1 + \frac{GK_i \operatorname{tg} \delta_k + 2 \operatorname{tg} \delta_{k+1} \operatorname{tg} \delta_{k+1}}{6} \right) \right] D_{i-1}, \end{aligned} \quad (4.10)$$

where:

$$D_{i-1} = 1 + \frac{GK_{i-1} \operatorname{tg}^2 \delta_{k-1} + \operatorname{tg} \delta_{k-1} \operatorname{tg} \delta_k + \operatorname{tg}^2 \delta_k}{3},$$

$$D_i = 1 + \frac{GK_i \operatorname{tg}^2 \delta_k + \operatorname{tg} \delta_k \operatorname{tg} \delta_{k+1} + \operatorname{tg}^2 \delta_{k+1}}{3}$$

and:

$$\begin{pmatrix} k = 1, 3, 5, \dots \\ i = 2, 4, 6, \dots \end{pmatrix}.$$

The ratio GK_i/EI_i is quite often approximately constant. This leads to a further simplification, as follows:

$$\text{Special Case 2} \quad \begin{cases} \text{Cross section: } EI = EI_i = \text{constant within span,} \\ GK/EI = \text{constant for entire system,} \\ \text{Same skew angle at each support: } \delta_k = \delta_{k+1} = \delta. \end{cases}$$

$$\begin{aligned} M_{k-1} \frac{l_{i-1}}{6EI_{i-1}} (1 - C) + M_k \cdot \left(\frac{l_{i-1}}{6EI_{i-1}} + \frac{l_i}{6EI_i} \right) (2 + C) + M_{k+1} \frac{l_i}{6EI_i} (1 - C) \\ = -[(\beta_{i-10} + \alpha_{i0}) (1 + C) - (\alpha_{i-10} + \beta_{i0}) C], \end{aligned} \quad (4.11)$$

where:

$$C = \frac{GK}{EI} \frac{\operatorname{tg}^2 \delta}{2}, \quad \begin{pmatrix} k = 1, 3, 5, \dots \\ i = 2, 4, 6, \dots \end{pmatrix}.$$

$$\text{Special Case 3} \quad \begin{cases} \text{Constant cross section along the entire beam,} \\ \text{Same skew angle at each support.} \end{cases}$$

$$\begin{aligned} M_{k-1} l_{i-1} (1 - C) + M_k (l_{i-1} + l_i) (2 + C) + M_{k+1} l_i (1 - C) \\ = -6EI[-\alpha_{i-10} C + (\beta_{i-10} + \alpha_{i0}) (1 + C) - \beta_{i0} C], \end{aligned} \quad (4.12)$$

where:

$$C = \frac{GK}{EI} \frac{\operatorname{tg}^2 \delta}{2}, \quad \begin{pmatrix} k = 1, 3, 5, \dots \\ i = 2, 4, 6, \dots \end{pmatrix}.$$

c) Forces and Deformations

The torsional moment induced by skewed supports is given by Eq. (4.2) wherein the support displacements α_i and β_i are determined by the expressions (4.7). Considering that

$$C_{i\beta k+1} \operatorname{tg} \delta_k = C_{i\beta k} \operatorname{tg} \delta_{k+1}$$

and

$$C_{i\alpha k} \operatorname{tg} \delta_{k+1} = C_{i\alpha k+1} \operatorname{tg} \delta_k,$$

the torsional moment in span i for the most general case (cross section variable and skew angle different from support to support) may be given by the expression:

$$\begin{aligned} T_i = \frac{-1}{\gamma_i D_i} [\alpha_{i0} \operatorname{tg} \delta_k + \beta_{i0} \operatorname{tg} \delta_{k+1} + M_k (\alpha_{ik} \operatorname{tg} \delta_k + \beta_{ik} \operatorname{tg} \delta_{k+1}) + \\ + M_{k+1} (\alpha_{ik+1} \operatorname{tg} \delta_k + \beta_{ik+1} \operatorname{tg} \delta_{k+1})] \end{aligned} \quad (4.13)$$

The determinant D_i is listed in the first column of table 4.2.

Expression (4.13) may be given in a more explicit manner for the special cases defined above.

Special Case 1 (EI_i, GK_i constant within one span, $\delta_k \neq \delta_{k+1}$):

$$T_i = -\frac{\frac{6EI_i}{l_i}(\alpha_{i0} \operatorname{tg} \delta_k + \beta_{i0} \operatorname{tg} \delta_{k+1}) + M_k(2 \operatorname{tg} \delta_k + \operatorname{tg} \delta_{k+1}) + M_{k+1}(\operatorname{tg} \delta_k + 2 \operatorname{tg} \delta_{k+1})}{6 \frac{EI_i}{GK_i} + 2(\operatorname{tg}^2 \delta_k + \operatorname{tg} \delta_k \operatorname{tg} \delta_{k+1} + \operatorname{tg}^2 \delta_{k+1})}. \quad (4.14)$$

Special Case 2 and 3 (EI_i, GK_i constant within one span and same skew angle at each support, $\delta_k = \delta_{k+1} = \delta$):

$$T_i = -\frac{\operatorname{tg} \delta}{\frac{EI_i}{GK_i} + \operatorname{tg}^2 \delta} \left[\frac{EI_i(\alpha_{i0} + \beta_{i0})}{l_i} + \frac{M_k + M_{k+1}}{2} \right] \quad (4.15a)$$

or with the substitution $C_i = \frac{GK_i}{EI_i} \frac{\operatorname{tg}^2 \delta}{2}$

$$T_i = -\frac{1}{\operatorname{tg} \delta} \frac{2C_i}{1 + 2C_i} \left[\frac{EI_i(\alpha_{i0} + \beta_{i0})}{l_i} + \frac{M_k + M_{k+1}}{2} \right]. \quad (4.15b)$$

The interpretation of the expression in brackets is as follows: $EI_i \alpha_{i0}$ represents (according to the conjugate beam method) the fictitious support reaction at the left end of member i which is loaded by the moment area M_{i0} . $EI_i \beta_{i0}$ is the corresponding reaction at the opposite member end. The sum of these two reactions is thus equal to the moment area. The first term in the brackets may therefore be written as:

$$\frac{EI_i(\alpha_{i0} + \beta_{i0})}{l_i} = \frac{\int_0^{l_i} M_{i0} dz}{l_i}. \quad (4.16)$$

It is equal to the average moment due to the applied loads in the member i . For a concentrated load P , it becomes

$$\frac{EI_i(\alpha_{i0} + \beta_{i0})}{l_i} = \frac{1}{2} M_{\max} = \frac{a_i b_i}{2 l_i} P \quad (4.16a)$$

and for a uniformly distributed load P ,

$$\frac{EI_i(\alpha_{i0} + \beta_{i0})}{l_i} = \frac{2}{3} M_{\max} = \frac{p l_i^2}{12}. \quad (4.16b)$$

The evaluation of the moment at any point along span i requires a knowledge of the end moments of the member. These end moments are designated as M_{ki} and M_{k+1i} and may be expressed by means of Eq. (4.3) in the form:

$$\left. \begin{aligned} M_{ki} &= M_k + \Delta M_{ki} = M_k + T_i \operatorname{tg} \delta_k, \\ M_{k+1i} &= M_{k+1} + \Delta M_{k+1i} = M_{k+1} + T_i \operatorname{tg} \delta_{k+1}. \end{aligned} \right\} \quad (4.17)$$

The moment at any point along the span is conveniently expressed as the superposition of simple beam moment and the proportionate contribution of the end moments which, written in terms of the nondimensional coordinates, $\zeta_i = z_i/l_i$ and $\zeta'_i = z'_i/l_i$, is:

$$M_i = M_{i0} + M_{ki} \zeta'_i + M_{k+1i} \zeta_i. \quad (4.18)$$

In order to plot the moment diagram one may advantageously plot first the base line between end moments upon which the simple beam moments M_{i0} are superposed.

Based on the end moments in Eq. (4.17), both the end shear Q and the support reactions F may be expressed as follows:

$$Q_i = Q_{i0} + \frac{M_{k+1i} - M_{ki}}{l_i}, \quad (4.19)$$

$$F_k = Q_{ki} - Q_{k+1i}. \quad (4.20)$$

The line of action of the reaction F acts somewhere along the bearing edge of the support but no longer intersects with the member axis even though the applied loads act without eccentricity. The point of application of this reaction has an x -coordinate x_{Fk} as determined by Eq. (4.21):

$$x_{Fk} = \frac{T_i - T_{i-1}}{F_k}. \quad (4.21)$$

The vertical deflection y of the member axis may likewise be determined as the superposition of the different deflection states of the simply supported base system.

$$y_i = y_{i0} + M_{ki} y_{ik} + M_{k+1i} y_{ik+1}. \quad (4.22)$$

Herein are:

y_{i0} = Deflection due to applied loads,

y_{ik} = Deflection due to $M_{ki} = 1$,

y_{ik+1} = Deflection due to $M_{k+1i} = 1$.

The last two deflection coefficients at location z are, according to the Reciprocal Theorem, equal to the angular rotations at the corresponding supports caused by a unit load $P = 1$ at z , i.e. $y_{ik} = \alpha_{i0}$ and $y_{ik+1} = \beta_{i0}$. Both α_{i0} and β_{i0} are listed in table 4.1 (in the section valid for the concentrated load $P = 1$).

Expressions for the vertical deflection of member locations which do not coincide with the member axis must include the torsional rotation φ . If this rotation is measured from a horizontal line and is positive when directed as shown in Fig. 4.2, it can be given by the expression:

$$\varphi(z_i) = \varphi(z_i = 0) + \int_0^{z_i} \varphi' dz. \quad (4.23)$$

Since in skew supported members $\varphi(z_i = 0) = \alpha_i \operatorname{tg} \delta_k$ (v. Fig. 4.3) and since, in Saint-Venant torsion $\varphi' = T/GK$, the relation given above may be

rewritten as

$$\varphi(z_i) = \alpha_i \operatorname{tg} \delta_k + \int_0^{z_i} \frac{T}{GK} dz. \quad (4.24)$$

where the angle α_i is given by Eq. (4.7).

d) Example: Three-Span Continuous Beam

The continuous beam shown in Fig. 4.5 is of uniform bending stiffness EI , uniform torsional rigidity GK and has identical skew angles δ at each support. It is subjected to the uniformly distributed load p acting only on the mid-span.

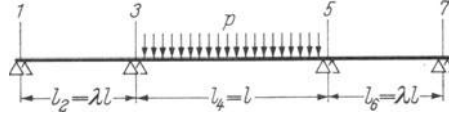


Fig. 4.5. Three-Span Continuous Beam.

The symmetries in both the system and load result in symmetry of the moments, i.e., $M_3 = M_5$, which reduces the general system (4.12) to one single equation:

$$M_3 l(\lambda + 1)(2 + C) + M_3 l(1 - C) = -6EI \left[+\frac{pl^3}{24EI} (1 + C) - \frac{pl^3}{24EI} C \right]$$

where

$$C = \frac{GK}{EI} \frac{\operatorname{tg}^2 \delta}{2},$$

from which:

$$M_3 = -\frac{3}{3 + 2\lambda + \lambda C} \frac{pl^2}{12}.$$

The quantities defined by Eqs. (4.15) to (4.21) may now be written explicitly as follows:

$$T_2 = T_6 = -\frac{2}{\operatorname{tg} \delta} \frac{C}{1 + 2C} \frac{M_3}{2} = +\frac{1}{\operatorname{tg} \delta} \frac{3C}{(1 + 2C)(3 + 2\lambda + \lambda C)} \frac{pl^2}{12}, \quad (4.25a)$$

$$T_4 = -\frac{2}{\operatorname{tg} \delta} \frac{C}{1 + 2C} \left(\frac{pl^2}{12} + M_3 \right) = -\frac{1}{\operatorname{tg} \delta} \frac{2\lambda C(2 + C)}{(1 + 2C)(3 + 2\lambda + \lambda C)} \frac{pl^2}{12}, \quad (4.25b)$$

$$M_{12} = M_{76} = T_2 \operatorname{tg} \delta = +\frac{3C}{(1 + 2C)(3 + 2\lambda + \lambda C)} \frac{pl^2}{12}, \quad (4.25c)$$

$$M_{32} = M_{56} = M_3 + T_2 \operatorname{tg} \delta = -\frac{3(1 + C)}{(1 + 2C)(3 + 2\lambda + \lambda C)} \frac{pl^2}{12}, \quad (4.25d)$$

$$M_{34} = M_{54} = M_3 + T_4 \operatorname{tg} \delta = -\frac{3 + 6C + 4\lambda C + 2\lambda C^2}{(1 + 2C)(3 + 2\lambda + \lambda C)} \frac{pl^2}{12}, \quad (4.25e)$$

$$Q_2 = -Q_6 = 0 + \frac{M_{32} - M_{12}}{\lambda l} = -\frac{1}{4\lambda(3 + 2\lambda + \lambda C)} pl, \quad (4.25f)$$

$$Q_4 = \left(\frac{1}{2} - \zeta_4\right) p l, \quad (4.25g)$$

$$F_1 = F_7 = Q_2 = -\frac{1}{4\lambda(3 + 2\lambda + \lambda C)} p l, \quad (4.25h)$$

$$F_3 = F_5 = \frac{p l}{2} - Q_2 = +\frac{2\lambda(3 + 2\lambda + \lambda C) + 1}{4\lambda(3 + 2\lambda + \lambda C)} p l, \quad (4.25i)$$

$$x_{F1} = -x_{F7} = \frac{T_2}{Q_2} = -\frac{1}{\operatorname{tg} \delta} \frac{\lambda C}{1 + 2C} l, \quad (4.25k)$$

$$x_{F3} = -x_{F5} = \frac{T_4 - T_2}{F_3} = -\frac{\lambda C}{3 \operatorname{tg} \delta} \cdot \frac{3 + 4\lambda + 2\lambda C}{(1 + 2C)(1 + 6\lambda + 4\lambda^2 + 2\lambda^2 C)} l. \quad (4.25l)$$

The foregoing expressions for the moments and some of the expressions for the shears and reactions may be checked as applied to the following limiting cases:

Supports without skew. The angle of the supports $\delta = 0$ corresponds to vanishing values for $\operatorname{tg} \delta$, C and $C/\operatorname{tg} \delta$ thus leading to $M_3 = M_{32} = M_{34} = -p l^2/(12 + 8\lambda)$ which is the expression for the support moment of the ordinary, continuous, three-span beam with a uniformly loaded central span. The torsional moments T_2 and T_4 vanish as does the eccentricity of the support reactions.

Fixed Ends of the Central Span: One arrives at fixed ends of the central span when the length of the outer spans is thought to approach zero in the limit. The constant $\lambda = 0$ leads, as expected, to $T_4 = 0$ and $M_3 = M_{34} = -p l^2/12$.

The Center Span as a Simply Supported Beam: Outer spans of infinite length do not offer any restraint to the central span which thus becomes equivalent to a simply supported beam. The limiting values corresponding to $\lambda \rightarrow \infty$ are:

$$\begin{aligned} T_4 &= -\frac{1}{\operatorname{tg} \delta} \frac{2C}{1 + 2C} \frac{p l^2}{12} = T, \\ M_{34} &= -\frac{2C}{1 + 2C} \frac{p l^2}{12} = M_s, \end{aligned} \quad (4.26)$$

$$x_{F3} = -x_{F5} = -\frac{l}{3 \operatorname{tg} \delta} \frac{C}{1 + 2C} = x_F.$$

Some numerical values for the moments, shears and eccentricities of the reactions will be given hereinafter. They were calculated for the system with three equal spans, $\lambda = 1$, and for a realistic ratio between torsional and flexural rigidity.

It will be shown in Section 4.4a that it is realistic to assume that narrow, rectangular solid or hollow cross sections have a ratio GK/EI of about 2. This introduces the simplification $C = \operatorname{tg}^2 \delta$ or $\operatorname{tg} \delta = \sqrt{C}$.

These assumptions reduce formulas (4.25) to the expressions given in the first column of Table 4.3. The values of these expressions are initially calculated for simple squared supports, then for small deviations ($\delta \sim \operatorname{tg} \delta$) from the simply supported case and finally for increasing skew angles of $\delta = 26.5^\circ, 35^\circ, 45^\circ, 55^\circ$ up to the fictitious limiting case $\delta = 90^\circ$.

A few numerical results are plotted in Fig. 4.6. This figure shows at the top a plan view of the system including the points of action of the support reactions for the angle $\delta = 45^\circ$. It may be observed that the reactions act everywhere on the side of the support which is closer to the loaded central span. This sketch is followed by the diagrams for the bending moments, torsional moments and shearing forces.

Table 4.3. Numerical Values for Different Support Skew Angles δ
 (System and Load According to Fig. 4.5, $\lambda = 1$, $GK/EI = 2$)

$\delta:$	arbitrary	0	$\approx \operatorname{tg} \delta$	26,5°	35°	45°	55°	90°
$C:$	$\operatorname{tg}^2 \delta$	0	$\ll 1$	0,25	0,5	1	2	∞
$12 \frac{T_2}{pl^2}:$	$+\frac{3\sqrt{C}}{(1+2C)(5+C)}$	0	$+0,6\delta$	+0,190	+0,193	+0,167	+0,121	+0
$12 \frac{T_4}{pl^2}:$	$-\frac{2\sqrt{C}(2+C)}{(1+2C)(5+C)}$	0	$-0,8\delta$	-0,286	-0,322	-0,333	-0,323	-0
$12 \frac{M_{12}}{pl^2}:$	$+\frac{3C}{(1+2C)(5+C)}$	0	0	+0,095	+0,136	+0,167	+0,171	0
$12 \frac{M_{32}}{pl^2}:$	$-\frac{3(1+C)}{(1+2C)(5+C)}$	-0,6	-0,6	-0,476	-0,409	-0,333	-0,257	-0
$12 \frac{M_{34}}{pl^2}:$	$-\frac{3+10C+2C^2}{(1+2C)(5+C)}$	-0,6	-0,6	-0,715	-0,773	-0,833	-0,885	-1
$\frac{Q_2}{pl}:$	$-\frac{1}{4(5+C)}$	-0,05	-0,05	-0,048	-0,045	-0,042	-0,036	-0
$\frac{x_{F1}}{l}:$	$-\frac{\sqrt{C}}{1+2C}$	0	$-\delta$	-0,333	-0,356	-0,333	-0,283	-0
$\frac{x_{F3}}{l}:$	$-\frac{\sqrt{C}(7+2C)}{3(11+24C+4C^2)}$	0	$-0,21\delta$	-0,072	-0,079	-0,077	-0,070	-0

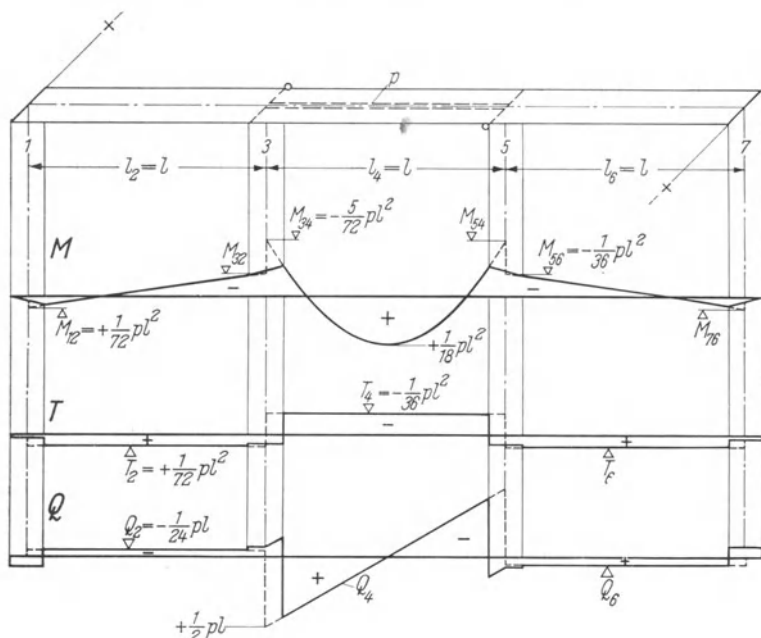


Fig. 4.6. Diagrams for the Bending Moments, Torsional Moments and Shearing Forces Caused by the Uniformly Distributed Load on the Central Span.

It is clearly apparent from the presented results that an increased value for C results in an increased restraint of the member at the support. The change induced in the bending moments, however, is quite different from the change in the torsional moments. This is illustrated by Figs. 4.7 and 4.8. While an increase of the skew angle to $\delta = 10^\circ$ does not change the bending moments appreciably, the torsional moments have already reached the half of their maximum value. This is another validation of the effectiveness of the iteration procedure presented in Section 4.1d in the case of small angles δ .

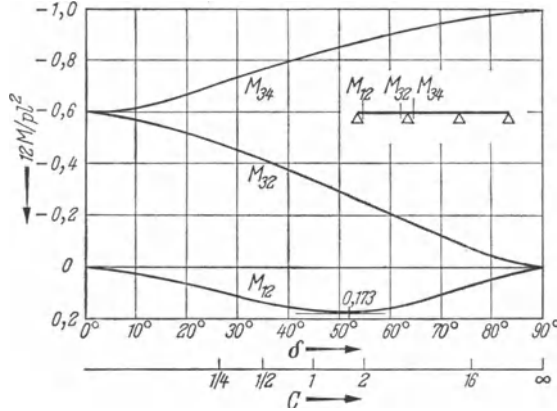


Fig. 4.7. Bending Moments as a Function of the Skew Angle δ .

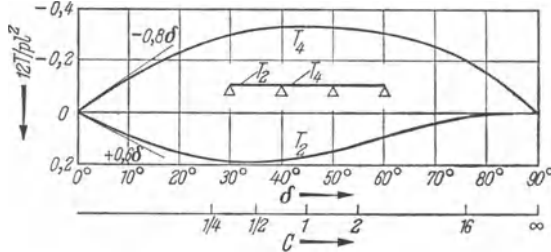


Fig. 4.8. Torsional Moments as a Function of the Skew Angle δ .

The bending moments in the central span vary almost uniformly from the simply supported, continuous beam ($\delta = 0$) to the beam on fixed supports ($\delta = 90^\circ$). The torsional moments, on the other hand, decrease with increasing large skew angle δ . Eq. (4.2) shows that this is due to the fact that the torsional moment not only increases with increasing skew angle but also with the sum of the angular displacements at the supports. The latter vanish in the case of fixed supports thus yielding zero torsional moments.

Exercise 4.1. *Skew Supported, Two-Span Beam.* Calculate the torsional moments, bending moments and shearing forces in a prismatic, continuous beam across two equal spans ($l_2 = l_4 = l$) and with equal skew angles of the three supports ($\delta_1 = \delta_3 = \delta_5 = \delta$):

- for dead load g ,
- for equally distributed live load on one span (e.g. $p_2 = p, p_4 = 0$).

Solutions:

$$C = \frac{GK}{EI} \frac{\operatorname{tg}^2 \delta}{2}.$$

Case a): Dead Load g

Torsional Moments:

$$T_2 = T_4 = -\frac{1}{\operatorname{tg} \delta} \frac{C}{2 + C} \frac{gl^2}{12}.$$

Bending Moments in Span 2 ($\zeta_2 = \zeta$, $\zeta'_2 = 1 - \zeta$):

$$M_2 = \frac{gl^2}{2} \zeta(1 - \zeta) - \frac{C + 3\zeta}{2 + C} \frac{gl^2}{12}.$$

M_4 and M_2 are symmetric with respect to the vertical line through the moment diagram at support 3.

Shearing Forces in Span 2 ($\zeta_2 = \zeta$):

$$Q_2 = \left(\frac{1}{2} - \zeta - \frac{1}{4(2+C)} \right) gl.$$

Q_4 and Q_2 are radially symmetric with respect to support 3.

Case b): Uniformly Distributed Load on Span 2

Torsional Moments:

$$T_2 = -\frac{pl^2}{\operatorname{tg} \delta} \frac{C(5+4C)}{24(2+C)(1+2C)}, \quad T_4 = \frac{pl^2}{\operatorname{tg} \delta} \frac{C}{8(2+C)(1+2C)}.$$

Support Moments based on $M_3 = -\frac{pl^2}{8(2+C)}$:

$$M_{12} = M_3 \frac{C(5+4C)}{3(1+2C)}, \quad M_{32} = M_3 \frac{3+11C+4C^2}{3(1+2C)},$$

$$M_{34} = M_3 \frac{1+C}{1+2C}, \quad M_{54} = -M_3 \frac{C}{1+2C}.$$

Shearing Forces:

$$Q_2 = \left(\frac{1}{2} - \zeta - \frac{1}{8(2+C)} \right) pl, \quad Q_4 = \frac{1}{8(2+C)} pl.$$

Remark: The support reactions together with their points of action may be determined from Eqs. (4.20) and (4.21). The diagrams of the bending moments, torsional moments and shearing forces are plotted in connection with the solution to Exercise 4.3, near the end of this chapter.

4.3 Eccentric Loads

a) Decomposition of Loads

Our understanding of the behavior of skew supported, continuous beams is now extended to include loads that are still vertical but which no longer act at the central axis of the member.

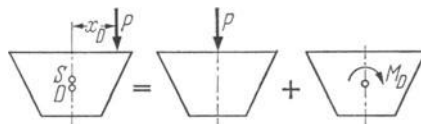


Fig. 4.9. Decomposition of Load.

The principle of superposition (small deformations and elasticity of material described by Hooke's law), permits analysis to be based on the effects of a single concentrated load P as shown in Fig. 4.9. The effect of load P at any location

is the same as the superposed effects of the load P acting in the plane of symmetry of the member and the concentrated torsional moment $M_D = Px_D$.

The additional problem to be considered in this section therefore deals with the effects of the applied torsional moment M_D on the skew supported, continuous beam. It will turn out that the three-moment equations given in section 4.2b may be utilized for this load as well.

b) System Acted Upon by a Concentrated Moment

The following investigation will again be based on the statically indeterminate base system of span i as shown in Fig. 4.10. The concentrated torsional moment M_{Di} acts at a distance a_i away from support k and distance b_i away from support $k+1$ (Fig. 4.10a).

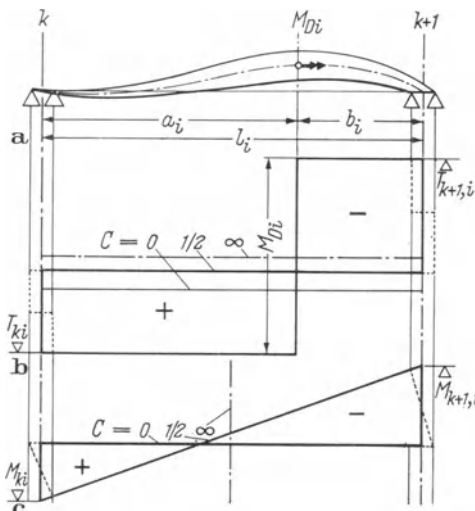


Fig. 4.10. Member i Acted Upon by a Concentrated Torsional Moment.

The torsional moment is no longer constant along the entire length of the member i but only within the sections of length a_i and b_i where it is equal to T_{ki} or $T_{k+1,i}$, respectively as shown in (Fig. 4.10 b). A displacement coefficient γ will be defined as follows:

General Case $GK_i = \text{konst.}$

$$\left. \begin{array}{lll} \gamma(z_i): & \int_0^{z_i} \frac{dz}{GK} & \frac{z_i}{GK_i} \\ \text{resp.} & \gamma(a_i): & \int_0^{a_i} \frac{dz}{GK} & \frac{a_i}{GK_i} \\ \text{and} & \gamma(b_i): & \int_0^{b_i} \frac{dz}{GK} & \frac{b_i}{GK_i} \end{array} \right\} \quad (4.27)$$

where

$$\gamma(a_i) + \gamma(b_i) = \gamma_i.$$

The equilibrium condition requires that the change in the torsional moment at $z = a_i$ has to be equal to the moment M_{Di} .

$$T_{ki} - T_{k+1i} = M_{Di}. \quad (4.28)$$

This relation is supplemented by the compatibility condition (4.1)

$$\alpha_i \operatorname{tg} \delta_k + T_{ki} \int_0^{a_i} \frac{dz}{GK} + T_{k+1i} \int_0^{b_i} \frac{dz}{GK} + \beta_i \operatorname{tg} \delta_{k+1} = 0. \quad (4.29)$$

Eqs. (4.28) and (4.29) may be solved for the torsional moments T_{ki} and T_{k+1i} which leads to the following relations when the definitions (4.27) are considered:

$$\left. \begin{aligned} T_{ki} &= +M_{Di} \frac{\gamma(b_i)}{\gamma_i} - \frac{\alpha_i \operatorname{tg} \delta_k + \beta_i \operatorname{tg} \delta_{k+1}}{\gamma_i}, \\ T_{k+1i} &= -M_{Di} \frac{\gamma(a_i)}{\gamma_i} - \frac{\alpha_i \operatorname{tg} \delta_k + \beta_i \operatorname{tg} \delta_{k+1}}{\gamma_i}. \end{aligned} \right\} \quad (4.30)$$

The relation between torsional moment and support moment, which necessarily reflects the influence of skew supports, is a consequence of the same considerations which previously led to Eqs. (4.3).

$$\left. \begin{aligned} \Delta M_{ki} &= T_{ki} \operatorname{tg} \delta_k, \\ \Delta M_{k+1i} &= T_{k+1i} \operatorname{tg} \delta_{k+1}. \end{aligned} \right\} \quad (4.31)$$

The total angular displacement at the supports may again be considered to be the superposition of different influences. The displacements α_{i0} and β_{i0} will be missing, however, leaving only the effects of the support moments M_k and M_{k+1} and their corrections ΔM_{ki} and ΔM_{k+1i} .

$$\left. \begin{aligned} \alpha_i &= M_k \alpha_{ik} + M_{k+1} \alpha_{ik+1} + \Delta M_{ki} \alpha_{ik} + \Delta M_{k+1i} \alpha_{ik+1}, \\ \beta_i &= M_k \beta_{ik} + M_{k+1} \beta_{ik+1} + \Delta M_{ki} \beta_{ik} + \Delta M_{k+1i} \beta_{ik+1}. \end{aligned} \right\} \quad (4.32)$$

The corrections ΔM_{ki} and ΔM_{k+1i} are given by Eqs. (4.31).

$$\begin{aligned} \alpha_i &= M_k \alpha_{ik} + M_{k+1} \alpha_{ik+1} + T_{ki} \alpha_{ik} \operatorname{tg} \delta_k + T_{k+1i} \alpha_{ik+1} \operatorname{tg} \delta_{k+1}, \\ \beta_i &= M_k \beta_{ik} + M_{k+1} \beta_{ik+1} + T_{ki} \beta_{ik} \operatorname{tg} \delta_k + T_{k+1i} \beta_{ik+1} \operatorname{tg} \delta_{k+1}. \end{aligned}$$

If finally the torsional moments T_{ki} and T_{k+1i} are introduced as given in Eqs. (4.30) and if the equations are ordered with respect to α_i and β_i , then these two equations may, by means of the substitutions

$$\left. \begin{aligned} \alpha_{iD} &= M_{Di} \frac{\gamma(b_i) \alpha_{ik} \operatorname{tg} \delta_k - \gamma(a_i) \alpha_{ik+1} \operatorname{tg} \delta_{k+1}}{\gamma_i}, \\ \beta_{iD} &= M_{Di} \frac{\gamma(b_i) \beta_{ik} \operatorname{tg} \delta_k - \gamma(a_i) \beta_{ik+1} \operatorname{tg} \delta_{k+1}}{\gamma_i} \end{aligned} \right\} \quad (4.33)$$

and the abbreviations defined in Table 4.2, be written in the following compact form:

$$\left. \begin{aligned} \alpha_i(1 + C_{i\alpha k}) + \beta_i C_{i\alpha k+1} &= M_k \alpha_{ik} + M_{k+1} \alpha_{ik+1} + \alpha_{iD}, \\ \alpha_i C_{i\beta k} + \beta_i(1 + C_{i\beta k+1}) &= M_k \beta_{ik} + M_{k+1} \beta_{ik+1} + \beta_{iD}. \end{aligned} \right\} \quad (4.34)$$

It was to be expected that these equations would deviate from those derived earlier (4.6) only in the load dependent elements. The generalized displacements α_{iD} and β_{iD} appear in place of α_{i0} and β_{i0} . The analysis of the system for a concentrated moment is thus reduced to the one conducted in Section 4.2. The three-moment equation developed therein may be used for this type of load if the corresponding generalized displacements given in Eq. (4.33) are used.

The calculation of the forces in the member follows exactly the pattern previously exhibited in Section 4.2c. The expressions for the torsional moments (4.13), (4.14) and (4.15), however, have to be modified slightly as a consequence of the moment M_{Di} . According to Eqs. (4.30) one has either to add the term $M_{Di}\gamma(b_i)/\gamma_i$ or to subtract the term $M_{Di}\gamma(a_i)/\gamma_i$ depending on whether the section is assumed to be to the left or to the right of the moment M_{Di} .

A single-span member of length l and with constant flexural and torsional rigidities EI and GK respectively, and having supports of the same skew angle δ will be analyzed as an example. The member is acted upon by the moment M_D at a distance a away from support A and at a distance b away from support B .

Eqs. (4.33) determine the generalized displacements α_D and β_D :

$$\begin{aligned} \alpha_D &= M_D \left[\frac{b}{l} \frac{l}{3EI} - \frac{a}{l} \frac{l}{6EI} \right] \operatorname{tg} \delta, \\ \beta_D &= M_D \left[\frac{b}{l} \frac{l}{6EI} - \frac{a}{l} \frac{l}{3EI} \right] \operatorname{tg} \delta, \end{aligned}$$

which, when introduced into Eq. (4.15b), lead to:

$$T = -M_D \frac{C}{1 + 2C} \frac{b - a}{l}$$

whereupon the torsional moments become:

$$\left. \begin{aligned} T_A &= M_D \frac{b}{l} - M_D \frac{C}{1 + 2C} \frac{b - a}{l}, \\ T_B &= -M_D \frac{a}{l} - M_D \frac{C}{1 + 2C} \frac{b - a}{l}. \end{aligned} \right\} \quad (4.35)$$

The first term in these expressions represents the torsional moment in a fixed-end member whereas the second term may be shown graphically to involve simply a reorientation of this moment diagram to a new base line. The shift of the base line depends on the skewness of the supports [expressed by the factor $C/(1 + 2C)$] and on the position of the applied, concentrated load M_D . There occurs no displacement of the base line whenever the skew angle δ of the supports vanishes ($C = 0$) or whenever the load M_D acts at the center of the member ($a = b$).

The changes in the bending moments at the supports are determined according to expressions (4.31).

The diagrams for both the torsional moments and the bending moments are plotted in Fig. 4.10b and 4.10c for the system properties $a = 2l/3$, $b = l/3$ and $\operatorname{tg} \delta = \sqrt{C}$.

The angular displacements at the supports are computed by means of Eqs. (4.32).

$$\alpha = \Delta M_A \frac{l}{3EI} + \Delta M_B \frac{l}{6EI} = \frac{M_D l \operatorname{tg} \delta}{6EI} \left(\frac{2b-a}{l} - 3 \frac{C}{1+2C} \frac{b-a}{l} \right),$$

$$\beta = \Delta M_A \frac{l}{6EI} + \Delta M_B \frac{l}{3EI} = \frac{M_D l \operatorname{tg} \delta}{6EI} \left(\frac{b-2a}{l} - 3 \frac{C}{1+2C} \frac{b-a}{l} \right).$$

These expressions are reduced for the given system properties to:

$$\alpha = 0,177 \frac{l M_D}{6EI}, \quad \beta = -0,530 \frac{l M_D}{6EI}.$$

Section 4.2c gives the method to compute the member deformations. They are again plotted in Fig. 4.10a for the geometrical assumptions given above.

c) System Acted Upon by a General Eccentric Load

The method of analysis for a concentrated moment which was explained in detail in the previous section will now be extended to an arbitrary torsional load.

The distribution of the torsional moments in the fixed-end base system (superscript f) shall be designated by $T_{i0}^{(f)}$ while its particular values at the member ends will be called $T_{ki}^{(f)}$ and $T_{k+1i}^{(f)}$. Fig. 3.2 showed specific examples of distributed applied torsional moment together with values at the fixed ends.

Eqs. (4.30) may now be written more generally to yield the fixed-end moments at the supports k and $k+1$ corrected by the effect of the flexural rotation at the corresponding support.

$$\left. \begin{aligned} T_{ki} &= T_{ki}^{(f)} - \frac{\alpha_i \operatorname{tg} \delta_k + \beta_i \operatorname{tg} \delta_{k+1}}{\gamma_i}, \\ T_{k+1i} &= T_{k+1i}^{(f)} - \frac{\alpha_i \operatorname{tg} \delta_k + \beta_i \operatorname{tg} \delta_{k+1}}{\gamma}. \end{aligned} \right\} \quad (4.36)$$

The same reasoning that led from the Eqs. (4.30) to (4.34) leads now to the most general form of Eqs. (4.33) for the generalized displacements.

$$\left. \begin{aligned} \alpha_{iD} &= T_{ki}^{(f)} \alpha_{ik} \operatorname{tg} \delta_k + T_{k+1i}^{(f)} \alpha_{i+k+1} \operatorname{tg} \delta_{k+1}, \\ \beta_{iD} &= T_{ki}^{(f)} \beta_{ik} \operatorname{tg} \delta_k + T_{k+1i}^{(f)} \beta_{i+k+1} \operatorname{tg} \delta_{k+1}. \end{aligned} \right\} \quad (4.37)$$

In order to illustrate this generalization of the theory, the single-span member of constant torsional and flexural rigidity but different skew angles of supports will be analyzed for the uniformly distributed torsional load m_D (moment per unit length). The expressions given for the fixed-end moments in connection with exercise 3.1 (in the position $z_i = 0$ and $z_i = 1$) reduce the general system for the generalized displacements (4.37) to:

$$\left. \begin{aligned} \alpha_{iD} &= \frac{m_D l_i^2}{12 EI_i} (2 \operatorname{tg} \delta_k - \operatorname{tg} \delta_{k+1}), \\ \beta_{iD} &= \frac{m_D l_i^2}{12 EI_i} (\operatorname{tg} \delta_k - 2 \operatorname{tg} \delta_{k+1}). \end{aligned} \right\} \quad (4.38)$$

These expressions reduce further for parallel supports ($\delta_k = \delta_{k+1} = \delta$).

$$\alpha_{iD} = -\beta_{iD} = \frac{m_D l_i^2}{12 EI_i} \cdot \operatorname{tg} \delta. \quad (4.39)$$

An *arbitrary eccentric load* is replaced by a load acting in the vertical plane of symmetry of the member and the torsional load (Fig. 4.9), each causing a certain generalized displacement. The total generalized displacements $\alpha_{i0} + \alpha_{iD}$ and $\beta_{i0} + \beta_{iD}$ are then introduced into the three-moment equations given in Section 4.2b whereupon the redundant quantities M_k may be calculated from the resulting system of equations. The influence of the angular rotations at the supports on the torsional moments in the member may be calculated by means of Eq. (4.13), (4.14) or (4.15). The formulation of Eq. (4.13) for this general eccentric load is:

$$T_i = -\frac{1}{\gamma_i D_i} [(\alpha_{i0} + \alpha_{iD}) \operatorname{tg} \delta_k + (\beta_{i0} + \beta_{iD}) \operatorname{tg} \delta_{k+1} + M_k (\alpha_{ik} \operatorname{tg} \delta_k + \beta_{ik} \operatorname{tg} \delta_{k+1}) + M_{k+1} (\alpha_{i k+1} \operatorname{tg} \delta_k + \beta_{i k+1} \operatorname{tg} \delta_{k+1})]. \quad (4.40)$$

The torsional moment $T_{i0}^{(f)}$ in the fixed-end base system has to be superposed on T_i in order to get the diagram of the torsional moments in the member. A similar superposition leads to the bending moments at the supports:

$$\left. \begin{aligned} M_{ki} &= M_k + (T_{ki}^{(f)} + T_i) \operatorname{tg} \delta_k = M_k + T_{ki} \operatorname{tg} \delta_k, \\ M_{k+1 i} &= M_{k+1} + (T_{k+1 i}^{(f)} + T_i) \operatorname{tg} \delta_{k+1} = M_{k+1} + T_{k+1 i} \operatorname{tg} \delta_{k+1}. \end{aligned} \right\} \quad (4.41)$$

Expressions (4.18), (4.19) and (4.20) for the bending moments, shearing forces and support reactions are still valid. The eccentricity of the resultant support reaction, however, should more precisely be formulated as follows:

$$x_{Fk} = \frac{T_{ki} - T_{k i-1}}{F_k}. \quad (4.42)$$

Exercise 4.2. *Obliquely Supported Three-Span Beam Subjected to Torsional Load.* Calculate expressions corresponding to Eqs. (4.25) if the central span of the system shown in Fig. 4.5 is acted upon by the uniformly distributed torsional moment m_D .

Solution

The regularities in the system and load immediately lead to the relations

$$\alpha_{40} = -\beta_{40} = \frac{m_D l_4^2}{12 EI} \operatorname{tg},$$

$$\alpha_{20} = \beta_{20} = \alpha_{60} = \beta_{60} = 0,$$

$$M_5 = -M_3,$$

where the latter reduces the system (4.12) to one single equation with the solution:

$$M_3 = -\frac{6EI}{l} \frac{1+2C}{1+2C+2\lambda+\lambda C} \alpha_{40}.$$

The evaluation of M_3 provides the basis to compute:

Torsional moments [v. Eqs. (4.40) and (4.15 b)]:

$$T_2 = -T_6 = \frac{C}{1 + 2C + \lambda(2 + C)} \frac{m_D l}{2},$$

$$T_4 = \left(1 - 2 \frac{z_4}{l}\right) \frac{m_D l}{2}.$$

Moments at the supports [v. Eqs. (4.41)]:

$$M_{12} = -M_{76} = \operatorname{tg} \delta \frac{C}{1 + 2C + \lambda(2 + C)} \frac{m_D l}{2},$$

$$M_{32} = -M_{56} = -\operatorname{tg} \delta \frac{1 + C}{1 + 2C + \lambda(2 + C)} \frac{m_D l}{2},$$

$$M_{34} = -M_{54} = \operatorname{tg} \delta \frac{\lambda(2 + C)}{1 + 2C + \lambda(2 + C)} \frac{m_D l}{2}.$$

Shearing forces [v. Eq. (4.19)]:

$$Q_2 = Q_6 = -\frac{\operatorname{tg} \delta}{2\lambda} \frac{1 + 2C}{1 + 2C + \lambda(2 + C)} m_D,$$

$$Q_4 = -\operatorname{tg} \delta \frac{\lambda(2 + C)}{1 + 2C + \lambda(2 + C)} m_D.$$

Support reactions [v. Eq. (4.20)]:

$$F_1 = -F_7 = -\frac{\operatorname{tg} \delta}{2\lambda} \frac{1 + 2C}{1 + 2C + \lambda(2 + C)} m_D,$$

$$F_3 = -F_5 = \frac{\operatorname{tg} \delta}{2\lambda} \frac{1 + 2C - 2\lambda^2(2 + C)}{1 + 2C + \lambda(2 + C)} m_D.$$

Eccentricities of the support reactions [v. Eq. (4.42)]:

$$x_{F1} = -x_{F7} = -\frac{1}{\operatorname{tg} \delta} \frac{\lambda C}{1 + 2C} l,$$

$$x_{F3} = -x_{F5} = \frac{\lambda}{\operatorname{tg} \delta} \frac{1 + C + \lambda(2 + C)}{1 + 2C - 2\lambda^2(2 + C)} l.$$

d) Example: Influence Surfaces

The influence line of a plane structure connects the influence coefficients plotted as ordinates at the point of load application. Since the eccentric position of a vertical unit load $P = 1$ has to be described by two coordinates (z_i and x , v. Fig. 4.2), the locus of all points representing influence coefficients will be a surface.

According to the procedure described in section 4.3 a, the eccentric, vertical load $P = 1$ is first decomposed into a unit load acting in the vertical plane through the member axis and into the moment $M_D = x$. Since the analysis

for either load was discussed extensively in the previous sections, the calculation of influence surfaces does not present any new problem.

To illustrate these introductory remarks the influence surfaces for the torsional moment and the bending moment in a single-span beam with equal skew angles of each support will be calculated and plotted for the following particular system properties:

$$\left. \begin{array}{l} \text{Considered cross section at } a = 2l/3 \text{ and } b = l/3, \\ GK/EI = 2, \\ C = 1/2, \text{ hence } \operatorname{tg} \delta = 1/\sqrt{2}. \end{array} \right\} \quad (4.43)$$

The torsional moment caused by the vertical load $P = 1$ in a and $b = l - a$, respectively can be calculated with the help of Eqs. (4.15b) and (4.16a).

$$T = -\frac{1}{\operatorname{tg} \delta} \frac{C}{1 + 2C} \frac{ab}{l}.$$

The torsional moment induced by the moment $M_D = x$ acting at the same position is given by the two Eqs. (4.35), each being valid for a different part of the member.

The superposition of the two types of load leads to:

$$\left. \begin{array}{l} T_A = \frac{l}{1 + 2C} \left\{ -\frac{C}{\operatorname{tg} \delta} \frac{ab}{l^2} + \frac{x}{l} \left[(1 + 2C) \frac{b}{l} - C \left(\frac{b}{l} - \frac{a}{l} \right) \right] \right\}, \\ T_B = \frac{l}{1 + 2C} \left\{ -\frac{C}{\operatorname{tg} \delta} \frac{ab}{l^2} + \frac{x}{l} \left[-(1 + 2C) \frac{a}{l} - C \left(\frac{b}{l} - \frac{a}{l} \right) \right] \right\}. \end{array} \right\}$$

The influence functions may be written in a more compact manner if the position of the unit load is described by the nondimensional coordinate parameters $a/l = \xi$, $b/l = \xi'$ and $x/l = \xi$.

$$\left. \begin{array}{l} T_A = \frac{l}{1 + 2C} \left[-\frac{C}{\operatorname{tg} \delta} \xi \xi' + \xi(C + \xi') \right] \\ T_B = \frac{l}{1 + 2C} \left[-\frac{C}{\operatorname{tg} \delta} \xi \xi' - \xi(C + \xi) \right] \end{array} \right\} \quad (4.44)$$

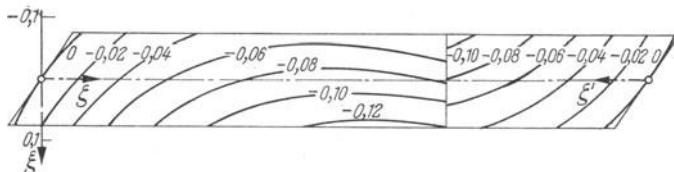


Fig. 4.11. Influence Surface for the Torsional Moment in the Cross Section $\xi = 2/3$, $\xi' = 1/3$ (Values are to be Multiplied by Pi).

Since the value T_A represents at the same time the torsional moment between the support A and the applied moment $M_D = x$, its expression represents the

influence surface which stretches from the cross section at $z = a$ to support B . The expression for T_B represents similarly the part of the influence surface which stretches from support A to the considered cross section.

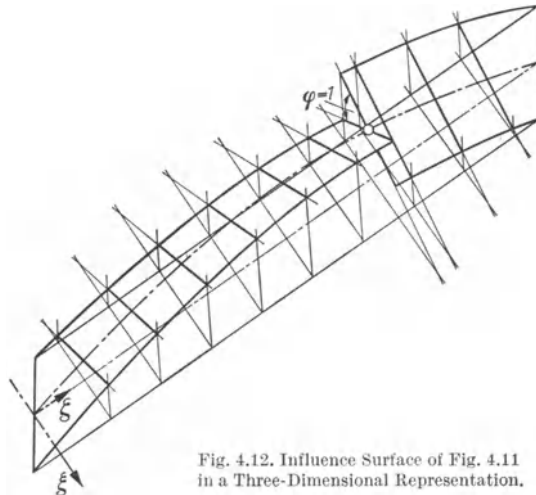


Fig. 4.12. Influence Surface of Fig. 4.11
in a Three-Dimensional Representation.

For the system with the assumed properties (4.43), the influence functions (4.44) may be written as follows:

$$\frac{T}{Pl} = \begin{cases} -0,354\zeta\zeta' + \xi(0,25 + 0,5\zeta') & \begin{cases} \zeta > 2/3 \\ \zeta' < 1/3 \end{cases} \\ -0,354\zeta\zeta' - \xi(0,25 + 0,5\zeta) & \begin{cases} \zeta < 2/3 \\ \zeta' > 1/3 \end{cases} \end{cases}$$

The shape of these surfaces is shown in Fig. 4.11 by a contour map presentation which is supplemented by the three-dimensional figure 4.12.

As a last example, the influence function for the bending moment in the same obliquely supported, single-span beam will be derived. Since no redundant quantities M_k and M_{k+1} need to be calculated, the expression for the bending moment in locations a and $b = l - a$, respectively, may be derived immediately from Eqs. (4.18) and (4.41).

$$M = M_0 + T_A \frac{b}{l} \operatorname{tg} \delta_A + T_B \frac{a}{l} \operatorname{tg} \delta_B.$$

The corresponding influence ordinates η have the same functional relationship:

$$\eta_M = \eta_{M_0} + \eta_{T_A} \frac{b}{l} \operatorname{tg} \delta_A + \eta_{T_B} \frac{a}{l} \operatorname{tg} \delta_B. \quad (4.45)$$

The ordinates η_{M_0} represent the influence surface for the moment in the statically determinate base system, the simple beam. This surface, which in the projection appears as the well-known triangle of height ab/l , may be described

analytically as follows:

$$\eta_{M_0} = \begin{cases} l \frac{b}{l} \zeta, & \text{for } \zeta < \frac{a}{l}, \\ l \frac{a}{l} \zeta', & \text{for } \zeta' < \frac{b}{l}. \end{cases} \quad (4.46)$$

The ordinates η_{T_A} and η_{T_B} constitute the influence surfaces for the torsional moments at the supports A and B . These functions are given by the expressions (4.44) for the case of equal, skew angles at the two supports, $\delta_A = \delta_B = \delta$. Introducing the expressions for η_{M_0} , η_{T_A} and η_{T_B} into Eq. (4.45), one arrives at the following description for the influence surface of the bending moment in locations a and $b = l - a$, respectively, for the single-span beam with equal skew angles at the supports:

$$\eta_M = l \left\{ \frac{\frac{b}{l} \zeta}{\frac{a}{l} \zeta'} - \frac{C}{1 + 2C} \zeta \zeta' + \frac{\xi \operatorname{tg} \delta}{1 + 2C} \left[\frac{b}{l} (C + \zeta') - \frac{a}{l} (C + \zeta) \right] \right\}, \text{ for } \begin{cases} \zeta < \frac{a}{l} \\ \zeta' > \frac{b}{l} \end{cases} \quad (4.47)$$

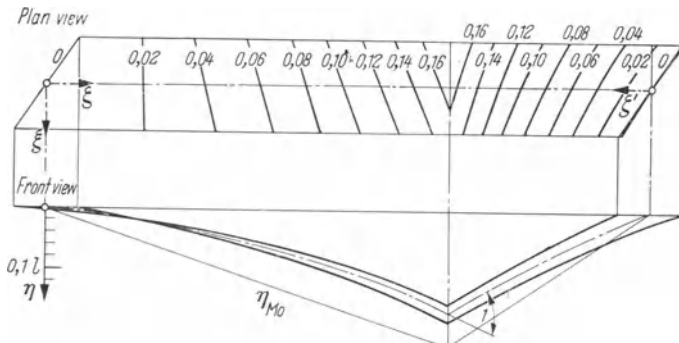


Fig. 4.13. Influence Surface for the Bending Moment in the Cross Section $\zeta = \frac{2}{3}$, $\zeta' = \frac{1}{3}$ ($M = \eta Pl$).

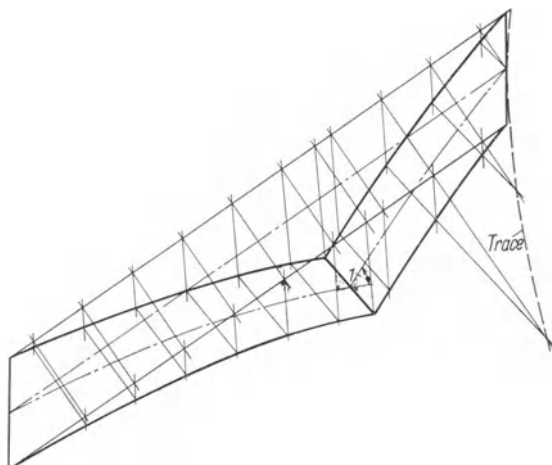


Fig. 4.14. Influence Surface of Fig. 4.13 in a Three-Dimensional Presentation.

Introducing into Eq. (4.47) the particular properties given by (4.43) for this illustrative case, the expression for the influence surface reduces to:

$$\eta_M = l \left\{ \begin{array}{l} \frac{1}{3} \zeta - \frac{1}{4} \zeta \zeta' + \frac{\sqrt{2}}{4} \xi \left(\frac{1}{6} - \zeta \right) \\ \frac{2}{3} \zeta' \end{array} \right\} \text{ for } \begin{cases} \zeta < \frac{2}{3} \\ \zeta > \frac{2}{3} \end{cases}$$

These influence surfaces are visualized in Figs. 4.13 and 4.14. For comparison with the case of zero skew angle, Fig. 4.13 also shows η_{M_0} (Eqs. 4.46) in the front view.

4.4 General Considerations

a) Member Constant C

It may be seen throughout the entire analysis that the member constant C (Table 4.2) is of great importance. All factors characterizing skew supports enter into this term.

One may expect in the most simple system having equal skew angles δ at the supports and constant torsional and flexural rigidity, that the member forces not only depend on span, skew angle and load, but also on the ratio between torsional and flexural rigidity, GK/EI . It may further be presumed that the effect of an increased ratio GK/EI will be similar to the effect of an increased obliqueness δ .

These presumed effects are illustrated by the following analytic form of the member constant C :

$$C = \frac{GK}{EI} \frac{\operatorname{tg}^2 \delta}{2}. \quad (4.48)$$

The parameter GK/EI will depend on the dimensions of the cross section. The following illustration for two special cases will give an idea of the range of the effects to be expected.

The narrow, rectangular, solid cross section shown in Fig. 4.1a has according to Eq. (1.9) the following approximate stiffness parameter:

$$\frac{GK}{EI} = \frac{\frac{E}{2(1+\nu)}}{\frac{E}{12} b t^3} \frac{1}{3} b t^3 = \frac{2}{1+\nu}. \quad (4.49)$$

The ratio between torsional and flexural rigidity is thus in this case ($b \gtrsim 4t$) independent of the dimensions of the cross section. If for example haunches in the members are neglected in the course of a preliminary analysis, a later consideration of the true member dimensions will not cause significant changes in the preliminary results. The member constants, however, are not completely independent of a nonuniform distribution of the structural material as may be seen from the first column in Table 4.2.

The stiffness parameter GK/EI for a *thin-walled, closed box section* of width b , height h and wall thickness t may be calculated by means of Bredt's formula (2.5).

$$\frac{GK}{EI} = \frac{\frac{E}{2(1+\nu)}}{\frac{E}{2}} \frac{\frac{4b^2h^2}{2(b+h)} t}{\frac{1}{2} bth^2 + \frac{2}{12} th^3} = \frac{2}{1+\nu} \frac{1}{\left(1 + \frac{h}{b}\right) \left(1 + \frac{1}{3} \frac{h}{b}\right)}. \quad (4.50)$$

In cases where the height of the cross section is small as compared to its width, the ratio GK/EI is almost independent of the dimensions and close to the value for the corresponding solid cross section.

Since Poisson's ratio ν is relatively small, the assumption $GK/EI = 2$ leading to $C = \operatorname{tg}^2 \delta$ which was made in a few previous examples should be in reasonable agreement with cases occurring in actual practice.

Values for the expression (4.48) will now be tabulated for a limited range of parameters in order to show the order of magnitude of C that may be expected.

Table 4.4. Values for $C = \frac{GK}{EI} \frac{\operatorname{tg}^2 \delta}{2}$

Skew Angle δ :	0°	15°	30°	45°	60°	75°	90°
$\frac{GK}{EI} = 2$	0	0,07	0,33	1,00	3,00	13,90	∞
$\frac{GK}{EI} = \frac{2}{1+\nu}$, $\begin{cases} \nu = 1/6 & 0 \\ \nu = 1/3 & 0 \end{cases}$	0	0,06	0,28	0,86	2,57	11,90	∞
$\frac{GK}{EI} = 1$	0	0,05	0,25	0,75	2,25	10,40	∞

b) Conditions at the Supports

The derivation of the fundamental relations that included the effect of skewed supports in Section 4.1 c assumed each support to consist of two discrete support elements acting at the outer edges of the member. This assumption is not at all necessary since neither the width of the member nor the distance between the support elements appears in the resulting relations. It was introduced to facilitate the visualization of the forces involved. The analysis of the system determines only the resultant support reaction with its point of application [Eqs. (4.20), (4.21) and (4.42)].

Consider again the single-span beam with skew supports, acted upon by a uniformly distributed load p . The resultant support reactions are $F_A = F_B = p \cdot 1/2$. Their distance from the member axis is given by the last of the expressions (4.26). They act furthermore on the lines which coincide with the bearing edges of the supports. The eccentricities of the reactions measured along these lines are given by:

$$r = \frac{|x|}{\cos \delta} = \frac{l}{3 \sin \delta} \frac{C}{1 + 2C}$$

and if C is replaced by Eq. (4.48) this becomes:

$$r = \frac{l}{6} \frac{\frac{GK}{EI} \sin \delta}{\cos^2 \delta + \frac{GK}{EI} \sin^2 \delta}. \quad (4.51)$$

Eq. (4.51) determines the position of the support reaction in terms of the polar coordinates r and δ . This function is plotted in a plan view of the member (Fig. 4.15) for values $GK/EI = 1, 2$ and for the entire range of the skew angle δ . It may be observed that Eq. (4.51) represents a semicircle of diameter $l/6$ for $GK/EI = 1$. Another observation with important practical consequences is that the biggest changes in the position of the reaction occur for small values of the skew angle δ . Thus a small deviation from the regular, rectangular support will cause a considerable change in bearing pressure distribution.

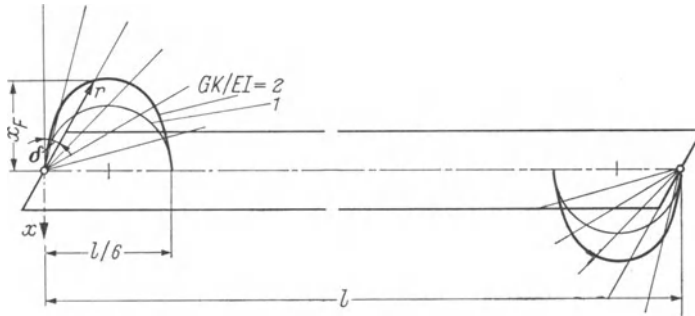


Fig. 4.15. Position of the Reaction as a Function of the Support Obliqueness δ for a Uniformly Loaded, Single-Span Member.

If a design provides for two separate support elements to carry the entire reactive load, then the two reactive forces may be calculated from the equilibrium condition alone. Suppose the two support elements are the distance $+\frac{d}{2}$ and $-\frac{d}{2}$ away from the member axis, then the corresponding bearing pressures $F_k\left(+\frac{d}{2}\right)$ and $F_k\left(-\frac{d}{2}\right)$ are given by the following expression:

$$F_k\left(\pm \frac{d}{2}\right) = \frac{F_k}{2} \pm \frac{T_{ki} - T_{k,i-1}}{d}. \quad (4.52)$$

If the reaction, on the other hand, consists of more than two support elements, or of a distributed bearing pressure, then the magnitude of these forces is undetermined but the value and point of application of their resultant is known. If for instance the line pressure per unit length of the bearing edge is supposed to be linearly distributed, then this pressure distribution is given by the expression:

$$\bar{\sigma}_k = \left[\frac{F_k}{d} + \frac{12(T_{ki} - T_{k,i-1})}{d^3} x \right] \cos \delta_k. \quad (4.53)$$

The sketch shown in Fig. 4.3b may lead to the assumption that portions close to the supports of the deflected member have to be replaced by the tangent planes in the theoretical support points. Since there is no further information

Summary of the Corrections

		In the region $0 \leq z'_{i-1} < e_k/2$
<i>Case 1: 2 separate support elements at $x = \pm \frac{d}{2}$</i>		
<i>T:</i>	$T_{i-1} + \left[\frac{F_k}{2} \frac{e_k}{\operatorname{tg} \delta_k} + (T_{ki} - T_{k i-1}) \right] \frac{1}{2}$	
<i>M:</i>	$M_{i-1} + \left[\frac{F_k}{2} \frac{e_k}{\operatorname{tg} \delta_k} + (T_{ki} - T_{k i-1}) \right] \cdot \left(\frac{1}{2} - \frac{z'_{i-1}}{e_k} \right) \cdot \operatorname{tg} \delta_k$	
<i>Q:</i>	$Q_{i-1} + \left[\frac{F_k}{2} \frac{e_k}{\operatorname{tg} \delta_k} + (T_{ki} - T_{k i-1}) \right] \cdot \frac{\operatorname{tg} \delta_k}{e_k}$	

Case 2: Line bearings

<i>T:</i>	$T_{i-1} + \frac{F_k}{2} \cdot \frac{e_k}{\operatorname{tg} \delta_k} \left[\frac{1}{4} - \left(\frac{z'_{i-1}}{e_k} \right)^2 \right] + (T_{ki} - T_{k i-1}) \left[1 - 8 \left(\frac{z'_{i-1}}{e_k} \right)^3 \right] \cdot \frac{1}{2}$	
<i>M:</i>	$M_{i-1} + \left\{ F_k \cdot \frac{e_k}{\operatorname{tg} \delta_k} \left[\frac{1}{4} - \left(\frac{z'_{i-1}}{e_k} \right)^2 \right] + (T_{ki} - T_{k i-1}) \left[1 - 8 \left(\frac{z'_{i-1}}{e_k} \right)^3 \right] \right\} \frac{\operatorname{tg} \delta_k}{2} -$ $- z'_{i-1} \left\{ F_k \left(\frac{1}{2} - \frac{z'_{i-1}}{e_k} \right) + \frac{3}{2} \frac{\operatorname{tg} \delta_k}{e_k} (T_{ki} - T_{k i-1}) \left[1 - 4 \left(\frac{z'_{i-1}}{e_k} \right)^2 \right] \right\}$	
<i>Q:</i>	$Q_{i-1} + F_k \left(\frac{1}{2} - \frac{z'_{i-1}}{e_k} \right) + \frac{3}{2} \cdot \frac{\operatorname{tg} \delta_k}{e_k} (T_{ki} - T_{k i-1}) \left[1 - 4 \left(\frac{z'_{i-1}}{e_k} \right)^2 \right]$	

at the Supports

At $z_{k-1} = z_i = 0$ (e.g. at k)	In the region $0 \leq z_i < e_k/2$
$F_k \left(\pm \frac{d}{2} \right) = \frac{F_k}{2} \pm \frac{T_{ki} - T_{k\ i-1}}{d}$	In the region $0 \leq z_i < e_k/2$
$M_k + \left(\frac{F_k}{2} \cdot \frac{e_k}{\operatorname{tg} \delta_k} + T_{k\ i-1} + T_{ki} \right) \frac{1}{2}$	$T_i + \left[\frac{F_k}{2} \cdot \frac{e_k}{\operatorname{tg} \delta_k} - (T_{ki} - T_{k\ i-1}) \right] \cdot \frac{1}{2}$
$M_k + \left(\frac{F_k}{2} \cdot \frac{e_k}{\operatorname{tg} \delta_k} + T_{k\ i-1} + T_{ki} \right) \frac{1}{2} \cdot \operatorname{tg} \delta_k$	$M_i + \left[\frac{F_k}{2} \cdot \frac{e_k}{\operatorname{tg} \delta_k} - (T_{ki} - T_{k\ i-1}) \right] \left(\frac{1}{2} - \frac{z_i}{e_k} \right) \cdot \operatorname{tg} \delta_k$
$\frac{Q_{k\ i-1} + Q_{k\ i}}{2} + (T_{ki} - T_{k\ i-1}) \frac{\operatorname{tg} \delta_k}{e_k}$	$Q_i - \left[\frac{F_k \cdot e_k}{2 \cdot \operatorname{tg} \delta_k} - (T_{ki} - T_{k\ i-1}) \right] \frac{\operatorname{tg} \delta_k}{e_k}$
$\bar{\sigma}_k = \left[\frac{F_k}{d} + \frac{12(T_{ki} - T_{k\ i-1})}{d^3} x \right] \cos \delta_k$	
$\left(\frac{F_k}{4} \cdot \frac{e_k}{\operatorname{tg} \delta} + T_{ki} + T_{k\ i-1} \right) \cdot \frac{1}{2}$	$T_i + \frac{F_k}{2} \cdot \frac{e_k}{\operatorname{tg} \delta_k} \left[\frac{1}{4} - \left(\frac{z_i}{e_k} \right)^2 \right] - (T_{ki} - T_{k\ i-1}) \left[1 - 8 \left(\frac{z_i}{e_k} \right)^3 \right] \cdot \frac{1}{2}$
$M_k + \frac{F_k}{4} \cdot \frac{e_k}{\operatorname{tg} \delta} + (T_{ki} + T_{k\ i-1}) \cdot \frac{\operatorname{tg} \delta_k}{2}$	$M_i + \left\{ F_k \frac{e_k}{\operatorname{tg} \delta_k} \left[\frac{1}{4} - \left(\frac{z_i}{e_k} \right)^2 \right] - (T_{ki} - T_{k\ i-1}) \left[1 - 8 \left(\frac{z_i}{e_k} \right)^3 \right] \right\} \frac{\operatorname{tg} \delta_k}{2}$ $- z_i \left\{ F_k \left(\frac{1}{2} - \frac{z_i}{e_k} \right) - \frac{3}{2} \frac{\operatorname{tg} \delta_k}{e_k} (T_{ki} - T_{k\ i-1}) \left[1 - 4 \left(\frac{z_i}{e_k} \right)^2 \right] \right\}$
$\frac{1}{2} Q_{k\ i-1} + \frac{1}{2} Q_{ki} + (T_{ki} - T_{k\ i-1}) \frac{3}{2} \cdot \frac{\operatorname{tg} \delta_k}{e_k}$	$Q_i - F_k \left(\frac{1}{2} - \frac{z_i}{e_k} \right) + \frac{3}{2} \cdot \frac{\operatorname{tg} \delta_k}{e_k} (T_{ki} - T_{k\ i-1}) \left[1 - 4 \left(\frac{z_i}{e_k} \right)^2 \right]$

required regarding the exact position of the support elements other than their oblique direction, they may be positioned arbitrarily close to each other. The boundary conditions are thus of mathematical nature and the analysis need only be based on the assumptions of ordinary structural analysis as mentioned in the preface.

In order to explain some of the discrepancies, one should recognize the differences between the theoretical and actually realized boundary conditions. The influence surfaces shown in Fig. 4.11, for instance, satisfy only the theoretical boundary conditions since support elements positioned away from the member axis do not exactly coincide with the line of zero torsional moment.

Thus, depending on the particular support arrangement, both the torsional moments and the bending moments will thus have to be corrected somewhat in the immediate vicinity of the supports. If the two elements of a support were positioned at the outer edges of the member, then the moment diagrams would be as shown in Fig. 4.6 or as indicated by means of dashed or dotted lines in Fig. 4.4 and 4.10, respectively.

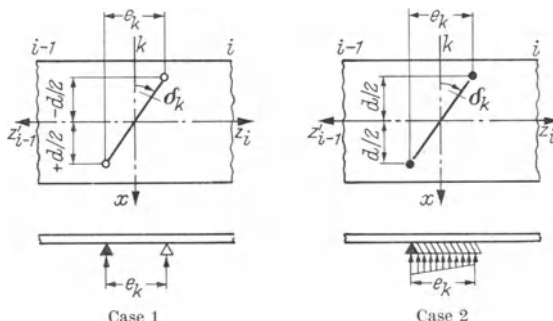
It was stated in section 4.4c that skew supports increase the end bending moments and reduce the in span moments. The end moments, on the other hand, may be favorably influenced by a suitable arrangement of the support elements. However, this usually increases shearing forces between these concentrated local support regions.

Exercise 4.3. Analytic Formulation of the Corrections at the Supports. The corrections in the member forces T , M and Q in the neighborhood of the supports may, within the limits of ordinary structural analysis, be given as a function of the reaction F_k and the torsional moment $T_{ki} - T_{ki-1}$.

Calculate these corrections for:

Case 1: Two support elements at a distance $\pm \frac{d}{2}$ away from the member axis [Eq. (4.52)]

Case 2: Support with linearly distributed bearing pressure [Eq. (4.53)].



The solutions are presented in the preceding table.

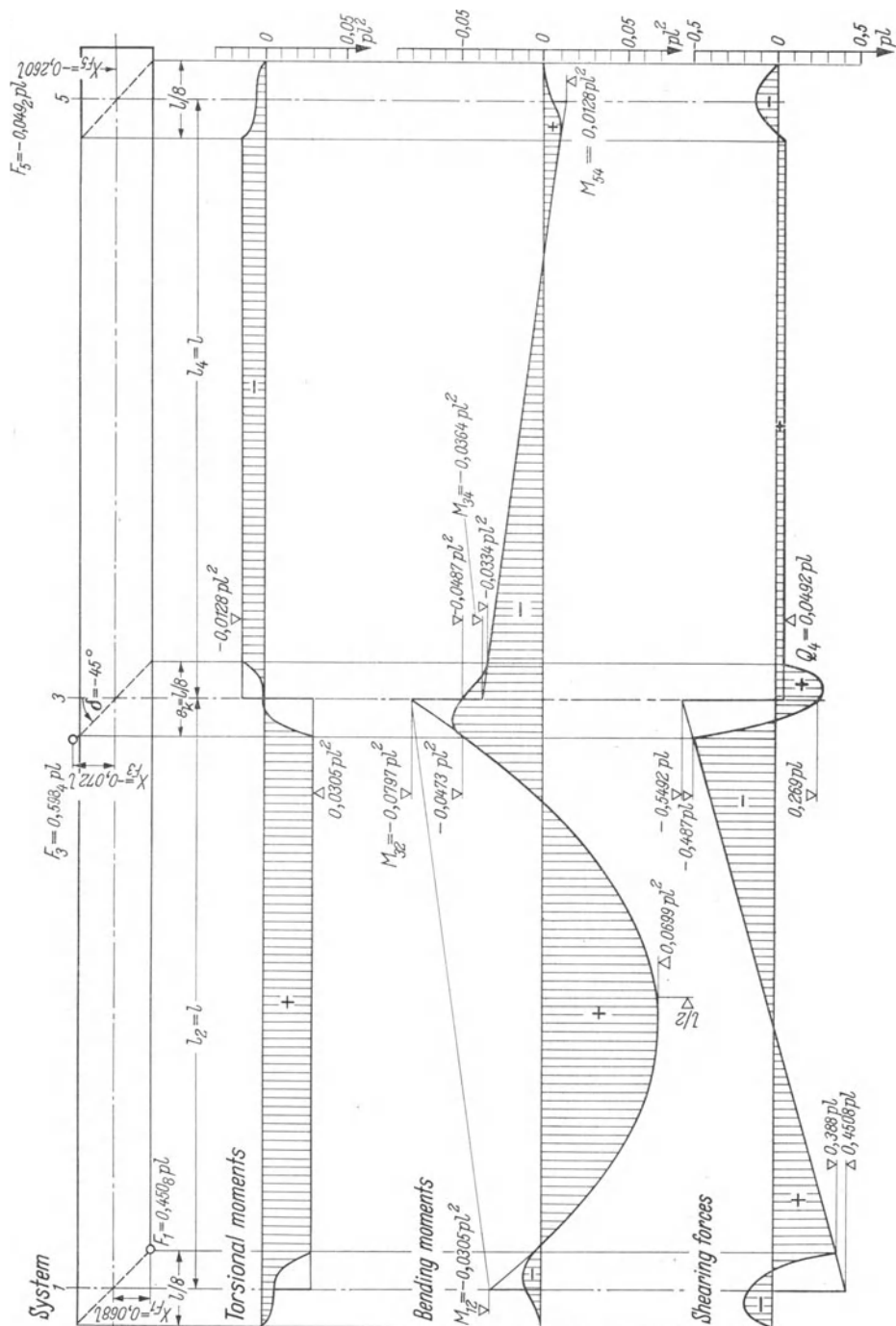
Exercise 4.4. Numerical Calculation of the Corrections at the Supports. Based on the solutions for a two-span beam in Exercise 4.1 calculate the diagrams for the torsional moments, bending moments and shearing forces which include their corrections at the supports.

Assumptions: Line bearing of the support: $d = l/8$.

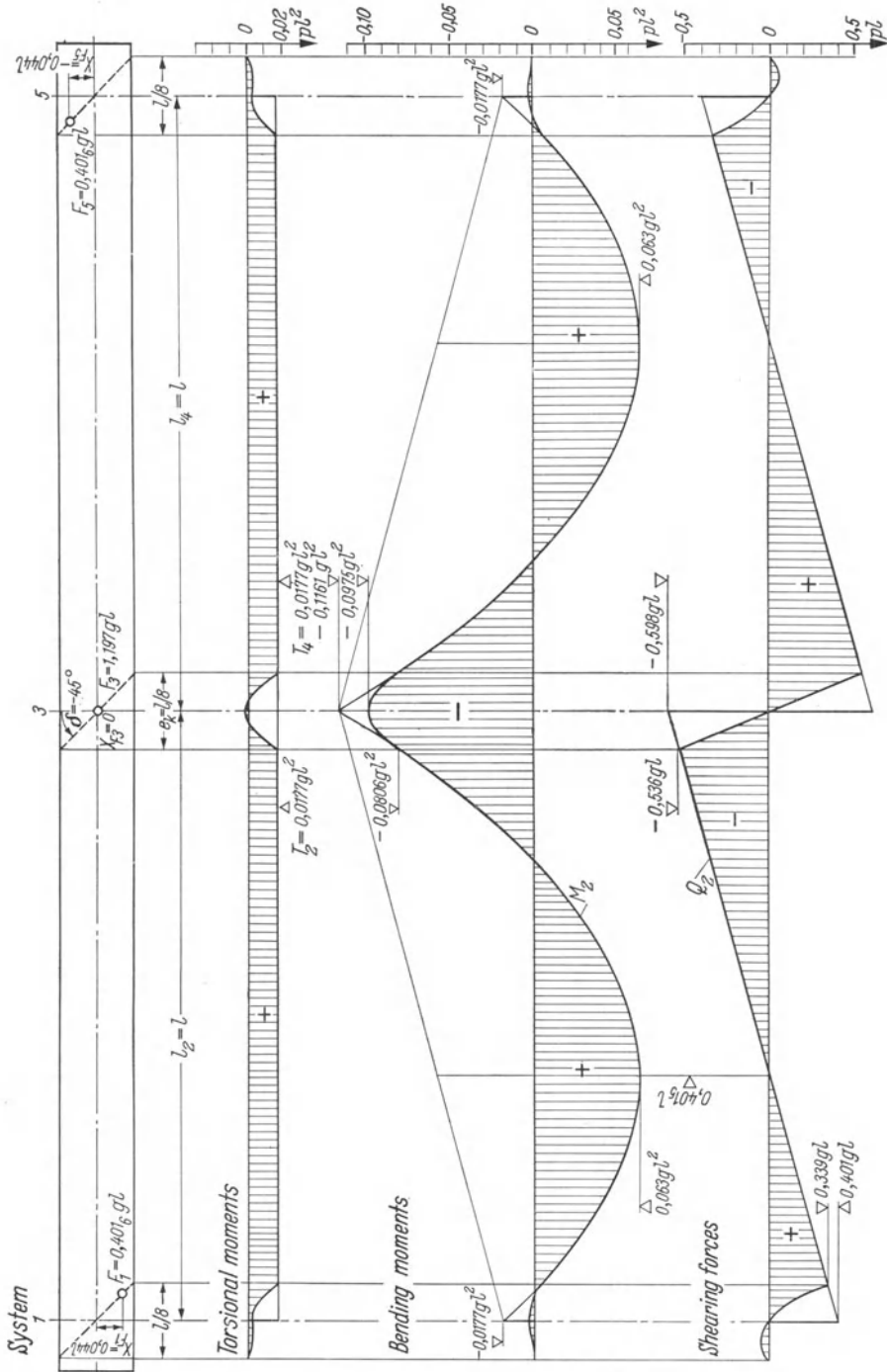
Skew angle: $\delta = -45^\circ (\tan \delta = -1)$.

Ratio between torsional and flexural rigidity: $GK/EI = 1,08$.

The results are presented in the two subsequent figures. They were obtained by a computer analysis which was programmed by E. KARAMUK, engineer with Basler & Hofmann, Zürich.



Solution to Exercise 4.4.a. Uniformly Distributed Dead Load



Solution to Exercise 4.4b. Uniformly Distributed Load on Span 2

c) Maximum Shearing Stresses Caused by Skewed Supports

Skewed supports reduce the flexural stresses in the span but result in increased shearing stresses. What portion of the shearing stresses may be attributed solely to the skewness of the supports? It is the purpose of this section to derive an upper limit for this portion of the shearing stresses if the system is subjected to centric loads only.

The torsional moment given by Eq. (4.15a) is equal to or smaller than the product of the maximum values of the two factors. The first factor, the quotient

$$Q = \frac{\operatorname{tg} \delta}{\frac{EI}{GK} + \operatorname{tg}^2 \delta}$$

vanishes for the obliqueness $\delta = 0^\circ$ as well as for $\delta = 90^\circ$. The quotient Q will thus assume an optimum value for some intermediate skew angle δ which is determined by the condition:

$$\frac{dQ}{d(\operatorname{tg} \delta)} = \frac{\frac{EI}{GK} + \operatorname{tg}^2 \delta - 2 \operatorname{tg}^2 \delta}{\left(\frac{EI}{GK} + \operatorname{tg}^2 \delta \right)^2} = 0$$

to be:

$$\operatorname{tg} \delta_{\text{opt}} = \sqrt{\frac{EI}{GK}}. \quad (4.54)$$

This leads to the inequality:

$$T_i \leq \frac{1}{2} \sqrt{\frac{GK_i}{EI_i}} \left[\frac{EI_i(\alpha_{i0} + \beta_{i0})}{l_i} + \frac{M_k + M_{k+1}}{2} \right]. \quad (4.55)$$

It was shown in relation with Eqs. (4.15) that the first expression in brackets represents the average bending moment in the span of length l_i . No matter what the particular load arrangement and the conditions at the member-end might be, this average value never exceeds the extreme value of the bending moment, e.g.

$$T_{\text{opt}} \leq \frac{1}{2} \sqrt{\frac{GK}{EI}} M_{\text{extr}}.$$

This inequality is now written in terms of stresses which will be calculated for the cross sections discussed in Section 4.4a. The expressions for the shearing stresses follow from Eq. (1.8) and (2.4).

Narrow Rectangular
Cross Section

$$\tau = 3 \frac{T}{bt^2},$$

$$\sigma = 6 \frac{M}{bt^2},$$

Hollow Box
Cross Section

$$\tau = \frac{T}{2bht},$$

$$\sigma = \frac{M}{bht \left(1 + \frac{1}{3} \frac{h}{b} \right)}.$$

For the narrow rectangular cross section one derives further $T_{\text{opt}} = \tau_{\text{opt}} b t^2 / 3$ and $M_{\text{extr}} = \sigma_{\text{extr}} b t^2 / 6$. If these simple relations together with the result (4.49) for the ratio GK/EI are introduced into the last inequality, one arrives at the following:

$$\tau_{\text{opt}} \leq \frac{1}{4} \sqrt{\frac{2}{1+\nu}} \sigma_{\text{extr}}.$$

A similar inequality may be derived for the rectangular, hollow box cross section:

$$\tau_{\text{opt}} \leq \frac{1}{4} \sqrt{\frac{2}{1+\nu}} \sigma_{\text{extr}} \sqrt{\sqrt{\frac{1 + \frac{1}{3} \frac{h}{b}}{1 + \frac{h}{b}}}}$$

For small height-width ratios h/b , the second square root is approximately equal to one. The inequality still holds if the square root is definitely replaced by one. Since Poissons's ratio ν varies between 0 and 1/2, the most unfavorable value for the first square root is $\sqrt{2}$. Thick, rectangular, solid cross sections would even reduce the value of GK/EI .

Thus it may be stated that the shearing stresses in rectangular, solid and hollow cross sections caused by the skewness of the supports alone do not exceed $\sqrt{2}/4$ times the extreme value of the flexural stress.

$$\tau_{\text{opt}} \leq 0,354 \sigma_{\text{extr}}. \quad (4.56)$$

This relation was derived for centric loads, but it is valid for arbitrary span ratios and structural materials.

d) Summary

Skew supported bridges require two types of compatibility conditions. One set of conditions places the member on the horizontal but *skewed supports* while the other concerns the continuity of slope of the deflected, longitudinal axis of the beam. Both types of conditions are formulated in Eqs. (4.1) and (4.8). They uncouple only for regularly supported, continuous beams, e.g. when $\operatorname{tg} \delta_k = \operatorname{tg} \delta_{k+1} = 0$.

It is customary in the analysis of continuous beams to take the support moments as redundant quantities. An obliquely supported, continuous beam, however, introduces two unknown moments M_{ki+1} and M_{ki} at each support k and the unknown torsional moment T_i in each span i . The total number of unknowns is thus three times the number of spans. If the analysis were based on these unknowns, then the aforementioned compatibility conditions would have to be supplemented by the equilibrium conditions for the moments at the supports.

$$M_{ki} - M_{ki-1} - (T_i - T_{i-1}) \operatorname{tg} \delta = 0. \quad (4.57)$$

It was nevertheless possible by an appropriate selection of a base system and the redundant quantities to arrive at equations which are completely analogous

to the well known three-moment equations of the ordinary continuous beam. The considerations which led to the selection of the base system and the redundants will be reviewed briefly.

The analysis is based on a statically indeterminate base system, a system of skew supported, single-span beams. The system of two simultaneous linear equations (4.6) describing the elastic properties of the base systems are solved once and for all, thus reducing the number of unknowns by the number of base systems. The remaining redundants are not actual moments at the supports—one would have to decide between the one to the left and the one to the right—but ideal transmission moments M_k which are not actually recognizable in the structure. These ideal quantities, however, make the analysis of a skew supported, continuous beam completely analogous to the analysis of the beam on regular supports.

The engineer applying these procedures does not need to repeat the development of the basic considerations over and over again because the fundamental equations and the forces in the members are expressed in terms of familiar displacement coefficients which may be determined for the *regularly supported, simple beam*. The general procedure for the analysis is as follows:

The supports and the spans are first numbered consecutively, assigning odd numbers k to the supports and even numbers i to the spans. The displacement coefficients are then calculated for each span just as for the regularly supported, continuous beam. The member constants C and D given by Table 4.2 may be computed later. This furnishes the basis for the formulation of the three-moment equations which are, in the order of increasing complexity of the system, provided in Eqs. (4.12), (4.11), (4.10) or (4.9). The solutions of the resulting system of equations are first used to calculate the torsional moments in each span. This is done by means of Eqs. (4.15b), (4.14) or (4.13) depending on the complexity of the system. The torsional moments simplify the evaluation of the moments at the supports (4.17), the distribution of the bending moments along the member (4.18), the shearing forces (4.19) and the resultant reactions (4.20). The lines of action of the latter are calculated by means of Eq. (4.21).

An eccentric load is divided into a centrally applied load and into a moment. The first part is treated as described above while the effect of the second may be analyzed by means of the same three-moment equation if Eqs. (4.37) are used to calculate the generalized displacements.

II. Warping Torsion

5 Stress Analysis

5.1 Notation

a) Sign Convention

The normal stress components σ and the shear stress components τ shall satisfy the following usual sign convention:

Stress components acting on a cross section whose outer normal points in the positive direction of some coordinate axis shall be considered to be positive whenever they point in the direction of a positive axis. If the cross section, on the other hand, has an outward normal pointing towards the negative part of the axis, then positive stress components point towards the negative parts of the coordinate axis as well.

Tensile stresses are therefore positive and compressive stresses negative.

The internal forces are the resultants of the stresses and will have the same sign convention. A positive shearing force is therefore directed as shown in Fig. 5.1 while a positive torsional moment acts as in Fig. 5.2.

b) Coordinate System

Tables of structural shapes refer their cross sections in general to the abscissa x and to the ordinate y . The axis z is therefore directed along the length of the member.

The positive y -axis is taken downward so that gravity loads cause positive deflections and if the coordinate system is assumed to be right-handed, one arrives at the configuration shown in Fig. 5.2.

c) Quantities Depending on the Coordinates x and y

According to a suggestion by BORNSCHEUER¹, the subscripts of the area integrals reflect the character of their integrand. The moment of inertia I_{xx} , for instance, is defined as follows:

$$I_{xx} = \int_F x x \, dF$$

¹ BORNSCHEUER, F. W.: Systematische Darstellung des Biege- und Verdrehvorganges, unter besonderer Berücksichtigung der Wölbkrafttorsion. Stahlbau 21 (1952) 1.

and the expression for the bending moment is similarly:

$$M_x = \int_F \sigma x \, dF.$$

If the quantities are no longer constants but variables, such as the statical moment \tilde{S} of a cut-off portion of the cross section, then a waved line is added at the top of the symbol:

$$\tilde{S}_x = \int_0^s x \, dF.$$

Quantities which involve the warping coordinate ω are furthermore characterized by the adjective “sectorial”. The reference point of the warping coordinate is indicated by an additional subscript unless the coordinate refers to the shear center.

d) Correlation of Signs for Quantities Depending on the Coordinate z

a) Bending in y -Direction. Consecutive differentiation of the elastic curve of a simple beam of constant flexural rigidity with respect to z leads in turn to the slope θ , the bending moment M , the shearing forces Q and to the load p . A dimensional analysis reveals that the second derivative must be of the form M/EI and cannot be equivalent to M itself. But still, even a variable flexural rigidity would not change the sign of the derived quantities. This means that on the basis of one sign convention, the differentiation procedure is able to determine the signs of the remaining quantities.

Consider for example the simply supported beam of length l , constant flexural rigidity and equally distributed load p_y . The boundary conditions

$$\eta(0) = \eta''(0) = \eta(l) = \eta''(l) = 0$$

determine the following correlated functions (notation: $\zeta = z/l$, derivatives with respect to z are denoted by primes):

$$f = + \frac{p_y l^4}{24} \zeta (1 - 2\zeta^2 + \zeta^3) = \eta(EI),$$

$$f' = + \frac{p_y l^3}{24} (1 - 6\zeta^2 + 4\zeta^3) = \Theta_y(EI),$$

$$f'' = - \frac{p_y l^2}{2} \zeta (1 - \zeta) = - M_y,$$

$$f''' = - \frac{p_y l}{2} (1 - 2\zeta) = - Q_y,$$

$$f'''' = + p_y = p_y.$$

These five functions are plotted in Fig. 5.1. They demonstrate that the integration of a positive lateral load (e.g. acting in the direction of the corresponding coordinate axis) leads to positive deflections as well. The correspondence between the signs of the first and the last function is therefore correct.

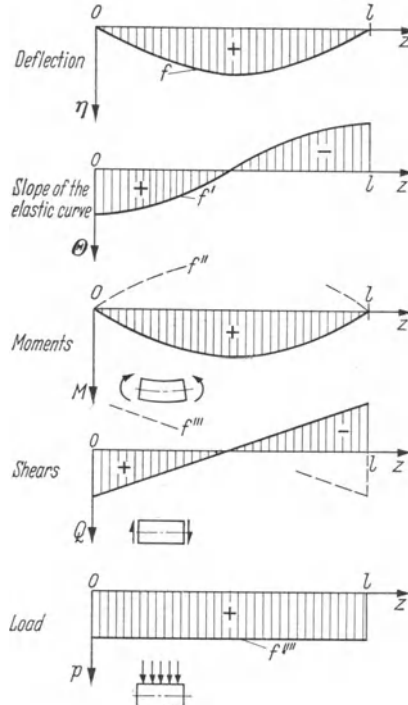


Fig. 5.1. The z -Dependent Elements for the Vertical Deflection of a Simple Beam.

The sign of the shearing forces has already been fixed when the sign convention for the stresses is established: A positive shearing force acting on a cross section whose outer normal is directed in $+z$ -direction points in $+y$ -direction, e.g. downwards. The shear in a simple beam which is subjected to vertical loads is positive in the vicinity of the support $z = 0$. The third derivative given above, however, is negative in this region. The shearing force corresponds therefore to the negative value of the third derivative.

The sign of the remaining two quantities, the slope θ_y and the bending moment M_y , is determined by means of the following convention:

$$\theta_y = +\eta', \quad Q_y = +M_y.$$

The first column of Table 5.1 summarizes the definitions presented above.

β) Pure Twist. It will be shown in Section 5.4 that the angle of twist φ and its derivatives for a thin-walled open cross section represent the same set of equations as the one derived above if the system is subjected to the boundary conditions:

$$\varphi(0) = \varphi''(0) = \varphi(l) = \varphi''(l) = 0.$$

In this analogy, the torsional moment T_ω corresponds to the shear while the warping moment M'_ω ¹ corresponds to the bending moment in the simple beam. A positive, e.g. clockwise torsional load m_D corresponds therefore to a twist with the same sense of rotation.

The torsional moment T_ω acting on a cross section with positive outward normal is said to be positive when pointing in $+\varphi$ -direction (Fig. 5.2). The equilibrium condition for the member element of length dz acted upon by the distributed torsional load m_D may thus be written as follows:

$$-T_\omega + m_D dz + \left(T_\omega + \frac{dT_\omega}{dz} dz \right) = 0.$$

This leads to the relation:

$$T'_\omega = -m_D,$$

which is equivalent to the connection between shear and load. In analogy to the relation $M'_y = +Q_y$ it is thus apparent that a dominating function, the warping moment M'_ω , may be defined as $M'_\omega = +T_\omega$.

The definition for the specific angle of twist $\theta_\omega, \varphi' = +\theta_\omega$, completes this new chain of functions which is summarized in the second column of Table 5.1.

Table 5.1. *Sign Connection Between the z-Dependent Quantities of a Member Under Pure Bending and Warping Torsion*

	Subjected to lateral load p_y	Subjected to torsional load m_D	Subjected to lateral load p_x
Displacement	η	φ	ξ
Slope	$\theta_y = +\eta'$	$\theta_\omega = +\varphi'$	$\theta_x = +\xi'$
Bending moment and warping m.	$M_y = -EI_{yy}\theta_y'$ $= -EI_{yy}\eta''$	$M_\omega = -EI_{\omega\omega}\theta_\omega'$ $= -EI_{\omega\omega}\varphi''$	$M_x = -EI_{xx}\theta_x'$ $= -EI_{xx}\xi''$
Shearing forces and torsional moments	$Q_y = +M'_y$ $= -(EI_{yy}\theta_y')'$ $= -(EI_{yy}\eta'')'$	$T_\omega = +M'_\omega$ $= -(EI_{\omega\omega}\theta_\omega')'$ $= -(EI_{\omega\omega}\varphi'')'$	$Q_x = +M'_x$ $= -(EI_{xx}\theta_x')'$ $= -(EI_{xx}\xi'')'$
Load	$p_y = -Q'_y$ $= -M''_y$ $= + (EI_{yy}\theta_y'')''$ $= + (EI_{yy}\eta'')''$	$m_D = -T'_\omega$ $= -M''_\omega$ $= + (EI_{\omega\omega}\theta_\omega'')''$ $= + (EI_{\omega\omega}\varphi'')''$	$p_x = -Q'_x$ $= -M''_x$ $= + (EI_{xx}\theta_x'')''$ $= + (EI_{xx}\xi'')''$

v) Bending in x -Direction. The sign convention set down for the y -direction will be valid for the x -direction as well (v. column 3 of Table 5.1). This statement seems trivial since it is really the prerequisite for a systematic treatment and the analogies of problems in flexure and torsion. Note that these sign conventions are different from those which assume moments to be positive whenever their vectors point in the positive direction of a coordinate axis.

f) Axial Forces. If the bending moments are not caused by lateral loads but by an eccentrically acting axial load with the coordinates x_N and y_N , then the

¹ HEILIG, R.: Der Schubverformungseinfluß auf die Wölbkrafttorsion von Stäben mit offenem Profil. Stahlbau 30 (1961) 97.

bending moments are given by:

$$M_x = +N x_N,$$

$$M_y = +N y_N.$$

A positive axial force causes tension.

5.2 Characteristic Behavior of Thin-Walled Cross Sections

In the "thin-walled" cross section the axial stresses and the shear stresses along the center line of the walls are assumed to be representative of the stress distribution over the cross section. The cross section may be arbitrarily shaped and may have constant or variable wall thickness.

The restriction to thin-walled cross sections introduces a considerable simplification in the analysis of stresses and deformations. The position of these quantities may be given by means of a curvilinear coordinate axis s which coincides with the center line of the cross section, has its origin in the boundary point 1 and ends in the boundary point n with the coordinate $s = b$ (Fig. 5.2a).

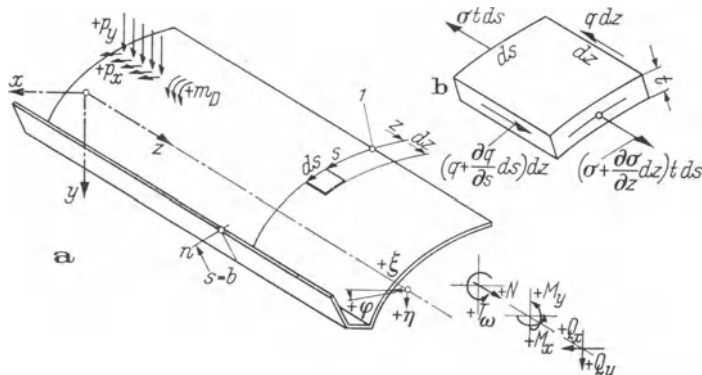


Fig. 5.2. Positive Quantities According to Definition.

- a) At the Member: Loads (p_x, p_y, m_D), Deformations (ξ, η, φ), Internal Forces ($Q_x, Q_y, N, M_x, M_y, T_\omega$);
- b) Stresses Acting at a Rectangular Wall Element.

Another consequence of thin walls is that Saint-Venant torsion has but little influence on the torsional moments and the angle of twist and therefore often may be neglected. (The torsion constant K is proportional to the cube of the wall thickness, and the value α , which, according to Section 10.2a, characterizes the torsional behavior, is relatively small.)

Fig. 5.2b shows the forces acting on a small, rectangular wall element. The shear flow q , product of shear stress and wall thickness

$$q = \tau t,$$

is again used instead of the shear stresses $\tau_{zs} = \tau_{sz}$.

Neglecting the normal stresses in the direction of the curvilinear coordinate represents a further simplification.

a) Equilibrium Condition for the Wall Element

The equilibrium condition for the wall element in Fig. 5.2b formulated for the longitudinal direction of the member is as follows:

$$\frac{\partial q}{\partial s} + \frac{\partial \sigma}{\partial z} t = 0. \quad (5.1)$$

b) Compatibility Condition

Figs. 5.3a and 5.3b show a front view and a top view of the wall element in both the original (solid-lined) and the displaced (dash-lined) position. Between the displacement w in the longitudinal direction, the displacement v along the arc and the change γ in the original right angle of the element ($\gamma = \tau/G$ = shearing strain), there exists the following differential relation:

$$\frac{\partial w}{\partial s} + \frac{\partial v}{\partial z} = \gamma. \quad (5.2)$$

c) The Tangential Displacement in Terms of ξ , η , φ

The letters ξ , η and φ denote the displacements of a small wall element in the x - and y -direction and the rotation around an axis which is parallel to the member axis (point P in Fig. 5.3e) respectively. The displacement v along the curvilinear coordinate s shall be expressed in terms of the displacements ξ , η and φ .

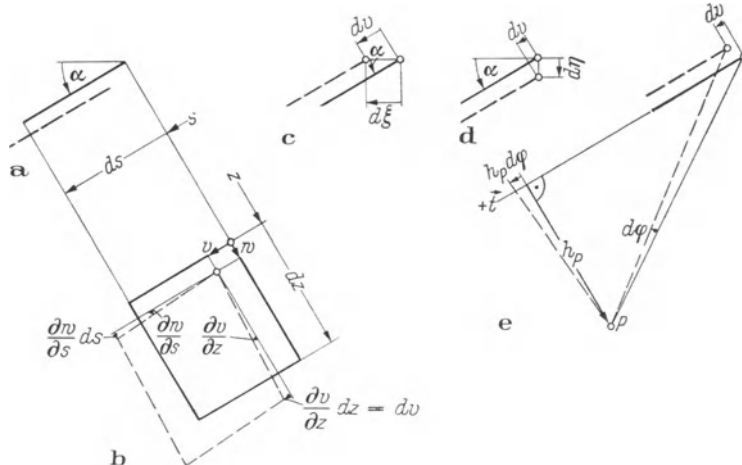


Fig. 5.3. Deformations and Displacements of a Wall Element.

If the increase of the displacement ξ from the position z to $z + dz$ is $d\xi$, then the corresponding increase of the tangential displacement dv is according to Fig. 5.3c $dv = d\xi \cos \alpha$. The quantity α is the angle between the positive x -axis and the positive tangential direction measured counterclockwise.

Fig. 5.3d leads to the corresponding relation $dv = d\eta \sin \alpha$. The point P is assumed to be the center of the rotation of the wall element (Fig. 5.3e). It is

at a distance h_P away from the tangent to the wall element (Fig. 5.3e). This distance shall be considered positive, when, in conjunction with the positive direction of the “ s ” coordinate, it creates a counter-clockwise couple. The tangential displacement dv caused by an increase of the rotation $d\varphi$ within the positions z and $z + dz$ is therefore $dv = h_P d\varphi$.

A superposition of these three contributions leads to:

$$dv = d\xi \cos \alpha + d\eta \sin \alpha + h_P d\varphi.$$

Since ξ , η and φ are functions of the coordinates s and z while α and h_P do not depend on z , this relation may be rewritten in the form:

$$\frac{\partial v}{\partial z} = \frac{\partial \xi}{\partial z} \cos \alpha + \frac{\partial \eta}{\partial z} \sin \alpha + h_P \frac{\partial \varphi}{\partial z}. \quad (5.3)$$

d) Assumptions

Three essential assumptions are made herein for the analysis of prismatic members with open, thin-walled cross sections:

1. Preservation of the Cross-Sectional Shape. This means that the functions $\xi(s, z)$, $\eta(s, z)$ and $\varphi(s, z)$ have to assume equal values in all points of the cross section. They must not depend on the cross-sectional coordinate s and are therefore representative for the entire cross section.

$$\xi = \xi(z), \quad \eta = \eta(z), \quad \varphi = \varphi(z). \quad (5.4)$$

2. Negligible Shear Deformations. This assumption, which is customary in theories on flexure, means mathematically that the shearing strain γ in Eq. (5.2) vanishes thus yielding the following simple relation between the longitudinal displacement w and the tangential displacement v :

$$\frac{\partial w}{\partial s} = - \frac{\partial v}{\partial z}. \quad (5.5)$$

3. Proportionality Between Stresses and Strains. The material shall satisfy Hooke’s law. Because of the simple state of stress shown in Fig. 5.2b, the strains, which are the first derivatives of the displacements, are related with the stresses by the following simple expression:

$$\sigma = E \frac{\partial w}{\partial z}. \quad (5.6)$$

e) The Six Equilibrium Conditions Written for a Cross Section

Six equilibrium conditions may be written for each cross section, each corresponding to one component of a general force or moment vector: Axial force N , bending moments M_x and M_y , torsional moment T_P with respect to a cross-sectional point P and the two shearing forces Q_x and Q_y . The equilibrium condi-

tions require the resultants of the internal forces to be equal to those obtained by a reduction of the external forces with respect to the cross section:

$$\begin{aligned} \int_F \sigma dF &= N, & a) \quad \int_s q h_P ds &= T_P, & d) \\ \int_F \sigma x dF &= M_x, & b) \quad \int_s q \cos \alpha ds &= Q_x, & e) \\ \int_F \sigma y dF &= M_y, & c) \quad \int_s q \sin \alpha ds &= Q_y. & f) \end{aligned} \quad (5.7)$$

5.3 Bending without Twist

a) Longitudinal Displacement w

Stresses will now be calculated for pure bending (bending without twist) of the member. Therefore, there are neither axial forces nor torsional moments and the right sides of Eqs. (5.7a) and (5.7d) vanish:

$$\int_F \sigma dF = 0, \quad \int_s q h_P ds = 0. \quad (5.8)$$

This is only possible if the member is acted upon by lateral loads whose lines of action go through the cross-sectional points P .

If Eq. (5.3) is introduced into Eq. (5.5) with the assumption $\partial \varphi / \partial z = 0$ and the preservation of the cross section [Eq. (5.4)], one arrives at:

$$\frac{\partial w}{\partial s} = - \frac{d\xi}{dz} \cos \alpha - \frac{d\eta}{dz} \sin \alpha,$$

which leads to:

$$w = -\xi' \int \cos \alpha ds - \eta' \int \sin \alpha ds + w_0(z).$$

Since

$$dX (= dx) = ds \cos \alpha, \quad dY (= dy) = ds \sin \alpha \quad (5.9)$$

one finally gets:

$$w = -\xi' X - \eta' Y + w_0(z). \quad (5.10)$$

The shift to capital letters for the coordinates will indicate that they refer to a coordinate system with the origin at an arbitrary position [as opposed to the system (x, y) whose origin is the center of gravity C]. The function $w_0(z)$ is yet undetermined but, according to Eq. (5.10), is simply the longitudinal displacement in the origin of the system (X, Y) .

Moreover, Eq. (5.10) shows that the longitudinal displacement w is linearly distributed across the cross section. The assumptions (5.4) and (5.5) include therefore Bernoulli-Navier's hypothesis of plane cross sections.

b) Axial Stress σ

Hooke's law (5.6) relates stresses and deformations. Based on the deformations given by Eq. (5.10), the expression for the stress becomes:

$$\sigma = -E\xi''X - E\eta''Y + Ew'_0(z).$$

The first of the conditions (5.8) determines $w'(z)$:

$$\begin{aligned} -E\xi'' \int_F X dF - E\eta'' \int_F Y dF + Ew \int_F dF &= 0, \\ Ew'_0(z) &= E\xi'' \frac{\int_F X dF}{F} + E\eta'' \frac{\int_F Y dF}{F}, \end{aligned}$$

whereupon:

$$\sigma = -E\xi'' \left(X - \frac{\int_F X dF}{F} \right) - E\eta'' \left(Y - \frac{\int_F Y dF}{F} \right).$$

Since the quotients in the brackets represent the coordinates of the center of gravity in the coordinate system (X, Y), the coordinate transformation

$$x = X - \frac{\int_F X dF}{F}, \quad y = Y - \frac{\int_F Y dF}{F}, \quad (5.11)$$

reduces the expression for the stress to the following simpler form:

$$\sigma = -E\xi''x - E\eta''y. \quad (5.12)$$

The axis x and y are therefore centroidal axis of the cross section.

The remaining unknown functions ξ'' and η'' in the expression (5.12) are determined by means of the equilibrium conditions (5.7 b) and (5.7 c):

$$\begin{aligned} -E\xi'' \int_F xx dF - E\eta'' \int_F xy dF &= M_x, \\ -E\xi'' \int_F xy dF - E\eta'' \int_F yy dF &= M_y. \end{aligned}$$

Solving this system of two simultaneous, linear equations for ξ'' and η'' leads to:

$$\begin{aligned} -E\xi'' &= \frac{M_y I_{yy} - M_y I_{xy}}{D}, \\ -E\eta'' &= \frac{M_y I_{xx} - M_x I_{xy}}{D}, \end{aligned} \quad (5.13)$$

where:

$$D = I_{xx}I_{yy} - I_{xy}^2. \quad (5.14)$$

The expression for the axial stresses (5.12) may now be rewritten in the form:

$$\sigma = \frac{(M_x I_{yy} - M_y I_{xy})x + (M_y I_{xx} - M_x I_{xy})y}{D} \quad (5.15a)$$

which, when arranged in terms of the forces M_x and M_y , becomes:

$$\sigma = \frac{I_{yy}x - I_{xy}y}{D} M_x + \frac{I_{xx}y - I_{xy}x}{D} M_y. \quad (5.15b)$$

If the numerator in Eq. (5.15a) is set equal to zero, the equation for the neutral axis corresponding to M_x and M_y is arrived at. The denominator of the same quotient represents the well-known invariant combination of the moments of inertia (5.14).

The axis x and y are said to be principal axis whenever the product of inertia $I_{xy} = 0$. In this case, Eq. (5.15b) reduces to:

$$\sigma = \frac{M_x}{I_{xx}} x + \frac{M_y}{I_{yy}} y. \quad (5.16)$$

e) Shear Stresses τ

The integration of the equilibrium condition (5.1) along the curvilinear coordinate s leads to:

$$q(s, z) = q_1(z) - \int_0^s \frac{\partial \sigma}{\partial z} t \, ds. \quad (5.17)$$

The constant of integration q_1 is a function of z . It represents the shear flow at the beginning of the region of integration and vanishes whenever the integration starts at a stress-free boundary of the cross section. It is assumed hereafter that this is the case (v. Fig. 5.2).

In Eqs. (5.15) only the moments are functions of z . According to the summary of Table 5.1, derivatives of these moments with respect to z are the resultant shearing forces. If therefore the derivative of expression (5.15a) is introduced into Eq. (5.17), the latter becomes:

$$q = -\frac{1}{D} \left[(Q_x I_{yy} - Q_y I_{xy}) \int_0^s x t \, ds + (Q_y I_{xx} - Q_x I_{xy}) \int_0^s y t \, ds \right].$$

The integrals in this expression represent statical moments of the portion of the cross section which stretches from 0 to s . If these integrals are denoted by \tilde{S}_x and \tilde{S}_y :

$$\tilde{S}_x = \int_0^s x \, dF, \quad \tilde{S}_y = \int_0^s y \, dF, \quad (5.18)$$

the formulas for the shear flows may be arranged as for the axial stresses [Eqs. (5.15 b) and (5.16)]:

$$q = -\frac{I_{yy}\tilde{S}_x - I_{xy}\tilde{S}_y}{D} Q_x - \frac{I_{xx}\tilde{S}_y - I_{xy}\tilde{S}_x}{D} Q_y, \quad (5.19)$$

or, with respect to principal axis:

$$q = -\frac{Q_x}{I_{xx}}\tilde{S}_x - \frac{Q_y}{I_{yy}}\tilde{S}_y. \quad (5.20)$$

d) Shear Center

The formulas for the axial stresses and the shear stresses derived above are valid only when the conditions set forth by Eqs. (5.8) are satisfied.

The first of these conditions asks for a vanishing axial force along the member and has already been utilized in the derivation of Eq. (5.12). The second condition requires that the moment of the shear flows with respect to the point P be zero. Since this point P shall furthermore coincide with the line of action of the applied forces, the point P represents a special point of the cross section which shall be denoted by D . This point is common to all shearing forces in the cross section which cause twist-free bending. The importance of this point was recognized first by R. MAILLART¹ and A. EGGENSCHWYLER² and was named "shear center" by the former.

The evaluation of the shear center will be made in reference to a coordinate system that has the center of gravity of the cross section as its origin. The position of this point D may therefore be given by the coordinates x_D and y_D .

If an arbitrary shearing force which passes through the shear center D is divided into components Q_x and Q_y , then the condition that each component and the corresponding shear flow reduce to the same torsional moment with respect to the center of gravity C may be formulated as follows:

$$\begin{aligned} \int_s q(Q_y) h_C ds &= Q_y x_D, \\ \int_s q(Q_x) h_C ds &= -Q_x y_D. \end{aligned} \quad (5.21)$$

Eq. (5.19) gives the shear flow for each of the two components ($Q_x = 0$ in the first case and $Q_y = 0$ in the second). Eq. (5.21) leads to the following general expression for the coordinates of the shear center:

$$\begin{aligned} x_D &= -\frac{1}{D} \left[I_{xx} \int_s \tilde{S}_y h_C ds - I_{xy} \int_s \tilde{S}_x h_C ds \right], \\ y_D &= +\frac{1}{D} \left[I_{yy} \int_s \tilde{S}_x h_C ds - I_{xy} \int_s \tilde{S}_y h_C ds \right]. \end{aligned} \quad (5.22)$$

¹ MAILLART, R.: Zur Frage der Biegung. Schweiz. Bauztg. 77 (1921) 195.

² EGGENSCHWYLER, A.: Über die Festigkeitsberechnung von Schiebetoren und ähnlichen Bauwerken. Diss. ETH Zürich, 1921.

These expressions simplify again for a system of principal axis ($I_{xy} = 0$):

$$\begin{aligned} x_D &= - \frac{\int \tilde{S}_y h_C ds}{I_{yy}}, \\ y_D &= + \frac{\int \tilde{S}_x h_C ds}{I_{xx}}. \end{aligned} \quad (5.23)$$

5.4 Twist

a) Basic Requirements and the Warping Function w

Pure twist φ around a center of rotation D requires that neither axial forces nor bending moments act on the cross section. Therefore, the equilibrium conditions (5.7 a, b and c) are changed accordingly:

$$\int_F \sigma dF = 0, \quad \int_F \sigma x dF = 0, \quad \int_F \sigma y dF = 0. \quad (5.24)$$

Vanishing displacements ξ and η and the first condition (5.4) reduce Eq. (5.3) to:

$$\frac{\partial v}{\partial z} = \varphi' h_D.$$

The consideration of the second condition (5.5) followed by the integration along the coordinate s leads finally to:

$$w = -\varphi' \int h_D ds + w_0(z).$$

The last expression shows that plane cross sections do not necessarily remain plane when the member is subjected to pure twist. The cross section *wraps* according to the longitudinal displacement w . The warping w is distributed linearly only for straight portions of the cross sections where the tangential distance h_D is constant and may thus be taken out of the integral sign.

The stress analysis for torsion and bending, however, may be made completely analogous if the integral with the integrand $h_D ds$ is assumed to be a coordinate. The calculation of stresses will again involve statical moments, moments of inertia and products of inertia which, for the purpose of distinction, shall be characterized by the adjective “sectorial” (v. Section 5.1 c). The newly introduced coordinate is moreover called sectorial coordinate and denoted by the symbol Omega. The capital letter Ω designates the coordinate with an arbitrarily positioned origin while the small letter ω stands for the normalized sectorial coordinate. This rule is therefore analogous to the convention for the remaining two cross-sectional coordinates X , x and Y , y respectively. With the definition:

$$d\Omega (= d\omega) = h_D ds. \quad (5.25)$$

the warping function may again be written as:

$$w = -\varphi' \Omega + w_0(z). \quad (5.26)$$

b) Warping Stresses

If the warping function (5.26) is introduced into Hooke's law, one arrives at the warping stress:

$$\sigma = -E\varphi''\Omega + Ew'_0(z).$$

The first of the conditions (5.24) serves to eliminate the constant of integration $w_0(z)$. The application of this condition leads to:

$$-E\varphi'' \int_F \Omega dF + Ew'_0(z) \int_F dF = 0,$$

from which follows:

$$Ew'_0(z) = E\varphi'' \frac{\int_F \Omega dF}{F}.$$

With the normalized sectorial coordinate

$$\omega = \Omega - \frac{\int_F \Omega dF}{F}, \quad (5.27)$$

the expression for the stress may be written in the form:

$$\sigma = -E\varphi''\omega. \quad (5.28)$$

The shear flow distribution follows from Eq. (5.1):

$$q = +E\varphi''' \int_0^s \omega t ds + q_1(z).$$

The constant of integration $q_1(z)$ is zero since it represents the shear flow at the beginning of the region of integration which was taken at a free boundary. With the substitution

$$\tilde{S}_\omega = \int_0^s \omega dF, \quad (5.29)$$

which may be designated as the "sectorial statical moment of the cut-off portion of the cross section", one arrives at:

$$q = +E\varphi''' \tilde{S}_\omega. \quad (5.30)$$

The equilibrium condition (5.7d) is utilized in order to eliminate the unknown angle of twist. If the torsional moment with respect to the point D is designated

by T_ω , this condition may be written as follows:

$$\int_s q h_D ds = T_\omega. \quad (5.31)$$

Considering the definition for the sectorial coordinate (5.25), integration by parts transforms the left side of Eq. (5.31) into:

$$\int_s q d\omega = q\omega \Big|_{s=0}^{s=b} - \int_s \frac{\partial q}{\partial s} \omega ds.$$

Eq. (5.1) and the condition for vanishing shear flows at free boundaries leads to:

$$\int_s q d\omega = 0 + \int_s \frac{\partial \sigma}{\partial z} \omega t ds,$$

which according to Eq. (5.28) is:

$$= -E\varphi''' \int_s \omega \omega dF,$$

or

$$= -E\varphi''' I_{\omega\omega}. \quad (5.32)$$

Therefore

$$\varphi''' = -\frac{T_\omega}{EI_{\omega\omega}}$$

and according to the definitions summarized in Table 5.1

$$\varphi'' = -\frac{M_\omega}{EI_{\omega\omega}}.$$

The warping stresses finally result from Eqs. (5.28) and (5.30):

$$\sigma = +\frac{M_\omega}{I_{\omega\omega}} \omega, \quad (5.33)$$

$$q = \tau t = -\frac{T_\omega}{I_{\omega\omega}} \tilde{S}_\omega. \quad (5.34)$$

c) Center of Twist

The calculation of the sectorial quantities assumes known coordinates x_D and y_D for the center of twist. This point may not be selected arbitrarily since the second and third condition (5.24) require zero flexural moments in the cross section. These conditions may be formulated in a different manner by means of relation (5.28):

$$\int_F \omega x dF = 0, \quad \int_F \omega y dF = 0. \quad (5.35)$$

If the tangent t to a wall element is at a distance h_D away from the origin C of the coordinate system (x, y) , then its distance from the point D with the coordinates x_D and y_D is given by:

$$h_D = h_C - x_D \sin \alpha + y_D \cos \alpha. \quad (5.36)$$

The angle α is the positive rotation of the x -axis necessary to have the positive branch of the x -axis coincide with the positive branch of the tangent (for signs v. Fig. 5.2):

If both sides of Eq. (5.36) are multiplied by ds :

$$h_D ds = h_C ds - x_D \sin \alpha ds + y_D \cos \alpha ds,$$

it may, by means of Eqs. (5.9) and (5.25), be written in the form:

$$d\omega_D = d\omega_C - x_D dy + y_D dx \quad (5.37)$$

which, when integrated along s and normalized, leads to:

$$\omega_D = \omega_C - x_D y + y_D x. \quad (5.38)$$

This transformation of the sectorial coordinate ω is now introduced into the equilibrium conditions (5.35), yielding the following relations:

$$\begin{aligned} \int_F \omega_C x dF - x_D \int_F y x dF + y_D \int_F x x dF &= 0, \\ \int_F \omega_C y dF - x_D \int_F y y dF + y_D \int_F x y dF &= 0. \end{aligned}$$

If the area-integrals are denoted as shown in Section 5.1c, the solutions to these two simultaneous linear equations may be written as follows:

$$\begin{aligned} x_D &= \frac{1}{D} (I_{xx} I_{y\omega} C - I_{xy} I_{x\omega} C), \\ y_D &= -\frac{1}{D} (I_{yy} I_{x\omega} C - I_{xy} I_{y\omega} C). \end{aligned} \quad (5.39)$$

The term D was defined in Eq. (5.14).

If the cross section refers to principal axis x and y , the product of inertia I_{xy} is zero and the solutions for the center of twist (5.39) reduce to:

$$x_D = \frac{I_{y\omega} C}{I_{yy}}, \quad y_D = -\frac{I_{x\omega} C}{I_{xx}}. \quad (5.40)$$

5.5 Miscellaneous Considerations

a) Properties of the Area Integrals

According to Eqs. (5.11) and (5.27), the coordinates x , y and ω are normalized such as to yield the value zero for the corresponding area integral. The statical moments for a portion of the cross section \tilde{S}_x , \tilde{S}_y and \tilde{S}_ω will therefore not only

be zero for the boundary $s = 0$ but also for the boundary $s = b$:

$$\begin{aligned}\tilde{S}_x(0) &= \tilde{S}_x(b) = 0, & \text{a)} \\ \tilde{S}_y(0) &= \tilde{S}_y(b) = 0, & \text{b)} \\ \tilde{S}_\omega(0) &= \tilde{S}_\omega(b) = 0. & \text{c)}\end{aligned}\quad (5.41)$$

Since the shear flows q are always given by some linear combination of the variables \tilde{S} , the physical condition asking for vanishing shear flows at the boundaries are therefore analytically satisfied as well.

Aside from the variables $x, y, \omega, \tilde{S}_x, \tilde{S}_y$ and \tilde{S}_ω , the cross-sectional constants $I_{xx}, I_{yy}, I_{\omega\omega}, I_{yx}, I_{x\omega}$ and $I_{y\omega}$ appear in the analysis. The latter are area integrals of all possible products of two coordinates. Because of the thin-walled cross sections, they reduce to line integrals which may be integrated by parts, e.g.:

$$I_{xx} = \int_0^b xx \, dF = x \tilde{S}_x \Big|_0^b - \int_0^b \tilde{S}_x \, dx.$$

Because of Eqs. (5.41), the first element of these integral transformations vanishes without exception thus yielding the following relations:

$$\begin{aligned}I_{xx} &= - \int_0^b \tilde{S}_x \, dx, & \text{a)} \\ I_{yy} &= - \int_0^b \tilde{S}_y \, dy, & \text{b)} \\ I_{\omega\omega} &= - \int_0^b \tilde{S}_\omega \, d\omega, & \text{c)} \\ I_{xy} &= - \int_0^b \tilde{S}_x \, dy = - \int_0^b \tilde{S}_y \, dx, & \text{d)} \\ I_{x\omega} &= - \int_0^b \tilde{S}_x \, d\omega = - \int_0^b \tilde{S}_\omega \, dx, & \text{e)} \\ I_{y\omega} &= - \int_0^b \tilde{S}_y \, d\omega = - \int_0^b \tilde{S}_\omega \, dy. & \text{f)}\end{aligned}\quad (5.42)$$

The sectorial quantities in these expressions may refer to an arbitrary point of reference.

b) Identity of Shear Center and Center of Twist

A comparison of the expressions (5.22) and (5.39) shows that they are identical if the following relations hold:

$$\int_0^b \tilde{S}_y h_C \, ds = -I_{y\omega} c, \quad \int_0^b \tilde{S}_x h_C \, ds = -I_{x\omega} c.$$

Since $hds = d\omega$, the relations represent simply the identities (5.42f) and (5.42e).

The shear center therefore is at the same time the center of twist. This particular point was therefore identified by the letter D right from the beginning.

c) The Equilibrium Conditions for the Shearing Forces

From a total of six equilibrium conditions (5.7), only four were used in Sections 5.3 and 5.4 for the analysis of pure bending and pure twist. The conditions a to d were utilized either as conditions for the applied loads or as a means of determining quantities which do not depend on the cross section.

The remaining equilibrium conditions (5.7e) and (5.7f) are nevertheless satisfied as will be demonstrated hereinafter.

With the help of Eq. (5.9), the two remaining equilibrium conditions (5.7e) and (5.7f) may be written in the form:

$$\int_0^b q \, dx = Q_x, \quad \int_0^b q \, dy = Q_y.$$

The validity of these conditions can be readily shown for the case of pure bending. If the shear flow is introduced as given by Eq. (5.19), a transformation of the left sides considering the identities (5.42) demonstrates at once the stated equivalence for each of the foregoing conditions.

A similar proof for pure twist introduces the shear flow q as given by Eq. (5.34). The integration which considers the identities (5.42e) and (5.42f) leads to expressions showing the sectorial products of inertia $I_{x\omega}$ and $I_{y\omega}$ as factors. The latter, however, are zero because of the conditions (5.35).

6 Numerical Calculation of the Cross-Sectional Constants

6.1 Computation Scheme

a) Geometrical Approximation

The cross section consists (exactly or approximately) of n narrow, rectangular elements. The centers of the elements will be numbered consecutively by the even numbers i while odd numbers k are assigned to the junctures of two adjacent elements and outer boundaries (v. Fig. 6.1).

Since the three coordinate distances x , y and ω vary linearly along the length of the element i which is of constant thickness t_i , the statical moments \tilde{S}_x , \tilde{S}_y and \tilde{S}_ω will show a parabolic distribution along each element. The shear flows which exhibit the same variation are therefore completely determined if they are known at three points, at the center of element i and at the junctures k and

$k + 1$ of the element. The variation of the axial stress is linear along the rectangular portions of the wall [v. Eq. (5.15) and (5.16)].

$$\sigma = \sigma_i + (\sigma_{k+1} - \sigma_k)u, \quad (6.1)$$

$$q = q_i + (q_{k+1} - q_k)u + (q_{k+1} - 2q_i + q_k)2u^2. \quad (6.2)$$

Herein is

$$u = \frac{s - s_i}{s_{k+1} - s_k}.$$

b) Required Quantities

In order to calculate the axial stresses and the shearing stresses in a cross section consisting of n rectangular elements for arbitrary lateral loads, the six variables

$$x, y, \omega \quad \text{and} \quad \tilde{S}_x, \tilde{S}_y, \tilde{S}_\omega,$$

have to be calculated in $2n + 1$ points.

They are supplemented by the moments of inertia

$$I_{xx}, I_{yy}, I_{\omega\omega} \quad \text{and} \quad I_{xy}, I_{x\omega}, I_{y\omega}.$$

A complete stress analysis requires therefore

$$6(2n + 1) + 6 = 12(n + 1)$$

numerical quantities. The cross-sectional area F and the coordinates of the center of gravity X_c , Y_c and of the shear center x_D and y_D appear as intermediate results.

It is the purpose of this section to develop a systematic computational scheme that will require a minimum number of simple steps to yield the desired numerical information. Although the following relations are readily adaptable to electronic computer analysis, the steps are nevertheless arranged for the application of a simple desk calculator¹.

c) Finite Difference Relations

The cross section is completely defined by the areas ΔF_i of the rectangular elements and by the coordinates X_k and Y_k of the element connections and outer boundaries. The definition of the cross section requires therefore altogether $3n + 2$ input values.

If the rectangular elements were defined by their thicknesses t_i instead of their areas, the latter could be determined as follows:

$$\underline{\underline{\Delta F_i}} = t_i \sqrt{(X_{k+1} - X_k)^2 + (Y_{k+1} - Y_k)^2}. \quad (6.3)$$

¹ Such a program for automatic computation was developed by JOHN WOLF at the Institute for Statics and Structural Engineering, Swiss Federal Institute of Technology, Zürich, of which B. THÜRLIMANN is the Head.

In order to avoid divisions when calculating the average of two coordinates, the tabulation will list $\Delta F_i/4$ instead of ΔF_i . Moreover, the fraction of ΔF_i shall appear twice, once between the points k and i and once between i and $k+1$.

$$\text{Input: } \frac{\Delta F_i}{4}, \quad \frac{\Delta F_i}{4}. \quad (\text{a})$$

The differentials dx , dy and $d\omega$ appear as finite differences and are of the order of magnitude of element widths [v. Eq. (5.9)]:

$$\Delta x_i = \Delta X_i = X_{k+1} - X_k, \quad (\text{x 1})$$

$$\Delta y_i = \Delta Y_i = Y_{k+1} - Y_k. \quad (\text{y 1})$$

Based on the expression for the distance between a straight line through the point $P(x, y)$ and the origin of the coordinate system, $h = x \sin \alpha - y \cos \alpha$, the following formula for the differential of the sectorial coordinate with respect to the center of gravity C , $d\omega_c$ [v. Eq. (5.25)], is arrived at:

$$d\omega_c = d\Omega_c = x \sin \alpha ds - y \cos \alpha ds.$$

This relation may be put into the following finite-difference form:

$$\Delta \omega_{ci} = \Delta \Omega_{ci} = x \Delta y_i - y \Delta x_i,$$

where x and y may be assumed to be the coordinates of any of the three tabulated points. The center of the rectangular element i will be selected for the purpose of symmetry:

$$\Delta \omega_{ci} = \Delta \Omega_{ci} = x_i \Delta y_i - y_i \Delta x_i, \quad (\omega_c 1)$$

whereas the alternate formula which involves the coordinates of the points k and $k+1$ shall only be used for the purpose of verification:

$$\Delta \omega_{ci} = \Delta \Omega_{ci} = x_k y_{k+1} - x_{k+1} y_k. \quad (\omega_c 1)_{\text{alt.}}$$

(Note that $\Delta \omega_{ci}$ represents twice the area of the triangle defined by the element i as base line and the point of reference C .)

After knowing the coordinates of the shear center, the transformed differences $\Delta \omega_i = \Delta \omega_{Di}$ may be calculated by means of Eq. (5.37):

$$\Delta \omega_i = \Delta \Omega_i = \Delta \omega_{ci} - x_D \Delta y_i + y_D \Delta x_i. \quad (\omega 1)$$

The coordinates X and Y of element junctures and boundaries k are either introduced directly as data:

$$\text{Input: } X_k, \quad (\text{x 2})$$

$$\text{Input: } Y_k, \quad (\text{y 2})$$

or indirectly as coordinate differences as for instance for Ω :

$$\Omega_{k+1} = \Omega_k + \Delta\Omega_i. \quad (\omega 2)$$

The starting value Ω_1 is completely arbitrary, e.g. $\Omega_1 = 0$.

A normalization of the coordinates requires the weighted average of the arbitrarily oriented coordinate distances X , Y and Ω . The areas of the rectangular elements or quantities proportional thereto will represent the weights. If half of the area ΔF_i is introduced as the weight, then the half of the contribution of element i to the statical moment with respect to an arbitrary origin of the coordinate system is:

$$\frac{1}{2} \Delta S_{X,i} = \frac{\Delta F_i}{4} (X_k + X_{k+1}), \quad (x 3)$$

$$\frac{1}{2} \Delta S_{Y,i} = \frac{\Delta F_i}{4} (Y_k + Y_{k+1}), \quad (y 3)$$

$$\frac{1}{2} \Delta S_{\Omega,i} = \frac{\Delta F_i}{4} (\Omega_k + \Omega_{k+1}), \quad (\omega 3)$$

The amount of the coordinate transformation may now be calculated by means of Eqs. (5.11) and (5.27).

$$\frac{\int_X dF}{\int_F dF} = \frac{\sum_i \frac{1}{2} \Delta S_{X,i}}{\sum_i 2 \frac{\Delta F_i}{4}} = X_0 = \frac{\sum(x3)}{\sum(a)}, \quad (X_0)$$

$$Y_0 = \frac{\sum(y3)}{\sum(a)}, \quad (Y_0)$$

$$\Omega_0 = \frac{\sum(\omega3)}{\sum(a)}. \quad (\Omega_0)$$

These provide the basis for the calculation of the coordinates of the cross-sectional points k and i with respect to the transformed coordinate system.

$$x_k = X_k - X_0, \quad x_i = 0,5(x_k + x_{k+1}), \quad (x 4)$$

$$y_k = Y_k - Y_0, \quad y_i = 0,5(y_k + y_{k+1}), \quad (y 4)$$

$$\omega_k = \Omega_k - \Omega_0, \quad \omega_i = 0,5(\omega_k + \omega_{k+1}). \quad (\omega 4)$$

The *statical moments* of cut-off portions are needed at all points i and k of the cross section. They are made up of contributions ΔS which are the product of the average of the end-coordinates and the area between:

$$\Delta S_{xik} = (x_i + x_k) \frac{\Delta F_i}{4}, \quad (x 5)$$

$$\Delta S_{yik} = (y_i + y_k) \frac{\Delta F_i}{4}, \quad (y 5)$$

$$\Delta S_{\omega ik} = (\omega_i + \omega_k) \frac{\Delta F_i}{4}. \quad (\omega 5)$$

The scheme for the computation of the differences ΔS may therefore be stated as follows:

“The sum of two consecutive coordinates shall be multiplied
by the area tabulated in between”. } (ΔS)

A successive addition of the differences ΔS yields the variables \tilde{S}_x , \tilde{S}_y and \tilde{S}_ω :

$$\tilde{S}_{xi} = \tilde{S}_{xk} + \Delta S_{xik}, \quad (x 6)$$

$$\tilde{S}_{yi} = \tilde{S}_{yk} + \Delta S_{yik}, \quad (y 6)$$

$$\tilde{S}_{\omega i} = \tilde{S}_{\omega k} + \Delta S_{\omega ik}. \quad (\omega 6)$$

The value 0 is assigned to the starting point 1. It will serve as a *check* of the calculations that the statical moments S vanish at the boundary point $n+1$.

$$\tilde{S}_{xn+1} = S_x = 0, \quad K (x 6)$$

$$\tilde{S}_{yn+1} = S_y = 0, \quad K (y 6)$$

$$\tilde{S}_{\omega n+1} = S_\omega = 0. \quad K (\omega 6)$$

The *statical moments of the second order*, I_{xx} , I_{yy} , $I_{\omega\omega}$, I_{xy} and the quantities used for the calculation of the shear center $I_{x\omega C}$ and $I_{y\omega C}$ are, without exception, determined from the relations (5.42).

These cross-sectional quantities result from an integration of the functions \tilde{S}_x , \tilde{S}_y and \tilde{S}_ω that were already calculated. Since these functions are parabolas for each element of the cross section (with known values at the ends and in the center of each element), Simpson's rule performs the integration exactly. The computation scheme may therefore be described as follows:

“The product of the weighted sum of the ordinates S (weights: 1, 4, 1) (column 7) and the corresponding coordinate difference shall be calculated for each element.” } (ΔI)

“The sum of the column multiplied by the factor $-1/6$ is equal to the statical moment of the second order.” } (I)

$$\bar{S}_{xi} = \tilde{S}_{xk} + 4\tilde{S}_{xi} + \tilde{S}_{xk+1}, \quad (x 7)$$

$$\bar{S}_{yi} = \tilde{S}_{yk} + 4\tilde{S}_{yi} + \tilde{S}_{yk+1}, \quad (y 7)$$

$$\bar{S}_{\omega i} = \tilde{S}_{\omega k} + 4\tilde{S}_{\omega i} + \tilde{S}_{\omega k+1}. \quad (\omega 7)$$

$$I_{xx} = -\frac{1}{6} \sum_i \bar{S}_{xi} \Delta x_i, \quad (x 8)$$

$$I_{xy} = -\frac{1}{6} \sum_i \bar{S}_{xi} \Delta y_i, \quad (x 9)$$

$$I_{x\omega C} = -\frac{1}{6} \sum_i \bar{S}_{xi} \Delta \omega_{Ci}, \quad (\text{x 10})$$

$$I_{yy} = -\frac{1}{6} \sum_i \bar{S}_{yi} \Delta y_i, \quad (\text{y 8})$$

$$I_{yx} = -\frac{1}{6} \sum_i \bar{S}_{yi} \Delta x_i = I_{xy}, \quad \text{K (y 9)}$$

$$I_{y\omega C} = -\frac{1}{6} \sum_i \bar{S}_{yi} \Delta \omega_{Ci}, \quad (\text{y 10})$$

$$I_{\omega\omega} = -\frac{1}{6} \sum_i \bar{S}_{\omega i} \Delta \omega_i, \quad (\omega 8)$$

$$I_{\omega x} = -\frac{1}{6} \sum_i \bar{S}_{\omega i} \Delta x_i = 0, \quad \text{K (\omega 9)}$$

$$I_{\omega y} = -\frac{1}{6} \sum_i \bar{S}_{\omega i} \Delta y_i = 0. \quad \text{K (\omega 10)}$$

d) The Set-Up of the Table

Arrangement. The results for each of the operations (x 1) to (x 10), (y 1) to (y 10) and (ω 1) to (ω 10) are listed in one column. Since each of the coordinates requires essentially the same operations, each is treated separately. This leads to the table x (6.1x), table y (6.1y) and table ω (6.1 ω).

The *Input Data* are characterized by means of the odd and even numbers which either denote junctures and outer boundaries or the centers of the different elements (Fig. 6.1).

The numerical analysis of a cross section is separated into the following steps:

1. Set-up and headings for the tables, definition of the cross section in columns (a), (x 2) and (y 2);
2. Calculation of columns (x 3) to (x 6);
Check $K(x 6)$;
Calculation of columns (y 3) to (y 6);
Check $K(y 6)$.
3. Calculation of columns (x 1), (y 1), (ω_C 1);
(x 7) to (x 10);
(y 7) to (y 10);
Check $K(y 9)$.
4. Evaluation of the coordinates x_D and y_D according to Eq. (5.39).
5. Calculation of the columns (ω 1) to (ω 10), check $K(\omega 9)$ and $K(\omega 10)$.

The two final checks $K(\omega 9)$ and $K(\omega 10)$ are very powerful inasmuch as they involve all the data and the intermediate results except those of column (ω 8).

All the *results* in the Tables 6.1 are framed by a solid line. The variables are listed in columns 4 and 6 and the statical moments of second order appear at the bottom of columns 8, 9 and 10.

The size of the tables may be slightly reduced if a desk calculator with some storage capacity is accessible. Columns 3 and 7 may be suppressed in this case since it is only the sum of column 3 which is of interest and column 7 lists numbers without a physical meaning.

6.2 Example

a) Cross-Sectional Quantities

The computation scheme developed above will now be applied to the cross section shown in Fig. 6.1.

The total number of quantities required for this cross section which consists of three narrow, rectangular elements amounts to $12(3 + 1) = 48$. These quantities are calculated in Tables 6.1 in which they are accentuated by a solid, rectangular frame. The quantities framed by a dotted line serve as a check on the accuracy of the calculations.

For the purpose of publication, Table 6.1 had to be divided up into three subtables. The division was made with respect to the correspondence with the three coordinates x , y and ω . This means that column (a) and the identification of the rows are repeated at the beginning of each table.

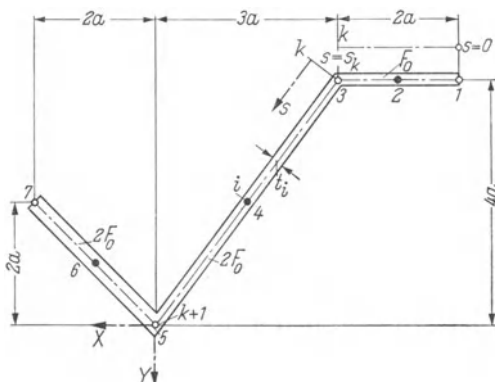


Fig. 6.1. Notation.

In order to facilitate an examination of the calculations, the auxiliary values $\Delta\omega_c$ which are used to calculate the differences $\Delta\omega$ are listed in the last column of Table 6.1y. They were originally placed in column (ω 1) but had to be erased in order to make room for the values $\Delta\omega$.

The calculations necessary to obtain the coordinates of the center of gravity and of the shear center are shown at the bottom of the tables.

b) Stresses

Under the assumption that a member with cross section properties analyzed above is subjected to a uniformly distributed vertical load \bar{p} and exhibits warping torsion only, the distribution of both the axial stresses and the shear stresses may be given.

The resultant of the load per unit length of the member ($p = \bar{p}7a$) is at a distance $x_D + a/2 = 1,65a$ away from the shear center (Fig. 6.2).

This load is resolved into components related to the shear center D as follows:

$$p_y = +p,$$

$$m_D = -1,65pa.$$

If the supports of the member are equivalent with respect to flexure and twist (e.g. if the boundary conditions for φ are the same as those for η), then the ratio between the bending moment M_y due to p_y and the warping moment M_ω due to m_D is the same as the ratio between the load components given above (v. Chapter 7):

$$M_\omega = -1,65aM_y.$$

The same relation holds between the shearing force Q_y and the torsional moment T_ω :

$$T_\omega = -1,65aQ_y.$$

The axial stresses for flexural and torsional loads are calculated by means of Eqs. (5.15b) and (5.33) and a superposition of the effects leads to the relation:

$$\begin{aligned}\sigma &= \left(\frac{I_{xx}}{D} y - \frac{I_{xy}}{D} x - \frac{1,65a}{I_{\omega\omega}} \omega \right) M_y, \\ &= \left(0,344 \frac{y}{a} - 0,195 \frac{x}{a} - 0,180 \frac{\omega}{a^2} \right) \frac{M_y}{aF_0},\end{aligned}$$

Eqs. (5.19) and (5.34) lead to a similar expression for the shear flows:

$$\begin{aligned}q &= \tau t = - \left(\frac{I_{xx}}{D} \tilde{S}_y - \frac{I_{xy}}{D} \tilde{S}_x - \frac{1,65a}{I_{\omega\omega}} \tilde{S}_\omega \right) Q_y, \\ &= - \left(0,344 \frac{\tilde{S}_y}{aF_0} - 0,195 \frac{\tilde{S}_x}{aF_0} - 0,180 \frac{\tilde{S}_\omega}{a^2 F_0} \right) \frac{Q_y}{a}.\end{aligned}$$

The distribution of both the axial and shear stress components is shown as projected on a horizontal line in Fig. 6.2.

Exercise 6.1. Horizontal Load. Calculate the axial stresses in the cross section shown in Fig. 6.1 if the element 2 of the member is subjected to a negative horizontal load.

Solution:

The general solution

$$\sigma = (-0,160305x + 0,194656y - 0,37267\omega) \frac{M_x}{a^2 F_0}$$

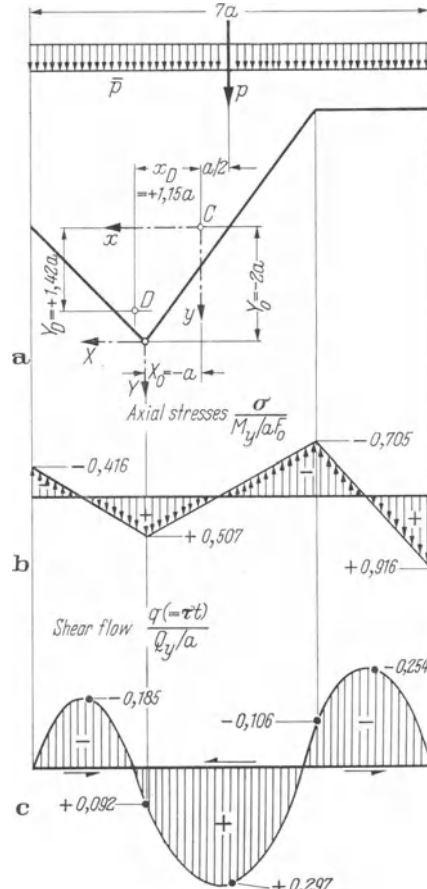


Fig. 6.2. Stresses Caused by a Uniformly Distributed Load Acting on the Profile Shown in Fig. 6.1.

Table 6.1 *x*

$$\text{Eq. } (X_0): X_0 = \frac{\Sigma(x3)}{\Sigma(a)} = \frac{-2,50 \cdot a \cdot F_0}{2,50 \cdot F_0} = -1,00a.$$

Table 6.1 *y*

Table 6.1 ω

$$\text{Eq. (}\Omega_0\text{: } \Omega_0 = \frac{\Sigma(\omega_3)}{\Sigma(a)} = \frac{+11,43a^2F_0}{2,50F_0} = +4,57a^2.$$

assumes the following particular values in:

$$\text{Point 1: } +1,957 \frac{M_x}{a F_0},$$

$$\text{Point 3: } -0,913 \frac{M_x}{a F_0},$$

$$\text{Point 5: } +0,261 \frac{M_x}{a F_0},$$

$$\text{Point 7: } -0,130 \frac{M_x}{a F_0}.$$

Exercise 6.2. *Theory of Warping Torsion Applied to a Folded Plate.* Consider the cross section shown in Fig. 11.3 to be of the thin-walled, open type and calculate:

- a) The sectorial moment of inertia $I_{\omega\omega}$ and the position of the shear center y_D with respect to the points 3 and 7.
- b) The axial stresses for the indicated load. The load p_8 gives rise to the bending moment $M_y = M_{s0}$.

Solutions:

$$\text{a) } I_{\omega\omega} = \frac{14}{27} c^4 F_0, \quad y_D = -\frac{11}{8} c.$$

$$\text{b) } \sigma_1 = -\frac{39}{28} \frac{M_{s0}}{c F_0},$$

$$\sigma_3 = +\frac{9}{7} \frac{M_{s0}}{c F_0},$$

$$\sigma_5 = -\frac{3}{4} \frac{M_{s0}}{c F_0},$$

$$\sigma_7 = -\frac{9}{7} \frac{M_{s0}}{c F_0},$$

$$\sigma_9 = +\frac{81}{28} \frac{M_{s0}}{c F_0}.$$

6.3 Built-Up Open Cross Sections

a) Sign Conventions

The curvilinear coordinate s which coincides with the wall center line of a thin-walled open cross section may be oriented in two different directions. It will be demonstrated below that either of these directions may be declared to be positive with identical results.

A change in the direction of the coordinate s (numbering starts from the opposite end of the cross section) means a sign-change for the differences Δx and Δy and for the variables \tilde{S} .

The coordinates x and y do not change their signs since they represent only a translation of the original system X and Y . The same holds for the sectorial coordinates Ω and ω but for different reasons. The differential of both Ω and ω is

defined by Eq. (5.25) as $h_D ds$. Since a change in the orientation of the curvilinear coordinate s changes the signs of both h_D and ds , the signs of the sectorial coordinates remain unchanged.

The signs of the variables \tilde{S}_x , \tilde{S}_y and \tilde{S}_ω , however are reversed and this in turn reverses the sign of the shear flow q . The latter is said to be positive if it points in the $+s$ -direction when acting on a cross section with positive outward normal. Therefore, a change in the direction of the curvilinear coordinate s reverses the sign of the shear flow q but the physical meaning of the result is still the same.

The moments of inertia are the sums of products which have statical moments and coordinate differences as factors. Since both factors change their sign when referring to the reversed coordinate s , their product is of course independent of the selected direction.

b) Branchings

Open, thin-walled cross sections which may no longer be described by a single, curvilinear coordinate s (v. e.g. Fig. 6.3a) require only slight changes in the computation scheme developed above. These changes are based on two conditions for the stresses at the branchpoints: Equal axial stresses in points which are common to several adjacent elements and continuity of the shear flows at these points. These two conditions require modifications in the calculation of the sectorial coordinate ω and of the statical moment of the cut-off portion.

The statical moments in each of the branches may be calculated separately starting from the free end and proceeding toward the common *branchpoint*. The statical moment immediately after this point is equal to the *sum* of the statical moments of all branches cut-off at the junction. There will *never be differences* if the cross section is of the open and thin-walled type.

For the purpose of analysis the cross section is referred to a principal curvilinear coordinate s which starts at some arbitrary free end and ends at another. This axis is again numbered consecutively as before. Secondary, curvilinear coordinates are then defined which have their origin at the free ends of the remaining branches. Each of the secondary coordinates is numbered separately with the assignment of different odd numbers to the origin.

The distribution of the variable \tilde{S} along the secondary branches is evaluated first (column 6). The values of \tilde{S} at the junctions represent differences ΔS for the distribution of the statical moments along the principal coordinate and are therefore introduced into column 5.

The sectorial coordinate Ω is likewise the result of a consecutive summing up of differences. It is first calculated along the principal curvilinear coordinate whereupon the distribution along the secondary branches is calculated backwards, starting from known values at the junctions.

c) Symmetries

Symmetries in a cross section may lead to a considerable simplification in the numerical analysis. If, for example, the cross section has one axis of symmetry, this axis may be made to coincide with the y -axis of the coordinate system. The

coordinates x and ω are thus antisymmetric with respect to the axis of symmetry. They don't need to be normalized and a calculation of the coordinate ω may be based at once on the differences $\Delta\omega$.

The area integrals I_{xy} and $I_{y\omega C}$ become zero since their integrand consists of one antisymmetric coordinate. It follows further from the first of Eqs. (5.39) that the shear center is positioned on the axis of symmetry.

The table for the numerical analysis may be reduced by some columns since the area integral is zero and no normalization of the coordinates is necessary (v. Table 6.2). If the symmetries and antisymmetries in the calculations were taken into account, the rows in Table 6.2 which correspond to the symmetric half of the cross section could have been omitted.

d) Concentrated Areas

Concentrated areas may be introduced as elements of vanishing width. Each shall again be defined by three points which, however, have the same coordinates. Only the shear flow immediately before and immediately after this element is of interest.

e) Composite Cross Sections

The well-known technique developed for the flexural analysis of composite cross sections may be applied for the torsional analysis of composite, thin-walled, open cross sections as well. A reference material with the modulus of elasticity E_0 is selected. Materials with different elastic moduli are related by means of the modular ratio $n = E/E_0$ which transforms the composite cross section with elementary areas ΔF_i to an equivalent cross section of the reference material E_0 with the elementary areas $\Delta F_i^* = n \cdot \Delta F_i$. The analysis of the transformed cross section yields imaginary stresses which have to be multiplied by the factor n of the corresponding material in order to become real.

f) Example

The cross section shown in Fig. 6.3 represents an example of a built-up, symmetric cross section with concentrated areas.

For the chosen proportions of the cross section, the center of gravity C is at a distance $a/2$ away from the floor slab.

The cross section is symmetric with respect to a vertical axis and the numerical simplifications explained in Section 6.3c may therefore be used. The remaining calculations are arranged in Table 6.2. The intermediate calculation leading to the y -coordinate of the shear center is the following:

$$y_D = -\frac{I_{x\omega C}}{I_{xx}} = -\frac{127}{110} a \cong -1,15a.$$

The headings of the columns x , y , ω and \tilde{S}_x , \tilde{S}_y , \tilde{S}_ω are especially accentuated since these variables represent the basis for the calculation of the axial stresses

Table

Eq. No.	(a)	(x1)	(x4)	(x5)	(x6)	(x7)	(x8)	(x10)
Notation	$\Delta F/4$	Δx	x	ΔS_x	\tilde{S}_x	$1 + 4 + 1$	I_{xx}	$I_{x_0} c$
Multiplier	F_0	a	a	$a F_0$	$a F_0$	$a F_0$	$a^2 F_0$	$a^3 F_0$
1			+2		0			
2	$\frac{1}{4}$	0	+2	+1	+1	+ 6	0	0
3	$\frac{1}{4}$		+2	+1	+2			
4	$\frac{1}{4}$	0	+2	+1	+3	+18	0	-72
5_4	$\frac{1}{4}$		+2	+1	+4			
5_6	$\frac{3}{2}$		+2	$\begin{matrix} +\frac{5}{2} \\ \leftarrow \end{matrix}$	$+\frac{13}{2}$			
6	$\frac{3}{2}$	-4	0	-3	$+\frac{19}{2}$	+51	-204	-102
7_6	$\frac{3}{2}$		-2	$-\frac{5}{2}$	$+\frac{13}{2}$			
7_8	$\frac{1}{4}$		-2	-1	+4			
8	$\frac{1}{4}$	0	-2	-1	+3	+18	0	-72
9	$\frac{1}{4}$		-2	-1	+2			
10	$\frac{1}{4}$	0	-2	-1	+1	+ 6	0	0
11	$\frac{1}{4}$		-2		0			
13			+3		0			
14	$\frac{1}{4}$	-1	$+\frac{5}{2}$	$+\frac{11}{8}$	$+\frac{11}{8}$	+ 8	-8	-4
5_{14}	$\frac{1}{4}$		+2	$+\frac{9}{8}$	$+\frac{5}{2}$			
15			-3		0			
16	$\frac{1}{4}$	+1	$-\frac{5}{2}$	$-\frac{11}{8}$	$-\frac{11}{8}$	- 8	-8	-4
7_{16}	$\frac{1}{4}$		-2	$-\frac{9}{8}$	$-\frac{5}{2}$			
	6					:(-6)	-220	-254

$$F = 12 = +\frac{110}{3} + \frac{127}{3}$$

6.2

(y_1)	(y_4)	(y_5)	(y_6)	(y_8)	(ω_1)	(ω_1)	(ω_4)	(ω_5)	(ω_6)	(ω_8)
Δy	y	ΔS_y	\tilde{S}_y	I_{yy}	$\Delta \omega_C$	$\Delta \omega$	ω	ΔS_ω	\tilde{S}_ω	$I_{\omega\omega}$
a	a	$a F_0$	$a F_0$	$a^2 F_0$	a^2	a^2	$\frac{a^2}{110}$	$\frac{a^2 F_0}{110}$	$\frac{a^2 F_0}{110}$	$\frac{a^4 F_0}{110}$
0	$+\frac{3}{2}$	0	$+\frac{3}{4}$	0	0	0	$+296$	$+148$	0	0
-2	$+\frac{3}{2}$	$+\frac{3}{4}$	$+\frac{3}{4}$	0	-23	-4	$+296$	$+148$	$+148$	0
0	$+\frac{3}{2}$	$+\frac{3}{2}$	$+\frac{1}{2}$	$+2$	-23	-4	$+296$	$+93$	$+296$	0
-2	$+\frac{1}{2}$	0	$+2$	-23	-4	-4	$+76$	-17	$+389$	8896
0	$-\frac{1}{2}$	$+\frac{1}{2}$	$+2$	-23	-4	-4	-144	-180	$+372$	$(-)$
-2	$-\frac{1}{2}$	$+\frac{3}{2}$	$+\frac{3}{2}$	0	0	-2	-144	-216	$+192$	0
0	$-\frac{1}{2}$	$-\frac{3}{2}$	0	0	-2	$+\frac{288}{110}$	-0	$+216$	-24	$\frac{288^2}{110}$
-2	$-\frac{1}{2}$	$-\frac{3}{2}$	$-\frac{3}{2}$	0	-23	-4	$+144$	$+192$	$+192$	$(+)$
0	$-\frac{1}{2}$	0	$-\frac{3}{2}$	-2	-23	-4	$+144$	$+180$	$+372$	0
-2	$+\frac{1}{2}$	$-\frac{1}{2}$	-2	-23	-4	-4	-76	$+17$	$+389$	8896
0	$+\frac{3}{2}$	$+\frac{1}{2}$	$-\frac{3}{2}$	0	0	0	-296	-93	$+296$	$(-)$
-2	$+\frac{3}{2}$	$+\frac{3}{2}$	$+\frac{3}{4}$	0	0	0	-296	-148	$+148$	0
0	$+\frac{3}{2}$	$+\frac{3}{2}$	0	0	0	0	-296	-148	0	0
-2	$-\frac{1}{2}$	0	0	0	0	0	-216	-99	0	0
0	$-\frac{1}{2}$	$-\frac{1}{4}$	$-\frac{1}{4}$	0	0	$-\frac{1}{2}$	$+\frac{72}{110}$	-180	-99	$\frac{288^2}{2 \cdot 110}$
-2	$-\frac{1}{2}$	$-\frac{1}{4}$	$-\frac{1}{2}$	0	0	0	-144	-81	-180	$(-)$
0	$-\frac{1}{2}$	0	0	0	0	0	$+216$	$+99$	0	0
-2	$-\frac{1}{2}$	$-\frac{1}{4}$	$-\frac{1}{4}$	0	0	$+\frac{1}{2}$	$-\frac{72}{110}$	$+180$	$+99$	$\frac{288^2}{2 \cdot 110}$
0	$-\frac{1}{2}$	$-\frac{1}{4}$	$-\frac{1}{2}$	0	0	0	$+144$	$+81$	$+180$	$(-)$
				$:(-6)$	-46				$:(-6)$	-17792

$$= +\frac{23}{3}$$

$$= +\frac{8896}{3}$$

Exercise 6.3. Calculate the cross-sectional quantities for the cross section shown in thickness of the floor seab ($t = 8F_0/6a$). The results are presented in the table below. In

Eq. No.	(a)	(x1)	(x4)	(x5)	(x6)	(x7)	(x8)	(x10)
Notation	$\Delta F/4$	Δx	x	ΔS_x	\tilde{S}_x	$1 + 4 + 1$	I_{xx}	$I_{x\omega c}$
Multiplier	F_0	a	a	$a F_0$	$a F_0$	$a F_0$	$a^2 F_0$	$a^3 F_0$
1			+2		0			
2	$\frac{1}{4}$	0	+2	+1	+1	+ 6	0	0
3	$\frac{1}{4}$		+2	+1	+2			
4	$\frac{1}{4}$	0	+2	+1	+3	+18	0	-72
5 ₄	$\frac{1}{4}$		+2	+1	+4			
5 ₆			+2	$+\frac{10}{3}$ ←	$+\frac{22}{3}$			
6	$\frac{4}{3}$	-4	0	$+\frac{8}{3}$	+10	$+\frac{164}{3}$	$-\frac{656}{3}$	$-\frac{328}{3}$
7 ₆	$\frac{4}{3}$		-2	$-\frac{8}{3}$	$+\frac{22}{3}$			
7 ₈			-2	$-\frac{10}{3}$ ←	+4			
8	$\frac{1}{4}$	0	-2	-1	+3	+18	0	-72
9	$\frac{1}{4}$		-2	-1	+2			
10	$\frac{1}{4}$	0	-2	-1	+1	+ 6	0	0
11	$\frac{1}{4}$		-2		0			
13			+3		0			
14	$\frac{1}{3}$	-1	$+\frac{5}{2}$	$+\frac{11}{6}$	$+\frac{11}{6}$	$+\frac{32}{3}$	$-\frac{32}{3}$	$-\frac{16}{3}$
5 ₁₄	$\frac{1}{3}$		+2	+3	$+\frac{10}{3}$			
15			-3		0			
16	$\frac{1}{3}$	+1	$-\frac{5}{2}$	$-\frac{11}{6}$	$-\frac{11}{6}$	$-\frac{32}{3}$	$-\frac{32}{3}$	$-\frac{16}{3}$
7 ₁₆	$\frac{1}{3}$		-2	-3	$-\frac{10}{3}$			
	6					:(-6)	-240	-264

$$F = 12F_0 \quad = \quad +40 \quad +44$$

Fig. 11.8. This cross section differs from the one shown in Fig. 6.3a only by its constant addition: $y_D = -11a/10$.

$(y1)$	$(y4)$	$(y5)$	$(y6)$	$(y8)$	(ω_1)	(ω_1)	(ω_4)	(ω_5)	(ω_6)	(ω_8)
Δy	y	ΔS_y	\tilde{S}_y	I_{yy}	$\Delta \omega_C$	$\Delta \omega$	ω	ΔS_ω	\tilde{S}_ω	$I_{\omega\omega}$
a	a	$a F_0$	$a F_0$	$a^2 F_0$	a^2	a^2	a^2	$a^2 F_0$	$a^2 F_0$	$a^4 F_0$
	$+\frac{3}{2}$		0				$+\frac{14}{5}$		0	
0	$+\frac{3}{2}$	$+\frac{3}{4}$	$+\frac{3}{4}$	0	0	0	$+\frac{14}{5}$	$+\frac{7}{5}$	$+\frac{7}{5}$	0
	$+\frac{3}{2}$	$+\frac{3}{4}$	$+\frac{3}{2}$				$+\frac{14}{5}$	$+\frac{7}{5}$	$+\frac{14}{5}$	
-2	$+\frac{1}{2}$	$+\frac{1}{2}$	$+2$	-23	-4	-4	$+\frac{4}{5}$	$+\frac{9}{10}$	$+\frac{37}{10}$	$-\frac{424}{5}$
	0		$+2$				$-\frac{6}{5}$	$-\frac{1}{10}$	$+\frac{18}{5}$	
	$-\frac{1}{2}$	$-\frac{2}{3}$	$+2$				$-\frac{6}{5}$	-2	$+\frac{8}{5}$	
	$-\frac{1}{2}$	$-\frac{4}{3}$	$+\frac{4}{3}$				$-\frac{6}{5}$	$-\frac{8}{5}$	$+\frac{8}{5}$	
0	$-\frac{1}{2}$	$-\frac{4}{3}$	-0	0	-2		$+\frac{12}{5}$	0	0	$+\frac{192}{25}$
	$-\frac{1}{2}$	$-\frac{4}{3}$					$+\frac{6}{5}$	$+\frac{8}{5}$	$+\frac{8}{5}$	
	$-\frac{1}{2}$	$-\frac{2}{3}$	-2				$+\frac{6}{5}$	$+2$	$+\frac{18}{5}$	
+2	$+\frac{1}{2}$	0	-2	-23	-4	-4	$-\frac{4}{5}$	$+\frac{1}{10}$	$+\frac{37}{10}$	$-\frac{424}{5}$
	$+\frac{1}{2}$	$+\frac{1}{2}$	-2				$+\frac{6}{5}$	$-\frac{9}{10}$	$+\frac{14}{5}$	
	$+\frac{3}{2}$	$+\frac{3}{2}$	$-\frac{3}{2}$				$-\frac{14}{5}$	$-\frac{7}{10}$	$-\frac{7}{5}$	
0	$+\frac{3}{2}$	$+\frac{3}{4}$	$-\frac{3}{4}$	0	0	0	$-\frac{14}{5}$	$-\frac{7}{5}$	$+\frac{7}{5}$	0
	$+\frac{3}{2}$	$+\frac{3}{4}$	0				$-\frac{14}{5}$	$-\frac{7}{5}$	0	
	$-\frac{1}{2}$	0					$-\frac{9}{5}$		0	
0	$-\frac{1}{2}$	$-\frac{1}{3}$	0				$-\frac{9}{5}$	$-\frac{11}{10}$	$-\frac{11}{10}$	$-\frac{96}{25}$
	$-\frac{1}{2}$	$-\frac{1}{3}$	$-\frac{1}{3}$	0	$-\frac{1}{2}$	$+\frac{3}{5}$	$-\frac{15}{10}$	$-\frac{9}{10}$	-2	
	$-\frac{1}{2}$	$-\frac{2}{3}$	$-\frac{2}{3}$				$-\frac{6}{5}$			
	$-\frac{1}{2}$	0					$+\frac{9}{5}$		0	
0	$-\frac{1}{2}$	$-\frac{1}{3}$	$-\frac{1}{3}$	0	$+\frac{1}{2}$	$-\frac{3}{5}$	$+\frac{15}{10}$	$+\frac{11}{10}$	$+\frac{11}{10}$	$-\frac{96}{25}$
	$-\frac{1}{2}$	$-\frac{1}{3}$	$-\frac{2}{3}$				$+\frac{6}{5}$	$+\frac{9}{10}$	$+2$	
				$:(-6)$	-46				$:(-6)$	$-\frac{848}{5}$
						$+\frac{23}{3}$				$+\frac{424}{15}$

and the shear stresses. The values are furthermore listed as nondimensional parameters which need to be multiplied by the multiplier given at the top of each

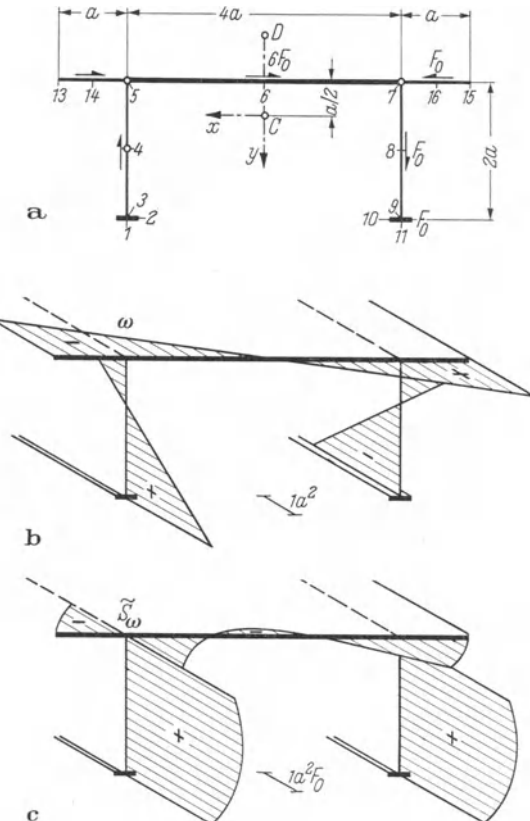


Fig. 6.3. An Example of a Built-Up, Open Cross Section.
a) Dimensions, b) Sectorial Coordinate ω , c) Sectorial Statical Moment \tilde{S}_ω .

column. The distribution of the variables ω and \tilde{S}_ω is shown in Figs. 6.3b and c respectively.

The underlined values at the bottom of the table represent nondimensional moments of inertia. After multiplication with the corresponding multiplier they become the actual moments of inertia.

$$I_{xx} = \frac{110}{3} a^2 F_0 \cong 36,7 a^2 F_0,$$

$$I_{yy} = \frac{23}{3} a^2 F_0 \cong 7,7 a^2 F_0,$$

$$I_{\omega\omega} = \frac{8896}{3 \cdot 110} a^4 F_0 \cong 27,0 a^4 F_0.$$

7 Analysis of Warping Structures

7.1 Introduction

a) Concept

Chapters 5 and 6 developed methods to determine stress distributions in individual cross sections. This chapter now will be concerned with the stress distribution along the length of members, retaining the assumption that the Saint-Venant part of the torsional resistance may be neglected.

The complete analogy between flexure and warping torsion as demonstrated by Table 5.1 will drastically simplify the solution to this new problem.

The different correspondences of problems in flexure and warping torsion are: Deflection η and twist φ , slope of the deflected axis θ_y and specific twist θ_ω , bending moment M_y and warping moment M_ω , shearing force Q_y and torsional moment T_ω and finally equally distributed load p_y and equally distributed torsional load m_D .

The different quantities defining the torsional deformations of members are easily visualized whenever they have a well defined physical meaning such as the twist φ and its derivative φ' , the distributed torsional load m_D and the torsional moment T_ω . The warping moment M_ω , however, must be accepted as defining a quantity which yields in analogy to the bending moment the axial stresses due to the restraint of warping deformations.

b) Usual Ways of Support

Since the differential operations for flexure in one principal plane of the member and for warping torsion are completely equivalent (v. Table 5.1), both equations will have analogous solutions when solved for the same boundary conditions.

Figs. 7.1, 7.2 and 7.3 show the distributions of torsional moments in members which are supported in different ways. The members are subjected to an equally distributed torsional load m_D in case one and three (Figs. 7.1 and 7.3) and to a concentrated torsional load M_D in case two (Fig. 7.2).

The analytic formulation of the boundary conditions is as follows:

Simply supported member (Fig. 7.1):

$$\begin{aligned} \varphi(z=0) &= 0, & \varphi(z=l) &= 0, \\ M_\omega(z=0) &= 0, & M_\omega(z=l) &= 0. \end{aligned} \tag{7.1}$$

Fixed-end member (Fig. 7.2):

$$\begin{aligned} \varphi(z=0) &= 0, & \varphi(z=l) &= 0, \\ \varphi'(z=0) &= 0, & \varphi'(z=l) &= 0. \end{aligned} \tag{7.2}$$

Compatibility condition at a support of a continuous member (Fig. 7.3):

$$\begin{aligned}\varphi'_{\text{left}} &= \varphi'_{\text{right}}, \\ \varphi &= 0.\end{aligned}\quad (7.3)$$

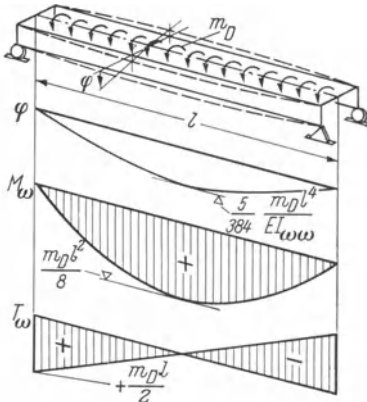


Fig. 7.1. Member on Supports Which Prevent Twist But Allow Warping (Simply Supported Beam in the Case of Bending).

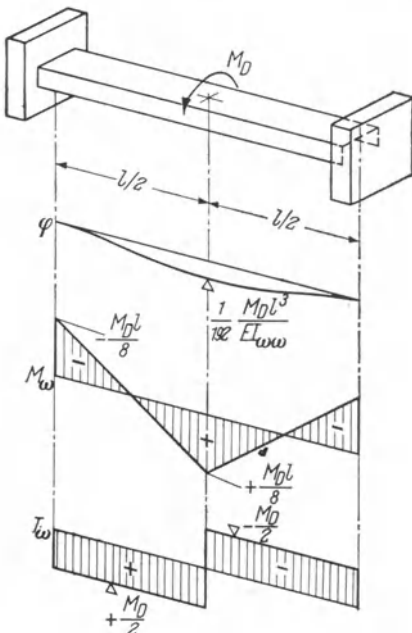


Fig. 7.2. Member on Supports Preventing Both Twist and Warping (Fixed-End Beam in the Case of Bending).

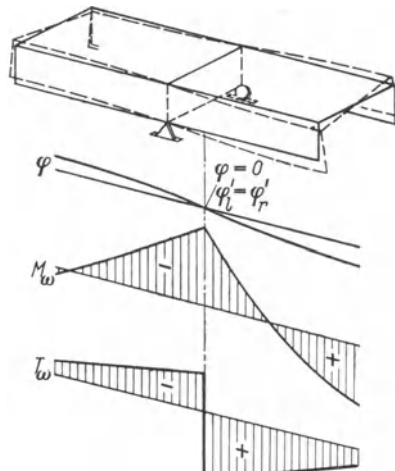


Fig. 7.3. Continuity Condition Requiring Zero Twist But Equal Warping at the Left and to the Right of a Support (Corresponding to the Support of a Continuous Beam).

c) Influence Lines

As a consequence of the analogy between warping torsion and flexure, the well-known influence lines for the bending moments, shearing forces and support reactions of a continuous, prismatic member may be used for the torsional analysis of this structure as well.

The influence lines for the bending moments have the dimension of a length, those for the shearing forces and support reactions are nondimensional. If, for instance, the concentrated torsional moment M_D with the dimension [force · length] is applied to an influence line for a bending moment, the result is of the dimension [force · length²] which is in fact the dimension of the warping moment M_ω .

7.2 Transverse Influence Lines

a) Meaning and Importance

Because of the similarity in the distribution of warping moments and bending moments and of torsional moments and shearing forces, the principle of superposition of bending stresses and warping stresses at the same time may be applied for all cross sections of a prismatic member. If one considers a particular point s of a cross section, e.g. the lower flange of a plate girder, the magnification factors for the stresses σ_s if the vertical load $P = 1$ deviates to either side of the axis through the shear center may be presented in the form of an influence line (v. Fig. 7.4).

Such a transverse influence line is valid for pure warping torsion for all cross sections of a prismatic member even if continuous over several spans and it may provide ample information for an analysis.

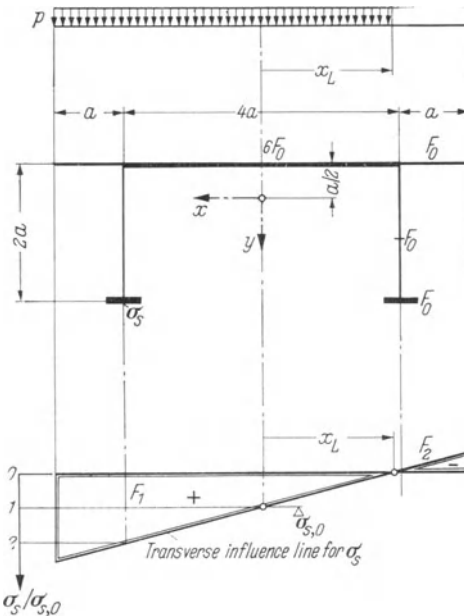


Fig. 7.4. Transverse Influence Line for Axial Stress in the Lower Flange of the Left Main Girder.

Consider as an example the transverse influence line for the stresses σ_s in the lower flange of the cross section shown in Fig. 7.4. If the stress in the flange s caused by a unit vertical load through the shear center is denoted by $\sigma_{s,0}$, it may be read from the transverse influence line that

1. the stress increases to $2,02 \sigma_{s0}$ if this load is applied at the left main girder,
2. the stress increases further to $2,53 \sigma_{s0}$ if this load moves further out to the left boundary of the floor slab and that
3. there is even a negative stress of $-0,53 \sigma_{s0}$ if the load acts at the right boundary of the floor slab.

Loads acting the indicated distance x_L away from the longitudinal shear center axis do not cause stresses in the left lower flange. Loads to the left of this dividing line increase the tensile stress in this flange, loads to the right decrease the stress. A uniformly distributed load therefore should be located as shown at the top of Fig. 7.4 in order to arrive at a maximum value for the stress in the left lower flange.

Moreover, the transverse influence line indicates the error that results if the flange stresses are simply calculated for the centric full load instead of for the critical partial load.

Since, in the case of a uniformly distributed vertical load, the flange stress is proportional to the area under the influence line in the loaded region, the area $(F_1 - F_2)$ represents the stress due to full load, σ_{s0} , while the area F_1 stands for the maximum axial stress $\sigma_{s\max}$.

The error defined as $(\sigma_{s0} - \sigma_{s\max})/\sigma_{s\max}$ may therefore be written as $(F_1 - F_2 - F_1)/F_1 = -F_2/F_1$ which is equal to the ratio between the two areas outlined in Fig. 7.4. For the dimensions of the above example cross section the error ratio is $-0,043$ which means that the full load stresses the lower flange by an amount $4,3\%$ less than the stress due to a load acting between $x = +3a$ and $x = -1,96a$.

b) The Calculation of Transverse Influence Lines

A vertical load P acting at a distance x away from the shear center may be divided up into the centric load P and into the concentrated torsional load $M_D = Px$. The axial stress at point s of a given cross section consists therefore of a flexural and torsional part as defined by Eqs. (5.16) and (5.33) respectively.

$$\sigma_s = \frac{M_y}{I_{yy}} y_s + \frac{M_\omega}{I_{\omega\omega}} \omega_s \quad (7.4a)$$

$$= \sigma_{s0} \left(1 + \frac{M_\omega}{M_y} \frac{I_{yy}}{I_{\omega\omega}} \frac{\omega_s}{y_s} \right). \quad (7.4b)$$

The flexural part of the axial stress produced with the load P at the shear center is denoted by δ_{s0} .

Because of the similarity in the distribution of the warping moments M_ω and the bending moments M_y , the ratio M_ω/M_y is equal to the ratio between the corresponding loads $M_D/P = Px/P = x$. The expression for the transverse influence line becomes therefore:

$$\frac{\sigma_s}{\sigma_{s0}} = 1 + \frac{\omega_s}{y_s} \frac{I_{yy}}{I_{\omega\omega}} x. \quad (7.5)$$

This expression represents a straight line with the ordinate +1 for loads through the shear center. The line may be located if the position of one more point, e.g. the abscissa x_L of the zero ordinate is known. The abscissa x_L is the solution of Eq. (7.5) for $\sigma_s = 0$.

$$x_L = -\frac{y_s}{\omega_s} \frac{I_{\omega\omega}}{I_{yy}}. \quad (7.6)$$

The quantities needed for the evaluation of this expression were calculated in Table 6.2 for the cross section shown in Fig. 7.4. The required ratio $I_{\omega\omega}/I_{yy}$ is:

$$\frac{I_{\omega\omega}}{I_{yy}} = \frac{\frac{8896}{3 \cdot 110} a^4 F_0}{\frac{23}{3} a^2 F_0} = \frac{4448}{1265} a^2. \quad (7.7)$$

The coordinates of the lower flange of the left main girder may be read from columns (y) and (ω) of Table 6.2. Since this flange was characterized by the number 1, the coordinates are written accordingly as $y_1 = +3a/2$ and $\omega_1 = 296a^2/110$. They lead finally to the following abscissa for the zero ordinate:

$$x_{L1} = -\frac{1668}{851} a \cong -1,96a. \quad (7.8a)$$

This numerical value was used in plotting the transverse influence line shown in Fig. 7.4.

The zero influence point for any other location in the cross section may now be calculated readily. The left boundary of the floor slab which is designated by the number 13, for instance, has the coordinates $y_{13} = -a/2$ and $\omega_{13} = -216a^2/110$. These values yield immediately the abscissa x_{L13} of the corresponding zero influence ordinate:

$$x_{L13} = -\frac{556}{621} a \cong -0,895a. \quad (7.8b)$$

The transverse influence line for point 13 is presented in Fig. 7.5 b. This line is considerably steeper than the one for the lower flange. It defines an error ratio of approximately $-0,3$ which means that the stresses in point 13 are underestimated by about 30% if they are determined for full load only.

It may be noticed that the ratio y/ω determines the error made by use of a full-load stress analysis. The mistake may reach 100% for $y = 0$ and $\omega \neq 0$ which are the coordinates of a point at $3/4$ the height of the web. The corresponding transverse influence line is vertical (Fig. 7.5c).

Another extreme case occurs not too far away from this point. The sectorial coordinate ω is zero for $y = +17a/100$. The zero ordinate is therefore at $x_L = \infty$, i.e. the corresponding transverse influence line is horizontal. The stress in the web at $y = 0,155a$ is independent of the eccentricity of the load.

These examples demonstrate that it is not correct to assign a load to each main girder according to the lever principle and to consider each half of the cross section independently.

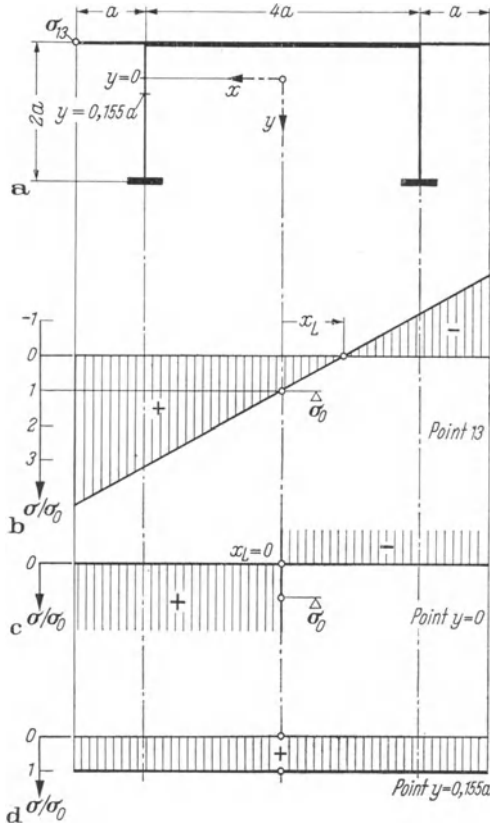


Fig. 7.5. Transverse Influence Lines for Axial Stresses.

Transverse influence lines may of course be derived for the shear stresses or the shear flows as well. The procedure is exactly analogous to the one for the axial stress. Again, the shear flow at a particular point s of a cross section consists of a flexural part [Eq. (5.20)] and a torsional part [Eq. (5.34)].

$$q_s = -\frac{Q_y}{I_{yy}} \tilde{S}_y(s) - \frac{T_\omega}{I_{\omega\omega}} \tilde{S}_\omega(s) \quad (7.9a)$$

$$= q_{s0} \left(1 + \frac{T_\omega}{Q_y} \frac{I_{yy}}{I_{\omega\omega}} \frac{\tilde{S}_\omega(s)}{\tilde{S}_y(s)} \right). \quad (7.9b)$$

The symbol q_{s0} denotes the shear flow for pure bending only. The ratio between the torsional moment and the shearing force T_ω/Q_y may again be expressed in terms of the corresponding loads as $M_D/P = Px/P = x$. This yields the following general expression for the transverse influence line:

$$\frac{q_s}{q_{s0}} = 1 + \frac{\tilde{S}_\omega(s)}{\tilde{S}_y(s)} \frac{I_{\omega\omega}}{I_{yy}} x. \quad (7.10)$$

This expression again represents a set of straight lines with each of the lines having a zero ordinate at x_L .

$$x_L = -\frac{\tilde{S}_y(s)}{\tilde{S}_w(s)} \frac{I_{wo}}{I_{yy}}. \quad (7.11)$$

This expression for the zero ordinate location is transformed into the one developed earlier [Eq. (7.6)] if the ratio \tilde{S}_y/\tilde{S}_w is replaced by the ratio y/w .

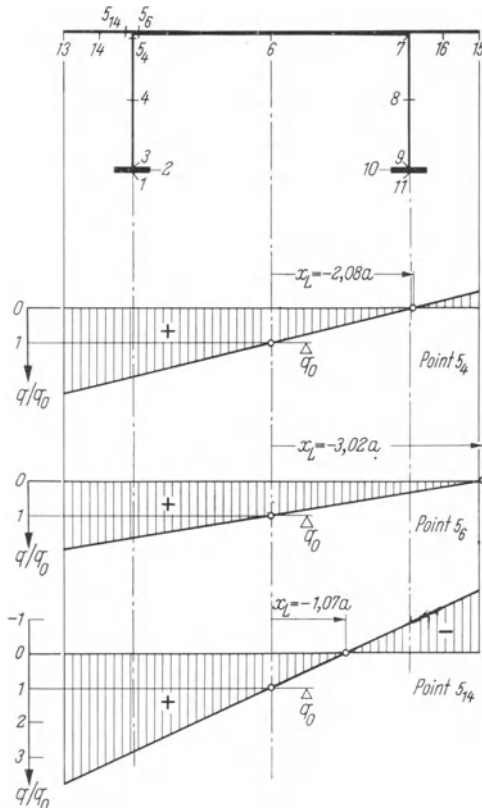


Fig. 7.6. Transverse Influence Lines for the Shear Flows in Branch Point 5.

Three frequently needed characteristic transverse influence lines for the shear flows in the cross section will now be calculated.

The constant given by Eq. (7.7) together with values calculated in Table 6.2 yield immediately values for the zero influence ordinates of the shear flows in:

Point 5₄ (top seam of the web):

$$x_L = -\frac{4448}{2139} a \cong -2,08a, \quad (7.12a)$$

Point 5₆ (connection with the intermediate floor slab):

$$x_L = -\frac{139}{46} a \cong -3,02a, \quad (7.12b)$$

Point 5₁₄ (connection with the cantilever portion of the floor slab):

$$x_L = -\frac{1112}{1035} a \cong -1,07 a. \quad (7.12 \text{c})$$

The transverse influence lines for the shear flows at these three points are plotted in Fig. 7.6.

7.3 The Continuous, Prismatic Bar

Although the torsional analysis of a continuous, prismatic bar with negligible Saint-Venant torsion-resistance may be reduced to a simple flexural analysis of the corresponding system, the elements of the three-warping-moment equation shall nevertheless be developed in order to facilitate the subsequent treatment of the mixed torsion.

a) Warping of the Member

The angular displacements at the supports of a simply supported beam

$$\begin{aligned} \alpha &= y'(\zeta=0), \\ \beta &= -y'(\zeta=1) \end{aligned} \quad (7.13 \text{a})$$

correspond to the torsional quantities φ' at the ends of a simply supported bar. The latter shall be denoted by the arabic letters a and b in order to reflect their analogy to the angles α and β .

$$\begin{aligned} a &= \varphi'(\zeta=0), \\ b &= -\varphi'(\zeta=1). \end{aligned} \quad (7.13 \text{b})$$

Table 7.1 presents expressions for the quantities a and b in a few special cases. They may be derived from the corresponding angular displacements simply by replacing EI_{yy} by $EI_{\omega\omega}$, P by M_D and p by m_D . The reversed coordinate going from the right to the left support shall again be denoted by z' or $\zeta' = z'/l$. The supports are consecutively numbered by the odd numbers k while even numbers i are attributed to the spans.

Table 7.1. Displacement Coefficients and Generalized Displacements for the Simply Supported, Prismatic Bar of Span i with Negligible Saint-Venant Torsion-Resistance

Displacement coefficients:

$$a_{ik}: \quad \frac{l_i}{3EI_{\omega\omega}},$$

$$a_{i+k+1} = b_{ik}: \quad \frac{l_i}{6EI_{\omega\omega}},$$

$$b_{i+k+1}: \quad \frac{l_i}{3EI_{\omega\omega}}.$$

Generalized displacements for the concentrated torsional moment M_D :

$$a_{i0}: \quad \frac{M_D l_i^2}{6 E I_{wo}} (\zeta'_i - \zeta''_i),$$

$$b_{i0}: \quad \frac{M_D l_i^2}{6 E I_{wo}} (\zeta_i - \zeta^3_i).$$

Generalized displacements for the distributed torsional load m_D :

$$a_{i0}: \quad \frac{m_D l_i^3}{24 E I_{wo}},$$

$$b_{i0}: \quad \frac{m_D l_i^3}{24 E I_{wo}}.$$

It may easily be recognized from an expression for the longitudinal displacement w that in fact the quantities a_i and b_i are related to the warping of the member ends. An expression for the longitudinal displacement w was presented in Eq. (5.26), $w = -\varphi' \Omega + w_0(z)$, and a relation for the unknown constant of integration $w_0(z)$ was given immediately afterwards:

$$w'_0(z) = \varphi'' \frac{\int \Omega dF}{F}.$$

If the sectorial coordinate is further normalized according to Eq. (5.27), the first derivative of the longitudinal displacement w may be simply given as $w' = \varphi''$ which after integration becomes:

$$w = -\varphi' \omega. \quad (7.14)$$

Eq. (7.14) omits the constant of integration intentionally since it indicates only a longitudinal rigid-body displacement of the entire member.

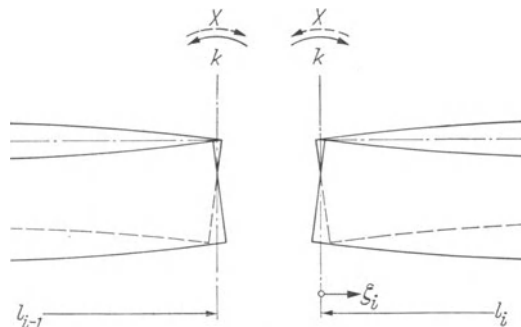


Fig. 7.7. Warping of U-shaped Cross Sections Under Torsional Load at the Support k . The Warping Moment X is Redundant Quantity.

Fig. 7.7 shows the warping deformations at the support k of two adjacent member ends of an originally continuous bar which was separated into independent base systems. The cross section is assumed to be symmetric and of the U-type with the web turned upwards.

While the coordinate ω describes the distribution of the warping deformations w along the walls of a thin-walled cross section, the derivative of the twist angle φ' is a measure of the intensity of the warping deformations which varies along the length of the member.

Since the shape of the warped cross section is the same for all cross sections of a prismatic, continuous bar, it suffices to formulate the compatibility conditions at the connections of the base systems in terms of the intensities φ' :

$$\varphi'(\zeta_{i-1} = 1) = \varphi'(\zeta_i = 0). \quad (7.15a)$$

This condition at the support k may be rewritten in terms of the deformation quantities defined in Eq. (7.13 b):

$$\begin{aligned} -b_{i-1} &= a_i, \\ b_{i-1} + a_i &= 0. \end{aligned} \quad (7.15b)$$

Eq. (7.15a) is identical to the first of the conditions (7.3) which was an immediate consequence of the analogy to the ordinary continuous-beam problem. The second of the conditions (7.3) is already satisfied by the base system.

b) The Forces in the Bar

The forces in the bar of the simply supported base system will, as usual, be designated by the subscript “zero”.

A *uniformly distributed* torsional load m_D causes the following warping moments $M_{\omega 0}$ and torsional moments $T_{\omega 0}$ in the base system:

$$\begin{aligned} M_{\omega 0} &= \frac{m_D l^2}{2} \zeta(1 - \zeta), \\ T_{\omega 0} &= \frac{m_D l}{2} (1 - 2\zeta). \end{aligned} \quad (7.16)$$

A *concentrated* torsional moment M_D acting at $z = c$ yields the following corresponding expressions:

$$\begin{aligned} \zeta < \frac{c}{l} &\quad \zeta > \frac{c}{l} \\ M_{\omega 0}: &\quad (l - c) M_D \zeta, \quad c M_D (1 - \zeta), \\ T_{\omega 0}: &\quad \left(1 - \frac{c}{l}\right) M_D, \quad -\frac{c}{l} M_D. \end{aligned} \quad (7.17)$$

These quantities have to be superimposed on those caused by the redundants. The latter are the warping moments X_k at the supports $k = 1, 3, 5, \dots$. The members are denoted by even numbers $i = 2, 4, 6, \dots$ such that the support to the left of member i is k and the one to the right $k + 1$.

$$M_{\omega i} = {}_0 M_{i0} + X_k(1 - \zeta_i) + X_{k+1} \zeta_i, \quad (7.18)$$

$$T_{\omega i} = {}_0 T_{i0} + \frac{X_{k+1} - X_k}{l_i}.$$

The total torsional moment absorbed by the support k is:

$$\begin{aligned} T_k &= T_{\omega i}(\zeta_i = 0) - T_{\omega i-1}(\zeta_{i-1} = 1), \\ &= T_{ki} - T_{k-1}. \end{aligned} \quad (7.19)$$

e) Three-Warping-Moment Equations

The continuous, prismatic bar is transformed into a base system consisting of successive, simply supported members i , each of which is connected at two consecutive supports. This base system already imposes equal torsional rotations at the supports (that is $\varphi_k = 0$). Only the warped cross sections at the member ends (Fig. 7.7) do not conform to each other. The condition for the compatibility of adjacent member ends is therefore formulated in Eq. (7.15b).

With the warping moments X_k as redundant quantities, the warping intensities b_{i-1} and a_i may be written as follows:

$$\begin{aligned} b_{i-1} &= b_{i-1,0} + b_{i-1,k-1}X_{k-1} + b_{i-1,k}X_k, \\ a_i &= a_{i,0} + a_{ik}X_k + a_{i,k+1}X_{k+1}. \end{aligned} \quad (7.20)$$

If these intensities are introduced into the compatibility condition (7.15b), one immediately arrives at the required three-warping-moment equations.

$$\begin{aligned} X_{k-1}b_{i-1,k-1} + X_k(b_{i-1,k} + a_{ik}) + X_{k+1}a_{i,k+1} &= -(b_{i-1,0} + a_{i,0}). \quad (7.21) \\ (k &= 1, 3, 5, \dots, \\ i &= 2, 4, 6, \dots). \end{aligned}$$

This system of equations may be simplified by means of expressions tabulated in Table 7.1.

$$\begin{aligned} X_{k-1}l_{i-1} + 2X_k(l_{i-1} + l_i) + X_{k+1}l_i &= -6EI_{\omega\omega}(b_{i-1,0} + a_{i,0}). \quad (7.22) \\ (k &= 1, 3, 5, \dots, \\ i &= 2, 4, 6, \dots). \end{aligned}$$

These three-warping-moment equations are completely equivalent to the three-moment equations of the continuous beam.

d) Influence Surfaces

Since two coordinates are required to determine the position of a moving single load $P = 1$, the influence function for any quantity may be represented as a surface. One coordinate, z_i , gives the position of the load along the length of the member and the other, x , indicates the eccentricity of the load with respect to the longitudinal axis.

Influence surfaces for warping moments or torsional moments alone are not of great interest since both the axial stresses and the shear stresses incorporate the

influence of bending and shear. It is therefore more useful to calculate influence surfaces for the stresses.

If the influence surface of the stress σ_s is denoted by $\eta(\sigma_s)$ and if η_M represents the influence line for the bending moment, then an expression for $\eta(\sigma_s)$ may be derived from Eq. (7.5):

$$\eta(\sigma_s) = \frac{\eta_M y_s}{I_{yy}} \left(1 + \frac{\omega_s}{y_s} \frac{I_{yy}}{I_{wo}} x \right). \quad (7.23)$$

Expression (7.23) may be looked upon as the product of the transverse influence line, the influence line for the bending moment and the constant factor y_s/I_{yy} which is simply the inverse of the section modulus. The influence surface is therefore a ruled surface which is completely determined by the zero ordinate location and the influence line for the bending moment divided by the section modulus.

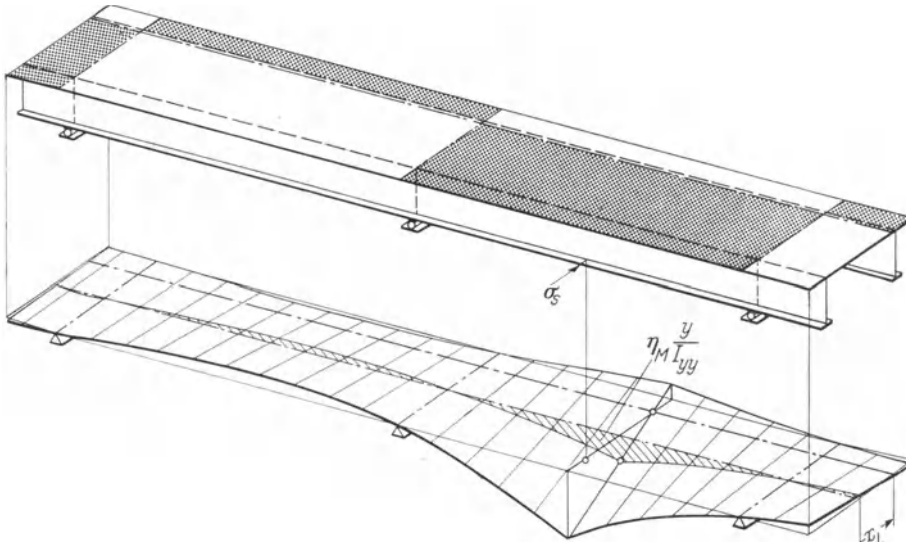


Fig. 7.8. Influence Surface for the Axial Stress σ_s in the Lower Flange of a Two-Span Continuous Beam. Positive Loads Acting in the Shaded Portions of the Floor Slab Cause Positive Stresses σ_s .

Fig. 7.8 shows such an influence surface for the axial stress σ_s in the lower flange of the cross section as defined in Fig. 7.4. The surface is plotted for the influence at midspan of a continuous beam with two equal spans. The influence is positive for the shaded portions of the floor slab and negative for the others.

The influence surface for the shear flow is defined by a similar expression. Eq. (7.10) is the basis for the following relation:

$$\eta(q_s) = -\frac{\tilde{S}_y(s)}{I_{yy}} \eta_Q \left(1 + \frac{\tilde{S}_o(s)}{\tilde{S}_y(s)} \frac{I_{yy}}{I_{wo}} x \right). \quad (7.24)$$

This influence function is, aside from the constant factor $-\tilde{S}_y(s) I_{yy}$, again the product of the influence line for the shear η_Q and the transverse influence line (expression in brackets).

Eq. (7.24) represents a ruled surface as well and maximum values for the shear stress result again from a checker board-type configuration of a uniformly distributed load.

7.4 Axial Forces

a) Relations

Until now, only the stresses due to lateral loads have been considered. The lateral load was divided up into a pure flexural part and into a pure torsional part. The system was then analyzed separately for bending and for torsion and the stresses due to each case were subsequently superposed.

If, for instance, the axes x and y coincide with the principal axes of a cross section and if ω represents the normalized sectorial coordinate, then the general expression for the axial stresses in a cross section is as follows:

$$\sigma = \frac{M_x}{I_{xx}} x + \frac{M_y}{I_{yy}} y + \frac{M_\omega}{I_{\omega\omega}} \omega. \quad (7.25)$$

If the lateral load leads to pure twist alone, the distribution of the axial stresses is described by the last term of expression (7.25). The stresses are termed warping stresses in this special case. Their distribution over the cross section is described by the sectorial coordinate ω . They are moreover proportional to the longitudinal displacements w of the cross sections under twist [Eq. (7.14)]. It is a consequence of Maxwell-Mohr's reciprocal theorem that an axial load, which acts at a point of the cross section whose longitudinal displacement w does not vanish, is bound to cause twist and therefore warping stresses¹.

If the position of an axial load P is given by the coordinates $x(P)$, $y(P)$ and $\omega(P)$, the resulting stress distribution may be put into the following form:

$$\sigma = \frac{P}{F} + \frac{Px(P)}{I_{xx}} x + \frac{Py(P)}{I_{yy}} y + \frac{P\omega(P)}{I_{\omega\omega}} \omega. \quad (7.26)$$

A tensile force P is assumed to be positive and the coordinates refer to principal axes through the center of gravity and the shear center, respectively.

Since the Saint-Venant torsional resistance is assumed to be negligible, a thin-walled, prismatic member acted upon by the axial load P at its ends leads to constant values for all quotients of Eq. (7.26).

If, on the other hand, one were to deal with mixed torsion, the problem of finding the contribution of Saint-Venant and warping torsion would have to be solved first. The warping stresses as expressed by the last term in the sum of Eq. (7.26) would vary along the member in accordance with the variation of the warping moment. This problem will be discussed in connection with Fig. 10.4.

If the axes x and y do not happen to be principal axes but are arbitrary, mutually orthogonal axes through the center of gravity of the cross section, the second

¹ It was V. Z. VLASOV who, to our knowledge, pointed out first that an axial load P may not be reduced with respect to the member axis without consideration of the warping moment $P\omega(P)$.

and third element in the sum of Eq. (7.26) will have to be rewritten in accordance with Eq. (5.15). This leads to the following, more general version of Eq. (7.26):

$$\sigma = \frac{P}{F} + P \frac{[x(P)I_{yy} - y(P)I_{xy}]x + [y(P)I_{xx} - x(P)I_{xy}]y}{I_{xx}I_{yy} - I_{xy}^2} + \frac{P \omega(P)}{I_{\omega\omega}} \omega. \quad (7.27)$$

b) Example

A prismatic member with the open, thin-walled cross section shown in Fig. 7.9 is acted upon by the axial load P at point 1 of the cross section. The distribution

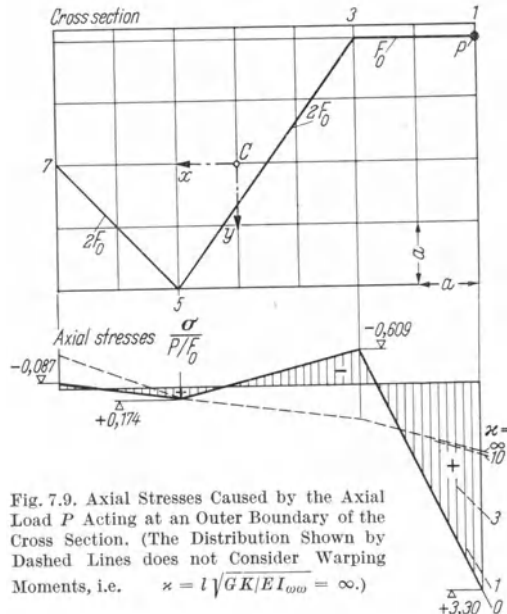


Fig. 7.9. Axial Stresses Caused by the Axial Load P Acting at an Outer Boundary of the Cross Section. (The Distribution Shown by Dashed Lines does not Consider Warping Moments, i.e. $\omega = l \sqrt{GK/EI_{\omega\omega}} = \infty$.)

of the axial stresses will be calculated for a member simply supported at its ends.

The characteristic quantities of this cross section were already calculated in Section 6.2a. The values needed in the subsequent calculations are as follows:

$$F = 5 F_0,$$

$$I_{xx} = 20 a^2 F_0,$$

$$I_{xy} = + \frac{34}{3} a^2 F_0,$$

$$I_{yy} = \frac{28}{3} a^2 F_0,$$

$$D = I_{xx}I_{yy} - I_{xy}^2 = + 58,2 a^4 F_0^2,$$

$$I_{\omega\omega} = 9,18 a^4 F_0.$$

The coordinates of the point of load application are

$$x(P) = -4a, \quad y(P) = -2a, \quad \omega(P) = -4,57a^2.$$

They complete the numerical information for the application of Eq. (7.27). This equation becomes:

$$\frac{\sigma}{P/F_0} = +0,200 - 0,252 \frac{x}{a} + 0,0916 \frac{y}{a} - 0,498 \frac{\omega}{a^2}. \quad (7.28)$$

This distribution of the axial stresses is plotted in Fig. 7.9. The distribution shown by a dashed line represents only the first three elements of the equation, i.e. it does not consider the warping moments.

8 Warping Torsion in Skew Supported Members

8.1 Introduction

a) Assumptions

Skew supported members in which Saint-Venant torsion is predominant were treated in Chapter 4. The same structural systems will now be analyzed under the assumption that the Saint-Venant torsional resistance may be neglected and that only warping resistance need be considered. Intermediate systems for which the two types of torsion should be treated jointly will be discussed in Chapter 10.

All treatments of skew supported members assume the extension of the support regions to be small as compared with the spans. The structure may thus be divided up into clearly defined structural members. Systems which clearly do not satisfy this condition would have to be treated as continuous beams on eccentrically placed supports whose number of spans would increase from n to $2n + 1$.

In order to facilitate the derivations, the member cross section is assumed to have at least one axis of symmetry and each support shall, at least to begin with, consist of two distinct support elements.

b) Notation

The system of notation developed in Chapter 4 will again be used wherever applicable. The spans will therefore be numbered consecutively by the even numbers $i = 2, 4, 6, \dots$ and the odd numbers $k = 1, 3, 5, \dots$ will be attributed to the supports. The meaning of the displacement coefficients a and b was explained in Table 7.1.

The obliqueness of the support k is defined by the angle δ_k which measures the angular deviation of the bearing axis from that of a regular, orthogonal support (Fig. 8.1 b).

It is appropriate to define the following new system parameters:

$$\begin{aligned}\varepsilon_{ki} &= \frac{e_k}{2l_i} \quad \left(= \frac{d}{2l_i} \operatorname{tg} \delta_k \right), \\ \varepsilon_{k+1,i} &= \frac{e_{k+1}}{2l_i} \quad \left(= \frac{d}{2l_i} \operatorname{tg} \delta_{k+1} \right).\end{aligned}\quad (8.1)$$

These compare the longitudinal displacement $\frac{e_k}{2}$ and $\frac{e_{k+1}}{2}$ of the distinct support elements k and $k + 1$ with the length l_i of span i . The signs of these parameters correspond to the signs of the angles δ_k and δ_{k+1} respectively, which are positive whenever directed as shown in Fig. 8.1 b.

Influence coefficients are usually characterized by double-subscripts, the first indicating their position and the second their cause. Double-subscripts are further used to characterize support quantities which need the specification as to whether they act immediately to the right or to the left of the support.

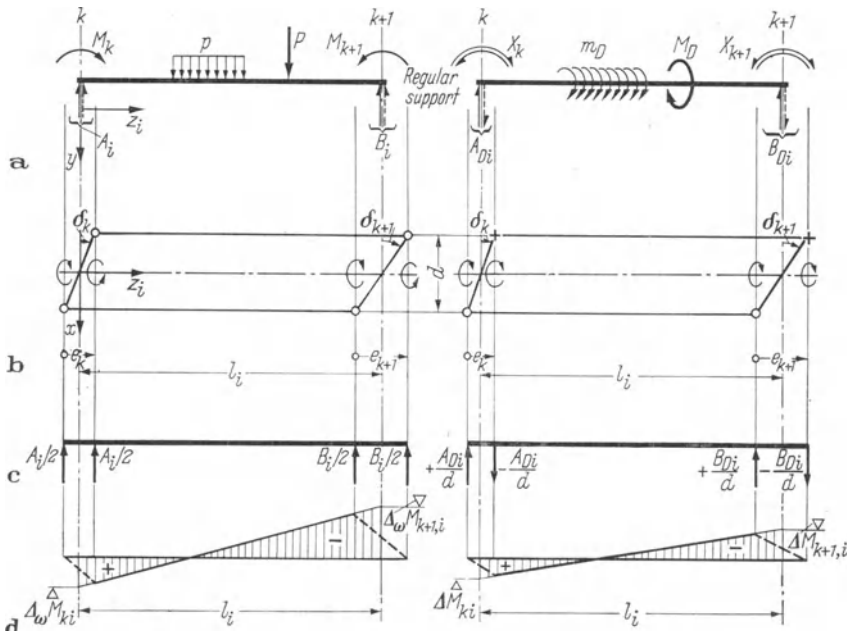


Fig. 8.1. Nomenclature Explained for the Base System of Span i , for Lateral Loads to the Left, for Torsional Loads to the Right.

The subscript ω is made to precede the symbol of some cross-sectional quantity (e.g. ωM_{ki}) if it cannot be omitted altogether. Quantities which belong to a simply and regularly supported base system show the number 0 either as subscript or, if the symbol shows two subscripts already, as superscripts (e.g. $Q_{ki}^{(0)}$). Fixed-end moments due to applied loads are termed $T_{ki}^{(f)}$ and $T_{k+1,i}^{(f)}$ in accordance with the nomenclature of Section 3.2 b.

8.2 Analysis

a) Base System

The original, continuous system is transformed into a chain of independent, skew supported members. The continuity is reestablished by means of the redundant moments M_k and warping moments X_k at intermediate supports. These redundant quantities are shown in Fig. 8.1a, the moments M_k to the left and the warping moments X_k to the right. They follow from compatibility conditions, one requiring equal slopes of the deflection curves at the supports and the other requiring compatible warping deformations of the adjacent cross sections [v. Eq. (7.15)].

$$\beta_{i-1} + \alpha_i = 0, \quad (8.2\text{a})$$

$$b_{i-1} + a_i = 0. \quad (8.2\text{b})$$

If the member were regularly supported, the angular displacements and the warping deformations could, by means of the law of superposition, be written as follows:

$$\alpha_i = M_k \alpha_{ik} + M_{k+1} \alpha_{i k+1} + \alpha_{i0}, \quad (8.3\text{a})$$

$$\beta_i = M_k \beta_{ik} + M_{k+1} \beta_{i k+1} + \beta_{i0}.$$

$$a_i = X_k a_{ik} + X_{k+1} a_{i k+1} + a_{i0}, \quad (8.3\text{b})$$

$$b_i = X_k b_{ik} + X_{k+1} b_{i k+1} + b_{i0}.$$

$$(k = 1, 3, 5, \dots,$$

$$i = 2, 4, 6, \dots)$$

The forces in the member would again be the superposition of those caused by the redundants and the applied loads. Eq. (7.18) shows this superposition for the case of warping moments and torsional moments.

The reactions at the supports are:

In the case of bending:

$$A_i = + Q_i(\zeta_i = 0) = + Q_{ki} = Q_{ki}^{(0)} + \frac{M_{k+1} - M_k}{l_i}, \quad (8.4)$$

$$B_i = - Q_i(\zeta_i = 1) = - Q_{k+1 i} = - Q_{k+1 i}^{(0)} - \frac{M_{k+1} - M_k}{l_i},$$

In the case of torsion:

$$A_{Di} = + T_i(\zeta_i = 0) = + T_{ki} = T_{ki}^{(0)} + \frac{X_{k+1} - X_k}{l_i}, \quad (8.5)$$

$$B_{Di} = - T_i(\zeta_i = 1) = - T_{k+1 i} = - T_{k+1 i}^{(0)} - \frac{X_{k+1} - X_k}{l_i}.$$

These reactions may be thought of as introduced at each member end by two distinct support elements. Each of these elements carries half of the total reaction in the case of lateral load and equal and opposite loads A_{Di}/d and B_{Di}/d respectively (positive at $x = + \frac{d}{2}$ and negative at $x = - \frac{d}{2}$) in the case of torsion.

If the line through the two support elements is rotated by the angle δ_k resp. δ_{k+1} out of its originally perpendicular position, the member is twisted by the angle φ_i . This motion is, because of the vanishing Saint-Venant torsional resistance, completely unrestrained.

The longitudinal displacements e_k and e_{k+1} of the support elements do nevertheless influence the forces in member i , as may be seen from Fig. 8.1 b–d. It may be noted by Fig. 8.1 c that the decomposition of the reaction A_i into the two parallel forces $A_i/2$ does not affect the moments outside the support region. This is no longer the case if the reactions represent couples. They lead to a moment distribution as shown to the right of Fig. 8.1 d. The corrections for the moments at the supports may, with consideration of Eq. (8.5), be written as follows:

$$\begin{aligned}\Delta M_{ki} &= \frac{A_{Di}}{d} e_k = + T_{ki} \operatorname{tg} \delta_k, \\ \Delta M_{k+1\ i} &= - \frac{B_{Di}}{d} e_{k+1} = + T_{k+1\ i} \operatorname{tg} \delta_{k+1}.\end{aligned}\quad (8.6)$$

The analysis of the warping moments requires additional information. They are calculated from the torsional moments M_D resulting from the reactions at the longitudinally displaced support elements. For the case shown to the left of Fig. 8.1 b, the moments M_D have the value $-A_i d/4$, $+A_i d/4$ and $-B_i d/4$, $+B_i d/4$, respectively.

The resulting distribution of the warping moments is the same as the bending moment distribution caused by analogous concentrated loads. This distribution is presented to the left of Fig. 8.1 d.

The corrections for the warping moments at the supports are, with consideration of Eq. (8.4), given by the following expressions:

$$\begin{aligned}\Delta_\omega M_{ki} &= \frac{A_i d}{4} e_k = + Q_{ki} \left(\frac{d}{2}\right)^2 \operatorname{tg} \delta_k, \\ \Delta_\omega M_{k+1\ i} &= - \frac{B_i d}{4} e_{k+1} = + Q_{k+1\ i} \left(\frac{d}{2}\right)^2 \operatorname{tg} \delta_{k+1}.\end{aligned}\quad (8.7)$$

The same reasoning will now be applied to the case shown on the right half of Fig. 8.1. The reactions of each end of the member lead to a pair of equal torsional moments which together constitute new reactions at the supports. The latter do not yield warping moments except within the support regions. Their influence on deformations is, as assumed, negligible.

In order to formulate expressions for the deformations of an obliquely supported member, relations between warping deformations and angular displacements at the supports are needed. The twist of a simply supported member with angular displacements α_i and β_i at the supports and negligible Saint-Venant torsion resistance is given by the expressions:

$$\begin{aligned}\varphi(\zeta_i = 0) &= \alpha_i \operatorname{tg} \delta_k \quad \text{and} \quad \varphi(\zeta_i = 1) = -\beta_i \operatorname{tg} \delta_{k+1} \\ \text{thus} \quad \varphi(\zeta_i) &= \alpha_i (1 - \zeta_i) \operatorname{tg} \delta_k - \beta_i \zeta_i \operatorname{tg} \delta_{k+1}, \\ \varphi'(\zeta_i) &= -\frac{1}{l_i} \alpha_i \operatorname{tg} \delta_k - \frac{1}{l_i} \beta_i \operatorname{tg} \delta_{k+1}.\end{aligned}\quad (8.8)$$

The additional quantities for the warping of the member are according to the definitions (7.13b):

$$\begin{aligned}\Delta a_i &= -\frac{\alpha_i \operatorname{tg} \delta_k + \beta_i \operatorname{tg} \delta_{k+1}}{l_i}, \\ \Delta b_i &= +\frac{\alpha_i \operatorname{tg} \delta_k + \beta_i \operatorname{tg} \delta_{k+1}}{l_i}.\end{aligned}\quad (8.9)$$

b) Deformations

The relations (8.3) for the deformation of regularly supported members have to be supplemented by the influence of skew supports, those for the angular displacements at the supports, Eqs. (8.3a), by the influence of ΔM and the warping deformations, Eqs. (8.3b), by the influence of ΔM_ω and Δa_i resp. Δb_i . The additional influences given by Eqs. (8.6), (8.7) and (8.9) lead together with Eqs. (8.3) to the member-end deformations tabulated below.

Table 8.1. Member-End Deformations for Skew Supports, $G K l^2 \ll EI_{\text{out}}$

Different Obliqueness, $\delta_k \neq \delta_{k+1}$

$$\alpha_i = M_k \alpha_{ik} + M_{k+1} \alpha_{i k+1} + \alpha_{i0} + T_{ki} \alpha_{ik} \operatorname{tg} \delta_k + T_{k+1 i} \alpha_{i k+1} \operatorname{tg} \delta_{k+1},$$

$$\beta_i = M_k \beta_{ik} + M_{k+1} \beta_{i k+1} + \beta_{i0} + T_{ki} \beta_{ik} \operatorname{tg} \delta_k + T_{k+1 i} \beta_{i k+1} \operatorname{tg} \delta_{k+1},$$

$$\begin{aligned}a_i &= X_k a_{ik} + X_{k+1} a_{i k+1} + a_{i0} + \left(\frac{d}{2}\right)^2 (Q_{ki} a_{ik} \operatorname{tg} \delta_k + Q_{k+1 i} a_{i k+1} \operatorname{tg} \delta_{k+1}) \\ &\quad - \frac{1}{l_i} (\alpha_i \operatorname{tg} \delta_k + \beta_i \operatorname{tg} \delta_{k+1}),\end{aligned}$$

$$\begin{aligned}b_i &= X_k b_{ik} + X_{k+1} b_{i k+1} + b_{i0} + \left(\frac{d}{2}\right)^2 (Q_{ki} b_{ik} \operatorname{tg} \delta_k + Q_{k+1 i} b_{i k+1} \operatorname{tg} \delta_{k+1}) \\ &\quad + \frac{1}{l_i} (\alpha_i \operatorname{tg} \delta_k + \beta_i \operatorname{tg} \delta_{k+1}).\end{aligned}$$

Equal Obliqueness, $\delta_k = \delta_{k+1} = \delta$

$$\alpha_i = \frac{l_i}{6EI_{yy}} (2M_k + M_{k+1}) + \alpha_{i0} + \frac{l_i \operatorname{tg} \delta}{6EI_{yy}} (2T_{ki} + T_{k+1 i})$$

$$\beta_i = \frac{l_i}{6EI_{yy}} (M_k + 2M_{k+1}) + \beta_{i0} + \frac{l_i \operatorname{tg} \delta}{6EI_{yy}} (T_{ki} + 2T_{k+1 i})$$

$$a_i = \frac{l_i}{6EI_{\omega\omega}} (2X_k + X_{k+1}) + a_{i0} + \frac{d^2 l_i \operatorname{tg} \delta}{24EI_{\omega\omega}} (2Q_{ki} + Q_{k+1 i}) - \frac{\operatorname{tg} \delta}{l_i} (\alpha_i + \beta_i)$$

$$b_i = \frac{l_i}{6EI_{\omega\omega}} (X_k + 2X_{k+1}) + b_{i0} + \frac{d^2 l_i \operatorname{tg} \delta}{24EI_{\omega\omega}} (Q_{ki} + 2Q_{k+1 i}) + \frac{\operatorname{tg} \delta}{l_i} (\alpha_i + \beta_i)$$

Part I

leading resp. to the ordinary three-moment and three-warping-moment equations

Part II

representing the influence of oblique supports, may be looked at as corrections in the generalized displacements, $\bar{\alpha}_{i0}, \bar{\beta}_{i0}, \bar{a}_{i0}, \bar{b}_{i0}$

Table 8.1 demonstrates that this system is described by ordinary three-moment equations for the unknowns M_k and three-warping-moment equations if the corrective terms of Part II are added to the deformations caused by the applied loads ($\alpha_{i0}, \beta_{i0}, \alpha_{i0}, b_{i0}$). The resulting system of equations may no longer be uncoupled since these corrective terms depend on the unknowns of the system, e.g., T_{ki} from X_k and X_{k+1} and Q_{ki} from M_k and M_{k+1} .

The solutions may be found by means of an iterative method. A first approximate value for the unknowns M_k and X_k may be calculated by neglecting the influence of the skew supports. This leads to a first approximation for the forces in the member and thereupon to the first corrections in the generalized displacements $\bar{\alpha}_{i0}, \bar{\beta}_{i0}, \bar{a}_{i0}, \bar{b}_{i0}$ (Part II of Table 8.1).

c) Member Forces

The support moments to the left and to the right of span i are the sum of the carry over moment and the correction ΔM . They immediately yield the distribution of the bending moments along the member.

Table 8.2. Summary of the Forces in an Obliquely Supported Member with $GKl^2 \ll EI_{\omega\omega}$

Bending	Twist
Moments at supports:	Warping moments at supports: $\omega M_{ki} = X_k + Q_{ki} \left(\frac{d}{2}\right)^2 \operatorname{tg} \delta_k$
$M_{k+1\ i} = M_{k+1} + T_{k+1\ i} \operatorname{tg} \delta_{k+1}$	$\omega M_{k+1\ i} = X_{k+1} + Q_{k+1\ i} \left(\frac{d}{2}\right)^2 \operatorname{tg} \delta_{k+1}$
Bending moments:	Warping moments: $M_{\omega i} = \omega M_{i0} + \omega M_{ki} (1 - \zeta_i) + \omega M_{k+1\ i} \zeta_i$
$M_i = M_{i0} + M_{ki}(1 - \zeta_i) + M_{k+1\ i} \zeta_i$	Torsional moments: $T_{\omega i} = T_i^{(i)} + (\omega M_{k+1\ i} - \omega M_{ki})/l_i$
Shearing forces:	Moment reaction on support: $F_k = Q_{ki} - Q_{k\ i-1}$
Force reaction on support:	Forces on support elements: $F_k^\pm = \frac{F_k}{2} \pm \frac{T_k}{d}$

The warping moments are now calculated. The derivation of the bending moments and the warping moments with respect to z_i yields shearing forces and torsional moments respectively. The difference of the latter at the supports again represents reactions. The corresponding expressions are summarized in Table 8.2.

If the torsional moments at the member ends, T_{ki} and T_{k+1i} , were known, all member forces could be calculated by means of known moments M_k and X_k simply by starting the calculation in the left upper corner of Table 8.2. This would successively lead to the shearing forces, support warping-moments and torsional moments.

In order to determine these unknown input quantities T_{ki} and T_{k+1i} , the above mentioned calculations are performed in a general manner. They finally lead to a system of two equations for the unknowns. The two solutions to this system may be obtained by means of the substitution

$$T_i = \frac{X_{k+1} - X_k}{l_i} + \frac{d}{2} (Q_{k+1 i}^{(0)} \varepsilon_{k+1 i} - Q_{ki}^{(0)} \varepsilon_{ki}) + \frac{d}{2l_i} (M_{k+1} - M_k) (\varepsilon_{k+1 i} - \varepsilon_{ki}) \quad (8.10a)$$

be written as follows:

$$T_{ki} = \frac{T_{k+1 i}^{(0)} + T_i - \varepsilon_{k+1 i} (\varepsilon_{k+1 i} - \varepsilon_{ki}) \Sigma M_{Di}}{1 - (\varepsilon_{k+1 i} - \varepsilon_{ki})^2}, \quad (8.10b)$$

$$T_{k+1 i} = \frac{T_{k+1 i}^{(0)} + T_i - \varepsilon_{ki} (\varepsilon_{k+1 i} - \varepsilon_{ki}) \Sigma M_{Di}}{1 - (\varepsilon_{k+1 i} - \varepsilon_{ki})^2}. \quad (8.10c)$$

d) Equal Skew Angles

The special case for equal skew angles δ is described by the parameter $\varepsilon_{ki} = \varepsilon_{k+1 i} = \varepsilon_i$. Eq. (8.10) yields the torsional moment:

$$T_{oi} = T_i^{(0)} + \frac{X_{k+1} - X_k}{l_i} - \frac{d}{2} \varepsilon_i \Sigma P_i \quad (8.11)$$

which enables the calculation of the bending moments at the supports:

$$\begin{aligned} M_{ki} &= M_k + T_{ki}^{(0)} \operatorname{tg} \delta + \frac{X_{k+1} - X_k}{l_i} \operatorname{tg} \delta - \varepsilon_i^2 l_i \Sigma P_i, \\ M_{k+1 i} &= M_{k+1} + T_{k+1 i}^{(0)} \operatorname{tg} \delta + \frac{X_{k+1} - X_k}{l_i} \operatorname{tg} \delta - \varepsilon_i^2 l_i \Sigma P_i \end{aligned} \quad (8.12)$$

and of the warping moments at the supports:

$$\begin{aligned} \omega M_{ki} &= X_k + Q_{ki}^{(0)} \left(\frac{d}{2} \right)^2 \operatorname{tg} \delta + (M_{k+1} - M_k) \varepsilon_i \frac{d}{2} - \varepsilon_i^2 l_i \Sigma M_{Di}, \\ \omega M_{k+1 i} &= X_{k+1} + Q_{k+1 i}^{(0)} \left(\frac{d}{2} \right)^2 \operatorname{tg} \delta + (M_{k+1} - M_k) \varepsilon_i \frac{d}{2} - \varepsilon_i^2 l_i \Sigma M_{Di}. \end{aligned} \quad (8.13)$$

These moments at the supports represent boundary values that permit determination of the distribution of bending moments and warping moments along the member.

The distribution of the torsional moments was given by Eq. (8.11). The equivalent expression for the shearing forces is:

$$Q_i = Q_{i0} + \frac{M_{k+1} - M_k}{l_i} - \frac{\sum M_{Di}}{l_i} \operatorname{tg} \delta. \quad (8.14)$$

8.3 Examples

a) Single-Span Beam on Skewed and Parallel Supports

The problem of a single-span beam on parallel and skew supports whose Saint-Venant torsional resistance is negligible was solved above. This simple system has no redundants ($M_k = M_{k+1} = X_k = X_{k+1} = 0$). All the forces in the member may therefore be calculated directly from Eqs. (8.11) to (8.14).

These forces shall nevertheless be given again using a simplified notation. Since there is only one span, the subscript i may be omitted. The support to the left (k) shall furthermore be denoted by A and the one to the right ($k + 1$) by B . M_0 and Q_0 denote the bending moments in the simply supported beam while $M_{\omega 0}$ and $T_{\omega}^{(P)}$ stand for the corresponding warping moments and torsional moments for which Eqs. (7.16) and (7.17) present some examples.

The skewness of the supports is defined by the longitudinal distance (e) and the transverse distance (d) between the two distinct support elements. The distance e may be either positive or negative depending on whether it defines a positive or a negative angle δ .

The Eqs. (8.12) for the bending moments at the supports simplify to:

$$\begin{aligned} M_A &= T_A^{(P)} \frac{e}{d} - \frac{e^2}{4l} \sum_A^B P, \\ M_B &= T_B^{(P)} \frac{e}{d} - \frac{e^2}{4l} \sum_A^B P \end{aligned} \quad (8.15)$$

and those for the warping moments (8.13) to:

$$\begin{aligned} M_{\omega A} &= Q_{A0} \frac{de}{4} - \frac{e^2}{4l} \sum_A^B M_D, \\ M_{\omega B} &= Q_{B0} \frac{de}{4} - \frac{e^2}{4l} \sum_A^B M_D. \end{aligned} \quad (8.16)$$

These moments represent boundary values of the distributed bending moments and warping moments respectively. The shearing forces and torsional moments are derived from expressions (8.14) and (8.11):

$$Q = Q_0 - \frac{e}{ld} \sum_A^B M_D, \quad (8.17)$$

$$T_{\omega} = T_{\omega 0} - \frac{de}{4l} \sum_A^B P. \quad (8.18)$$

Simple expressions for the forces in the member may be derived for the case of a uniformly distributed load p in which $M_{\omega_0} = 0$ and therefore $T_{A0} = T_{B0} = 0$ and $Q_{A0} = -Q_{B0} = pl/2$. The member forces in this case are:

$$\begin{aligned} M &= \frac{pl^2}{8} \left[4\zeta(1-\zeta) - 2\left(\frac{e}{l}\right)^2 \right], \\ Q &= \frac{pl}{2} (1-2\zeta), \\ M_\omega &= \frac{pl^3}{8} \frac{d}{l} \frac{e}{l} (1-2\zeta), \\ T_\omega &= -\frac{pl^3}{4} \frac{d}{l} \frac{e}{l}. \end{aligned} \tag{8.19}$$

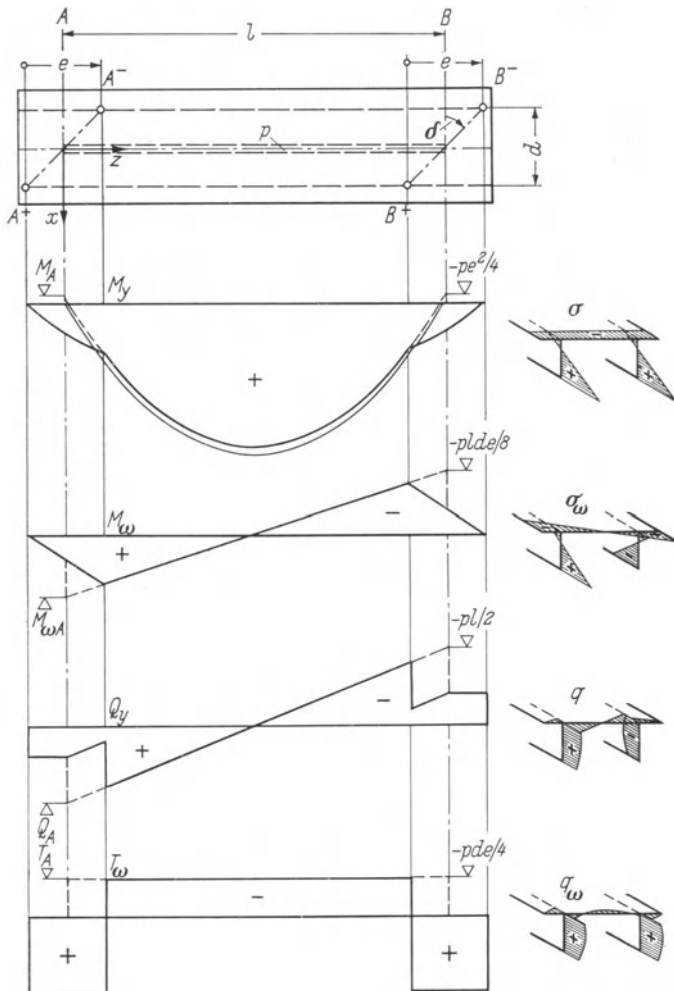


Fig. 8.2. Forces in a Skew Supported, Single-Span Beam Under Uniformly Distributed Load, $GKl^2 \ll EI_{\omega\omega}$.

These functions are plotted in Fig. 8.2 for the geometric assumptions $e/l = d/l = 1:5$. It may be observed that skewed supports have but little influence on the bending moments in the case of centric loads. The maximum value at mid-span is merely reduced to $1 - 2(e/l)^2 = 23/25$ of the maximum moment in a simply supported beam. The shearing forces remain unchanged as long as the skew supports remain parallel.

The forces acting on the distinct support elements may be calculated with the expression at the bottom of Table 8.2. They are denoted by A^+ , A^- and B^+ , B^- depending on whether they act on the positive or negative side of the x -axis.

$$\begin{aligned} A^- &= \frac{pl}{4} \left(1 + \frac{e}{l}\right), & B^- &= \frac{pl}{4} \left(1 - \frac{e}{l}\right), \\ A^+ &= \frac{pl}{4} \left(1 - \frac{e}{l}\right), & B^+ &= \frac{pl}{4} \left(1 + \frac{e}{l}\right). \end{aligned} \quad (8.20)$$

Fig. 8.2 shows the distribution of all the internal force components caused by the uniformly distributed load p , i.e. the bending moment M_y , the warping moment M_ω , the shearing force Q_y and the torsional moment T_ω . The distribution of the axial stresses for the first two cases and of the shear flows in the other is shown to the right of the same figure (v. Table 6.2).

The corrections of the different diagrams within the support regions are a consequence of the selected support arrangement. The reactions F and T were divided up into forces acting at the distinct support points. The corrections together with the purely theoretical values M_A , $M_{\omega A}$, Q_A and T_A are of course only valid within the scope of ordinary statics.

The extreme value for the warping moment occurs at $\zeta = e/2l$ and amounts to:

$$\max M_\omega = \frac{pl^3}{8} \frac{d}{l} \frac{e}{l} \left(1 - \frac{e}{l}\right) = \frac{pl^3}{250}.$$

Whether this warping moment is an important design quantity or not may be judged only on the basis of its effect on the axial stresses. The maximum stresses in the lower flange caused by this warping moment shall therefore be compared with those due to the maximum bending moment.

$$\frac{\max \sigma_\omega}{\max \sigma} = \frac{\frac{pl^3}{8} \frac{d}{l} \frac{e}{l} \left(1 - \frac{e}{l}\right) \frac{\omega}{I_{\omega\omega}}}{\frac{pl^2}{8} \left[1 - 2\left(\frac{e}{l}\right)^2\right] \frac{y}{I_{yy}}} = \frac{\frac{e}{l} - \left(\frac{e}{l}\right)^2}{1 - 2\left(\frac{e}{l}\right)^2} d \frac{\omega}{y} \frac{I_{yy}}{I_{\omega\omega}}.$$

The quotient $y I_{\omega\omega} / d I_{yy}$ represents, according to Eq. (7.6), the coordinate x_L of the zero influence ordinate. It may be observed from Fig. 7.4 that x_L for stresses in the lower flange is approximately $d/2$. Since, furthermore, (e/l) is small as compared to one, the last expression reduces to the following approximate relation:

$$\frac{\max \sigma_\omega}{\max \sigma} = \frac{e}{l} \frac{d}{x_L} \simeq 2 \frac{e}{l}. \quad (8.21)$$

In this example, the warping stresses would amount to about 40% of the bending stresses. They should not be added, however, since these maximum values occur in different places, one at an interior support element and the other at mid-span. The situation is different for the shear flows where maximum values occur in the same location.

b) Two-Span Beam on Skewed Supports

Consider the continuous beam over two equal spans and with variable skewness of the supports ($\delta_1 = 0$, $\delta_3 = \delta$, $\delta_5 = 0$) subjected to the uniformly distributed, centric load p .

The character of the system and the load is expressed by $T_{20} = T_{40} = 0$, $Q_{12}^{(0)} = -Q_{32}^{(0)} = Q_{34}^{(0)} = -Q_{54}^{(0)} = pl/2$, $\epsilon_{12} = \epsilon_{54} = 0$, $\epsilon_{32} = \epsilon_{34} = \epsilon = e/2l$ and $M_1 = M_5 = X_1 = X_5 = 0$ which, by means of Eqs. (8.10), lead to:

$$T_{12} = T_{32} = \frac{\frac{X_3}{l} - \frac{d}{2} \frac{pl}{2} \frac{e}{2l} + \frac{d}{2l} \frac{e}{2l} M_3}{1 - \epsilon^2}. \quad (8.22a)$$

$$T_{34} = T_{54} = \frac{-\frac{X_3}{l} - \frac{d}{2} \frac{pl}{2} \frac{e}{2l} + \frac{d}{2l} \frac{e}{2l} M_3}{1 - \epsilon^2}. \quad (8.22b)$$

The system of equations for the remaining redundants M_3 and X_3 ,

$$2(l_2 + l_4)M_3 = -6EI_{yy}(\beta_{20} + \alpha_{40} + \bar{\beta}_{20} + \bar{\alpha}_{40}),$$

$$2(l_2 + l_4)X_3 = -6EI_{\omega\omega}(\bar{b}_{20} + \bar{a}_{40}),$$

may even be reduced further because of $\beta_2 = \alpha_4$ and $\bar{b}_{20} + \bar{a}_{20} = 0$ which immediately yield $X_3 = 0$ (v. Table 8.1).

The torsional moments (8.22a) and (8.22b) are therefore no longer different from each other.

From Table 8.1 follows the relation:

$$\bar{\beta}_{20} = \bar{\alpha}_{40} = \frac{le^2}{3EI_{yy}} \frac{-\frac{p}{8} + \frac{M_3}{4l^2}}{1 - \epsilon^2},$$

which brings the first equation of the system above into the following form:

$$4lM_3 = -6EI_{yy} \left(2 \frac{pl^3}{24EI_{yy}} + 2 \frac{le^2}{24EI_{yy}} \frac{-p + 2 \frac{M_3}{l^2}}{1 - \epsilon^2} \right).$$

This relation determines:

$$M_3 = -\frac{pl^2}{8} (1 - 5\epsilon^2) \quad (8.23)$$

and:

$$T_2 = T_4 = -\frac{5}{32} p d e.$$

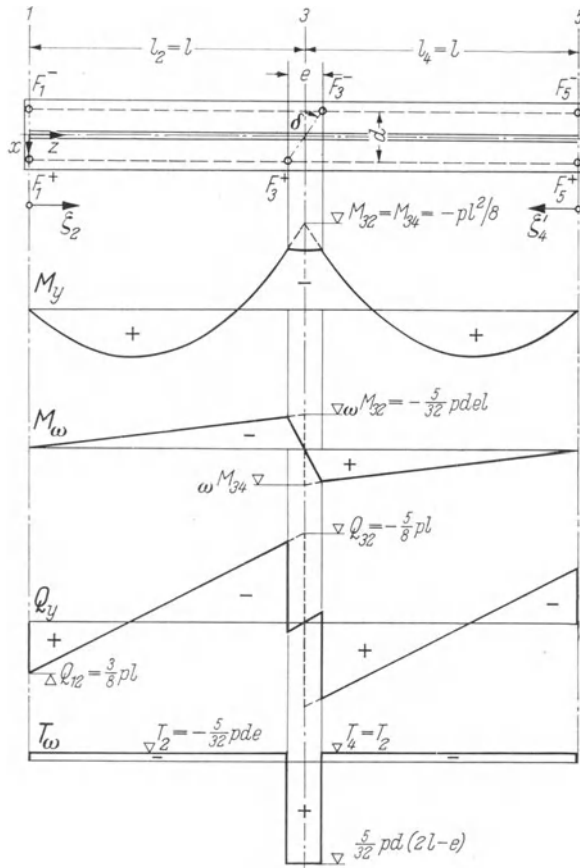


Fig. 8.3. Forces in a Two-Span, Continuous Beam with an Oblique, Intermediate Support under a Uniformly Distributed, Lateral Load. $EI_{\omega\omega} \gg GKl^2$.

Expressions for the forces in the continuous system may now be formulated. For span 2 they become:

$$M_2 = \frac{pl^2}{8} (3\zeta_2 - 4\zeta_2^2), \quad (8.24a)$$

$$Q_2 = pl \left(\frac{3}{8} - \zeta_2 \right), \quad (8.24b)$$

$$M_{\omega 2} = -\frac{5}{32} p le d \zeta_2, \quad (8.24c)$$

$$T_2 = -\frac{5}{32} p d e. \quad (8.24d)$$

The distribution of the forces in span 4 is either symmetric or antisymmetric to the one in span 2 as may be seen from Fig. 8.3. The reactions at the supports are:

$$\begin{aligned} F_1^- &= F_5^+ = \frac{3}{16} pl \left(1 + \frac{5}{6} \frac{e}{l} \right), \\ F_1^+ &= F_5^- = \frac{3}{16} pl \left(1 - \frac{5}{6} \frac{e}{l} \right), \\ F_3^+ &= F_3^- = \frac{5}{8} pl. \end{aligned} \quad (8.25)$$

Fig. 8.3 shows further the behavior of the forces at the supports again assuming the validity of the ordinary statics. The total reaction F_3 was, for this purpose, again divided up into the two equivalent forces F_3^+ and F_3^- each acting at a distinct support point.

A prime effect of skewed supports is to reduce the bending moments. The corresponding decrease in axial stresses, however, is usually offset, at least in part, by the warping stresses.

III. Mixed Torsion

9 Internal Forces

9.1 Elements of the Analysis

a) Differential Equation

The interaction of Saint-Venant torsion (T_s) and warping torsion (T_ω) requires consideration whenever both effects are of the same order of magnitude. At any point z along the member, the torsional moment T is equal to the sum of two effects:

$$T = T_s + T_\omega. \quad (9.1)$$

The Saint-Venant part of the torsional moment is proportional to the first derivative of the angle of twist φ , v. Eq. (1.1).

$$T_s = G K \varphi'. \quad (9.2)$$

The warping torsion, on the other hand, is (according to Table 5.1) proportional to the first derivative of the warping moment M_ω . The warping moment is defined as

$$M_\omega = -E I_{\omega\omega} \varphi''. \quad (9.3)$$

Thus

$$T_\omega = -(E I_{\omega\omega} \varphi''). \quad (9.4)$$

The signs of the torsional moments are determined by the following convention: A torsional moment acting on a cross section with a positive outward normal is positive whenever it causes a positive rotation (in $+\varphi$ -sense) of the cross section. Conversely, a torsional moment acting on a cross section with a negative outward normal must turn in the negative φ -sense to be positive.

The symbol m_D denotes an externally applied torsional load per unit length and is positive if applied in the positive φ -sense.

The equilibrium condition for a member element of length dz may thus be formulated as follows:

$$-T + m_D dz + \left(T + \frac{dT}{dz} dz \right) = 0,$$

which simplifies to:

$$-\frac{dT}{dz} = m_D.$$

If the torsional moment T is, according to Eq. (9.1), divided up into the two components T_s and T_ω and if the latter are introduced according to the expressions (9.2) and (9.4), the following fundamental differential equation for mixed torsion results:

$$(EI_{\omega\omega}\varphi'')'' - (GK\varphi')' = m_D. \quad (9.5)$$

Since the following theory is restricted to prismatic members, this linear fourth-order differential equation will have constant coefficients:

$$EI_{\omega\omega}\varphi'''' - GK\varphi'' = m_D. \quad (9.6)$$

b) Solution for an Infinitely Long Bar

The general solution to the homogeneous part of the differential equation (9.6) is of the form:

$$\varphi = C_1 + C_2 \frac{z}{d} + C_3 e^{-z/d} + C_4 e^{+z/d}$$

where d^* , the “characteristic length”, is:

$$d = \sqrt{\frac{EI_{\omega\omega}}{GK}}.$$

The symbols C_1 , C_2 , C_3 and C_4 represent constants of integration.

The general solution (9.7) could of course be written in terms of hyperbolic functions. The independent variable z , which is the length coordinate of the bar, will in any case be normalized by means of the characteristic length d which depends only on the cross section of the bar. If the bar is of finite length l , then l may serve as the reference distance for the normalization of the coordinate z .

Consider, for example, the semi-infinite bar which is fixed at the origin and which transmits from its far (infinitely distant) end a constant torsional moment M_D . The boundary conditions are:

$$\varphi\left(\frac{z}{d} = 0\right) = 0, \quad (a)$$

$$\varphi'\left(\frac{z}{d} = 0\right) = 0, \quad (b)$$

$$\varphi'\left(\frac{z}{d} = \infty\right) = \text{finite}, \quad (c)$$

$$T\left(\frac{z}{d} = \infty\right) = M_D. \quad (d)$$

Condition (9.8c) states the fact that φ' must remain finite for large values of z/d . Therefore $C_4 = 0$.

* The characteristic length d , sometimes termed the “torsion-bending constant” and designated as “ a ” in English references, is tabulated for I-shaped sections in design manuals of major U.S. steel companies. It is also tabulated for British sections in Publication No. 31 of the British Constructional Steelwork Association.

This result means that the expression for the angle of twist (9.7) in the case of large arguments $z/d \gg 1$ reduces to:

$$\varphi \left(\frac{z}{d} \gg 1 \right) = C_1 + C_2 \frac{z}{d} \quad (9.9)$$

The second and third derivative of the expression vanish and with them the warping moment M_ω and the torsional moment T_ω . The Saint-Venant torsional moment $T_s = G K \varphi'$ becomes therefore the only resistance to the applied load M_D .

This shows that mixed torsion uncouples and becomes pure Saint-Venant torsion if the total torsional moment stays constant over a distance which greatly exceeds the reference distance d .

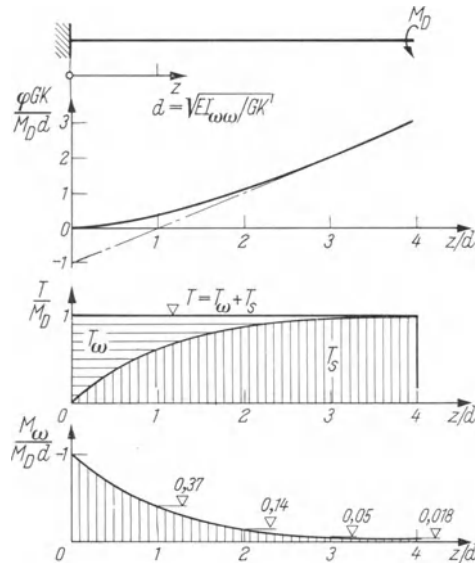


Fig. 9.1. Distribution of the Twist φ , Torsional Moment T , Warping Moment M_ω in a Semi-Infinite Bar Under the Constant Torsional Moment M_D .

The boundary condition (9.8d) requires that $G K C_2/d = M_D$ which determines the constant C_2 . The conditions (a) and (b), finally, yield $C_1 = -C_3$ and $C_2 = C_3$. The final solution to this simple example is therefore the following:

$$\begin{aligned} \varphi &= \frac{M_D d}{G K} \left(-1 + \frac{z}{d} + e^{-z/d} \right), \\ T_s &= G K \varphi' = M_D (1 - e^{-z/d}), \\ M_\omega &= -EI_{\omega\omega}\varphi'' = -M_D d e^{-z/d}, \\ T_\omega &= -EI_{\omega\omega}\varphi''' = +M_D e^{-z/d}. \end{aligned} \quad (9.10)$$

These solutions are presented in Fig. 9.1.

e) Solution for the Bar of Finite Length l

It is appropriate to base the discussion of this problem on a general solution which is written in terms of hyperbolic functions as the linearly independent integrals of the differential equation. The length coordinate z will, as was mentioned above, be normalized by means of the bar length l .

If $\bar{\varphi}$ denotes the particular solution of the differential equation, $\zeta = \frac{z}{l}$ the normalized coordinate and if

$$\varkappa = \sqrt{\frac{G K l^2}{E I_{\omega\omega}}} = \frac{l}{d} \quad (9.11)$$

replaces the given, nondimensional expression, the differential equation (9.6) and its solution may be written in the following way:

$$\begin{aligned} \varphi'''' - \frac{\varkappa^2}{l^2} \varphi'' &= \frac{m_D}{E I_{\omega\omega}}, \\ \varphi &= C_1 + C_2 \zeta + C_3 \sin \varkappa \zeta + C_4 \cos \varkappa \zeta + \bar{\varphi}. \end{aligned} \quad (9.12)^1$$

The constants C_1 , C_2 , C_3 and C_4 again represent constants of integration which may be determined from four prescribed boundary conditions of the bar.

The primes denote derivatives with respect to z . Derivatives with respect to the normalized coordinate ζ have thus to be corrected by:

$$d\zeta/dz = 1/l.$$

The deformations of the bar and the internal forces are summarized below in their general form

The angle of twist φ :

$$\varphi = C_1 + C_2 \zeta + C_3 \sin \varkappa \zeta + C_4 \cos \varkappa \zeta + \bar{\varphi}. \quad (9.13)$$

The angle of twist per unit length φ' :

$$\varphi' = C_2 \frac{1}{l} + C_3 \frac{\varkappa}{l} \cos \varkappa \zeta + C_4 \frac{\varkappa}{l} \sin \varkappa \zeta + \bar{\varphi}'. \quad (9.14)$$

The warping moment $M_\omega = -EI_{\omega\omega}\varphi''$:

$$M_\omega = -GK(C_3 \sin \varkappa \zeta + C_4 \cos \varkappa \zeta) - EI_{\omega\omega} \bar{\varphi}''. \quad (9.15)$$

The torsional moment $T = GK\varphi' - EI_{\omega\omega}\varphi'''$:

$$T = GK \left(\frac{C_2}{l} + \bar{\varphi}' \right) - EI_{\omega\omega} \bar{\varphi}'''. \quad (9.16)$$

¹ Note that $\sin \varkappa \zeta$ and $\cos \varkappa \zeta$, as transposed from the German text, are hyperbolic functions, usually denoted as $\sinh \varkappa \zeta$ and $\cosh \varkappa \zeta$, respectively, in English texts.

It may again be recognized from Eq. (9.16) that the total torsional moment T stays constant in regions of the bar to which no torsional moment is applied and the particular solution $\bar{\varphi}$ in such cases vanishes.

d) Particular Solutions

This section presents a small selection of particular solutions $\bar{\varphi}$ for a number of different load arrangements¹.

The particular solutions for the cases (9.17 a to d) may be found by means of assumptions which express the principal character of the loading function.

An assumption for the particular solution of case (9.17e) must reflect the jump-discontinuity of the torsional moment at the point $\zeta = \alpha$ which, furthermore, must be expressed in terms of solutions to the homogeneous differential equation (9.12). The concentrated torsional moment M_D yields a discontinuity in the expression for the warping torsion which might be formulated as follows:

$$\begin{aligned} -EI_{\omega\omega}\bar{\varphi}'''(\zeta < \alpha) &= 0, \\ -EI_{\omega\omega}\bar{\varphi}'''(\zeta > \alpha) &= -M_D \cos \varkappa(\zeta - \alpha). \end{aligned}$$

The particular solution in the region $\zeta < \alpha$ may be assumed to be zero. In the region $\zeta > \alpha$, it may be calculated from the above assumption considering that the warping moment, thus $\bar{\varphi}''$, $\bar{\varphi}'$ and $\bar{\varphi}$ are continuous at the point α and are therefore actually zero because of the particular solution $\bar{\varphi}$ for $\zeta < \alpha$.

1. Uniformly distributed torsional load :

$$m_D = m \quad \rightarrow \bar{\varphi} = -\frac{m}{2} \frac{l^2}{GK} \zeta^2. \quad (9.17 \text{ a})$$

2. Linearly distributed torsional load :

$$m_D = m\zeta \quad \rightarrow \bar{\varphi} = -\frac{m}{6} \frac{l^2}{GK} \zeta^3. \quad (9.17 \text{ b})$$

3. Parabolically distributed torsional load :

$$m_D = m\zeta^2 \quad \rightarrow \bar{\varphi} = -\frac{m}{12} \frac{l^2}{GK} \zeta^4 - m \frac{EI_{\omega\omega}}{(GK)^2} \zeta^2. \quad (9.17 \text{ c})$$

4. Sinusoidally distributed torsional load :

$$m_D = m \sin \alpha \zeta \quad \rightarrow \bar{\varphi} = m \frac{l^4}{EI_{\omega\omega}} \frac{\sin \alpha \zeta}{\alpha^2(\alpha^2 + \varkappa^2)}. \quad (9.17 \text{ d})$$

¹ Graphical presentation of solutions (9.17a), (9.17b) and (9.17c), as well as additional particular solutions will be found in Handbook 1963 of the Bethlehem Steel Corporation (USA) and in Publication No. 31 of the British Constructional Steelwork Association.

5. Concentrated torsional moment M_D acting in the position $\zeta = \alpha = a/l$ (v. Fig. 9.4):

$$\begin{aligned}\bar{\varphi}(\zeta < \alpha) &= 0, \\ \bar{\varphi}(\zeta > \alpha) &= \frac{M_D l}{GK} \left[\frac{1}{\alpha} \sin \alpha (\zeta - \alpha) - (\zeta - \alpha) \right].\end{aligned}\quad (9.17e)$$

e) Boundary Conditions

Two boundary conditions may be formulated for each end of the bar. This leads to a total of four boundary conditions which serve to determine the four as yet unknown constants of integration C_1 , C_2 , C_3 and C_4 . The deformations and internal forces follow thereupon from Eqs. (9.13) to (9.16). Examples for two sets of boundary conditions are given by Eqs. (7.1) and (7.2). These conditions are still valid even though Chapter 7 neglects the influence of Saint-Venant torsion. The geometric boundary conditions (e.g. those referring to φ and φ') are not affected by this simplification and the condition for M_ω in Eqs. (7.1) as one of the statical conditions (e.g. those giving information about M_ω and T) remains unchanged as well.

For a free end of a member at $z = l$, the two corresponding statical conditions would be as follows:

$$\begin{aligned}M_\omega(z=l) &= 0, \\ T(z=l) &= 0.\end{aligned}\quad (9.18)$$

The symbol T represents the total torsional moment as given by Eq. (9.16).

If a member is simply supported at $\zeta = 0$ the corresponding two boundary conditions reduce the number of integration constants in the general solution by two. A new set of expressions corresponding to Eqs. (9.13) to (9.16) will be derived for this special case.

The boundary conditions at the point $\zeta = 0$ are:

$$\varphi(\zeta=0) = 0 \quad \text{and} \quad M_\omega(\zeta=0) = 0,$$

and any particular solution vanishes at this point as well, $\bar{\varphi}(\zeta=0) = 0$. Eqs. (9.13) and (9.15) lead therefore to the integration constants:

$$C_1 = -C_4, \quad C_4 = -\frac{l^2}{\alpha^2} \bar{\varphi}''(\zeta=0),$$

which in turn yield the following simplified system of general solutions:

$$\begin{aligned}\varphi &= \frac{l^2}{\alpha^2} (1 - \cos \alpha \zeta) \bar{\varphi}''(\zeta=0) + C_2 \zeta + C_3 \sin \alpha \zeta + \bar{\varphi}, \\ \varphi' &= -\frac{l}{\alpha} \bar{\varphi}''(\zeta=0) \sin \alpha \zeta + \frac{C_2}{l} + C_3 \frac{\alpha}{l} \cos \alpha \zeta + \bar{\varphi}', \\ M_\omega &= EI_{\omega\omega} \bar{\varphi}''(\zeta=0) \cos \alpha \zeta - C_3 GK \sin \alpha \zeta - EI_{\omega\omega} \bar{\varphi}'', \\ T &= GK \left(\frac{C_2}{l} + \bar{\varphi}' \right) - EI_{\omega\omega} \bar{\varphi}'''.\end{aligned}\quad (9.19)$$

If the member is, aside from the hinged support at $\zeta = 0$, acted upon only by a torsional load at the other end, the particular solution vanishes and the general solutions simplify even further to:

$$\begin{aligned}\varphi &= C_2 \zeta + C_3 \sin \alpha \zeta, \\ \varphi' &= \frac{C_2}{l} + C_3 \frac{\alpha}{l} \cos \alpha \zeta, \\ M_\omega &= -GK C_3 \sin \alpha \zeta, \\ T &= C_2 \frac{GK}{l}.\end{aligned}\tag{9.20}$$

The total torsional moment T is of no interest since the stress calculation must be based on the two components T_s and T_ω . This does not present any new problem, however, since the derivative of the angle of twist, φ' , needs only the multiplier GK to determine the Saint-Venant torsional moment T_s . The torsional moment T_ω may be calculated from the difference $T - T_s$ or obtained directly from the derivative of the warping moment M_ω with respect to z .

9.2 Examples of the Simply Supported Member

a) Warping Moment at the End of the Member

If a warping moment X is introduced at the end $z = l$ of a member which is simply supported at both ends, the situation at the supports is described by the boundary conditions:

$$\begin{aligned}\varphi(\zeta = 0) &= 0, & \varphi(\zeta = 1) &= 0, \\ M_\omega(\zeta = 0) &= 0, & M_\omega(\zeta = 1) &= X.\end{aligned}\tag{9.21}$$

The simple supports at the end $z = 0$ and the vanishing particular solution $\bar{\varphi}$ reduce the general solutions (9.13) to (9.16) to the simple expressions (9.20).

The conditions at the right support determine the remaining two constants $C_3 = -X/GK \sin \alpha$ and $C_2 = X/GK$. The solutions to this problem are therefore as follows:

$$\begin{aligned}\varphi &= \frac{X}{GK} \left(\zeta - \frac{\sin \alpha \zeta}{\sin \alpha} \right), \\ \varphi' &= \frac{X}{GKl} \left(1 - \alpha \frac{\cos \alpha \zeta}{\sin \alpha} \right), \\ M_\omega &= X \frac{\sin \alpha \zeta}{\sin \alpha}, \\ T &= \frac{X}{l}.\end{aligned}\tag{9.22}$$

These functions of the independent variable ζ are plotted in Fig. 9.2 for the special case $\alpha = 1$.

b) Twisted Supports

The two supports of a simply supported bar are twisted by the angle φ_A and φ_B respectively. Since the member carries no lateral load, the particular solution $\bar{\varphi}$ is again zero and the problem is completely described by the boundary conditions:

$$\begin{aligned}\varphi(\zeta=0) &= \varphi_A, & \varphi(\zeta=1) &= \varphi_B, \\ M_\omega(\zeta=0) &= 0, & M_\omega(\zeta=1) &= 0.\end{aligned}\quad (9.23)$$

If Eq. (9.15) is used to determine the two constants C_3 and C_4 from the two statical boundary conditions, one immediately arrives at $C_3 = C_4 = 0$ which means that the warping moment is zero throughout. The remaining boundary conditions yield $C_1 = \varphi_A$ and $C_2 = \varphi_B - \varphi_A$. This problem has therefore the following solutions:

$$\begin{aligned}\varphi &= \varphi_A + (\varphi_B - \varphi_A)\zeta, \\ \varphi' &= \frac{\varphi_B - \varphi_A}{l}, \\ M_\omega &= 0, \\ T &= \frac{GK}{l} (\varphi_B - \varphi_A).\end{aligned}\quad (9.24)$$

Since the torsional moment T_ω is the derivative of the warping moment M_ω , T_ω vanishes as well. It is therefore apparent that members which are free to warp at each end and which are subjected to a constant torsional moment exhibit only Saint-Venant torsional resistance.

c) Uniformly Distributed Torsional Load

The boundary conditions of a simply supported bar of the length l are those of Eqs. (7.1). Since both the system and the load show symmetry with respect to the center of the span, it is appropriate to introduce a new coordinate system

$$\xi = \zeta - \frac{l}{2} \quad (9.25)$$

which has its origin at this point.

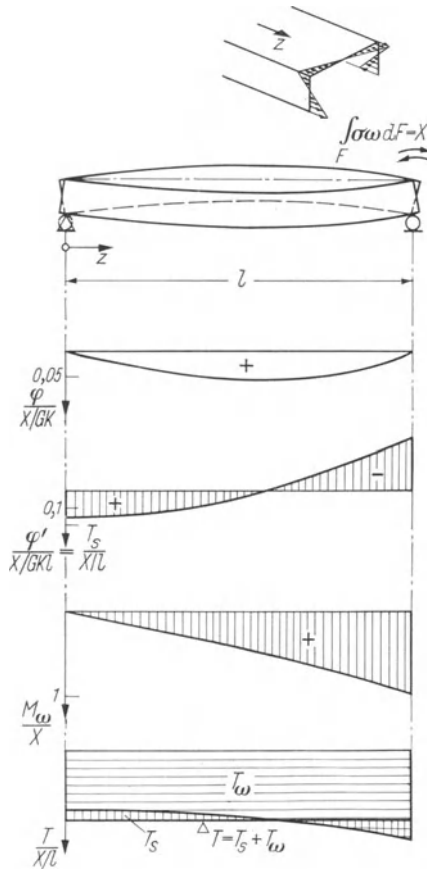


Fig. 9.2. Distribution of the Quantities φ , φ' , M_ω , T_ω , T_s and T in a Simply Supported Bar Whose Right End is Acted Upon by the Warping Moment X (Figures are Plotted for $\alpha = 1$).

It is a consequence of this symmetry that constants of integration belonging to the odd functions in the expression for the angle of twist (9.13) must vanish. Therefore: $C_2 = C_3 = 0$.

The remaining two constants follow from the boundary conditions:

$$\begin{aligned}\varphi(\xi = \frac{l}{2}) &= 0, \\ M_\omega(\xi = \frac{l}{2}) &= 0.\end{aligned}\tag{9.26}$$

The particular solution corresponding to the uniformly distributed torsional load m_D is given by Eq. (9.17a). The expressions for this solution and its first, second and third derivative are:

$$\begin{aligned}\bar{\varphi} &= -\frac{m_D}{2} \frac{l^2}{GK} \xi^2, \\ \bar{\varphi}' &= -m_D \frac{l}{GK} \xi, \\ \bar{\varphi}'' &= -\frac{m_D}{GK}, \\ \bar{\varphi}''' &= 0.\end{aligned}$$

Eqs. (9.13) and (9.15) together with the boundary conditions (9.26) lead to the following conditions for the constants C_1 and C_4 :

$$\begin{aligned}C_1 + C_4 \cos \frac{\varkappa}{2} - \frac{m_D l^2}{8GK} &= 0, \\ C_4 \cos \frac{\varkappa}{2} - \frac{EI_{\omega\omega}}{(GK)^2} m_D &= 0.\end{aligned}$$

The solutions for this system of equations are:

$$\begin{aligned}C_4 &= +\frac{EI_{\omega\omega}}{(GK)^2 \cos \frac{\varkappa}{2}} m_D = +\frac{m_D l^2}{GK} \frac{1}{\varkappa^2 \cos \frac{\varkappa}{2}}, \\ C_1 &= \frac{m_D l^2}{GK} \left(\frac{1}{8} - \frac{1}{\varkappa^2} \right).\end{aligned}$$

These are then introduced into Eqs. (9.13) to (9.16) to provide the solution of the given problem.

$$\begin{aligned}\varphi &= \frac{m_D l^2}{GK} \left[\left(\frac{1}{8} - \frac{1}{\varkappa^2} \right) - \frac{1}{2} \xi^2 + \frac{\cos \varkappa \xi}{\varkappa^2 \cos \frac{\varkappa}{2}} \right], \\ \varphi' &= -\frac{m_D l}{GK} \left(\xi - \frac{\sin \varkappa \xi}{\varkappa \cos \frac{\varkappa}{2}} \right), \\ M_\omega &= \frac{m_D l^2}{\varkappa^2} \left(1 - \frac{\cos \varkappa \xi}{\cos \frac{\varkappa}{2}} \right), \\ T &= -m_D l \xi.\end{aligned}\tag{9.27}$$

These solutions are plotted in Fig. 9.3 for the parameter $\kappa = 3$.

The total torsional moment T may be divided up into the Saint-Venant part

$$T_s = GK\varphi' = -m_D l \left(\bar{\xi} - \frac{\sin \kappa \bar{\xi}}{\kappa \cos \frac{\kappa}{2}} \right) \quad (9.28a)$$

and into the warping part

$$T_\omega = -m_D l \frac{\sin \kappa \bar{\xi}}{\kappa \cos \frac{\kappa}{2}}. \quad (9.28b)$$

The maximum value for the angle of twist φ occurs at mid-span, i.e. for $\bar{\xi} = 0$.

$$\max \varphi = \frac{m_D l^2}{8 GK} \left(1 - \frac{\left(\frac{4}{\kappa}\right)^2}{1 + \operatorname{Ctg}^2 \frac{\kappa}{4}} \right). \quad (9.29)$$

Both the Saint-Venant torsional moment T_s and the warping torsional moment T_ω have maximum values at the ends of the member, i.e. for $\bar{\xi} = \pm 1/2$.

$$\begin{aligned} \max T_s &= GK\varphi' \left(\bar{\xi} = \pm \frac{1}{2} \right) \\ &= \pm \frac{m_D l}{2} \left(1 - \frac{2}{\kappa} \operatorname{Tg} \frac{\kappa}{2} \right), \end{aligned} \quad (9.30a)$$

$$\max T_\omega = \pm \frac{m_D l}{2} \frac{2}{\kappa} \operatorname{Tg} \frac{\kappa}{2}. \quad (9.30b)$$

The maximum value for the warping moment, finally, occurs at mid-span, i.e. for $\bar{\xi} = 0$.

$$\max M_\omega = \frac{m_D l^2}{\kappa^2} \left(1 - \frac{1}{\cos \frac{\kappa}{2}} \right). \quad (9.31)$$

d) Concentrated Torsional Load

The structural system and the applied notation are shown in Fig. 9.4. A particular solution which corresponds to the concentrated torsional load M_D was presented in Eq. (9.17e) assuming $\bar{\varphi}''(\xi = 0) = 0$. For this simply supported

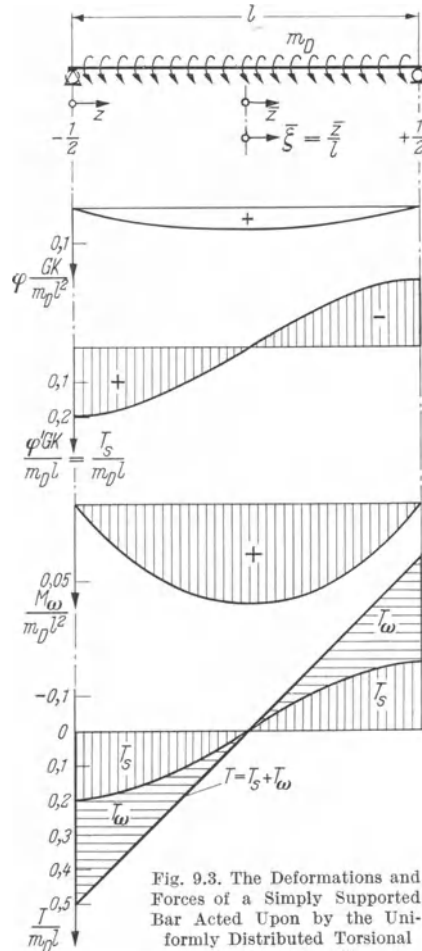


Fig. 9.3. The Deformations and Forces of a Simply Supported Bar Acted Upon by the Uniformly Distributed Torsional Load m_D ($\kappa = 3$).

system, the two constants of integration C_2 and C_3 of Eqs. (9.19) may be determined as follows ($\beta = b/l = 1 - \alpha$):

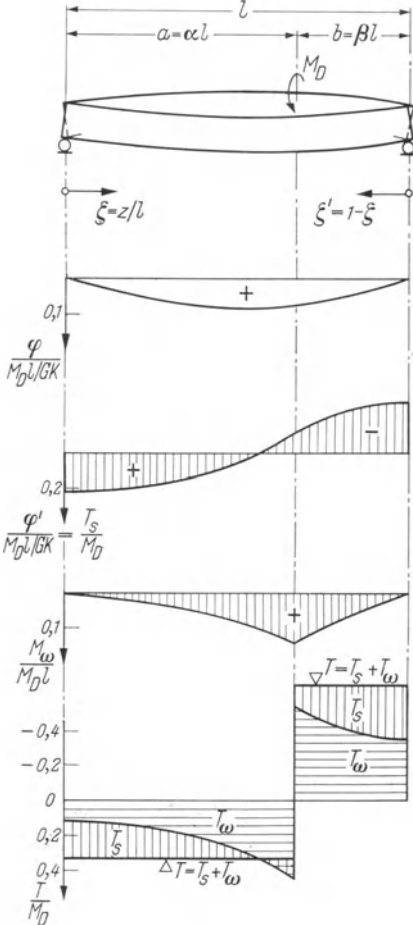


Fig. 9.4. Distribution of the Quantities φ , φ' , M_ω , T_ω , T_s , and T in a Simply Supported Bar which is Acted Upon by the Concentrated Torsional Load M_D ($\varkappa = 3$, $\alpha = 2/3$).

The solution for the adjacent region $\alpha < \zeta \leq 1$ where the particular solution $\bar{\varphi}$ is given by the second of Eqs. (9.17 e) follows from Eqs. (9.19). The solution for the angle of twist φ becomes:

$$\varphi = \frac{M_D l}{GK} \left[\beta \zeta - \frac{\sin \varkappa \beta}{\varkappa \sin \varkappa} \sin \varkappa \zeta + \frac{1}{\varkappa} \sin \varkappa (\zeta - \alpha) - (\zeta - \alpha) \right],$$

which by means of the relations $\beta = 1 - \alpha$ and

$$\sin \varkappa (1 - \alpha) \sin \varkappa \zeta = \sin \varkappa \sin \varkappa (\zeta - \alpha) + \sin \varkappa \alpha \sin \varkappa (1 - \zeta)$$

may be reduced to:

$$\varphi = \frac{M_D l}{GK} \left[\alpha (1 - \zeta) - \frac{\sin \varkappa \alpha}{\varkappa \sin \varkappa} \sin \varkappa (1 - \zeta) \right].$$

$$\varphi(\zeta = 1) = 0$$

$$C_2 + C_3 \sin \varkappa + \frac{M_D l}{GK} \left(\frac{1}{\varkappa} \sin \varkappa \beta - \beta \right) = 0,$$

$$M_\omega(\zeta = 1) = 0$$

$$-C_3 G K \sin \varkappa - EI_{\omega\omega} \frac{M_D \varkappa}{GK l} \sin \varkappa \beta = 0.$$

The second equation yields immediately

$$C_3 = -\frac{M_D l}{GK} \frac{\sin \varkappa \beta}{\varkappa \sin \varkappa}$$

whereupon the first determines

$$C_2 = \beta \frac{M_D l}{GK}.$$

If these constants of integration are introduced into Eqs. (9.20), one arrives at a solution which is valid in the region $\zeta < \alpha$ where the particular solution $\bar{\varphi} = 0$.

$$\begin{aligned} \varphi &= \frac{M_D l}{GK} \left(\beta \zeta - \frac{\sin \varkappa \beta}{\varkappa \sin \varkappa} \sin \varkappa \zeta \right), \\ \varphi' &= \frac{M_D}{GK} \left(\beta - \frac{\sin \varkappa \beta}{\sin \varkappa} \cos \varkappa \zeta \right), \\ M_\omega &= M_D l \frac{\sin \varkappa \beta}{\varkappa \sin \varkappa} \sin \varkappa \zeta, \\ T &= \beta M_D. \end{aligned} \quad \left. \begin{array}{l} \\ \\ \\ \end{array} \right\} 0 \leq \zeta < \alpha \quad (9.32 \text{a})$$

If, finally, the reversed coordinate

$$\zeta' = 1 - \zeta$$

is introduced, the state of the member in the region $0 \leq \zeta' < \beta$ is described by the following expressions:

$$\left. \begin{aligned} \varphi &= \frac{M_D l}{GK} \left(\alpha \zeta' - \frac{\sin \varkappa \alpha}{\varkappa \sin \varkappa} \sin \varkappa \zeta' \right), \\ \varphi' &= \frac{M_D}{GK} \left(-\alpha + \frac{\sin \varkappa \alpha}{\sin \varkappa} \cos \varkappa \zeta' \right), \\ M_\omega &= M_D l \frac{\sin \varkappa \alpha}{\varkappa \sin \varkappa} \sin \varkappa \zeta', \\ T &= -\alpha M_D. \end{aligned} \right\} \quad 0 \leq \zeta' < \beta \quad (9.32 \text{ b})$$

The solutions (9.32) are plotted in Fig. 9.4 for the system parameters $\varkappa = 3$, $\alpha = 2/3$ and $\beta = 1/3$. In order to facilitate the plot of diagrams for the deformations and forces and as an aid for the quick calculation of governing design stresses, the solutions (9.32) shall be supplemented by the following expressions:

The *angle of twist* φ at the point of application of the moment M_D amounts to:

$$\varphi(\zeta = \alpha) = \frac{M_D l}{GK} \left(\alpha \beta - \frac{\sin \varkappa \alpha \sin \varkappa \beta}{\varkappa \sin \varkappa} \right). \quad (9.33)$$

This angle vanishes at the supports in order to satisfy the boundary conditions. The total twist angle φ at these three points follows immediately from the expressions for the Saint-Venant torsional moment T_s (9.34).

The *first derivative* φ' multiplied by the stiffness GK represents the Saint-Venant torsional moment T_s . It assumes maximum values at the ends of the bar and its value at the point of the applied moment is always smaller.

$$\begin{aligned} T_s(\zeta = 0) &= GK \varphi'(\zeta = 0) = M_D \left(\beta - \frac{\sin \varkappa \beta}{\sin \varkappa} \right). \\ T_s(\zeta' = 0) &= GK \varphi'(\zeta' = 0) = M_D \left(-\alpha + \frac{\sin \varkappa \alpha}{\sin \varkappa} \right), \\ T_s(\zeta = \alpha) &= \frac{M_D}{2} \left(\beta - \alpha - \frac{\sin \varkappa (\beta - \alpha)}{\sin \varkappa} \right). \end{aligned} \quad (9.34)$$

The slope of the torsional moment T_s is zero at the ends of the bar and equal to the warping moment (9.35) multiplied by $-GK/E I_{\omega\omega}$ at the point of load application.

The *warping moments* increase steadily from the value zero at the ends of the bar up to the maximum value

$$M_\omega(\zeta = \alpha) = M_D l \frac{\sin \varkappa \beta \sin \varkappa \alpha}{\varkappa \sin \varkappa}. \quad (9.35)$$

The slope of the warping moment M_ω is equivalent to the *torsional moment* T_ω which assumes the following values in the three considered points of the bar:

$$\begin{aligned} T_\omega(\zeta = 0) &= M_D \frac{\sin \alpha \beta}{\sin \alpha}, \\ T_\omega(\zeta = \alpha) &= M_D \frac{\sin \alpha \beta \cos \alpha}{\sin \alpha}, \\ T_\omega(\zeta' = \beta) &= -M_D \frac{\sin \alpha \cos \alpha \beta}{\sin \alpha}, \\ T_\omega(\zeta' = 0) &= -M_D \frac{\sin \alpha \alpha}{\sin \alpha}. \end{aligned} \tag{9.36}$$

All the expressions derived in this section may be looked upon as influence functions η_s for the quantities S if α (and therefore $\beta = 1 - \alpha$) is assumed to be the independent variable and if ζ (and therefore $\zeta' = 1 - \zeta$) is held fixed. The torsional moment M_D has to be taken as unity in this case. The quantity S may either be φ , φ' , M_ω , T or any of the two components T_s and T_ω .

The utilization of the influence line η_s for an arbitrarily variable torsional load $m_D = m(\alpha)$ [resp. $m_D = m(\beta)$] is as usual: The quantity S results from the integration of the product $\eta_s \cdot m(\alpha) da = \eta_s m(\alpha) l d\alpha$ [resp. $\eta_s m(\beta) db = \eta_s m(\beta) l d\beta$].

When applying these influence functions, careful attention should be paid to their region of validity. If the influence functions for a certain quantity S are denoted by $\eta_s(\beta, \zeta)$ when derived from the corresponding solution (9.32a) and by $\eta_s(\alpha, \zeta')$ when derived from (9.32b), the quantity S may be calculated from the expression:

$$S(\zeta) = l \int_0^\zeta \eta_s(\alpha, \zeta') m(\alpha) d\alpha + l \int_0^{\zeta'} \eta_s(\beta, \zeta) m(\beta) d\beta. \tag{9.37}$$

The reversed coordinate ζ' has to be replaced by $1 - \zeta$ if S is not accepted in the form $S(\zeta, \zeta')$.

A great number of these influence lines were calculated by C. F. KOLLMRUNNER and N. HAJDIN and presented in tabular form¹.

9.3 Continuous Beams

a) Three-Warping-Moment Equations

The torsional analysis of a continuous beam will again be based on a chain of consecutive, simply supported members as defined by Eqs. (7.1). Continuity is reestablished by means of the redundant warping moments X_k at intermediate supports. The redundant quantities follow from conditions asking for compatible

¹ KOLLMRUNNER, C. F., and N. HAJDIN: Wölbkrafttorsion dünnwandiger Stäbe mit offenem Profil. Report, Part 1, Vol. 29, Zürich, October 1964, Published by: Schweizer Stahlbau-Vereinigung.

deformations of adjacent member ends which, in the case of prismatic members, means equal twist rates (v. Section 7.3a).

Since the base system, the redundant quantities and the compatibility conditions are equivalent to those for the continuous system with negligible Saint-Venant torsion treated in Section 7.3, the three-warping-moment equations (7.21) derived therein are valid for mixed torsion as well. Only the numerical values for the displacement coefficients a_{ik} and b_{ik} as well as those for the generalized displacements a_{i0} and b_{i0} will have to be calculated anew. In other words: The expressions given in Table 7.1 have to be replaced by new ones. These new expressions for prismatic members under mixed torsion are given in Table 9.1.

The first two coefficients of Table 9.1 are calculated from the second expression of the solutions (9.22) by putting $\zeta = 1$ and afterwards $\zeta = 0$. The sum of these two coefficients is needed frequently and is also listed.

The generalized displacements may be derived from the formulas for φ' in the solutions (9.27) and (9.32). The resulting expressions are given in Table 9.1, one set of equations giving the influence of a uniformly distributed torsional load m_D and the other the influence of a concentrated torsional moment M_D . The last two of these equations may be transformed immediately into influence functions for the generalized displacements a_{i0} and b_{i0} by putting the torsional moment M_D equal to one and assuming the coordinates of load application α_i and β_i to be independent variables. These influence functions may be used to calculate the generalized displacements for an arbitrarily distributed torsional load.

Table 9.1. Displacement Coefficients and Generalized Displacements for the Prismatic, Simply Supported Member i under Mixed Torsion, $x_i = \sqrt{G K_i l_i^2 / E I_{woi}}$

Displacement coefficients:

$$a_{ik} = b_{i k+1} = \frac{1}{G K_i l_i} (\kappa_i \operatorname{Ctg} \kappa_i - 1),$$

$$a_{i k+1} = b_{ik} = \frac{1}{G K_i l_i} \left(1 - \frac{\kappa_i}{\operatorname{Sin} \kappa_i} \right),$$

$$a_{ik} + a_{i k+1} = \frac{\kappa_i}{G K_i l_i} \operatorname{Tg} \frac{\kappa_i}{2}.$$

Generalized displacements for the uniformly distributed torsional load m_D :

$$a_{i0} = b_{i0} = \frac{m_D l_i}{2 G K_i} \left(1 - \frac{2}{\kappa_i} \operatorname{Tg} \frac{\kappa_i}{2} \right).$$

Generalized displacements for the concentrated torsional moment M_D acting at $\alpha_i = a_i/l_i$ resp. $\beta_i = b_i/l_i$, ($\alpha_i + \beta_i = 1$):

$$a_{i0} = \frac{M_D}{G K_i} \left(\beta_i - \frac{\operatorname{Sin} \kappa_i \beta_i}{\operatorname{Sin} \kappa_i} \right),$$

$$b_{i0} = \frac{M_D}{G K_i} \left(\alpha_i - \frac{\operatorname{Sin} \kappa_i \alpha_i}{\operatorname{Sin} \kappa_i} \right).$$

b) Deformations and Forces

All quantities, φ , φ' , M_ω , T and the two components T_s and T_ω , result from the superposition of different influences acting on the base system. The solutions (9.27) and (9.32) represent examples for the distribution of these quantities in the base system.

The influence of the redundant X_{k+1} on the forces and deformations in the simply supported member i is described by the expressions (9.22). In order to obtain the influence of the redundant X_k on the member, the coordinate ζ need only be replaced by $\zeta' = 1 - \zeta$.

These simple considerations lead to the following general expressions for the deformations and forces in the member i which is situated between the supports k and $k + 1$:

$$\begin{aligned}\varphi_i &= \varphi_{i0} + \frac{X_k}{GK_i} \left(\zeta^i - \frac{\sin \varkappa_i \zeta'_i}{\sin \varkappa_i} \right) + \frac{X_{k+1}}{GK_i} \left(\zeta_i - \frac{\sin \varkappa_i \zeta_i}{\sin \varkappa_i} \right), \\ \varphi'_i &= \varphi'_{i0} - \frac{X_k}{GK_i l_i} \left(1 - \varkappa_i \frac{\cos \varkappa_i \zeta'_i}{\sin \varkappa_i} \right) + \frac{X_{k+1}}{GK_i l_i} \left(1 - \varkappa_i \frac{\cos \varkappa_i \zeta_i}{\sin \varkappa_i} \right), \\ M_{\omega i} &= \omega M_{i0} + X_k \frac{\sin \varkappa_i \zeta'_i}{\sin \varkappa_i} + X_{k+1} \frac{\sin \varkappa_i \zeta_i}{\sin \varkappa_i}, \\ T_i &= T_{i0} + \frac{X_{k+1} - X_k}{l_i}.\end{aligned}\tag{9.38}$$

The Saint-Venant torsional moment T_s is equal to φ'_i multiplied by the stiffness GK while the warping torsional moment T_ω is either its supplement to the total torsional moment T or equal to the first derivative of $M_{\omega i}$.

An extensive summary of closed solutions was presented by F. W. BORNSCHEUER¹.

This surprisingly simple analysis of a complicated statical system is possible only because of the selection of an appropriate base system. This base system, however, is statically indeterminate because the calculation of its reactions at the supports is a one time statically indeterminate problem. If twist were avoided at only one end of each member the total torsional moments T would follow from equilibrium conditions only.

In any case, the base system is infinitely indeterminate because the total torsional moment T may be divided up into the Saint-Venant torsional moment T_s and into the warping torsional moment T_ω only after determination of the angle of twist φ and its derivative with respect to z .

The basis for reducing the problem to one having as few redundants as there are intermediate supports results from the fact that the base system itself already satisfies the most important geometrical conditions. The angles of twist at the member ends are compatible; they are zero. Only the continuity of the derivative φ' is required and introduced by means of compatibility conditions.

¹ BORNSCHEUER, F. W.: Beispiel und Formelsammlung zur Spannungsberechnung dünnwandiger Stäbe mit wölbbehindertem Querschnitt. Der Stahlbau 22 (1953) 35–41.

The statical conditions are satisfied as a consequence of geometrical compatibility. The redundant quantities X_k cause the warping moments M_ω and the corresponding axial stresses to be equal at two adjacent member ends. The same situation holds for the Saint-Venant torsional moments and the corresponding shear stresses because they are proportional to the continuous function φ' . The warping shear stresses, however, show jump discontinuities at the supports which correspond to the total jump in the torsional moment at these points.

c) Examples

a) Symmetric, Three-Span Continuous Beam. Consider the symmetric, continuous, prismatic beam shown at the top of Fig. 9.5. The central span of this system is acted upon by the uniformly distributed torsional load m_D . This load is counteracted by the reactions at four supports which prevent twist but allow warping of the beam.

The torsional properties of the three members in the system are described by the parameters:

$$\varkappa_4 = \varkappa = \sqrt{\frac{l^2 G K}{E I_{\omega\omega}}}$$

$$\varkappa_2 = \sqrt{\frac{l_2^2 G K}{E I_{\omega\omega}}} = \lambda \varkappa$$

Because of the symmetry in the system and load ($X_1 = X_7 = 0$, $X_3 = X_5$), there remains only one unknown redundant which is determined by the following equation:

$$X_3(b_{23} + a_{43}) + X_3 a_{45} = -(b_{20} + a_{40}).$$

This equation yields:

$$X_3 = X = -\frac{b_{20} + a_{40}}{b_{23} + a_{43} + a_{45}}.$$

If the generalized displacements for uniformly distributed load and the displacement coefficients as given in Table 9.1 are introduced, one arrives at the following expression for the redundant X :

$$X = -\frac{m_{D2} l^2 \left(\frac{\lambda}{2} - \frac{1}{\varkappa} \operatorname{Tg} \frac{\lambda \varkappa}{2} \right) + m_{D4} l^2 \left(\frac{1}{2} - \frac{1}{\varkappa} \operatorname{Tg} \frac{\varkappa}{2} \right)}{\varkappa \operatorname{Ctg} \lambda \varkappa - \frac{1}{\lambda} + \varkappa \operatorname{Tg} \frac{\varkappa}{2}}. \quad (9.39)$$

This expression includes the solutions for load acting along the entire length of the bar ($m_{D2} = m_{D4}$), along the end spans only ($m_{D4} = 0$) and finally along the central span only ($m_{D2} = 0$, $m_{D4} = m_D$). Only the last case for which

$$X = -m_D l^2 \frac{\frac{1}{2} - \frac{1}{\varkappa} \operatorname{Tg} \frac{\varkappa}{2}}{\varkappa \operatorname{Ctg} \lambda \varkappa - \frac{1}{\lambda} + \varkappa \operatorname{Tg} \frac{\varkappa}{2}} \quad (9.40)$$

will be considered further.

For the parameters $\varkappa = 3$ and $\lambda = 1/2$ used in Fig. 9.5, the redundant warping moment X becomes:

$$X = -0,0492 m_D l^2. \quad (9.41)$$

The set of expressions for the deformations and the forces in the continuous beam may now be calculated from the solutions for the simply supported member

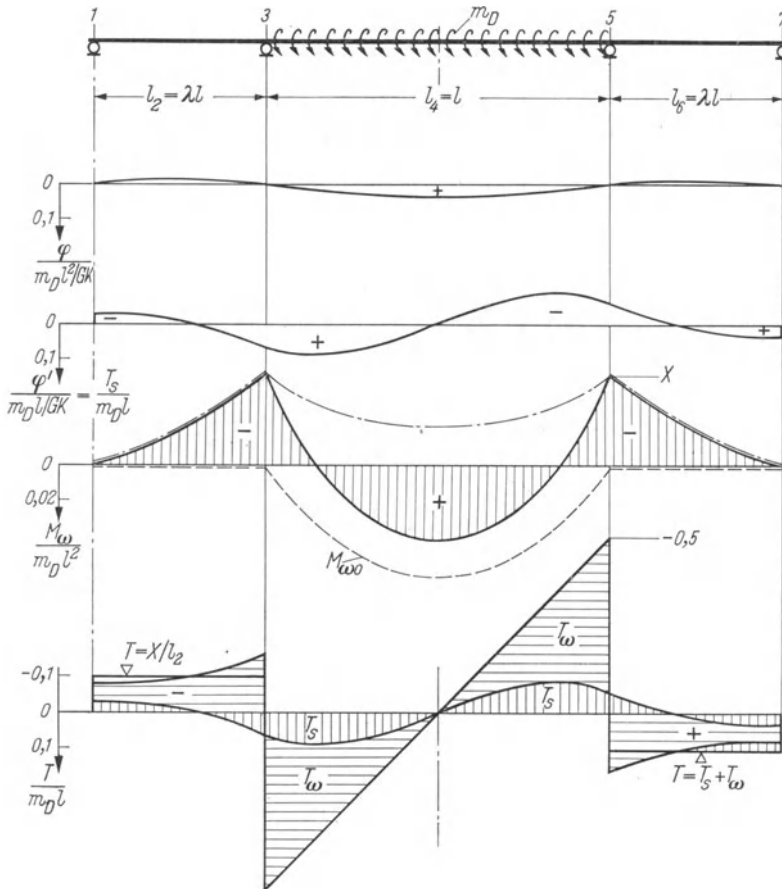


Fig. 9.5. The Deformations and Forces of a Three-Span Continuous Bar with a Uniformly Distributed Torsional Load m_D at its Central Span ($\varkappa = 3$, $\lambda = 1/2$).

which are given in a general form by Eqs. (9.38). These equations require expressions for deformations of the base system under applied loads. These deformations vanish for the outer spans and for the central span they are given by Eqs. (9.27).

It is always advantageous to reflect the symmetries of the system and the load in the analytical expressions by means of an appropriate selection of the coordinate system. The appropriate coordinate system for the symmetric central span is $\zeta = \xi - 1/2$. If further the two equal redundant quantities X_k and X_{k+1} are denoted by X and if the span subscript i is omitted, the Eqs. (9.38) may be rewritten

in the form :

$$\begin{aligned}\varphi &= \varphi_0 + \frac{X}{GK} \left(1 - \frac{\cos \frac{\pi \xi}{2}}{\cos \frac{\pi}{2}} \right), \\ \varphi' &= \varphi'_0 - \frac{X}{GKl} \frac{\pi \sin \frac{\pi \xi}{2}}{\cos \frac{\pi}{2}}, \\ M_\omega &= M_{\omega 0} + X \frac{\cos \frac{\pi \xi}{2}}{\cos \frac{\pi}{2}}, \\ T &= T_0.\end{aligned}\tag{9.42}$$

The distribution of these quantities is plotted in Fig. 9.5 for the system parameters $\pi = 3$ and $\lambda = 1/2$. Curves are shown successively for the angle of twist φ , the twist rate φ' (which is proportional to the Saint-Venant torsional moment T_s) and the warping moments M_ω . This latter curve is supplemented by a dashed line giving the warping moments $M_{\omega 0}$ in the base system and by a dash-dot line for the warping moments M_ω caused by the redundants X . The sum of these two supplementary curves represents the warping moment M_ω . Finally, the difference between the total torsional moment T and the Saint-Venant torsional moment T_s represents the warping torsional moment T_ω .

The end restraint of the central span depends not only on the member constant π but also on the length of the adjacent span. The two special cases, a vanishing length and an infinite length of the end span, are of particular interest.

If the parameter λ tends to zero, the solutions approach those for the fixed-end member under uniformly distributed torsional load m_D .

The value of expression (9.40) approaches the following fixed-end warping moment if $\lambda \rightarrow 0$:

$$X = -\frac{m_D l^2}{\pi^2} \left(\frac{\pi}{2} \operatorname{Ctg} \frac{\pi}{2} - 1 \right).\tag{9.43}$$

The redundant warping moment for the other extreme case, $\lambda \rightarrow \infty$, becomes:

$$X = -\frac{m_D l^2}{\pi^2} \frac{\frac{\pi}{2} - \operatorname{Tg} \frac{\pi}{2}}{1 + \operatorname{Tg} \frac{\pi}{2}}.\tag{9.44}$$

The last expression does not vanish as long as π is different from zero. This means that there is a restraint to the warping at supports whenever the member is extended beyond.

β) The Fixed-End Member Under Uniformly Distributed Torsional Load. This system with the boundary conditions (7.2) is a special case of the system discussed above. The redundant warping moment is given by Eq. (9.43), the solutions for the simply supported base system by the expressions (9.27) and the superposition is performed according to Eqs. (9.42).

The combination of these expressions results in the following:

$$\begin{aligned}\varphi &= \frac{m_D l^2}{8GK} \left(1 - 4\bar{\zeta}^2 - 4 \frac{\cos \frac{\zeta}{2} - \cos \alpha \bar{\zeta}}{\alpha \sin \frac{\zeta}{2}} \right), \\ \varphi' &= \frac{m_D l}{GK} \left(-\bar{\zeta} + \frac{1}{2} \frac{\sin \alpha \bar{\zeta}}{\sin \frac{\zeta}{2}} \right), \\ M_\omega &= \frac{m_D l^2}{\alpha^2} \left(1 - \frac{\alpha}{2} \frac{\cos \alpha \bar{\zeta}}{\sin \frac{\zeta}{2}} \right), \\ T &= -m_D l \bar{\zeta}.\end{aligned}\tag{9.45}$$

The angle of twist and the warping moment at mid-span ($\bar{\zeta} = 0$) are:

$$\varphi_{\max} = \frac{m_D l^2}{8GK} \left(1 - \frac{4}{\alpha} \operatorname{Tg} \frac{\alpha}{4} \right),\tag{9.46}$$

$$M_\omega = \frac{m_D l^2}{\alpha^2} \left(1 - \frac{\frac{\alpha}{2}}{\sin \frac{\alpha}{2}} \right).\tag{9.47}$$

The warping moment vanishes for the coordinates

$$\bar{\zeta} = \pm \frac{1}{\alpha} \operatorname{ArCos} \frac{2}{\alpha} \sin \frac{\alpha}{2}.\tag{9.48}$$

The Saint-Venant torsional moment assumes a maximum value at these two points. It vanishes together with φ' at midspan and at the fixed ends where, therefore, the total torsional moment and the warping torsional moment are equal. The warping torsional moment at the fixed ends is simply:

$$|T_\omega|_{\max} = \frac{m_D l}{2}.\tag{9.49}$$

10 Miscellaneous Problems

10.1 Stress Analysis of Rolled Sections

a) General Considerations

It was the purpose of Chapter 9 to determine deformations and internal forces in members which carry torsional moments both by means of Saint-Venant and warping torsion (mixed torsion). The solutions to this problem did not depend on any particular assumption concerning the shape of the cross section. All geometric and elastic properties of a structural member were considered in one

nondimensional parameter α which, aside from the normalization length l , is a function of the ratio between the Saint-Venant torsional rigidity GK and the warping rigidity $EI_{\omega\omega}$ [v. Eq. (9.11)].

Procedures for the determination of the axial stresses and the shear stresses in terms of the internal moments T , T_ω and M_ω were previously developed separately for Saint-Venant torsion (in Chapters 1 and 2) and for warping torsion (in Chapters 5 and 6).

Although the calculation of stresses in a structural member with mixed torsion presents no new problem, the necessary numerical procedures will nevertheless be illustrated by means of a few typical examples. The rolled I-, L- and T-sections are very well suited for this purpose. Their walls are thick enough to yield components T_s and T_ω which may be of the same order of magnitude. They represent furthermore three completely different types of cross sections in that the first has two, the second one and the third no axis of symmetry.

The calculations will subsequently be carried out for each of the three types of cross sections in a general manner. Tables for structural shapes define the shape of such cross sections by means of the flange width b , the flange thickness t , the depth of section h and the web thickness d . In the following calculations, the web shall be made dependent on the flange in that the parameter γ represents the ratio between depth of web and flange width and the parameter ϱ the ratio between web area and flange area. The flange width and the flange area are therefore assumed to be the units for the definition of the cross section.

The following notation holds therefore for the three types of cross section shown in Figs. 10.1, 10.2 and 10.3:

$$\begin{aligned} c &= \text{flange width} \quad \begin{cases} = b & \text{for I-shapes,} \\ = b - \frac{d}{2} & \text{for L- and T-shapes,} \end{cases} \\ F_f &= \text{flange area} = ct, \\ \gamma &= \frac{\text{depth of web}}{\text{flange width}} = \frac{h-t}{c}, \\ \varrho &= \frac{\text{web area}}{\text{flange area}} = \frac{(h-t)d}{ct} = \gamma \frac{d}{t}. \end{aligned} \tag{10.1}$$

This system for the notation assumes the depth of the web to stretch from one center line of the flange to the other. This means that in each flange a small area amounting to web thickness times the half of the flange thickness is considered twice. This small additional area compensates in part for the neglected fillets at the connection between web and flange. The mistakes caused by this approximation do not in general exceed those caused by the rolling tolerances.

The basic equation (1.16) leads by means of the notation defined above (10.1) to the following expression for the torsion constant:

$$K = \frac{\eta}{3} \left[2c \left(\frac{F_f}{c} \right)^3 + \gamma c \left(\frac{\varrho F_f}{\gamma c} \right)^3 \right] = \frac{\eta}{3} \frac{F_f^3}{c^2} \left(2 + \frac{\varrho^3}{\gamma^2} \right). \tag{10.2}$$

For rolled sections, the correction factor η assumes values between 1,0 and 1,3 (v. Section 1.4)¹.

Aside from the regions at the flange ends and at the fillets between flange and web, the Saint-Venant shear stresses τ_s are linearly distributed across the walls of thickness t . At the boundary they reach the maximum $\max \tau_s$.

$$\max \tau_s = \frac{T_s}{K} t. \quad (10.3)$$

This leads to the following expression for the maximum Saint-Venant shear stresses¹ in the undisturbed regions of the flanges of all I-, L- and T-sections:

$$\max \tau_s = \frac{3\gamma^2}{\eta(2\gamma^2 + \varrho^3)} \frac{T_s c}{F_f^2}. \quad (10.4)$$

The shear stresses in the web reduce in proportion to the reduced web thickness.

b) I-Sections

The shear center D of this doubly symmetric cross section coincides with the center of gravity C . The expression for the normalized sectorial coordinate ω may be written down at once if both the definition and the symmetries of the cross section are considered. If the axes x and y of the cross section are made to coincide with the principal axes which are at the same time axes of symmetry (Fig. 10.1 a), the normalized sectorial coordinate ω is given by the simple expression:

$$\omega = xy. \quad (10.5)$$

The sectorial moment of inertia follows now directly from the definition and may again be written in terms of the notation (10.1):

$$I_{\omega\omega} = \int \omega^2 dF = \frac{\gamma^2}{24} c^4 F_f. \quad (10.6)$$

Since the sectorial coordinate ω vanishes for the entire web, only the flanges make a contribution to the sectorial moment of inertia. The coordinate x is a constant for the two flanges and may therefore be put in front of the integral which, aside from the negligible contribution of the web, is equal to the moment of inertia I_{yy} of the cross section.

The value of the sectorial moment of inertia $I_{\omega\omega}$ of an I-section may therefore be calculated from two items of data which are listed in available tables of structural shapes. It is equal to the moment of inertia I_{yy} with respect to the web axis multiplied by the square of the distance between the center of the flange and the center of gravity of the cross section.

¹ Tables listing accurate values of the torsion constant as well as other torsional properties for all rolled shapes are available through the major steel producers in the USA and Great Britain.

The sectorial statical moment \tilde{S}_ω varies parabolically along the flange (v. Fig. 10.1 c) and reaches an extreme value of

$$\max \tilde{S}_\omega = \int_{c/2}^0 \omega \, dF = -\frac{\gamma}{16} c^2 F_f. \quad (10.7)$$

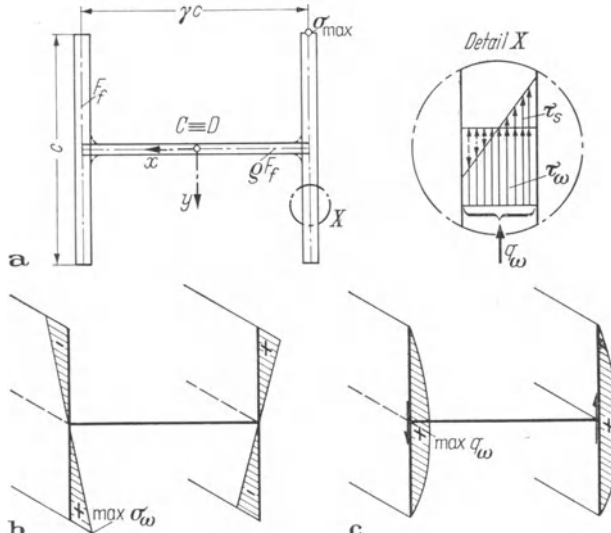


Fig. 10.1. Torsion of an I-Section:
a) Notation, b) Axial Stresses σ_ω , c) Shear Flow q_ω .

The warping stresses σ_ω are now proportional to the sectorial coordinate ω while the shear flow $q_\omega = \tau_\omega t$ resulting from the warping torsional moment T_ω is proportional to the sectorial statical moment \tilde{S}_ω . The distribution of the warping stresses along the center line of the flanges is plotted in Figs. 10.1 b and c.

Thus a knowledge of the maximum values of the axial stress σ_ω and the shear flow q_ω is all that is needed to visualize the warping stresses in a symmetric I-section.

The basic relations (5.33) and (5.34),

$$\sigma_\omega = \frac{M_\omega}{I_{\omega\omega}} \omega, \quad q_\omega = -\frac{T_\omega}{I_{\omega\omega}} \tilde{S}_\omega,$$

lead to the following two maximum stresses:

$$\max \sigma_\omega = \frac{6}{\gamma} \frac{M_\omega}{c^2 F_f}, \quad \max \tau_\omega = \frac{3}{2\gamma} \frac{T_\omega}{c^2}. \quad (10.8 \text{ a, b})$$

Finally, the Saint-Venant and the warping states of stress may be superposed to complete the analysis of torsional stresses in this cross section. This superposition confines itself to the shear stresses which are added according to the detail shown in Fig. 10.1 a.

c) L -Sections

This cross section exhibits only one plane of symmetry. Considerably more information than for the I-section is needed to define the state of stress for this type of structural shape.

The analytical procedure that will be developed may easily be modified for application to a singly symmetric bridge cross section consisting of a floor slab and two main girders.

Uniformly distributed lateral loads are resolved into three components p_x , p_y , m_D with respect to the shear center and concentrated lateral loads are similarly resolved into components P_x , P_y , M_D (v. Fig. 5.2). Each of these components is positive if it points in the direction of the corresponding positive coordinate. The structural system is thereafter analyzed separately for each of the three sets of load components. The components pointing in x - and y -direction lead to a flexural analysis of the system which yields the internal forces (M_x , Q_x) and (M_y , Q_y) respectively. The torsional analysis, finally, results in the warping moments M_ω , warping torsional moments T_ω and Saint-Venant torsional moments T_s . Solutions of the last problem are presented in Sections 9.2 and 9.3 for a number of different structural systems.

The axial stresses and shear flows in a cross section oriented as in Fig. 10.2 are [according to Eqs. (5.16), (5.20) and (5.33), (5.34)] given by the following expressions:

$$\sigma = +\frac{M_x}{I_{xx}}x + \frac{M_y}{I_{yy}}y + \frac{M_\omega}{I_{\omega\omega}}\omega, \quad (10.9a)$$

$$\tau t = q = -\frac{Q_x}{I_{xx}}\tilde{S}_x - \frac{Q_y}{I_{yy}}\tilde{S}_y - \frac{T_\omega}{I_{\omega\omega}}\tilde{S}_\omega. \quad (10.9b)$$

A clearly arranged scheme for the numerical calculation of the moments of inertia I_{xx} , I_{yy} , $I_{\omega\omega}$, the coordinates x , y , ω and the statical moments \tilde{S}_x , \tilde{S}_y , \tilde{S}_ω was developed in Chapter 6. The same calculations are carried out in Table 10.1 for the L-section using the notations (10.1). The columns ($x4$), ($y4$) and ($\omega4$) give the ordinary and the sectorial coordinates of the consecutively numbered points in the cross section of Fig. 10.2. The three variable statical moments appear in the columns ($x6$), ($y6$) and ($\omega6$) and the moments of inertia and the coordinate y_D of the shear center, finally, are presented at the bottom of the table in the following form:

$$I_{\omega\omega} = \frac{\gamma^2(3+2\varrho)}{12(6+\varrho)} c^4 F_f, \quad (10.10)$$

$$y_D = -\frac{4(3+\varrho)}{(2+\varrho)(6+\varrho)} c. \quad (10.11a)$$

The shear center is therefore the distance

$$e = \frac{3}{6 + \varrho} c \quad (10.11\text{b})$$

away from the center line of the web.

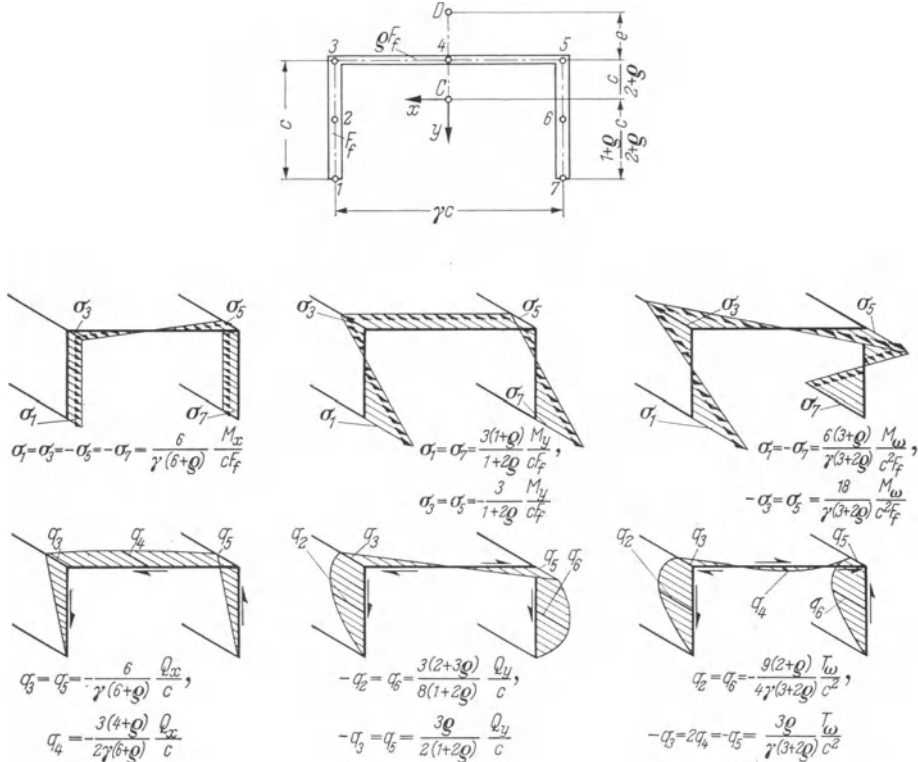


Fig. 10.2. Distribution of the Flexural Stresses and the Warping Stresses in the T-Section.

Fig. 10.2 shows the distribution of the axial stress and of the shear flow for each of the three components of the applied load (bending from lateral load in x -direction, bending from lateral load in y -direction and torsion in $+\varphi$ -direction). The arrangement of the six stress figures corresponds to the configuration of the six elements in the stress formulas (10.9).

The axial stresses σ are proportional to the coordinates x , y and ω while the shear flows q are proportional to the variable statical moments \tilde{S}_x , \tilde{S}_y and \tilde{S}_ω . The plotted stress patterns show the stresses along the center lines of the small rectangular elements and not along outer fibers for which they might become extreme. The shear flow q has to be divided by the wall thickness in order to arrive at the shear stress. The latter is constant across the rectangular elements in contrast to the distribution resulting from Saint-Venant torsion (v. detail in Fig. 10.1 a)).

Table 10.1.

Eq. No.	(a)	(x1)	(x4)	(x5)	(x6)	(x7)	(x8)	(x10)
Notation	$\Delta F/4$	Δx	x	ΔS_x	\tilde{S}_x	$1 + 4 + 1$	I_{xx}	$I_x \omega c$
Multiplier	F_f	c	c	$c F_f$	$c F_f$	$c F_f$	$c^2 F_f$	$c^3 F_f$
1			$\frac{\gamma}{2}$		0			
	$\frac{1}{4}$			$\frac{\gamma}{4}$				
2		0	$\frac{\gamma}{2}$		$\frac{\gamma}{4}$	$\frac{3\gamma}{2}$	0	$-\frac{3\gamma^2}{4}$
	$\frac{1}{4}$			$\frac{\gamma}{4}$				
3			$\frac{\gamma}{2}$		$\frac{\gamma}{2}$			
	$\frac{\varrho}{4}$			$\frac{\varrho\gamma}{8}$				
4		$-\gamma$	0		$\frac{\gamma(4+\varrho)}{8}$	$\frac{\gamma(6+\varrho)}{2}$	$-\frac{\gamma^2(6+\varrho)}{2}$	$-\frac{\gamma^2(6+\varrho)}{2(2+\varrho)}$
	$\frac{\varrho}{4}$			$-\frac{\varrho\gamma}{8}$				
5			$-\frac{\gamma}{2}$		$\frac{\gamma}{2}$			
	$\frac{1}{4}$			$-\frac{\gamma}{4}$				
6		0	$-\frac{\gamma}{2}$		$\frac{\gamma}{4}$	$\frac{3\gamma}{2}$	0	$-\frac{3\gamma^2}{4}$
	$\frac{1}{4}$			$-\frac{\gamma}{4}$				
7			$-\frac{\gamma}{2}$		0			
	$1 + \frac{\varrho}{2}$						$-\frac{\gamma^2(6+\varrho)}{2}$	$-\frac{2\gamma^2(3+\varrho)}{2+\varrho}$
	$F = 2 + \varrho$						$+\frac{\gamma^2(6+\varrho)}{12}$	$+\frac{\gamma^2(3+\varrho)}{3(2+\varrho)}$

$$y_D = -\frac{I_{x\omega c}}{I_{xx}} = -\frac{\gamma^2(3+\varrho)12}{3(2+\varrho)\gamma^2(6+\varrho)} c = -4 \frac{3+\varrho}{(2+\varrho)(6+\varrho)} c$$

The Analysis of L-Section

(y_1)	(y_4)	(y_5)	(y_6)	(y_8)	(ω_1)	(ω_4)	(ω_5)	(ω_6)	(ω_8)
Δy	y	ΔS_y	\tilde{S}_y	I_{yy}	$\Delta \omega_C$	$\Delta \omega$	ω	ΔS_ω	\tilde{S}_ω
c	c	$\frac{c F_f}{8(2+\varrho)}$	$c F_f$	$c^2 F_f$	c^2	c^2	$\frac{\gamma c^2 F_f}{16(6+\varrho)}$	$c^2 F_f$	$c^4 F_f$
-1	$\frac{1+\varrho}{2+\varrho}$		0				$\frac{\gamma(3+\varrho)}{2(6+\varrho)}$	0	
		$2+3\varrho$					$+3(2+\varrho)$		
	$\frac{\varrho}{2(2+\varrho)}$		$\frac{2+3\varrho}{8(2+\varrho)}$	$-\frac{1+2\varrho}{2+\varrho}$	$-\frac{\gamma}{2}$	$-\frac{\gamma}{2}$	$\frac{\gamma\varrho}{4(6+\varrho)}$	$\frac{3\gamma(2+\varrho)}{16(6+\varrho)}$	$-\frac{\gamma^2(3+2\varrho)}{4(6+\varrho)}$
		$-2+\varrho$					$-(6-\varrho)$		
	$-\frac{1}{2+\varrho}$		$\frac{\varrho}{2(2+\varrho)}$				$-\frac{3\gamma}{2(6+\varrho)}$	$\frac{\gamma\varrho}{4(6+\varrho)}$	
0	-4ϱ						-6ϱ		
	$-\frac{1}{2+\varrho}$		0	0	$-\frac{\gamma}{2+\varrho}$	$\frac{3\gamma}{6+\varrho}$	\uparrow \downarrow	0	$-\frac{\gamma\varrho}{8(6+\varrho)}$
		-4ϱ					$+6\varrho$		
	$-\frac{1}{2+\varrho}$		$-\frac{\varrho}{2(2+\varrho)}$				$\frac{3\gamma}{2(6+\varrho)}$	$\frac{\gamma\varrho}{4(6+\varrho)}$	
		$-2+\varrho$					$+(6-\varrho)$		
$+1$	$\frac{\varrho}{2(2+\varrho)}$		$-\frac{2+3\varrho}{8(2+\varrho)}$	$-\frac{1+2\varrho}{2+\varrho}$	$-\frac{\gamma}{2}$	$-\frac{\gamma}{2}$	$-\frac{\gamma\varrho}{4(6+\varrho)}$	$\frac{3\gamma(2+\varrho)}{16(6+\varrho)}$	$-\frac{\gamma^2(3+2\varrho)}{4(6+\varrho)}$
		$2+3\varrho$					$-3(2+\varrho)$		
	$\frac{1+\varrho}{2+\varrho}$		0				$-\frac{\gamma(3+\varrho)}{2(6+\varrho)}$	0	
				$-\frac{2(1+2\varrho)}{2+\varrho}$					$-\frac{\gamma^2(3+2\varrho)}{2(6+\varrho)}$
				$+\frac{1+2\varrho}{6+3\varrho}$					$+\frac{\gamma^2(3+2\varrho)}{12(6+\varrho)}$

Table 10.2.

Eq. No.	(a)	(x1)	(x4)	(x5)	(x6)	(x8)	(y1)	(y4)	(y5)	(y6)
Notation	$\Delta F/4$	Δx	x	ΔS_x	\tilde{S}_x	I_{xx}	Δy	y	ΔS_y	\tilde{S}_y
Multiplier	F_f	c	c	cF_f	cF_f	c^2F_f	c	c	cF_f	cF_f
1			$\frac{\gamma}{2}$		0			1		0
	$\frac{1}{4}$			$\frac{\gamma}{4}$					$\frac{3}{8}$	
2		0	$\frac{\gamma}{2}$		$\frac{\gamma}{4}$	0	-1	$\frac{1}{2}$		$\frac{3}{8}$
	$\frac{1}{4}$			$\frac{\gamma}{4}$					$\frac{1}{8}$	
3			$\frac{\gamma}{2}$		$\frac{\gamma}{2}$			0		$\frac{1}{2}$
	$\frac{\varrho}{4}$			$\frac{\gamma\varrho}{8}$					0	
4		$-\gamma$	0	$\frac{\gamma(4+\varrho)}{8}$	$-\frac{\gamma^2(6+\varrho)}{2}$	0	0			$\frac{1}{2}$
	$\frac{\varrho}{4}$			$-\frac{\gamma\varrho}{8}$					0	
5			$-\frac{\gamma}{2}$		$\frac{\gamma}{2}$			0		$\frac{1}{2}$
	$\frac{1}{4}$			$-\frac{\gamma}{4}$					$-\frac{1}{8}$	
6		0	$-\frac{\gamma}{2}$		$\frac{\gamma}{4}$	0	-1	$-\frac{1}{2}$		$\frac{3}{8}$
	$\frac{1}{4}$			$-\frac{\gamma}{4}$					$-\frac{3}{8}$	
7			$-\frac{\gamma}{2}$		0			-1		0
	$1 + \frac{\varrho}{2}$					$-\frac{\gamma^2(6+\varrho)}{2}$				
	$F = 2 + \varrho$					$\frac{\gamma^2(6+\varrho)}{12}$				

$$D = I_{xx}I_{yy} - I_{xy}^2 = \frac{\gamma^2(3 + 2\varrho)}{36} c^4 F_f^2$$

The Analysis of L-Sections

(y8)	(y9)	(ω₁)	(ω₂)	(ω₃)	(ω₄)	(ω₅)	(ω₆)	(ω₈)
I_{yy}	I_{yx}	$\Delta\omega_c = \Delta\omega$	Ω	$\Delta S_\Omega/2$	$\boxed{\omega}$	ΔS_ω	$\boxed{\tilde{S}_\omega}$	$I_{\omega\omega}$
$c^2 F_f$	$c^2 F_f$	c^2	c^2	$c^2 F_f$	c^2	$\frac{\gamma c^2 F_f}{16(2+\varrho)}$	$c^2 F_f$	$c^4 F_f$
-2	0	$-\frac{\gamma}{2}$	0	$-\frac{\gamma}{8}$	$+\frac{\gamma(1+\varrho)}{2(2+\varrho)}$	0	$+\frac{\gamma(2+3\varrho)}{16(2+\varrho)}$	$-\frac{\gamma^2(1+2\varrho)}{4(2+\varrho)}$
0	-3γ	0	$-\frac{\gamma}{2}$	$-\frac{\gamma\varrho}{4}$	$+\frac{\gamma\varrho}{4(2+\varrho)}$	$-2+\varrho$	$+\frac{\gamma\varrho}{4(2+\varrho)}$	
-2	0	$+\frac{\gamma}{2}$	$-\frac{\gamma}{2}$	$-\frac{\gamma\varrho}{4}$	$-\frac{\gamma}{2(2+\varrho)}$	-4ϱ	0	0
			$-\frac{\gamma}{2}$	$-\frac{\gamma\varrho}{4}$	$-\frac{\gamma}{2(2+\varrho)}$	-4ϱ	$-\frac{\gamma\varrho}{4(2+\varrho)}$	
-4	-3γ			$-\frac{\gamma(1+\varrho)}{4}$			$-\frac{\gamma^2(1+2\varrho)}{2(2+\varrho)}$	
$+\frac{2}{3}$	$+\frac{\gamma}{2}$						$+\frac{\gamma^2(1+2\varrho)}{12(2+\varrho)}$	

$$\text{Eq. } (\Omega_0): \Omega_0 = \frac{\Sigma(\omega_3)}{\Sigma(a)} = -\frac{\gamma(1+\varrho)c^2 F_f 2}{4(2+\varrho) F_f} = -\frac{\gamma(1+\varrho)}{2(2+\varrho)} c^2$$

The Saint-Venant shear stress as given by Eq. (10.4) completes the picture of all possible stress distributions which may occur in this type of structural section.

d) L-Sections

Since no axis of symmetry may be attributed to this type of cross section, the direction of the principal axis is initially unknown. The cross section has point symmetry, however, and the center of gravity and the shear center therefore coincide and are thus known in advance.

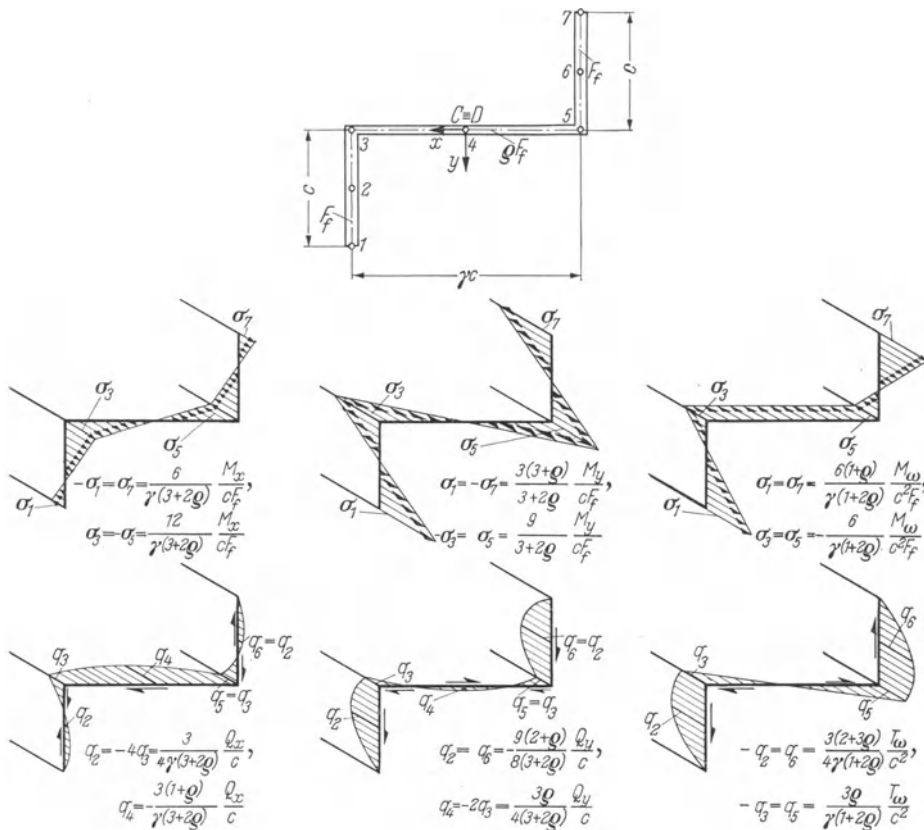


Fig. 10.3. Distribution of the Flexural Stresses and the Warping Stresses in the L-Section.

The analysis of this cross section is again conducted according to the numerical procedure developed in Chapter 6. The necessary calculations are arranged in Table 10.2. Because of the special symmetry, the simplified procedure of Table 6.2 may be used to calculate quantities depending on x and y and the procedure of Table 6.1 ω to calculate sectorial quantities.

According to the formulas (5.15 b), (5.33) and (5.19), (5.34), the general expressions for the stresses in a cross section which is referred to an arbitrary rectangular

coordinate system through the center of gravity are as follows:

$$\sigma = \frac{I_{yy}x - I_{xy}y}{D} M_x + \frac{I_{xx}y - I_{xy}x}{D} M_y + \frac{\omega}{I_{\omega\omega}} M_\omega, \quad (10.12a)$$

$$\tau t = q = -\frac{I_{yy}\tilde{S}_x - I_{xy}\tilde{S}_y}{D} Q_x - \frac{I_{xx}\tilde{S}_y - I_{xy}\tilde{S}_x}{D} Q_y - \frac{\tilde{S}_\omega}{I_{\omega\omega}} T_\omega \quad (10.12b)$$

where

$$D = I_{xx}I_{yy} - I_{xy}^2.$$

Fig. 10.3 again shows separately the stress patterns for each of the six elements in expressions (10.12). The distribution for the axial stress is plotted for the center line of the walls. Again, the shear stresses from flexure and warping torsion have to be supplemented by those resulting from Saint-Venant torsion [Eqs. (10.3) and (10.4)].

10.2 Approximate Solutions

a) The Parameter \varkappa as an Index for the Torsional Behavior

According to the definition (9.11) the parameter \varkappa is equal to the ratio between the member length l and the characteristic length d which depends only on the member cross section. The square of this reference distance d is equal to the ratio between the warping rigidity $E I_{\omega\omega}$ and the Saint-Venant torsion rigidity GK [v. Eq. (9.7)]. It may be anticipated, therefore, that the parameter \varkappa will give some indication as to whether Saint-Venant torsion or warping torsion predominates and thus whether the structural system has to be analyzed for mixed torsion.

$$\varkappa^2 = \frac{l^2 GK}{EI_{\omega\omega}}$$

If the numerator in this expression for \varkappa^2 is large as compared to the denominator, one may expect that Saint-Venant torsion is predominant. There will be a certain region for \varkappa where neither Saint-Venant nor warping torsion may be neglected (mixed torsion) and, finally, a region of small values for \varkappa where only warping torsion needs to be considered.

To develop some judgement as to the extent of these regions and on how they are influenced by the dimensions of the structural member, a member with the cross section of Fig. 6.1 will be considered. The cross section properties were calculated in Section 6.2. Since the thicknesses of the three rectangular elements were $t_6 = t$, $t_4 = t \sqrt{2}/5$ and $t_2 = t/\sqrt{2}$, respectively, the Saint-Venant torsion constant becomes:

$$K = \frac{1}{3} \sum_{i=2,4,6} b_i t_i^3 = \frac{157}{150} F_0 t^2 = 1,05 F_0 t^2. \quad (10.13)$$

If further $E/G = 2,6$, the torsion parameter \varkappa becomes:

$$\varkappa = l \sqrt{\frac{GK}{EI_{\omega\omega}}} = 0,21 \frac{l}{a} \frac{t}{a}. \quad (10.14)$$

If the length a is looked at as a constant reference length, one immediately recognizes that the value of κ is proportional to the product of member length and wall thickness. Since in the case of open, thin-walled cross sections the parameter κ may always be written in the form (10.14), one may formulate the following rule: In the case of thin-walled, open cross sections, Saint-Venant torsion will dominate in long members, warping torsion in short ones.

If, on the other hand, the slenderness of the member is kept constant, e.g. $l/a = 30$, the value κ is governed by the ratio t/a .

The lowest values for κ occur for cold formed sections whose wall thickness parameters are in the region $t/a < 0,1$ thus leading to $\kappa < 0,6$. The boundaries of such sections are usually flanged, a peculiarity which increases the warping rigidity as opposed to the Saint-Venant torsional rigidity. The κ -values for rolled shapes are considerably higher. Ordinary L-sections have ratios $t/a \approx 1:3$ which yields a κ between 2 and 3.

b) Shear Deformation

The torsional rigidity of closed, thin-walled cross sections may be between ten and a hundred times greater than the torsional rigidity of the corresponding open cross sections. Thus closed cross sections behave very much like solid sections for which Saint-Venant developed his theory on torsion.

It will be shown below that members with dominating Saint-Venant torsional rigidity (high values for κ) exhibit large shear stresses close to the point of load application whose influence on the deformations may no longer be neglected. These regional disturbances, however, may not be treated by means of the simple member statics.

Saint-Venant's principle helps to get around these difficulties. It states, applied in this context, that if a system of forces (internal forces) is replaced by an equivalent system of forces (reactions), the disturbances caused by the latter are of limited extent.

As an example, the problem treated in Section 7.4 b will be solved for mixed torsion. A member with the cross section shown in Fig. 7.9 is acted upon by an eccentrically applied axial force P . Both the axial force and the bending moments remain constant along the entire length of the member. The first two elements (contributions of axial force and bending) in the stress formula (7.27) therefore remain unchanged. The warping moments with the values

$$X = P\omega(P)$$

at the member ends, however, vary along the length of the member if the Saint-Venant torsional rigidity does not vanish (as assumed in Section 7.4 b). Thus the torsional moments T_s and T_ω vary along the length of the member.

$$\text{Eq. (9.42) yields:} \quad M_\omega = X \frac{\cos \kappa \bar{\zeta}}{\cos \frac{\kappa}{2}}, \quad (10.15 \text{ a})$$

$$T_\omega = -T_s = \frac{X}{l} \kappa \frac{\sin \kappa \bar{\zeta}}{\cos \frac{\kappa}{2}}. \quad (10.15 \text{ b})$$

Eqs. (10.15) are written in terms of the coordinate ξ which has the origin at mid-span. They are plotted in Fig. 10.4. The torsional moments at the member-ends increase with increasing ζ and approach $\zeta X/l$ for large values of ζ .

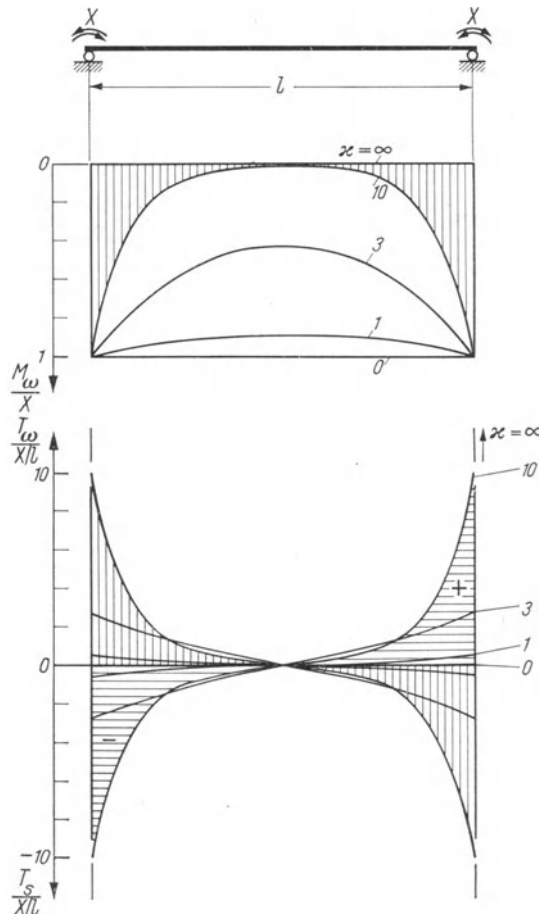


Fig. 10.4. Distribution of the Warping Moments M_ω and of the Two Components T_s and T_ω in a Member Under the End Warping Moments X .

Away from the member ends (for which the ordinary statical analysis is not able to give a reliable solution) it may be observed that the warping stresses vanish along the member for large values of ζ (for about $\zeta > 10$). Only in such cases is it permissible to resolve the effects of the axial force P with respect to the centroidal member axes and to calculate the stresses by means of the well known stress formulas.

Fig. 7.9 shows the stress distribution in the cross section at mid-span for the two limiting cases; pure warping torsion ($\zeta = 0$) and pure Saint-Venant torsion ($\zeta = \infty$). Even though these two limiting cases cannot occur in an actual member, they are nevertheless valuable in establishing limits for the actual stress distribution as was shown in Fig. 7.9 for the parameters $\zeta = 1$, 3 and 10.

The two limiting cases have additional significance in providing a basis for the development of approximate expressions when limiting conditions are approached. Approximate relations for both large and small values for α will be derived in the next two sections.

Members acted upon by a uniformly distributed torsional load m_D and by a concentrated torsional moment M_D will serve as examples. If the local influence of warping moments at the member ends is also considered, the basis for the approximate analysis of continuous systems will be complete.

e) Large α -Values, Limiting Case and Approximation for $\max M_\omega$

If α is very large, approximate expressions for a simply supported member under the uniformly distributed torsional load m_D may be derived from the solutions (9.27).

$$\frac{m_D l^2}{G 8 K} (1 - 4 \bar{\zeta}^2),$$

$$G K \varphi' = -m_D l \bar{\zeta} = T_s = T, \quad (10.16)$$

$$M_\omega = T_\omega = 0.$$

These expressions coincide exactly with those for the member with only Saint-Venant torsion (Section 3.2).

If, however, an approximation for the warping moment M_ω for large α -values is desired, one may read from the corresponding relation of Eqs. (9.27)

$$M_\omega = \frac{m_D l^2}{\alpha^2} = m_D \frac{E I_{\omega\omega}}{G K}. \quad (10.17a)$$

which, according to Eq. (5.33), yields the following warping stresses:

$$\sigma_\omega = \frac{E}{G} \frac{m_D \omega}{K}. \quad (10.17b)$$

The Eqs. (9.32) lead to corresponding expressions for the member under the concentrated torsional moment M_D . For extremely large values of α , these expressions again coincide with those for pure Saint-Venant torsion in Table 3.2a.

The previous section mentions that an ordinary structural analysis will not determine the true state of stress in the close neighbourhood of concentrated loads. With this limitation kept in mind, the warping moment at the fixed end of a member may be derived from the corresponding expression of the solutions (9.10).

$$\max M_\omega = -T^{(f)} d. \quad (10.18)$$

$T^{(f)}$ refers to the total torsional moment at the fixed end and d is the characteristic length as defined by Eq. (9.7).

If a concentrated torsional moment M_D acts at a large distance from the nearest support, warping restraint effects are produced on each side of the point

of load application. The warping moment

$$\max M_\omega = \frac{M_D}{2} d, \quad (10.19\text{a})$$

$$= \frac{M_D l}{2\kappa}. \quad (10.19\text{b})$$

Both the warping moment and the warping stresses decrease to either side of the disturbance according to the law $e^{-z/d}$ [v. curve at the bottom of Fig. 9.1 and corresponding expression of the solutions (9.10)]. The same holds true for a warping moment X applied at a member end. For large values of κ its decrease with increasing distance z from the member end is given by the expression:

$$M_\omega = X e^{-z/d}. \quad (10.20)$$

This expression and the corresponding relation for the warping stress are very unreliable if the characteristic length d is smaller than the breadth of the cross section. Since the warping stresses are usually small in this case, the resulting error is not significant.

d) Small κ -Values, Limiting Case and Approximation

The warping moment in a simply supported member which is acted upon by a warping moment X at the right end of the member (Fig. 9.2) is given by Eqs. (9.22).

$$M_\omega = X \frac{\sin \kappa \zeta}{\sin \kappa}$$

If both numerator and denominator are expanded in a Taylor series, this expression becomes:

$$\begin{aligned} M_\omega &= X \frac{\kappa \zeta + \frac{1}{3!}(\kappa \zeta)^3 + \frac{1}{5!}(\kappa \zeta)^5 + \dots}{\kappa + \frac{1}{3!}\kappa^3 + \frac{1}{5!}\kappa^5 + \dots}, \\ &= X \frac{\zeta + \frac{\kappa^2}{6}\zeta^3 + \frac{\kappa^4}{120}\zeta^5 + \dots}{1 + \frac{\kappa^2}{6} + \frac{\kappa^4}{120} + \dots}. \end{aligned} \quad (10.21)$$

This expression leads immediately to the limiting solution $M_\omega = X \zeta$ for vanishing values κ (pure warping torsion) which might have been derived from the analogy of warping torsion and bending.

In addition to this limiting solution, approximate solutions for $\kappa > 0$ with any desired degree of accuracy may be derived. The accuracy depends only on the number of terms considered in the series.

Sets of approximate solutions will now be derived for all cases treated in Section 9.2. All terms of higher than second order in \varkappa are neglected. The subsequent expressions are immediately transformed into those for pure warping torsion if \varkappa^2 is put equal to zero. They represent furthermore approximate solutions for mixed torsion if the parameter \varkappa does not exceed a certain value which depends on the required accuracy (e.g. $\varkappa < 2$). The warping torsional moment T_ω is given instead of the total torsional moment T .

For a warping moment X acting at the right end of a member [derived from the solutions (9.22) for small values \varkappa]:

$$\begin{aligned}\varphi &= \frac{Xl^2}{EI_{\omega\omega}} \frac{\zeta(1 - \zeta^2) + \frac{\varkappa^2}{20}\zeta(1 - \zeta^4)}{6 + \varkappa^2}, \\ \varphi' &= \frac{Xl}{6EI_{\omega\omega}} \frac{1 - 3\zeta^2 + \frac{\varkappa^2}{20}(1 - 5\zeta^4)}{1 + \frac{\varkappa^2}{6}}, \\ M_\omega &= X \frac{\zeta + \frac{\varkappa^2}{6}\zeta^3}{1 + \frac{\varkappa^2}{6}}, \\ T_\omega &= \frac{X}{l} \frac{1 + \frac{\varkappa^2}{2}\zeta^2}{1 + \frac{\varkappa^2}{6}}.\end{aligned}\tag{10.22}$$

For uniformly distributed torsional load m_D [derived from the solutions (9.27) for small values \varkappa]:

$$\begin{aligned}\varphi &= \frac{5}{384} \frac{m_D l^4}{EI_{\omega\omega}} \frac{1 - \frac{8}{5}\bar{\zeta}^2(3 - 2\bar{\zeta}^2) + \frac{\varkappa^2}{300}(7 - 30\bar{\zeta}^2 + 32\bar{\zeta}^6)}{1 + \frac{\varkappa^2}{8}}, \\ \varphi' &= -\frac{m_D l^3}{24EI_{\omega\omega}} \frac{\bar{\zeta}(3 - 4\bar{\zeta}^2) + \frac{\varkappa^2}{80}\bar{\zeta}(5 - 16\bar{\zeta}^4)}{1 + \frac{\varkappa^2}{8}}, \\ M_\omega &= \frac{m_D l^2}{8} \frac{1 - 4\bar{\zeta}^2 + \frac{\varkappa^2}{48}(1 - 16\bar{\zeta}^4)}{1 + \frac{\varkappa^2}{8}}, \\ T_\omega &= -m_D l \bar{\zeta} \frac{1 + \frac{\varkappa^2}{6}\bar{\zeta}^2}{1 + \frac{\varkappa^2}{8}}.\end{aligned}\tag{10.23}$$

For concentrated torsional load M_D at $\zeta = \alpha$ and $\zeta' = \beta$ [derived from the solutions (9.32) for small values z]:

$$\left. \begin{aligned} \varphi &= \frac{M_D l^3}{6 EI_{\omega\omega}} \frac{\beta \zeta}{1 + \frac{z^2}{6}} \left[1 - \beta^2 - \zeta^2 + \frac{z^2}{20} \left(1 - \beta^4 - \zeta^4 - \frac{10}{3} \beta^2 \zeta^2 \right) \right], \\ \varphi' &= \frac{M_D l^2}{6 EI_{\omega\omega}} \frac{\beta}{1 + \frac{z^2}{6}} \left[1 - \beta^2 - 3\zeta^2 + \frac{z^2}{20} (1 - \beta^4 - 10\beta^2\zeta^2 - 5\zeta^4) \right], \\ M_\omega &= M_D l \frac{\beta \zeta}{1 + \frac{z^2}{6}} \left[1 + \frac{z^2}{6} (\beta^2 + \zeta^2) \right], \\ T_\omega &= M_D \frac{\beta}{1 + \frac{z^2}{6}} \left[1 + \frac{z^2}{6} (\beta^2 + 3\zeta^2) \right]. \end{aligned} \right\} \begin{matrix} 0 \leq \zeta < \alpha \\ (10.24) \end{matrix}$$

The solutions in the region $0 \leq \zeta' < \beta$ are similar to those above. The coordinate β is replaced by α , ζ by ζ' and signs of the odd functions φ' and T_ω are reversed.

The displacement coefficients and the generalized displacements according to Eq. (7.13b) are derived from the second equation in the sets (10.22), (10.23) and (10.24) by putting $\bar{\zeta} = \pm 1/2$ and $\zeta = 0$ and 1, respectively.

The following quantities are again valid for small values of z and they are written without span subscripts.

Displacement coefficients:

$$\begin{aligned} a_{ik} = b_{ik+1} &= \frac{l}{3EI_{\omega\omega}} \frac{1 + \frac{z^2}{10}}{1 + \frac{z^2}{6}}, \\ a_{i k+1} = b_{ik} &= \frac{l}{6EI_{\omega\omega}} \frac{1 + \frac{z^2}{20}}{1 + \frac{z^2}{6}}. \end{aligned} \quad (10.25)$$

Generalized displacements for uniformly distributed torsional load m_D :

$$a_0 = b_0 = \frac{m_D l^3}{24EI_{\omega\omega}} \frac{1 + \frac{z^2}{40}}{1 + \frac{z^2}{8}}. \quad (10.26)$$

Generalized displacements for the concentrated torsional load M_D at $\zeta = \alpha$ and $\zeta' = \beta$:

$$\begin{aligned} a_0 &= \frac{M_D l^3}{6EI_{\omega\omega}} \beta \frac{1 - \beta^2 + \frac{z^2}{20} (1 - \beta^4)}{1 + \frac{z^2}{6}}, \\ b_0 &= \frac{M_D l^2}{6EI_{\omega\omega}} \alpha \frac{1 - \alpha^2 + \frac{z^2}{20} (1 - \alpha^4)}{1 + \frac{z^2}{6}}. \end{aligned} \quad (10.27)$$

These expressions for the displacements at the member ends are the bases for the formulation of approximate three-warping-moment equations for small \varkappa (warping torsion dominates).

Expressions for the deformations and internal forces corresponding to Eqs. (9.38) may be formulated by means of the approximate solutions (10.22) which represent the influence of the warping moment X at one end of the member.

Frequently, as a consequence of symmetry in the system and the load, a member is acted upon by equal warping moments X at each end. In this case, the expressions for the deformations and internal forces are as follows [derived from Eqs. (9.42) for small values \varkappa]:

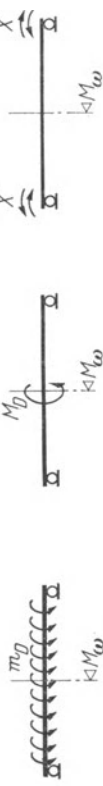
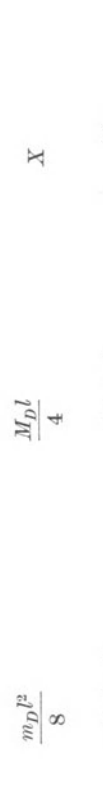
$$\begin{aligned}\varphi &= \varphi_0 + \frac{X l^2}{8 EI_{\omega\omega}} \frac{1 - 4\bar{\xi}^2 + \frac{\varkappa^2}{48} (1 - 16\bar{\xi}^4)}{1 + \frac{\varkappa^2}{8}}, \\ T_s &= GK\varphi' = T_{s0} - \varkappa^2 \frac{X}{l} \frac{\bar{\xi} + \frac{\varkappa^2}{6}\bar{\xi}^3}{1 + \frac{\varkappa^2}{8}}, \\ M_\omega &= M_{\omega 0} + X \frac{1 + \frac{\varkappa^2}{2}\bar{\xi}^2}{1 + \frac{\varkappa^2}{8}}, \\ T_\omega &= T_{\omega 0} + \varkappa^2 \frac{X}{l} \frac{\bar{\xi} + \frac{\varkappa^2}{6}\bar{\xi}^3}{1 + \frac{\varkappa^2}{8}}.\end{aligned}\tag{10.28}$$

e) The Accuracy of Approximate Solutions

The accuracy of the different approximate solutions for the problem of mixed torsion will be examined hereinafter. The warping moments at mid-span of the simply supported member will be compared. These warping moments are calculated for the three different types of load as treated above, i.e. uniformly distributed torsional load m_D , concentrated torsional moment M_D at mid-span, and equal warping moments X at the two member ends.

To arrive at a nondimensional presentation of the results, the warping moments $M_\omega(\varkappa)$ are compared with the warping moment $M_\omega(\varkappa = 0)$ for pure warping torsion which in any case assumes the greatest possible value. These reference values were calculated and discussed in Chapter 7 and are summarized in the first line of Table 10.3. The approximations for small values of \varkappa are derived from the third equation of the solutions (10.23), (10.24) and (10.28) and the corresponding exact values from the solutions (9.27), (9.32) and (9.42) by putting $\bar{\xi} = 0$ or $\zeta = 1/2$.

Table 10.3. Comparison of Different Solutions to the General Torsion Problem (Basis for the Curves in Fig. 10.5)

		
Pure warping torsion: ($\kappa = 0$)	$\frac{M_o l}{m_D l^2}$	$\frac{M_o l}{4}$
Dominating warping torsion: ($\kappa \gtrsim 2$)	$\frac{48 + \kappa^2}{48 + 6\kappa^2}$	$\frac{12 + \kappa^2}{12 + 2\kappa^2}$
Mixed torsion: ($0 \leq \kappa < \infty$)	$\frac{8}{\kappa^2} \left(1 - \frac{1}{\cos \frac{\kappa}{2}} \right)$	$\frac{2}{\kappa} \operatorname{Tg} \frac{\kappa}{2}$
Dominating Saint-Venant torsion: ($\kappa \lesssim 5$)	$\frac{M_o(\kappa)}{M_o(\kappa = 0)}$	$\frac{2}{\kappa}$
Pure Saint-Venant torsion: ($\kappa = \infty$)	$\frac{M_o(\kappa)}{M_o(\kappa = 0)}$	0

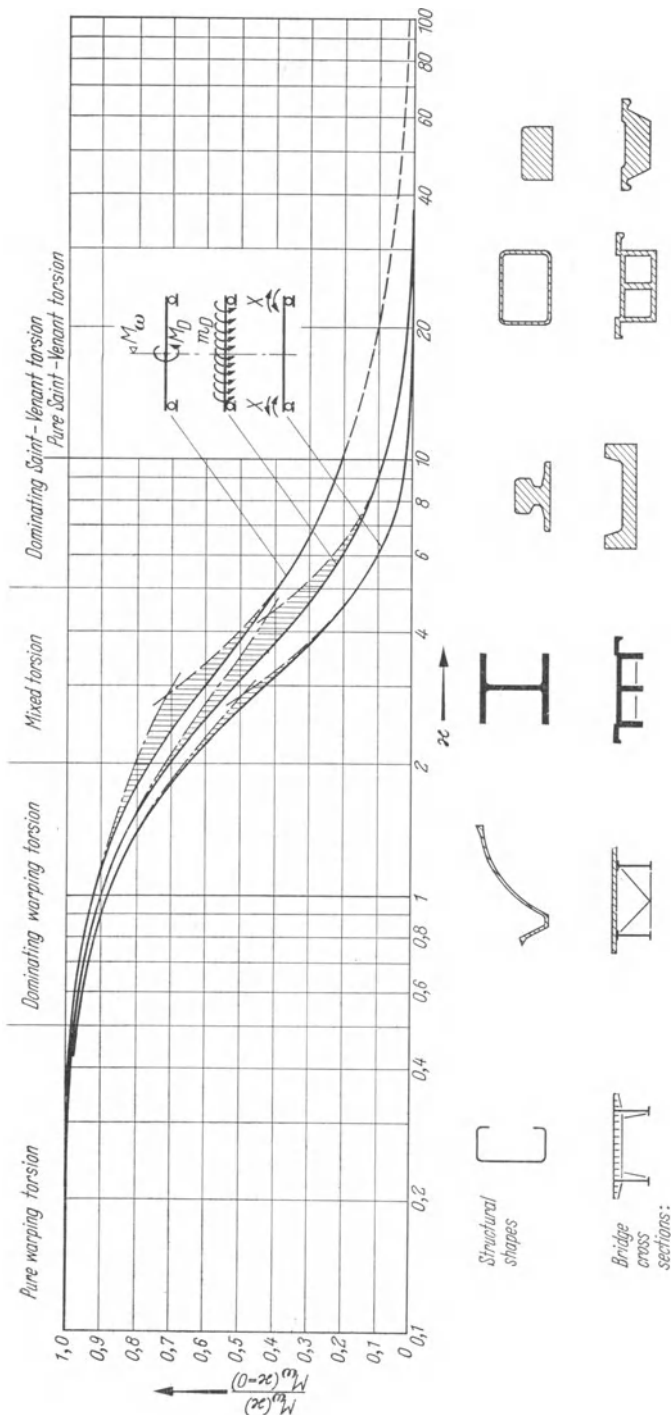


Fig. 10.5. Warping Moments $M_w = M_w(x)$ at Mid-Span of a Simply Supported Member Subjected to Three Different Types of Load.

The approximations for large ζ -values are given for each of the three considered cases by Eqs. (10.17a), (10.19b) and (10.20). Note with reference to Eq. (10.20) that equal warping moments act at each end of the member and that $z = l/2$.

These formulas are summarized in Table 10.3 and plotted with respect to the logarithmic scale ζ in Fig. 10.5. These curves extend between the ordinates $M_w(\zeta)/M_w(\zeta = 0) = 1$ (pure warping torsion) and $M_w(\zeta)/M_w(\zeta = 0) = 0$ (pure Saint-Venant torsion). Neither of these limits is reached by the plotted curves since no actual structural member will ever be able to assume a ζ -value of zero or infinity. However, the curves demonstrate decisively that within large regions of small and large ζ -values one torsional component may be neglected as opposed to the other without appreciable error. The previous chapters demonstrated the great simplifications that thereby resulted in the solution of torsional problems.

It may be observed from Fig. 10.5 that (with the exception of the member acted upon by the concentrated torsional moment M_D) the warping stresses do not exceed 10% of the maximum possible values in the case of large ζ (about $\zeta > 10$). It also is noted, that these theoretical warping stresses occur at the point of load application and are therefore to be accepted with some reservation.

As mentioned in Section 10.2, members with large values of ζ show such abrupt changes in the axial stresses that the shear stresses and shear deformations resulting therefrom may no longer be neglected. The actual warping restraint is therefore smaller than that calculated without consideration of shear deformations. The theory as presented herein therefore overestimates the warping moments under the load. Fig. 10.5 presents therefore these questioned results by a broken line.

The approximate solutions for small and large ζ -values are indicated by a dash-and-dot line. Their deviations from the corresponding exact solutions are accented by the cross-hatched regions. It is seen that the approximation both for warping torsion and Saint-Venant torsion is excellent. One might well assume therefore that the two approximate solutions would in themselves be satisfactory for the entire range of mixed torsion ($0 < \zeta < \infty$).

It is also possible to develop approximate solutions for the intermediate range of ζ -values. The maximum warping moment in the uniformly loaded, simply supported member (intermediate solid curve of Fig. 10.5), for instance, might be approximated by the following formula:

$$\max M_w = \frac{m_D l^2}{8 + \frac{5}{6} \zeta^2} = \frac{m_D l^2}{8 + \frac{5}{6} \frac{l^2 G K}{E I_{w\omega}}}. \quad (10.29)$$

Various typical shapes and bridge cross sections are shown at the bottom of Fig. 10.5. They are placed in the range of ζ -values in which they are most likely to be found.

1a) Pure warping torsion: Cold-formed profiles (folded sheet metal or rolled strips) may usually be analyzed for pure warping torsion only. Open bridge cross sections with steel floor slabs reinforced by open, longitudinal ribs also belong to this group.

1 b) Warping torsion dominates: The reinforced concrete floor slabs of open, composite bridge cross sections increase the Saint-Venant torsional rigidity by such an amount that a correction of the analysis for pure warping torsion is indicated. The same thing holds for slender cylindrical shells.

2) Mixed torsion: This group includes the rolled structural shapes and reinforced-concrete slab bridges. There exist, however, post-tensioned concrete bridges which belong rather to group 1 b.

3 a) Saint-Venant torsion dominates: The application of these formulas seems indicated for all composite solid and hollow cross sections.

3 b) Pure Saint-Venant torsion: This may be assumed to govern in all compact solid and hollow cross sections. Special attention must be given to the problem of concentrated loads which may not be treated by means of the methods developed in this text.

The foregoing is but an approximate classification because the exact position of a cross section along the α -scale does not only depend on the cross section itself but also on the length of the member and on the character of the applied load. Every member, for instance, exhibits only Saint-Venant torsion if the two member ends are merely twisted with respect to each other without any restraint of warping (v. Section 9.2 b).

Occasionally, either warping or Saint-Venant torsion is arbitrarily neglected. This may occur whenever ultimate load considerations ask for an admissible state of stress in order to find a lower bound for the ultimate load. It conforms with the theory of plasticity that if a structure exhibits two ways to carry a torsional moment (warping torsion and Saint-Venant torsion) one only needs to consider one in order to arrive at an admissible state of stress.

Of importance in Saint-Venant torsion theory is the assumption that all elements of a cross section undergo the same angle of twist. The effect of warping torsion, on the other hand, is not altered appreciably if the shape of the cross section is not exactly maintained. It is therefore advisable to completely neglect Saint-Venant torsion in cross sections which are very sensitive to such changes of shape (e.g. composite plate girder bridges).

10.3 The Skew Supported Bar with Mixed Torsion

a) Introduction

The notation is the same as the one applied in Chapters 4 and 8 where skew supported systems were analyzed either on the basis of pure Saint-Venant torsion or pure warping torsion. It must be noted that the distance d is the difference in the x -coordinates of two distinct bearing elements and not the characteristic length defined by Eq. (9.7).

The reservations made in Section 10.2 b concerning the analysis of stresses in regions of supports must be observed. They not only apply to the inaccurate evaluation of warping stresses because of neglected shear deformations but also to the complex state of stress around the concentrated, eccentric reactions which may only be analyzed by means of a two- or even three-dimensional theory of elasticity. The principal factors which may be determined with good accuracy

are the resultants of the stresses, the moments, the shears and the torsional moments.

b) Base System and Compatibility Conditions

The base system consisting of a chain of skew supported, single-span members will again be assumed. The compatibility conditions are the same as those given for the case of pure warping torsion, v. Eq. (8.2).

Even the compatibility conditions for the statically indeterminate base system remain unchanged since geometrical conditions do not depend on whether the member deforms under pure Saint-Venant torsion, pure warping torsion or under mixed torsion. Conditions (4.1) are therefore valid as well. Since, according to the solutions (9.24), twisted member ends cause only Saint-Venant torsional moments T_s , independent of the parameter α , Eq. (4.2) is applicable for any torsion resistant member. One may further conclude from the solutions (9.24) that the warping intensities Δa_i and Δb_i in the case of mixed torsion are the same as those determined for pure warping torsion only [Eqs. (8.9)].

Skew supports influence the bending moments and the warping moments at the supports as formulated by expressions (8.6) and (8.7). The resulting changes have to be considered in the subsequent calculation of the member-end deformations. It may be concluded however from what was said above that the expressions for α_i , β_i , a_i and b_i summarized in Table 8.1 remain unchanged except for the first two which have to include the influence of T_i according to Eq. (4.2).

The expressions for T_{ki} and T_{k+1i} which would have to be introduced into the first two equations of Table 8.1 are still given by Eqs. (8.10a–c) because the total torsional moment T has exactly the form as that of the warping torsional moment in Table 8.2 even though the expression for the warping moment changes, v. Eq. (9.38). This may give an idea as to how involved this problem becomes if mixed torsion has to be considered. Because of the influence of T_i , the expressions for α_i and β_i are, according to Eq. (4.2), not even in an explicit form.

In order to simplify the expressions for the angular displacements α_i and β_i at the supports, the coordinate differences between the two bearing elements d and e_k are assumed to be negligible as compared with the span length l_i . This assumption simplifies considerably the expressions (8.10a–c) and gives rise to the following implicit formulas for the angular displacements at the supports [T_i according to Eq. (4.2)]:

$$\begin{aligned} \alpha_i = & M_k \alpha_{ik} + M_{k+1} \alpha_{ik+1} + \alpha_{i0} \\ & + T_{ki}^{(i)} \alpha_{ik} \operatorname{tg} \delta_k + T_{k+1i}^{(i)} \alpha_{ik+1} \operatorname{tg} \delta_{k+1} \\ & + (\alpha_{ik} \operatorname{tg} \delta_k + \alpha_{ik+1} \operatorname{tg} \delta_{k+1}) (X_{k+1} - X_k) / l_i \\ & - (\alpha_{ik} \operatorname{tg} \delta_k + \alpha_{ik+1} \operatorname{tg} \delta_{k+1}) (\alpha_i \operatorname{tg} \delta_k + \beta_i \operatorname{tg} \delta_{k+1}) / \gamma_i. \end{aligned} \quad (10.30)$$

$$\begin{aligned} \beta_i = & M_k \beta_{ik} + M_{k+1} \beta_{ik+1} + \beta_{i0} \\ & + T_{ki}^{(i)} \beta_{ik} \operatorname{tg} \delta_k + T_{k+1i}^{(i)} \beta_{ik+1} \operatorname{tg} \delta_{k+1} \\ & + (\beta_{ik} \operatorname{tg} \delta_k + \beta_{ik+1} \operatorname{tg} \delta_{k+1}) (X_{k+1} - X_k) / l_i \\ & - (\beta_{ik} \operatorname{tg} \delta_k + \beta_{ik+1} \operatorname{tg} \delta_{k+1}) (\alpha_i \operatorname{tg} \delta_k + \beta_i \operatorname{tg} \delta_{k+1}) / \gamma_i. \end{aligned}$$

Each of the Eqs. (10.30) are written on four lines and the corresponding elements on each of these lines may be interpreted in a similar way.

The first line of each expression represents the ordinary three-moment equation for a continuous beam on regular supports ($\operatorname{tg} \delta_k = \operatorname{tg} \delta_{k+1} = 0$). The second line represents according to Eqs. (4.37) the generalized displacements α_{iD} and β_{iD} for torsional loads while the third line might similarly be considered to give the influence of the warping moments.

$$\begin{aligned}\alpha_{iX} &= (\alpha_{ik} \operatorname{tg} \delta_k + \alpha_{i,k+1} \operatorname{tg} \delta_{k+1}) \frac{X_{k+1} - X_k}{l_i} \\ \beta_{iX} &= (\beta_{ik} \operatorname{tg} \delta_k + \beta_{i,k+1} \operatorname{tg} \delta_{k+1}) \frac{X_{k+1} - X_k}{l_i}.\end{aligned}\quad (10.31)$$

The expressions on the fourth line, by means of the member constants in Table 4.2, may be written as $-(\alpha_i C_{i\alpha k} + \beta_i C_{i\alpha k+1})$ resp. $-(\alpha_i C_{i\beta k} + \beta_i C_{i\beta k+1})$. Since these are functions of the angular displacements α_i and β_i , they are more appropriately written on the left side of Eqs. (10.30). The latter are, by means of the abbreviations introduced above, reduced to the following system of equations for the unknowns α_i and β_i :

$$\begin{aligned}\alpha_i(1 + C_{i\alpha k}) + \beta_i C_{i\alpha k+1} &= \alpha_{i0} + \alpha_{iD} + \alpha_{iX} + M_k \alpha_{ik} + M_{k+1} \alpha_{i,k+1}, \\ \alpha_i C_{i\beta k} + \beta_i(1 + C_{i\beta k+1}) &= \beta_{i0} + \beta_{iD} + \beta_{iX} + M_k \beta_{ik} + M_{k+1} \beta_{i,k+1}.\end{aligned}\quad (10.32)$$

These equations differ from the system (4.6) only by the additional generalized displacements α_{iD} and α_{iX} resp. β_{iD} and β_{iX} from which α_{iD} and β_{iD} were already introduced in Chapter 4.

The generalized displacements α_{i0} and β_{i0} occur alone in the case of centric loads and pure Saint-Venant torsion. They must be supplemented by α_{iD} and α_{iX} respectively if mixed torsion requires consideration. If the load is purely torsional, the generalized displacements remain α_{iD} and β_{iD} in the case of pure Saint-Venant torsion and $\alpha_{iD} + \alpha_{iX}$ and $\beta_{iD} + \beta_{iX}$ in the case of mixed torsion.

If, finally, pure warping torsion may be assumed, the left side and not the right side of Eqs. (10.32) is modified. The four member constants $C_{i\alpha k}$ to $C_{i\beta k+1}$ become zero in this case.

Hence it appears that the procedures and solutions discussed in Chapter 4 may be applied for the determination of the moments M_k if only the generalized displacements are modified by the influence of the warping moments according to Eqs. (10.31).

The warping moments X_k , however, are as yet unknown. They have to be determined by means of the compatibility conditions (8.2b) which, according to Section 7.3, lead to the three-warping-moment equations (7.21). They include the coefficients a_{ik} and the generalized displacements a_{i0} given by Table 9.1. The latter, however, have to be modified by the influence of skew supports as given by Part II of Table 8.1.

An iterative procedure may again be used to solve this very involved problem. A first approximation for the moment M_k may be obtained from the simplified

three-moment equations of Chapter 4 which neglect the influence of warping moments, i.e. α_{iX} and β_{iX} are set equal to zero. The resulting values for M_k , α_i and β_i are thereafter assumed to represent first approximations of the generalized displacements in the three-warping-moment equations.

These equations determine the warping moments X_k as initial values for a second cycle of the iteration which now includes first approximations for α_{iX} and β_{iX} .

Only for a few continuous spans is it practicable to calculate closed solutions of the coupled three-moment and three-warping-moment equations.

c) Internal Forces

The torsional moments caused by the angular displacements at the supports of the regularly supported member and by the redundant moments M_k and M_{k+1} are given by:

$$\begin{aligned} T_{ii} = & -\frac{1}{\gamma_i D_i} [(\alpha_{i0} + \alpha_{iD} + \alpha_{iX}) \operatorname{tg} \delta_k + (\beta_{i0} + \beta_{iD} + \beta_{iX}) \operatorname{tg} \delta_{k+1} \\ & + M_k(\alpha_{ik} \operatorname{tg} \delta_k + \beta_{ik} \operatorname{tg} \delta_{k+1}) + M_{k+1}(\alpha_{ik+1} \operatorname{tg} \delta_k + \beta_{ik+1} \operatorname{tg} \delta_{k+1})] \end{aligned} \quad (10.33)$$

which, according to Eqs. (9.38) leads to the following expressions for the total torsional moments T_i , the Saint-Venant torsional moments T_{si} and the warping torsional moments $T_{\omega i}$, respectively, in span i :

$$\left. \begin{aligned} T_i &= T_{i0} + \frac{\omega M_{k+1i} - \omega M_{ki}}{l_i} + T_{ii}, \\ T_{si} &= s T_{i0} - \frac{\omega M_{ki}}{G K_i l_i} \left(1 - \zeta_i \frac{\cos \zeta_i \zeta'_i}{\sin \zeta_i} \right) + \frac{\omega M_{k+1i}}{G K_i l_i} \left(1 - \zeta_i \frac{\cos \zeta_i \zeta_i}{\sin \zeta_i} \right) + T_{ii}, \\ T_{\omega i} &= \omega T_{i0} - \frac{\omega M_{ki}}{l_i} \zeta_i \frac{\cos \zeta_i \zeta'_i}{\sin \zeta_i} + \frac{\omega M_{k+1i}}{l_i} \zeta_i \frac{\cos \zeta_i \zeta_i}{\sin \zeta_i}. \end{aligned} \right\} \quad (10.34)$$

The warping moments at the supports ωM_{ki} and ωM_{k+1i} are given by Table 8.2.

The total torsional moments at the member ends, T_{ki} and T_{k+1i} , as determined by the first of Eqs. (10.34), provide together with the redundant moments M_k and M_{k+1} for the calculation of the bending moments at the supports. The necessary relations are listed in the upper left corner of Table 8.2. All subsequent relations given in this table therefore are also valid except those for the warping moments which must be modified in accordance with Eqs. (9.38).

As in the case of pure warping torsion, the member-end values T_{ki} and T_{k+1i} are not known at the outset. The considerations which led to the expressions (8.10), however, show that Eqs. (8.10b) and (8.10c) for T_{ki} and T_{k+1i} respectively are still valid if Eq. (8.10a) for T_i is supplemented by T_{ii} of Eq. (10.33).

If the distances d and s_k between the two bearing elements are small compared to the span length l_i , one may put $\omega M_{ki} = X_k$ and $\omega M_{k+1i} = X_{k+1}$.

IV. Folded Plates

Introduction

A primary condition for the flexural and torsional analysis of thin-walled members is that the shape of the cross section is maintained, either inherently by the cross section itself or by means of transverse stiffeners or diaphragms. What happens if this important condition is no longer satisfied?

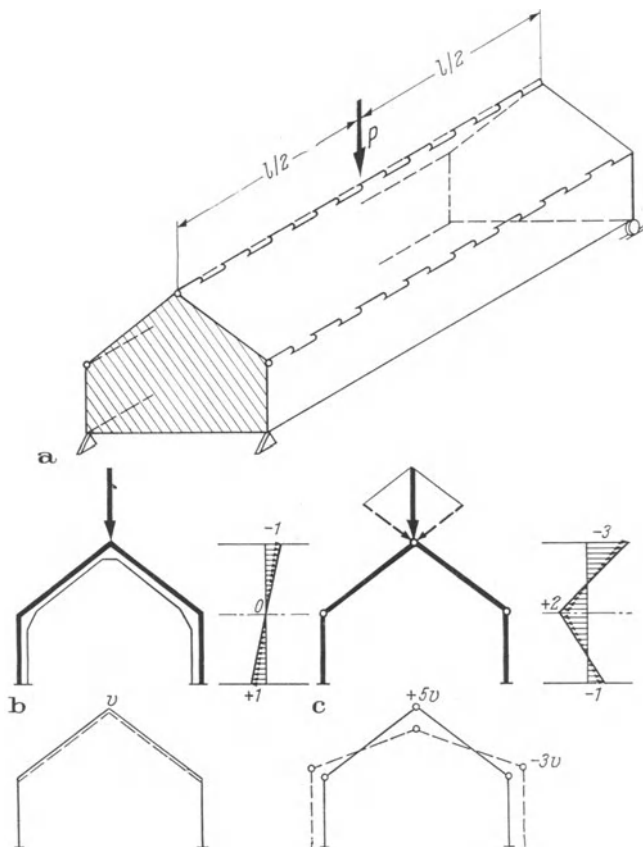


Fig. 11.1. Comparison of the Ordinary Bending Theory and the Folded-Plate Theory.

A member consisting of a number of plane plates must, of course, show a state of stress which is in equilibrium with the applied loads.

This Chapter deals with the idealized member consisting of a number of plane plates that are hinged together along their longitudinal edges and whose Saint-Venant torsional rigidity is negligible. This type of structure is called a Folded Plate.

Fig. 11.1 illustrates the differences in the behavior between a simple structure viewed either as a simple beam or as a folded plate. The structure consists of four longitudinal plates and two rigid end walls or diaphragms (Fig. 11.1 a).

It is assumed in the first case that a cross frame is introduced at mid-span which completely maintains the shape of the cross section. This rigid frame induces therefore a linear stress distribution over the entire cross section and makes each cross-sectional point undergo the same vertical deflection (Fig. 11.1 b).

In the second case, the four plates are no longer forced to maintain the shape of the cross section. In the limit, the mutual restraints between adjacent plates are assumed to be hinged connections (Fig. 11.1 c). The stresses are set linear across the individual plates, but are nevertheless not independent from each other. The longitudinal deformations and therefore the axial stresses must be equal at the hinged connections of two adjacent plates. The shape of the cross section, however, changes because different points of the cross section undergo different vertical deflections. The deflections of the two outer plates may even be negative.

Of course, the hinges between two plates do not occur in actuality. However, the bending rigidities of the plates themselves are usually too small to prevent the deformation of the cross section. The two different types of structural behavior may therefore be considered to be limiting cases for the stresses and deformations of the actual structure.

One of the first publications dealing with folded plates was a dissertation by H. SCHWYZER¹. A very recent state-of-the-art survey² was presented by a committee in the United States. It lists more than a hundred references to which the reader may refer for further information.

11 General Analysis of Folded Plates

11.1 Systems of Equations

a) Three-Shear Equations

In order to arrive at a general solution for this new type of structure, the individual plates are first considered separately whereupon the conditions for the compatibility at the hinges are formulated.

A partial view of the separated plate i with the width c_i and thickness t_i is given in Fig. 11.2. The part of the plate as illustrated stretches from the sup-

¹ SCHWYZER, H.: Statische Untersuchung der aus ebenen Tragflächen zusammengesetzten räumlichen Tragwerke. Diss. ETH Zürich, 1920.

² Committee on Masonry and Reinforced Concrete: Phase I Report on Folded Plate Construction. ASCE, ST6, Dec. 1963, p. 365—400.

port A_i to the cross section at z_i which is acted upon by the internal forces M_i and N_i .

The shear stresses τ or the shear flows $q = \tau \cdot t$ exerted by the adjacent plates $i - 1$ and $i + 1$ in the edges k and $k + 1$ are equated to the resultant edge forces $R_k(z)$ as follows:

$$R_k = \int_0^z \tau t \, dz = \int_0^z q_k \, dz. \quad (11.1)$$

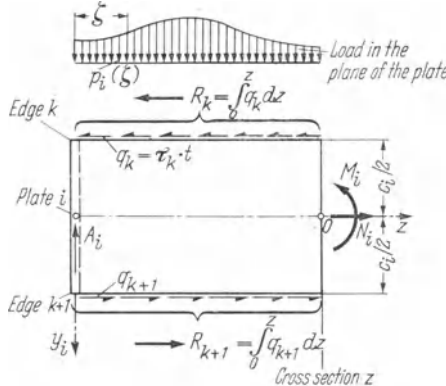


Fig. 11.2. Positive Internal Forces Acting in the Position z of Plate i of a Folded Plate (Plates $i = 2, 4, 6, \dots, n$ and Edges $k = 1, 3, 5, \dots, n + 1$).

The internal forces $M(z)$ and $N(z)$ may now be expressed in terms of the edge forces and applied loads. The condition for the moment equilibrium with respect to the point 0 is:

$$\underbrace{A_i z - \int_0^z p_i(\xi) (z - \xi) \, d\xi}_{M_{i0}} - R_k \frac{c_i}{2} - R_{k+1} \frac{c_i}{2} - M_i = 0.$$

The first two elements together represent the simple-beam bending moment M_{i0} in plate i due to the applied load in the plane of the plate $p_i(\xi)$. This reduces the equilibrium condition to:

$$M_i = M_{i0} - \frac{c_i}{2} (R_k + R_{k+1}). \quad (11.2)$$

The equilibrium condition in the z -direction may be formulated as follows:

$$N_i = R_k - R_{k+1}. \quad (11.3)$$

The bending moment and the axial force cause the following edge stresses σ_k and σ_{k+1} if the stress distribution is assumed to be linear in each plate:

$$\begin{aligned} \sigma_k &= -\frac{M_i}{W_i} + \frac{N_i}{F_i}, \\ \sigma_{k+1} &= +\frac{M_i}{W_i} + \frac{N_i}{F_i}, \end{aligned} \quad (11.4)$$

W_i signifies the section modulus and F_i the area of the rectangular cross section of plate i . They are connected by the following relation:

$$W_i = \frac{c_i^2 t_i}{6} = F_i \frac{c_i}{6}. \quad (11.5)$$

These relations may be summarized in the following expressions for the edge stresses σ_k and σ_{k+1} :

$$\left. \begin{aligned} \sigma_k &= -\frac{M_{i0}}{W_i} + 4 \frac{R_k}{F_i} + 2 \frac{R_{k+1}}{F_i}, \\ \sigma_{k+1} &= +\frac{M_{i0}}{W_i} - 2 \frac{R_k}{F_i} - 4 \frac{R_{k+1}}{F_i}. \end{aligned} \right\} \quad (11.6)$$

The deformations at the common edge of two adjacent plates have to be equal. If this compatibility condition is expressed in terms of stresses and written for the edge k , it becomes:

$$+\frac{M_{i-10}}{W_{i-1}} - 2 \frac{R_{k-1}}{F_{i-1}} - 4 \frac{R_k}{F_{i-1}} = -\frac{M_{i0}}{W_i} + 4 \frac{R_k}{F_i} + 2 \frac{R_{k+1}}{F_i}$$

or, if rearranged with respect to the unknown edge forces:

$$R_{k-1} \frac{1}{F_{i-1}} + R_k \frac{1}{F_{i-1}} \left(\frac{1}{F_{i-1}} + \frac{1}{F_i} \right) + R_{k+1} \frac{1}{F_i} = \frac{1}{2} \left(\frac{M_{i-10}}{W_{i-1}} + \frac{M_{i0}}{W_i} \right) \quad (11.7)$$

$$\left(\begin{array}{cccccc} k: & 1 & 3 & 5 & \dots & \text{edges} \\ i: & 2 & 4 & 6 & \dots & \text{plates} \end{array} \right).$$

If this compatibility condition is formulated for each edge, one ends up with a system of as many equations as there are unknown edge forces. The solutions of this system of equations must be introduced into Eqs. (11.6) in order to arrive at the edge stresses in all plates of the structure.

b) Three-Stress Equations

The defining system of equations for a folded plate may as well be written in terms of unknown edge stresses instead of edge forces. This may be accomplished if the Eqs. (11.6) are first solved for R_k and R_{k+1}

$$\left. \begin{aligned} R_k &= \frac{F_i}{6} \left(\frac{M_{i0}}{W_i} + 2\sigma_k + \sigma_{k+1} \right) \\ R_{k+1} &= \frac{F_i}{6} \left(\frac{M_{i0}}{W_i} - \sigma_k - 2\sigma_{k+1} \right) \end{aligned} \right\} \quad (11.8)$$

and if afterwards the two adjacent edge forces of each edge are made to be equal.

The compatibility condition becomes, if formulated for the edge k :

$$\frac{F_{i-1}}{6} \left(\frac{M_{i-10}}{W_{i-1}} - \sigma_{k-1} - 2\sigma_k \right) = \frac{F_i}{6} \left(\frac{M_{i0}}{W_i} + 2\sigma_k + \sigma_{k+1} \right).$$

If rearranged with respect to the unknown edge shears, this condition reduces to the required three-stress equation.

$$\sigma_{k-1} F_{i-1} + \sigma_k 2(F_{i-1} + F_i) + \sigma_{k+1} F_i = \frac{M_{i-10}}{W_{i-1}} F_{i-1} - \frac{M_{i0}}{W_i} F_i. \quad (11.9)$$

$$\begin{pmatrix} k: & 1 & 3 & 5 & \dots \text{edges} \\ i: & 2 & 4 & 6 & \dots \text{plates} \end{pmatrix}$$

A folded plate may therefore be analyzed either by means of the three-shear equations (11.7) or the three-stress equations (11.9). The first system yields the edge forces at once and the stresses are found after evaluating the additional expressions (11.6). The solution of the second system, on the other hand, leads directly to the quantities which are of prime interest, the stresses, and the edge forces follow thereafter from Eqs. (11.8).

The number of unknowns in the two systems of equations (11.7) and (11.9) is not necessarily equal. In the case of an open cross section, the system (11.9) which immediately yields the stresses has two more unknowns than the system (11.7) because the vanishing edge forces at the free boundaries are known in advance. If the cross section is closed, however, both systems have as many unknowns as there are plane plates.

e) Example

The two methods of analysis discussed above will now be applied to a folded plate whose cross section is shown in Fig. 11.3.

The system (11.7) written for the edges 3, 5 and 7 looks as follows:

$$R_3 2 \left(\frac{1}{F_2} + \frac{1}{F_4} \right) + R_5 \frac{1}{F_4} = 0,$$

$$R_3 \frac{1}{F_4} + R_5 2 \left(\frac{1}{F_4} + \frac{1}{F_6} \right) + R_7 \frac{1}{F_6} = 0,$$

$$R_5 \frac{1}{F_6} + R_7 2 \left(\frac{1}{F_6} + \frac{1}{F_8} \right) = \frac{1}{2} \frac{M_{80}}{W_8}.$$

Introducing the properties of the individual plates (v. Fig. 11.3)

$$F_2 = F_8 = ct = F_0,$$

$$F_4 = F_6 = \frac{5}{3} c \cdot \frac{3}{5} t = F_0,$$

$$W_8 = \frac{tc^2}{6} = \frac{F_0 c}{6}$$

one arrives at the following solutions to the given system of equations:

$$\begin{aligned} R_3 &= +\frac{1}{112} \frac{F_0}{W_8} M_{80} = +\frac{3}{56} \frac{M_{80}}{c}, \\ R_5 &= -\frac{4}{112} \frac{F_0}{W_8} M_{80} = -\frac{3}{14} \frac{M_{80}}{c}, \quad (11.10) \\ R_7 &= +\frac{15}{112} \frac{F_0}{W_8} M_{80} = +\frac{45}{56} \frac{M_{80}}{c}. \end{aligned}$$

The axial stresses in the edges of the folded plate follow from Eqs. (11.6).

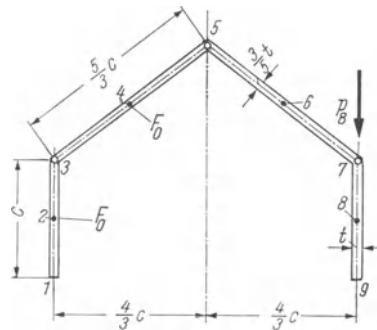


Fig. 11.3. Cross Section of the Folded Plate Used in the Example.

$$\begin{aligned} \sigma_1 &= +\frac{1}{56} \frac{M_{80}}{W} = +\frac{3}{28} \frac{M_{80}}{c F_0}, \\ \sigma_3 &= -\frac{1}{28} \frac{M_{80}}{W} = -\frac{3}{14} \frac{M_{80}}{c F_0}, \\ \sigma_5 &= +\frac{1}{8} \frac{M_{80}}{W} = +\frac{3}{4} \frac{M_{80}}{c F_0}, \quad (11.11) \\ \sigma_7 &= -\frac{13}{28} \frac{M_{80}}{W} = -\frac{39}{14} \frac{M_{80}}{c F_0}, \\ \sigma_9 &= +\frac{41}{56} \frac{M_{80}}{W} = +\frac{123}{28} \frac{M_{80}}{c F_0}. \end{aligned}$$

The same values for the axial stresses could have been calculated immediately from the system (11.9) which, when applied to this example, becomes:

$$\begin{aligned} \sigma_1 2F_2 + \sigma_3 F_2 &= 0, \\ \sigma_1 F_1 + \sigma_3 2(F_2 + F_4) + \sigma_5 F_4 &= 0, \\ \sigma_3 F_4 + \sigma_5 2(F_4 + F_6) + \sigma_7 F_6 &= 0, \\ \sigma_5 F_6 + \sigma_7 2(F_6 + F_8) + \sigma_9 F_8 &= -\frac{F_8}{W_8} M_{80}, \\ \sigma_7 F_8 + \sigma_9 2F_8 &= +\frac{F_8}{W_8} M_{80}. \end{aligned}$$

The edge forces may be calculated from the solutions to this system of equations by means of Eqs. (11.8). Of course, the results must be equivalent to those given above (11.10).

11.2 Equivalent Load System

a) Components in the Plane of the Plates

It was assumed in this analysis of a folded plate that the applied loads act in the planes of the plates. If this is not true, it is necessary to determine the reactions of the individual plates at the hinges by consideration of a transverse strip of each plate. The effect of these reactions is then resolved into loads acting in the plane of the plates. The latter, finally, lead to the desired bending moments M_{i0} in each plate.

If, for instance, the folded plate shown in Fig. 11.1 is assumed to have the same cross section as shown in Fig. 11.3, the following bending moments would have to be introduced for a stress analysis at mid-span:

$$\begin{aligned} M_{20} &= 0, \\ M_{40} &= -\frac{5}{6} P \frac{l}{4}, \\ M_{60} &= +\frac{5}{6} P \frac{l}{4}, \\ M_{80} &= 0. \end{aligned} \tag{11.12}$$

b) Separation of Variables

The stresses in a thin-walled, prismatic structure may be expressed as functions of the two coordinates s and z . The curvilinear coordinate s defines a position

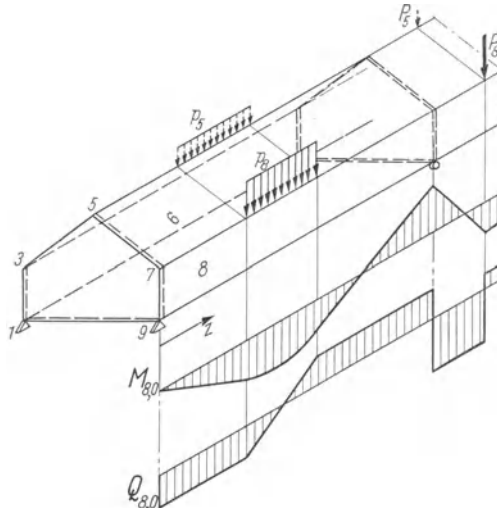


Fig. 11.4. Affinitive Load.

in the transverse direction while the coordinate z determines the position of a cross section in the longitudinal direction.

So far, no assumption has been made concerning the variation of the load in a longitudinal direction. A possible assumption for the disposition of the load on a folded plate with the cross section of Fig. 11.3 is shown in Fig. 11.4. The presentation in this figure is restricted to the end-span of a continuous folded-plate structure. It shows further the moment diagram M_{80} and the shear diagram Q_{80} for the indicated loads.

Since it is clearly apparent that it isn't necessary to know the z -dependent quantities in order to calculate the stress distribution over the cross section, the independent variables s and z in the expressions for the stresses may be separated. This property may be expressed as follows:

$$\text{Res} = f_1(s) \cdot f_2(z).$$

Such functions $f_1(s)$ and $f_2(z)$ for the specific example described above are plotted in Fig. 11.5 for the axial stresses and in Fig. 11.6 for the shear stresses.

c) Affinitive Loads

It may be seen from the systems (11.7) and (11.9) that an arbitrary external moment M_{i0} may be attributed to any plate i .

This simple analysis, however, is only applicable if the deformations of the plates are compatible to each other. This requires that both the loads and the edge forces are affinitive to each other. This requirement is satisfied by the loads shown in Fig. 11.4.

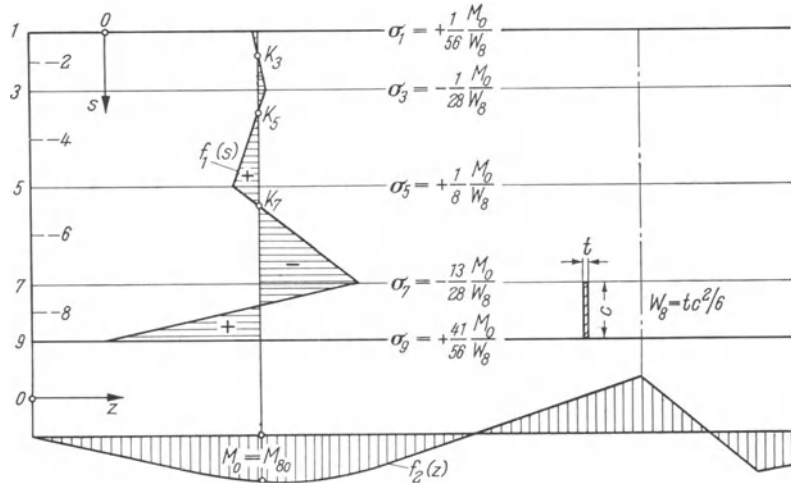


Fig. 11.5. Distribution of the Axial Stresses in Longitudinal and Transverse Direction Presented at the Developed Folded Plate of Figs. 11.3 and 11.4.

If there exists affinity among the loads and therefore among the plate moments M_{i0} , the latter may be expressed in terms of a common moment distribution M_0 and an individual coefficient μ_i which expresses the relation between

the moment M_{i0} and the reference moment M_0 :

$$M_{i0} = \mu_i M_0. \quad (11.13)$$

The solutions to the systems of equations may be written similarly in terms of M_0 as common factor.

In order to express both the systems of equations and their solutions in a nondimensional manner, the dimensions of the structure will refer to those of a reference plate with the width c , the thickness t and the cross-sectional area F . Therefore:

$$\begin{aligned} F &= ct, \\ W &= \frac{cF}{6}. \end{aligned} \quad (11.14)$$

The edge forces R_k and the axial stresses σ_k may now be written in terms of the reference quantities M_0 , c , F and the nondimensional parameters \varkappa_k and λ_k .

$$R_k = \varkappa_k \frac{M_0}{c}, \quad (11.15)$$

$$\sigma_k = \lambda_k \frac{M_0}{W} = \lambda_k \frac{6M_0}{cF}, \quad (11.16)$$

If the loads do not satisfy the condition of affinity, they must be divided into affinitive groups leading to separate states of stresses which thereafter may be superimposed. If of the loads p_5 , p_8 , P_5 and P_8 in Fig. 11.4 the ratio between p_5 and p_8 is different from the ratio between P_5 and P_8 , it is necessary to analyze separately the effect of two different load arrangements, either of (p_5, p_8) and (P_5, P_8) or of (p_5, P_5) and (p_8, P_8) .

It must be noted finally that the supports of all plates must be equivalent. In the example of Fig. 11.4, this is accomplished by means of diaphragms. Rigid cross frames would serve the same purpose. They prevent deflections of the plates in their planes but do not impose any other restraint. It would drastically complicate the analysis if, for example, a support were placed on the line of action of the load P_8 in Fig. 11.4. In such a case, the reaction would have to be introduced as a redundant quantity to be determined from a compatibility condition.

11.3 Shear Stresses

a) General Analysis

It is assumed that the edge forces and the axial stresses do already exist in the form of Eqs. (11.15) and (11.16), i.e. the coefficients \varkappa and λ are already calculated.

The shear flow along the edge k according to Eq. (11.1) is defined as:

$$q_k = \frac{dR_k}{dz}, \quad (11.17)$$

which means that in view of Eq. (11.15) known values \varkappa_k determine the values of the shear flows q_k as well:

$$\frac{dR_k}{dz} = \varkappa_k \frac{Q_0}{c},$$

therefore

$$q_k (= \tau t) = \varkappa_k \frac{Q_0}{c}. \quad (11.18)$$

The shear flows along the edges are therefore proportional to the reference shear diagram Q_0 .

The shear flow at a point on plate i which is at a distance away from edge k follows now from the well-known equilibrium condition for a small rectangular plate element. It is equal to the shear flow q_k at the boundary reduced by the total change in axial stress between the edge and s' [v. Eq. (5.17)].

$$q(s', z) = q_k(z) - \int_0^{s'} \frac{\partial \sigma}{\partial z} t \, ds'. \quad (11.19)$$

Since the axial stresses are linearly distributed over the width of each plate segment,

$$\sigma_i(s', z) = \left[\lambda_k + (\lambda_{k+1} - \lambda_k) \frac{s'}{c_i} \right] \frac{M_0(z)}{W}, \quad (11.20)$$

their integration for constant wall thickness t yields a second order polynomial in s' . The distribution of the shear stresses is therefore parabolic with the initial value q_k for $s' = 0$ and the value q_{k+1} for $s' = c_i$.

Calculation of the shear flow at the center of the plate will therefore completely determine the distribution of the shear flows in plate i . The integration of Eq. (11.19) from $s' = 0$ to $s' = \frac{c_i}{2}$ assuming the linear distribution of Eq. (11.20) yields the following value for the shear flow in the center of plate i :

$$q_i = q_k - F_i \frac{3\lambda_k + \lambda_{k+1}}{8} \frac{Q_0}{W}. \quad (11.21 \text{ a})$$

If q_k is introduced as given by Eq. (11.18) and if one observes the transformations (11.14), Eq. (11.21 a) may be written in the following alternate form:

$$q_i = \left[\varkappa_k - (3\lambda_k + \lambda_{k+1}) \frac{3}{4} \frac{F_i}{F} \right] \frac{Q_0}{c_i}. \quad (11.21 \text{ b})$$

If the three-shear equations are not used for the analysis of a folded plate, the derivatives of the edge forces are of primary interest rather than the forces.

The derivative of Eqs. (11.8) with respect to z , the notations defined in Eqs. (11.13) to (11.16) and Eq. (11.21 b) lead therefore to the following set of

Table 11.1. Shear Flows and Shear Stresses for the Example of Fig. 11.3

Reference	Fig. 11.3		Eq. (11.10)	Eq. (11.11)	Eq. (11.18) Eq. (11.22)	$\tau = q/t$
Notation	c_i	t_i	α_k	λ_k	q	$\tau_{k,i}, \tau_i, \tau_{k+1,i}$
Dim. or Multipl.	c	t			$\frac{Q_0}{c}$	$\frac{Q_0}{ct}$
1				$+\frac{1}{56}$	0	0
2	1	1			$-\frac{3}{224}$	$-\frac{3}{224}$
3			$+\frac{3}{56}$	$-\frac{1}{28}$	$+\frac{3}{56}$	$+\frac{5}{56}$
4	$\frac{5}{3}$	$\frac{3}{5}$			$+\frac{9}{224}$	$+\frac{15}{224}$
5			$-\frac{3}{14}$	$+\frac{1}{8}$	$-\frac{3}{16}$	$-\frac{5}{16}$
6	$\frac{5}{3}$	$\frac{3}{5}$			$-\frac{33}{224}$	$-\frac{55}{224}$
7			$+\frac{45}{56}$	$-\frac{13}{28}$	$+\frac{45}{56}$	$+\frac{45}{56}$
8	1	1			$+\frac{291}{224}$	$+\frac{291}{224}$
9				$+\frac{41}{56}$	0	0

Presented in

Fig. 11.6a

Fig. 11.6b

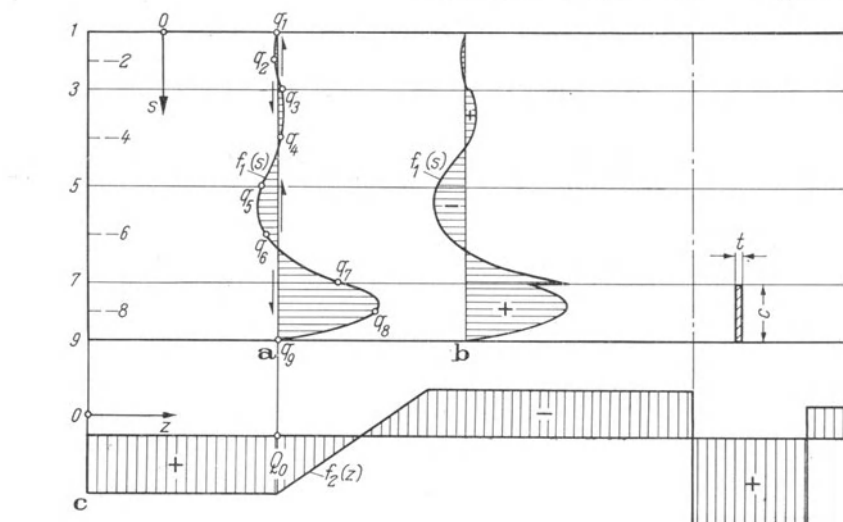


Fig. 11.6. Distribution of the Shear Flows (a), the Shear Stresses (b) in Transverse Direction and (c) in Longitudinal Direction Presented at the Developed Folded Plate of Fig. 11.3 and 11.4.

expressions for the direct evaluation of the shear flows from the axial stresses:

$$\begin{aligned} q_k &= \left[\mu_i + (2\lambda_k + \lambda_{k+1}) \frac{F_i}{F} \right] \frac{Q_0}{c}, \\ q_i &= \left[\mu_i + \frac{1}{4} (-\lambda_k + \lambda_{k+1}) \frac{F_i}{F} \right] \frac{Q_0}{c}, \\ q_{k+1} &= \left[\mu_i - (\lambda_k + 2\lambda_{k+1}) \frac{F_i}{F} \right] \frac{Q_0}{c}. \end{aligned} \quad (11.22)$$

Herein are:

- μ_i Ratio between the load in plate i and the reference load,
- λ_k, λ_{k+1} Nondimensional axial stresses according to Eq. (11.16),
- F_i Cross-sectional area of plate i ,
- F, c Cross-sectional area and width of the reference plate,
- Q_0 Shearing force due to the reference load.

Exercise 11.1. Verify by means of Simpson's rule that the resultant of the shear flows in plate i as defined by Eqs. (11.22) assumes the value $\mu_i \frac{Q_0}{c}$.

b) Example

The example discussed in Section 11.1c will now be analyzed with respect to shear stresses. If plate 8 is selected to be the reference plate, the values for α may immediately be taken from the solutions (11.10) and those for λ from the results (11.11). Both sets of values are listed once again in the second and third column of Table 11.1.

Eq. (11.18) is applied to calculate the shear flows at the edges k while those at the centers of the plates i follow from Eq. (11.22). The resulting distribution of the shear flow is plotted in Fig. 11.6a.

The shear stress, finally, is equal to the shear flow divided by the plate thickness t_i (last column of Table 11.1 and Fig. 11.6b).

11.4 General Formulation

a) Plates of Variable Thickness and with Protruding Portions

The three-shear equations and three-stress equations in Section 11.1 were derived under the assumption that all plates have thin rectangular cross sections and that they are connected to adjacent plates along their longitudinal edges.

Both assumptions shall be dropped hereinafter. Fig. 11.7 illustrates a plate i that is not only of variable thickness but also extends beyond the hinges connecting the adjacent plates.

The considerations which led to the basic relations for the special case treated above remain essentially the same. Only the formulation of the different elements in the expressions becomes more complicated since two parameters per plate (cross-sectional area F_i and section modulus W_i) are no longer sufficient to com-

pletely characterize the structure. The following four independent properties are selected to describe plate i :

I_i Moment of inertia of plate i ,

F_i Cross-sectional area of plate i ,

a_i Distance between the hinge of the previous plate and the center line of plate i ,

b_i Distance between the hinge of the subsequent plate and the center line of plate i .

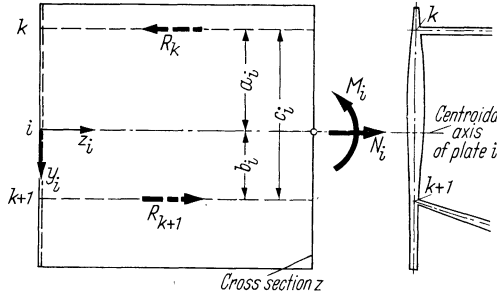


Fig. 11.7. General Shape of Plate i .

If no contiguous plate precedes or follows plate i , the distances a_i and b_i respectively may be assumed as the distance from the centroidal axis to the plate boundary or to any other line in which the stresses are of particular interest.

The distance between the two hinges of plate i will be denoted by $c_i = a_i + b_i$.

b) Axial Forces

As a further generalization, axial forces N_{i0} resulting from applied loads will be included in the analysis. The eccentricity e_i of the force N_{i0} in plate i is described by the coordinate y_i of the line of action both with respect to magnitude and sign. Tension is assumed to be positive. Both the force N_{i0} and its eccentricity e_i may be variable in z .

For the purpose of a stress analysis, the eccentric axial force N_{i0} is resolved into a bending moment $e_i N_{i0}$ and a force N_{i0} at the centroid of the cross section.

This eccentric axial force always occurs in prestressed constructions where the load V_i applied by the cables is negative. The effect of prestressing is therefore analyzed by means of the following forces at the center of the cross section:

$$\begin{aligned} M_{i0} &= -V_i e_i, \\ N_{i0} &= -V_i. \end{aligned} \quad (11.23)$$

The eccentricity e_i is positive whenever the cable lies in the part of the cross section with the greater edge number.

c) Formulation of Expressions for the Axial Stresses and Shear Stresses

The definition of the edge forces R_k (11.1) and of the bending moment M_{i0} caused by external loads in the plane of plate i is not affected by the generalization of the problem. The modified relations for the internal forces originally

given by Eqs. (11.2) and (11.3), however, are as follows:

$$\begin{aligned} M_i &= M_{i0} - a_i R_k - b_i R_{k+1}, \\ N_i &= N_{i0} + R_k - R_{k+1}. \end{aligned} \quad (11.24)$$

These lead to the following expression for the *axial stresses* in plate i :

$$\sigma_i(y_i, z) = \frac{M_{i0} - a_i R_k - b_i R_{k+1}}{I_i} y_i + \frac{N_{i0} + R_k - R_{k+1}}{F_i}. \quad (11.25)$$

The change of this stress along a prismatic member is:

$$\frac{\partial \sigma_i}{\partial z} = \frac{\frac{dM_{i0}}{dz} - a_i q_k - b_i q_{k+1}}{I_i} y_i + \frac{\frac{dN_{i0}}{dz} + q_k - q_{k+1}}{F_i}.$$

The derivative of the moment M_{i0} in the case of pure transverse load $dM_{i0}/dz = +Q_{i0}$, i.e. is equal to the shear for this load. The same derivative for the “prestressing” load (if changes in the cable force and therefore friction losses are neglected), is approximately equal to:

$$\begin{aligned} Q_{i0} &= \frac{dM_{i0}}{dz} \cong -V_i \sin \alpha \\ \frac{dN_i}{dz} &\cong 0. \end{aligned} \quad (11.26)$$

The angle α represents the slope of the cable axis with respect to the longitudinal axis of plate i . It is positive if the eccentricity of the cable is increasing with increasing coordinate z .

The subsequent calculation of shear stresses assumes further a constant value for the axial force N_{i0} , i.e. $dN_{i0}/dz = 0$.

If the statical moment of the cut-off portion of the plate cross section between the boundary y_{-r} and the section y is denoted by \tilde{S}_i and the corresponding cross-sectorial area by \tilde{F}_i

$$\tilde{S}_i = \int_{y_{-r}}^{y_i} y_i dF_i, \quad \tilde{F}_i = \int_{y_{-r}}^{y_i} dF_i, \quad (11.27 \text{a and b})$$

the shear flow in plate i according to Eq. (11.19) may be defined as follows:

Cantilever portion beyond the hinge k (i.e. for $y_i < -a_i$):

$$q(y_i, z) = \bar{q}_i \quad (11.28 \text{a})$$

Portion between the hinges k and $k + 1$ (i.e. for $-a_i < y_i < +b_i$):

$$q(y_i, z) = \bar{q}_i + q_k. \quad (11.28 \text{b})$$

Cantilever portion beyond the hinge $k + 1$ (i.e. for $y_i > +b_i$):

$$q(y, z) = \bar{q}_i + q_k - q_{k+1}. \quad (11.28 \text{c})$$

These three relations are written in terms of \bar{q}_i which is given by the expression:

$$\bar{q}_i = -\frac{Q_{i0} - a_i q_k - b_i q_{k+1}}{I_i} \tilde{S}_i - \frac{q_k - q_{k+1}}{F_i} \tilde{F}_i. \quad (11.28 \text{d})$$

The shear flow at the plate boundary y_{+p} becomes zero as well as at the boundary y_{-p} . This may be immediately confirmed if the value of Eq. (11.28) for $\bar{S}_i = 0$ and $\bar{F}_i = F_i$ is introduced into Eq. (11.28c).

The shear stresses τ follow from the shear flows q in the usual manner, $\tau = q/t$.

d) Three-Shear and Three-Stress Equations

If Eq. (11.25) is first written for $y_i = -a_i$ and afterwards for $y_i = +b_i$, one arrives at the following more general version of Eqs. (11.6) for the axial stresses in the edges k and $k+1$:

$$\left\{ \begin{array}{l} \sigma_k = -M_{i0} \frac{a_i}{I_i} + R_k \left(\frac{a_i^2}{I_i} + \frac{1}{F_i} \right) + R_{k+1} \left(\frac{a_i b_i}{I_i} - \frac{1}{F_i} \right) \\ \sigma_{k+1} = +M_{i0} \frac{b_i}{I_i} - R_k \left(\frac{a_i b_i}{I_i} - \frac{1}{F_i} \right) - R_{k+1} \left(\frac{b_i^2}{I_i} + \frac{1}{F_i} \right) \end{array} \right\} \quad (11.29)$$

The subsequent three-shear equations for the unknown edge forces again follow from the conditions requiring compatible edge deformations and therefore equal stresses.

$$\begin{aligned} R_{k-1} \left(\frac{a_{i-1} b_{i-1}}{I_{i-1}} - \frac{1}{F_{i-1}} \right) + R_k \left(\frac{b_{i-1}^2}{I_{i-1}} + \frac{a_i^2}{I_i} + \frac{1}{F_{i-1}} + \frac{1}{F_i} \right) + R_{k+1} \left(\frac{a_i b_i}{I_i} - \frac{1}{F_i} \right) \\ = +M_{i-10} \frac{b_{i-1}}{I_{i-1}} + M_{i0} \frac{a_i}{I_i} \end{aligned} \quad (11.30)$$

$$(k = 1, 3, 5, \dots,$$

$$i = 2, 4, 6, \dots)$$

This system of equations becomes equivalent to the system (11.7) if the plates are connected to each other at their longitudinal edges.

In order to formulate the three-stress equations, the edge forces R_k and R_{k+1} must first be calculated explicitly from Eqs. (11.29).

$$\left\{ \begin{array}{l} R_k = \frac{M_{i0}}{a_i + b_i} + \sigma_k \frac{b_i^2 F_i + I_i}{(a_i + b_i)^2} + \sigma_{k+1} \frac{a_i b_i F_i - I_i}{(a_i + b_i)^2} \\ R_{k+1} = \frac{M_{i0}}{a_i + b_i} - \sigma_k \frac{a_i b_i F_i - I_i}{(a_i + b_i)^2} - \sigma_{k+1} \frac{a_i^2 F_i + I_i}{(a_i + b_i)^2} \end{array} \right\} \quad (11.31)$$

If these edge forces are subsequently equated at common edges, the following more general three-stress equations are arrived at:

$$\begin{aligned} \sigma_{k-1} \frac{a_{i-1} b_{i-1} F_{i-1} - I_{i-1}}{(a_{i-1} + b_{i-1})^2} + \sigma_k \left(\frac{a_{i-1}^2 F_{i-1} + I_{i-1}}{(a_{i-1} + b_{i-1})^2} + \frac{b_i^2 F_i + I_i}{(a_i + b_i)^2} \right) + \sigma_{k+1} \frac{a_i b_i F_i - I_i}{(a_i + b_i)^2} \\ = +\frac{M_{i-10}}{a_{i-1} + b_{i-1}} - \frac{M_{i0}}{a_i + b_i} \end{aligned} \quad (11.32)$$

$$(k = 1, 3, 5, \dots,$$

$$i = 2, 4, 6, \dots)$$

e) Example

Fig. 11.8 shows a symmetric bridge cross section which at the top of the right main girder is acted upon by an arbitrary system of loads.

In accordance with the above considerations, this cross section consists basically of only three plates, 2, 4 and 6. The first and the last are of variable thickness while the intermediate plate stretches beyond the two connecting hinges.

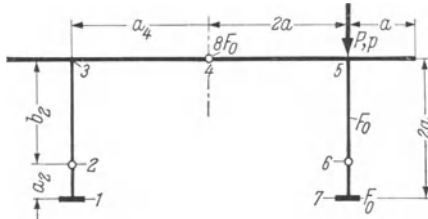


Fig. 11.8. Bridge Cross Section.

thickness while the intermediate plate stretches beyond the two connecting hinges.

The three plates are characterized by the following values:

Plate 2:

$$\begin{aligned} a_2 &= \frac{1}{2} a, & b_2 &= \frac{3}{2} a, \\ F_2 &= 2F_0, \\ I_2 &= \frac{5}{6} a^2 F_0. \end{aligned}$$

Plate 4:

$$\begin{aligned} a_4 &= 2a, & b_4 &= 2a, \\ F_4 &= 8F_0, \\ I_4 &= 24a^2 F_0. \end{aligned}$$

Plate 6:

$$\begin{aligned} a_6 &= \frac{3}{2} a, & b_6 &= \frac{1}{2} a, \\ F_6 &= 2F_0, \\ I_6 &= \frac{5}{6} a^2 F_0. \end{aligned}$$

If the bending moment for the load shown in Fig. 11.8 is denoted by M_0 , the bending moments in the plates in terms of this reference moment are:

$$M_{20} = M_{40} = 0,$$

$$M_{60} = +M_0.$$

(11.34)

Since there are only two unknown edge forces (R_3 and R_5), the system (11.30) reduces to two equations with two unknowns:

$$\begin{aligned} R_3 \left(\frac{b_2^2}{I_2} + \frac{a_4^2}{I_4} + \frac{1}{F_2} + \frac{1}{F_4} \right) + R_5 \left(\frac{a_4 b_4}{I_4} - \frac{1}{F_4} \right) &= M_{20} \frac{b_2}{I_2} + M_{40} \frac{a_4}{I_4}, \\ R_3 \left(\frac{a_4 b_4}{I_4} - \frac{1}{F_4} \right) + R_5 \left(\frac{b_4^2}{I_4} + \frac{a_6^2}{I_6} + \frac{1}{F_4} + \frac{1}{F_6} \right) &= M_{40} \frac{b_4}{I_4} + M_{60} \frac{a_6}{I_6}. \end{aligned}$$

The solutions of this system for the plate properties (11.33) and the load definition (11.34) are as follows:

$$\begin{aligned} R_3 &= -\frac{15}{2 \cdot 23 \cdot 53} \frac{M_0}{a}, \\ R_5 &= +\frac{3 \cdot 419}{2 \cdot 23 \cdot 53} \frac{M_0}{a}. \end{aligned} \quad (11.35)$$

These solutions determine the axial stresses in the edges 1, 3, 5 and 7 by means of Eq. (11.29)

$$\left. \begin{aligned} \sigma_1 &= -\frac{3}{23 \cdot 53} \frac{M_0}{a F_0}, \\ \sigma_3 &= +\frac{24}{23 \cdot 53} \frac{M_0}{a F_0}, \\ \sigma_5 &= -\frac{183}{23 \cdot 53} \frac{M_0}{a F_0}, \\ \sigma_7 &= +\frac{480}{23 \cdot 53} \frac{M_0}{a F_0}. \end{aligned} \right\} \quad (11.36)$$

In order to verify these values, they shall subsequently be determined from the three-stress equations (11.32). The coefficients of the three-stress equations and the matrix of the system for this particular example are as follows:

$$\begin{array}{lll} \frac{a_i b_i F_i - I_i}{(a_i + b_i)^2} & \frac{a_i^2 F_i}{(a_i + b_i)^2} & \frac{b_i^2 F_i + I_i}{(a_i + b_i)^2} \\ \text{Plate 2 } (i=2): & \frac{1}{6} F_0 & \frac{1}{3} F_0 & \frac{4}{3} F_0 \\ \text{Plate 4 } (i=4): & \frac{1}{2} F_0 & \frac{7}{2} F_0 & \frac{7}{2} F_0 \\ \text{Plate 6 } (i=6): & \frac{1}{6} F_0 & \frac{4}{3} F_0 & \frac{1}{3} F_0 \end{array}$$

$$\left. \begin{array}{l} \sigma_1 \quad \sigma_3 \quad \sigma_5 \quad \sigma_7 \\ \frac{4}{3} F_0 \quad \frac{1}{6} F_0 \quad \quad \quad = 0 \\ \frac{1}{6} F_0 \quad \left(\frac{1}{3} + \frac{7}{2} \right) F_0 \quad \frac{1}{2} F_0 \quad = 0 \\ \frac{1}{2} F_0 \quad \left(\frac{7}{2} + \frac{1}{3} \right) F_0 \quad \frac{1}{6} F_0 \quad = -\frac{M_0}{2a} \\ \frac{1}{6} F_0 \quad \frac{4}{3} F_0 \quad \quad \quad = +\frac{M_0}{2a} \end{array} \right\} \quad (11.37a)$$

Eqs. (11.37) may be reduced to the system

$$\left. \begin{array}{l} \sigma_1 \quad \sigma_3 \quad \sigma_5 \quad \sigma_7 \\ 8 \quad 1 \quad \quad \quad = 0 \\ 1 \quad 23 \quad 3 \quad = 0 \\ \quad 3 \quad 23 \quad 1 \quad = -3 \frac{M_0}{a F_0} \\ \quad \quad 1 \quad 8 \quad = +3 \frac{M_0}{a F_0} \end{array} \right\} \quad (11.37b)$$

which is in fact satisfied by the solutions (11.36).

f) Deformations

The curvature v'' ; of each plate i may be calculated from the distribution of the axial stresses. It is equal to the difference of the edge strains, $\varepsilon_{k+1} - \varepsilon_k$, divided by their distance, $a_i + b_i = c_i$.

$$v''_i = -\frac{\sigma_{k+1} - \sigma_k}{E c_i}. \quad (11.38)$$

The integration of this differential equation with respect to certain boundary conditions would yield the deflection of plate i . However, the relationship to existing well known expressions for deflections due to bending is readily developed.

Since

$$v''_i = -\frac{M_i}{E I_i}$$

the comparison with Eq. (11.38) leads to

$$\frac{M_i}{I_i} = -\frac{\sigma_{k+1} - \sigma_k}{c_i}. \quad (11.39)$$

In order to apply well-known deflection formulas to this problem, their factor M/I needs only to be replaced by $A\sigma_i/c_i$.

If the deflection of one plate is known, the deflections of the remaining plates may be calculated therefrom. The ratio between the deflections of two different plates is, because of the required affinity between the loads and the equivalence of the supports, equal to the ratio between the corresponding curvatures

$$\frac{v_i}{v_{i+1}} = \frac{\sigma_{k+1} - \sigma_k}{\sigma_{k+2} - \sigma_{k+1}} \cdot \frac{c_{i+1}}{c_i}. \quad (11.40)$$

The deflections of a simply supported, single-span folded plate under uniformly distributed load and concentrated load will hereinafter be given as an example.

1. Uniformly distributed load p along the span of length l :

$$\text{max. deflection} = \frac{5}{384} \frac{pl^4}{EI} = \frac{pl^2}{8I} \cdot \frac{5l^2}{48E}$$

thus

$$\max v_i = \frac{\sigma_{k+1} - \sigma_k}{c_i} \frac{5l^2}{48E}. \quad (11.41)$$

2. Concentrated load at the position

$$\zeta = \frac{z}{l} \quad \text{resp.} \quad \zeta' = \frac{z'}{l}:$$

Deflection v at the positions $\alpha = \frac{a}{l}$ and $\beta = \frac{b}{l}$, respectively:

$$v = \begin{cases} \frac{Paz'}{lI} \cdot \frac{l^2}{6E} (1 - \alpha^2 - \zeta'^2) & \text{for } \alpha \leq \zeta, \\ \frac{Pzb}{lI} \cdot \frac{l^2}{6E} (1 - \beta^2 - \zeta^2) & \text{for } \alpha \geq \zeta, \end{cases}$$

thus

$$v_i = \begin{cases} \frac{\Delta\sigma_i}{c_i} \cdot \frac{l^2}{6E} (1 - \alpha^2 - \zeta'^2) & \text{for } \alpha \leq \zeta, \\ \frac{\Delta\sigma_i}{c_i} \cdot \frac{l^2}{6E} (1 - \beta^2 - \zeta^2) & \text{for } \alpha \geq \zeta. \end{cases} \quad (11.42)$$

Deflection at the position of the concentrated load, $\zeta = \alpha, \zeta' = \beta$:

$$v_i = \frac{\sigma_{k+1} - \sigma_k}{c_i} \cdot \frac{l^2}{3E} \alpha \beta, \quad (11.43 \text{ a})$$

and if the load is furthermore acting at mid-span ($\alpha = \beta = 1/2$):

$$v_i = \frac{\sigma_{k+1} - \sigma_k}{c_i} \frac{l^2}{12E}. \quad (11.43 \text{ b})$$

Consider again as an example the cross section shown in Fig. 11.3. If the deflection of the plate 8 at the position z is denoted by v_8 , the deflections of the remaining

plates in the same point may be derived from Eq. (11.40) considering the results (11.11).

$$\frac{v_6}{v_8} = \frac{-\frac{39}{14} - \frac{3}{4}}{\frac{123}{28} + \frac{39}{14}} \cdot \frac{c}{\frac{5}{3}c} = -\frac{99}{335},$$

$$\frac{v_4}{v_8} = \frac{\frac{3}{4} + \frac{3}{14}}{\frac{123}{28} + \frac{39}{14}} \cdot \frac{c}{\frac{5}{3}c} = +\frac{27}{335},$$

$$\frac{v_2}{v_8} = \frac{-\frac{3}{14} - \frac{3}{28}}{\frac{123}{28} + \frac{39}{14}} \cdot \frac{c}{c} = -\frac{15}{335}.$$

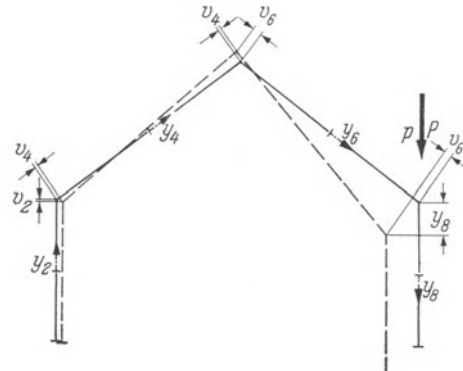


Fig. 11.9. Deformation of the Folded Plate
Defined in Fig. 11.3.

A deflection v is positive whenever pointing towards the higher numbered edge member. Fig. 11.9 visualizes the relative deformations calculated above.

12 Core Point Method

12.1 Introduction

a) Different Methods of Solution

The three-element equations which were derived for the analysis of a folded plate are very similar to the three-moment equations for a continuous beam. There are therefore as many possible methods of solution as there are methods to solve the three-moment equations. There exists, for instance, a stress distribution method in complete analogy to the moment distribution method¹.

This chapter presents a semi-graphical method which was developed by K. BASLER while attending a course of Prof. B. THÜRLIMANN² at the Lehigh University, Bethlehem, Pa. This method has its continuous-beam analogy in the fixed-point method of Prof. M. RITTER³.

The core point method uses the two boundary points of the core on the center line of a plate cross section. These two points correspond to the two fixed points in each span of a continuous beam. In a manner analogous to the decay of the moments by means of straight lines through fixed points, the attenuation of the

¹ WINTER, G., and M. PEI: Hipped Plate Construction. J. Amer. Concrete Inst. **43** (1947).

² THÜRLIMANN, B.: Selected Topics in Concrete Structures. Lecture Notes, Course C.E. 411, Lehigh University, Bethlehem, Pa., 1958.

³ e.g. Repetitorium der Vorlesung Massivbau von Prof. Dr. M. RITTER, ETH, Zürich: AIV-Verlag.

axial stresses follows straight lines through the core points. Both cases assume that external loads act on only one span or plate at the same time.

These semi-graphical methods have the advantage of facilitating the visualization of the moment or stress distribution and thus allowing quick estimates without the need to solve the complete system of defining equations.

b) Introductory Example

The folded plate having the cross section shown in Fig. 11.3 will again be used to illustrate the fundamental concepts of this method. Plate 8 is again the only one acted upon by an external load.

Plate 2 is first thought to be separated from the adjacent plate 4 (v. Fig. 12.1 a). The only force acting on plate 2 is the edge force R_3 which represents an eccentrically applied axial force. The stress distribution in plate 2 is now completely

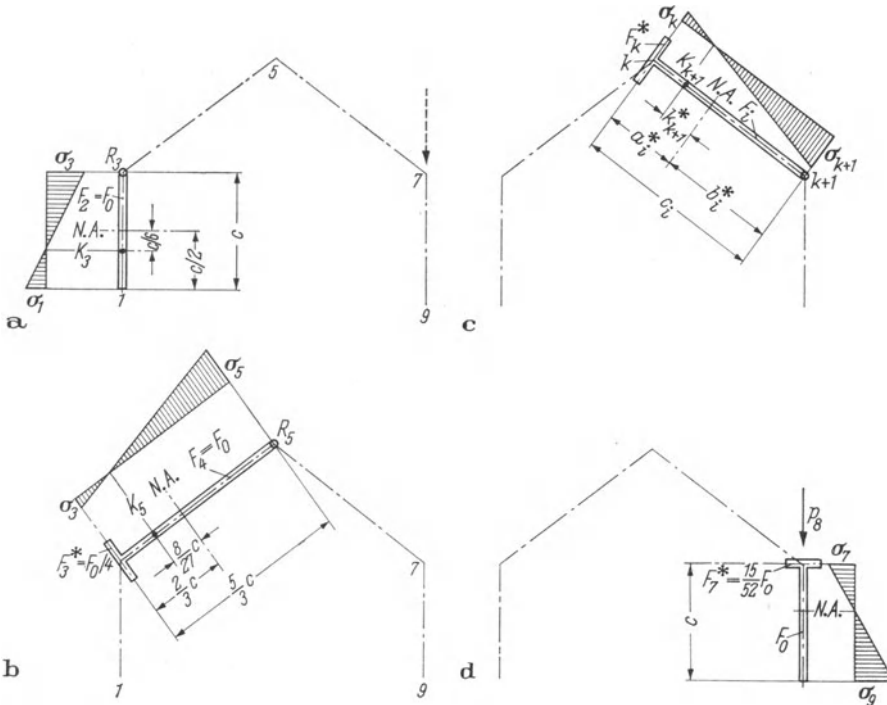


Fig. 12.1. Illustration of the Core Point Method.

determined since it vanishes in the core point K_3 which corresponds to edge 3. Since in plates with rectangular cross section the core point is one sixth of width c away from the neutral axis, the ratio between the two boundary stresses of plate 2 $\sigma_1/\sigma_3 = -1/2$ (v. Fig. 12.1 a).

The resultant R_3 of the axial stresses is calculated as the product of the cross-sectional area F_2 and the stress at the center of gravity and amounts to $\sigma_3 F_0/4$.

The edge force R_3 determines the influence of plate 2 on plate 4. This edge force may be substituted by the stress σ_3 acting over the ideal¹ area F^* which in this case amounts to $F_0/4$.

Plate 4 may now be separated from plate 6 as shown in Fig. 12.1 b. The axial stresses in this plate are again a consequence of the edge force R_5 only. The position of the core point K_5 may be determined from the changed geometry of the cross section. It determines the ratio between the two boundary stresses $\sigma_3/\sigma_5 = -2/7$ as well as the ideal area $F_5^* = 2F_0/7$.

If this described procedure is carried out from plate to plate, one will finally arrive at a plate in which the stresses may be determined by a simple flexural analysis (Fig. 12.1 d). This flexural analysis yields numerical quantities for two edge stresses from which the remaining edge stresses may be determined by means of the known edge-stress ratios. This last sequence of calculations may of course be carried out graphically. The stress distribution outside the loaded plate is represented by a chain of straight lines which include the core points. This sequence of straight lines from the edge 7 to 1 is shown in Fig. 11.5 in the developed state of the cross section.

12.2 Plates Connected at their Boundaries

a) Recurrence Relations

The very elementary analysis described above may be simplified in two ways. Firstly, it suffices to know the ratio between the edge stresses and the ideal area. The center of gravity and the core of the ideal plate cross section do not need to be determined. Secondly, the steps of computation are the same for all plates. It is therefore sufficient to devise two relations, a relation for the ratio between the edge strains and a recurrence relation for the ideal areas.

With the notation of Fig. 12.1 c, the problem may be stated as follows:

If a plate i is defined by its area F_i , its width c_i and its ideal area F_k^* from the previous recurrence step, calculate the edge-stress ratio and the following ideal area F_{k+1}^* .

It will be shown in Section 12.4 that the two required relations do not depend on the width c_i . They may be presented in the following simple form:

$$\frac{\sigma_k}{\sigma_{k+1}} = - \frac{1}{2 + 6 \frac{F_k^*}{F_i}}, \quad (12.1)$$

$$F_k^* = \frac{F_i}{4} \frac{F_i + 4F_k^*}{F_i + 3F_k^*}. \quad (12.2)$$

¹ The term “ideal” as used in this development refers to an imaginary or fictitious area that is added to the real area.

b) Application of the Recurrence Relations

The relations (12.1) and (12.2) assume the following values when applied to the cross section of Fig. 11.3 ($F_0 = ct$):

$$\left. \begin{array}{ll} \text{Eq. (12.1)} & \text{Eq. (12.2)} \\ F_1^* = 0 & \\ \frac{\sigma_1}{\sigma_3} = -\frac{1}{2}, & F_3^* = \frac{1}{4} F_0, \\ \frac{\sigma_3}{\sigma_5} = -\frac{2}{7}, & F_5^* = \frac{2}{7} F_0, \\ \frac{\sigma_5}{\sigma_7} = -\frac{7}{26}, & F_7^* = \frac{15}{52} F_0. \end{array} \right\} \quad (12.3)$$

The area F_7^* becomes a part of the last cross section, v. Fig. 12.1d. The cross-sectional values for this new section may either be calculated independently or by means of the formulas summarized in Table 12.1 (Section 12.4). With the moment of inertia

$$I_8^* = \frac{28}{201} c^2 F_0 \quad (12.4a)$$

and the section moduli

$$W_7^* = \frac{14}{39} c F_0, \quad (12.4b)$$

$$W_9^* = \frac{28}{123} c F_0, \quad (12.4c)$$

the edge stresses of plate 8 become:

$$\sigma_7 = -\frac{M_{80}}{W_7^*} = -\frac{39}{14} \frac{M_{80}}{c F_0},$$

$$\sigma_9 = +\frac{M_{80}}{W_9^*} = +\frac{123}{28} \frac{M_{80}}{c F_0}.$$

The remaining edge stresses are calculated by means of the edge-strain ratios given in Eqs. (12.3).

$$\sigma_5 = -\frac{7}{26} \sigma_7 = +\frac{3}{4} \frac{M_{80}}{c F_0},$$

$$\sigma_3 = -\frac{2}{7} \sigma_5 = -\frac{3}{14} \frac{M_{80}}{c F_0},$$

$$\sigma_1 = -\frac{1}{2} \sigma_3 = +\frac{3}{28} \frac{M_{80}}{c F_0}.$$

These edge stresses are identical to those given by Eqs. (11.11).

12.3 General Folded Plate

a) Recurrence Relations

If the plates are again allowed to stretch beyond the hinges and to be of variable thickness (Fig. 11.7), the recurrence relations will change but the considerations leading to them remain the same. The following expressions are formulated in terms of the plate parameters introduced in Section 11.4a, that is the area F_i , the moment of inertia I_i and the two hinge distances a_i and b_i .

The general formulation of the edge-stress ratios is as follows:

$$\frac{\sigma_k}{\sigma_{k+1}} = - \frac{F_i a_i b_i - I_i}{I_i + F_i b_i^2 + F_k^* (a_i + b_i)^2}. \quad (12.5)$$

The recurrence relation for the calculation of the ideal area F_{k+1}^* from the preceding ideal area F_k^* becomes:

$$F_{k+1}^* = \frac{F_i I_i + F_k^* (I_i + a_i^2 F_i)}{I_i + b_i^2 F_i + F_k^* (a_i + b_i)^2}. \quad (12.6)$$

The derivation of these two relations will be shown in the next section after having demonstrated their application to a particular example.

b) Example

The general folded plate shown in Fig. 11.8 whose plates were characterized in Eqs. (11.33) will now be analyzed by means of the relations (12.5) and (12.6).

The recursion starts with $F_1^* = 0$ (one might as well assume $F_1^* = F_0$ if plate 2 is thought to consist of the web only). The successive application of the recurrence relations leads to:

Relation: (12.5) (12.6)

Initial value: $F_1^* = 0$

First step: $\frac{\sigma_1}{\sigma_3} = -\frac{1}{8}$ $F_3^* = \frac{5}{16} F_0$ (12.7)

Second step: $\frac{\sigma_3}{\sigma_5} = -\frac{8}{61}$ $F_5^* = \frac{419}{122} F_0$ (12.8)

The area F_5^* becomes a part of the I -shaped cross section of the equivalent member whose stresses and deformations for a given load may be determined. The top flange of this member has the area $F_5^* = 419 F_0 / 122$.

With the web area F_0 , depth of web $2a$ and area of the bottom flange F_0 , the moment of inertia and section moduli of this equivalent member become:

$$I_6^* = \frac{2 \cdot 23 \cdot 53}{3 \cdot 221} a^2 F_0, \quad (12.9a)$$

$$W_5^* = \frac{23 \cdot 53}{183} a F_0, \quad (12.9b)$$

$$W_7^* = \frac{23 \cdot 53}{480} a F_0. \quad (12.9c)$$

If the bending moment for the load acting in the plane of plate 6 is denoted by M_0 , expressions for the axial stresses in the edges 5 and 7 may be formulated. The stresses in the edges 3 and 1 follow from the edge-stress ratios (12.8) and (12.7). The results of this analysis are identical to those derived earlier [Eqs. (11.36)] by means of a different method.

The shear stresses τ or the shear flows $q = \tau t$ (where t is the plate thickness) may be calculated from the relations (11.28) which again are written in terms of the plate characteristics (11.33). In calculating the statical moments of cut-off portions according to Eq. (11.27a), one has to be well aware of the sign of coordinate y_i . The centroidal axis divides each isolated plate into two parts. The coordinate y is positive in the part whose edge carries the higher edge number (v. Fig. 11.7). It is therefore the sense of the edge numbering that defines the direction of a positive shear flow.

Since the edge force is equal to the ideal area multiplied by the stress acting therein,

$$R_k = F_k^* \sigma_k, \quad (12.10)$$

the shear flow in the corresponding edge is according to Eq. (11.1)

$$q_k = F_k^* \frac{d\sigma_k}{dz}. \quad (12.11)$$

The shear flows for this specific example may thus be calculated by means of the edge stresses summarized by Eqs. (11.36) and the areas F_3^* and F_5^* of Eqs. (12.7) and (12.8):

$$\begin{aligned} q_3 &= -\frac{15}{2 \cdot 23 \cdot 53} \frac{Q_0}{a}, \\ q_5 &= +\frac{3 \cdot 419}{2 \cdot 23 \cdot 53} \frac{Q_0}{a}. \end{aligned} \quad (12.12)$$

The shear flow distribution resulting therefrom is plotted in Fig. 12.2b.

The deflection of plate 6 may be calculated by means of the equivalent member with the moment of inertia I_6^* of Eq. (12.9a) for the load acting in the plane of plate 6. The folded plate and, consequently, its equivalent members may be continuous over several spans. If it is further specified that the folded plate has

one single span of length l and that plate 6 is acted upon by the uniformly distributed load p_6 , the equivalent member has its maximum deflection v_6 at mid-span:

$$v_6 = \frac{5}{384} \frac{p_6 l^4}{E I_6^*}. \quad (12.13)$$

Since the boundary conditions are the same for all plates (v. Section 11.2b), the ratio between the plate deflections is the same as the corresponding ratio between the curvatures. The curvatures, however, are equal to the difference of the edge strains divided by the distance between the edges.

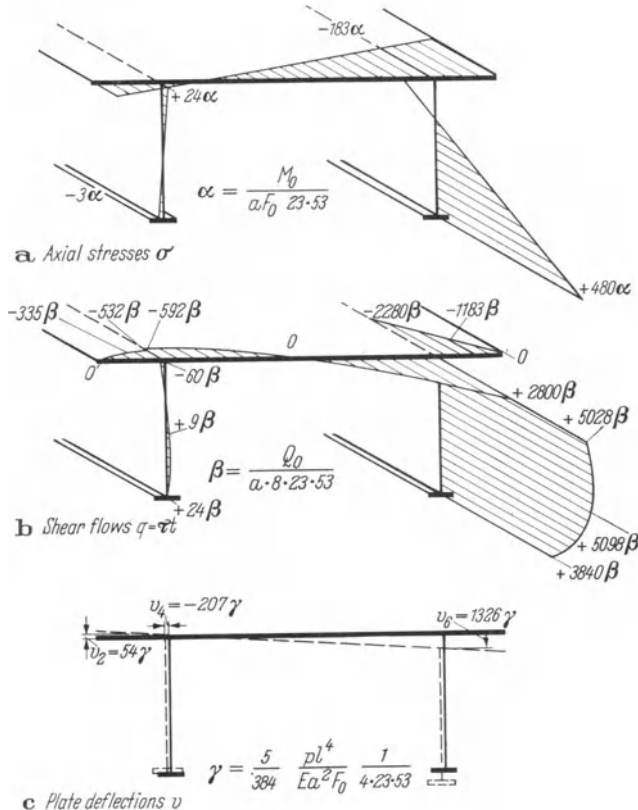


Fig. 12.2. Results of the Example 12.3b.

The following relation may therefore be derived for the ratio between the deflections of two consecutive plates:

$$\frac{v_i}{v_{i+1}} = \frac{\frac{\sigma_{k+1} - \sigma_k}{E_i(a_i + b_i)}}{\frac{\sigma_{k+2} - \sigma_{k+1}}{E_i(a_{i+1} + b_{i+1})}} = \frac{\sigma_{k+1} - \sigma_k}{\sigma_{k+2} - \sigma_{k+1}} \cdot \frac{a_{i+1} + b_{i+1}}{a_i + b_i}. \quad (12.14)$$

For the values of this specific example, Eqs. (11.36) and (11.33), these ratios become:

$$\frac{v_4}{v_6} = \frac{\sigma_5 - \sigma_3}{\sigma_7 - \sigma_5} \cdot \frac{a_6 + b_6}{a_4 + b_4} = \frac{-183 - 24}{480 + 183} \cdot \frac{2a}{4a} = -\frac{3 \cdot 23}{2 \cdot 13 \cdot 17},$$

$$\frac{v_2}{v_4} = \frac{\sigma_3 - \sigma_1}{\sigma_5 - \sigma_3} \cdot \frac{a_4 + b_4}{a_2 + b_2} = \frac{24 + 3}{-183 - 24} \cdot \frac{4a}{2a} = -\frac{6}{23}.$$

These determine the absolute values of the plate deflections by introduction of the known initial value v_6 given by Eq. (12.13). If the moment of inertia I_6^* is further replaced by expression (12.9a), the deflections at mid-span become:

$$\begin{aligned} v_6 &= +\frac{5}{384} \frac{p_6 l^4}{E a^2 F_0} \frac{3 \cdot 13 \cdot 17}{2 \cdot 23 \cdot 53}, \\ v_4 &= -\frac{5}{384} \frac{p_6 l^4}{E a^2 F_0} \frac{3^2}{2^2 \cdot 53}, \\ v_2 &= +\frac{5}{384} \frac{p_6 l^4}{E a^2 F_0} \frac{3^3}{2 \cdot 23 \cdot 53}. \end{aligned} \quad (12.15)$$

These deflections may be used to sketch the shape of the deflected cross-section of the folded plate. This is done in Fig. 12.2c.

Exercise 12.1. *Deflections.* Use Eq. (11.41) to verify the deflections given by Eqs. (12.15).

12.4 Miscellaneous Considerations

a) Derivation of the Recurrence Relations

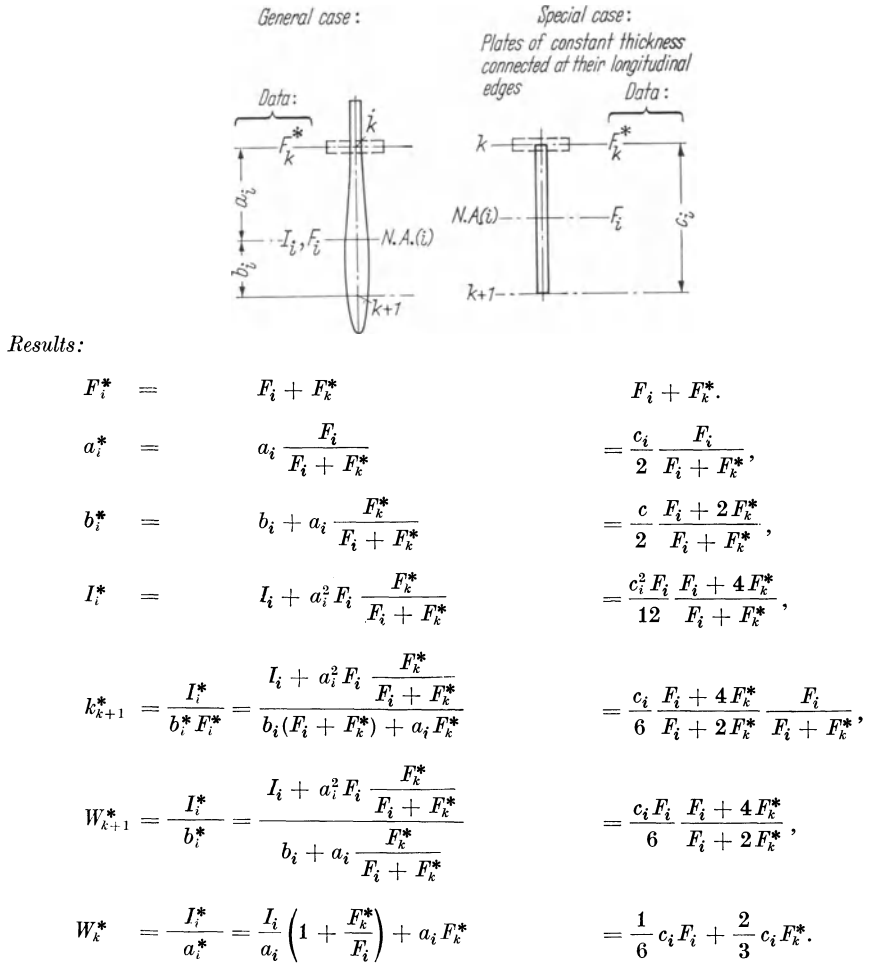
The special and general versions of the recurrence relations (12.1), (12.2) and (12.5), (12.6) which were stated without proof in the previous sections shall be derived hereinafter. The derivations are based on the plate characteristics F_i , I_i , a_i and b_i as defined in Section 11.4 a and as illustrated at the top of Table 12.1. The ideal area F_k^* is the result of the preceding recursion step and is therefore assumed to be known.

Initially, the cross-sectional properties of the plate cross section i as modified by the ideal area F_k^* must be calculated. Table 12.1 presents a summary of required formulas based on simple derivations, both for the general case and for the special case of constant plate thickness and with no protruding plate portions.

The new ideal area F_{k+1}^* is defined as the resulting edge force divided by the axial stress σ_{k+1} acting at the edge $k + 1$:

$$F_{k+1}^* = \frac{\int \sigma dF}{\sigma_{k+1}}. \quad (12.16a)$$

Table 12.1. Collection of Formulas for the Analysis of Folded Plates



Since the area integral in the numerator is equal to the stress at the centroid multiplied by the total area F_i^* , an alternate form of Eq. (12.16a) is:

$$F_{k+1}^* = \frac{\sigma_i F_i^*}{\sigma_{k+1}}. \quad (12.16b)$$

The stress ratio σ_i/σ_{k+1} is equal to the ratio between the distances k_{k+1}^* and $(b_i^* + k_{k+1}^*)$.

$$F_{k+1}^* = \frac{k_{k+1}^*}{b_i^* + k_{k+1}^*} F_i^*. \quad (12.16c)$$

Expressions for the quantities k_{k+1}^* , b_i^* and F_i^* are listed in Table 12.1. If these expressions are introduced into Eq. (12.16c), some simple algebraic manipulations transform the latter into formula (12.6) for the general case and into formula (12.2) for the special case.

If the ratio between the edge stresses,

$$\frac{\sigma_k}{\sigma_{k+1}} = -\frac{a_i^* - k_{k+1}^*}{b_i^* + k_{k+1}^*}, \quad (12.17)$$

undergoes a similar algebraic transformation, it reduces to Eq. (12.5) in the general case and to Eq. (12.1) in the special case.

These considerations prove the validity of the two sets of recurrence relations stated above.

b) Bracketing

The core-point method provides a simple mechanism for determining the behavior of folded plates which may be used to arrive at quick estimates for the stresses due to some particular load.

Consider as an example plate i of the saw-tooth roof shown in Fig. 12.3 a.

In order to calculate the stresses in this plate caused by the load P_i , it suffices to consider the system shown in Fig. 12.3 b.

Plate i is thought to be attached to a top flange and a lower flange whose cross-sectional areas F_k^* and F_{k+1}^* have to satisfy the following inequalities:

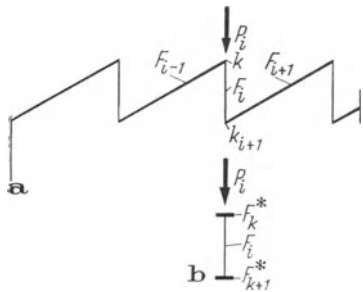


Fig. 12.3. Approximation for the Interior Plate of a Saw-Tooth Roof.

$$\begin{aligned} \frac{1}{4} F_{i-1} &< F_k^* & < \frac{1}{3} F_{i-1}, \\ \frac{1}{4} F_i &< F_{k+1}^* & < \frac{1}{3} F_i. \end{aligned} \quad (12.18a)$$

These inequalities are justified by means of the recurrence relations (12.2). The ideal area F_k^* of the preceding recursion step may vary between zero and infinity. If these two extreme values are introduced into Eq. (12.2), one arrives at the lower bound $F_i/4$ and the upper bound $F_i/3$ for the area F_{k+1}^* .

A realistic estimate of the area F^* results from the following considerations: If one assumes that all plates have the same cross-sectional area F and that the plate under consideration is preceded by many equivalent plates, the two consecutive areas F_k^* and F_{k+1}^* will be approximately equal, $F_k^* = F_{k+1}^* = F^*$. If this is introduced into the recurrence relation (12.2), it yields the following estimate:

$$F^* = \frac{F}{\sqrt{12}} \cong 0.29 F, \quad (12.18b)$$

which by means of Eq. (12.1) gives rise to the corresponding edge-stress ratio:

$$\frac{\sigma_k}{\sigma_{k+1}} = -\frac{1}{2 + \sqrt{3}} \cong -0.27. \quad (12.18c)$$

It was noted that Eqs. (12.18) are valid for the interior plates of a uniform and wide-spread folded plate structure. They need to be modified somewhat for end plates.

Consider for this purpose the end portion of an arbitrary folded-plate structure shown in Fig. 12.4. The ideal areas and the edge-stress ratios in the edges 3 and 5 follow immediately from the recurrence relations (12.2) and (12.1):

$$F_3^* = \frac{F_2}{4}, \quad (12.19a)$$

$$\frac{\sigma_1}{\sigma_3} = -\frac{1}{2}.$$

$$F_5^* = F_4 \frac{F_2 + F_4}{3F_2 + 4F_4}, \quad (12.19b)$$

$$\frac{\sigma_3}{\sigma_5} = -\frac{2F_4}{3F_2 + 4F_4}.$$

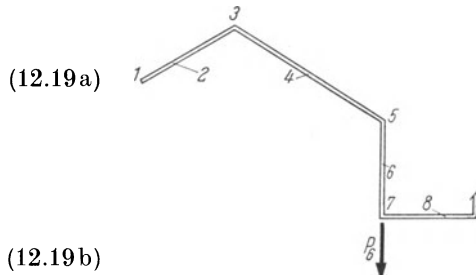


Fig. 12.4. End-Plates of a Wide-Spread Folded-Plate Structure.

The values given by Eqs. (12.19b) are quite generally applicable for a plate which is close to the edge of a folded-plate structure. They lead to stresses which represent an upper bound for the precise values but which are in any case more accurate than those calculated from either of the bounds of the inequalities (12.18a).

c) The Substitute Two-Plate Structure

It will be shown in Section 13.2a that the folded-plate analysis and the bending analysis are equivalent whenever the structure consists of only two plates. A load acting at the hinge of the two plates does not need to be divided up with respect to the planes of the plates.

Consider as an example the folded plate shown in Fig. 12.5. This cross section is a substitute for the cross section of Fig. 11.3. The stresses will be calculated for the structural system and the load shown in Fig. 11.1a.

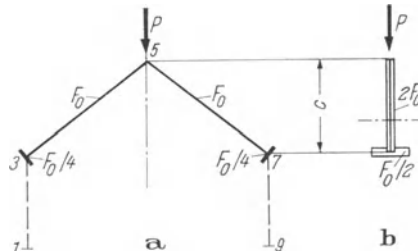


Fig. 12.5. Example for a Substituting Two-Plate Cross Section.

Nonloaded end-plates may be replaced by concentrated areas at the edges which are one fourth of the corresponding plate area. They exhibit furthermore an edge-stress ratio of $-1/2$. The reduced cross section shown in Fig. 12.5a may thus be used to calculate the center of gravity and the moments of inertia for the admissible flexural analysis.

The formulation of expressions for the stresses may be simplified even more if the substitute two-plate cross section is transformed into the equivalent section

of Fig. 12.5b for which the section moduli are tabulated in Table 12.1. The formulas given therein yield the following expressions for the edge stresses:

$$\begin{aligned}\sigma_5 &= -\frac{Pl}{4} \frac{9}{4cF_0}, \\ \sigma_3 = \sigma_7 &= +\frac{Pl}{4} \frac{6}{4cF_0}, \\ \sigma_1 = \sigma_9 &= -\frac{Pl}{4} \frac{3}{4cF_0}.\end{aligned}\quad (12.20)$$

These results were used to plot Fig. 11.1c.

d) Closed Cross Sections

The analysis of a closed folded plate is not essentially different from that described in Sections 11.1 and 11.4. It is also of interest that the number of unknowns is now the same for both the three-shear and three-stress equations. The elements in the matrix, however, may no longer be grouped as a uniform diagonal band.

The core point method and its advantageous property of providing a close bound to the exact solution (v. Section 12.4b) readily provides an approximate

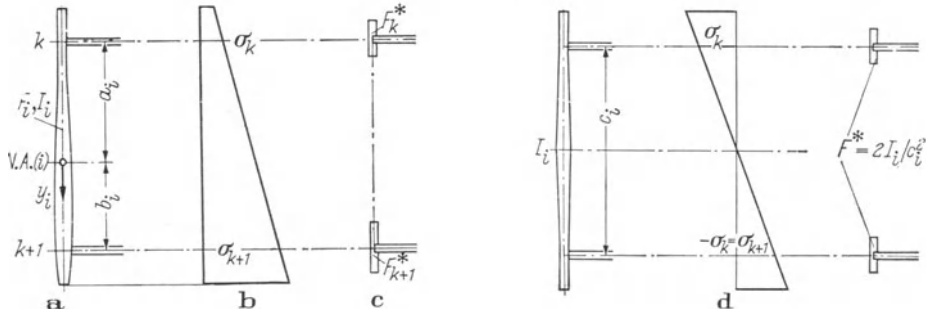


Fig. 12.6. The Opening of a Closed Folded Plate.

solution of the problem. Such an approximation is reached if the closed folded plate is opened at a plate which is as far away as possible from any loaded plate. The exact point of separation may be given for those plates for which the edge-stress ratio is known.

Fig. 12.6 shows again a plate of general cross section which is preceded by plate $i - 1$ and followed by plate $i + 1$. The ideal areas F_i^* and F_{k+1}^* whose effect is equivalent to that of plate i shall be calculated.

They result from the following two conditions:

$$\sigma_k F_k^* + \sigma_{k+1} F_{k+1}^* = \int_{F_i} \sigma_i dF_i, \quad (12.21a)$$

$$-\sigma_k F_k^* a_i + \sigma_{k+1} F_{k+1}^* b_i = \int_{F_i} \sigma_i y_i dF_i. \quad (12.21b)$$

The linear distribution of the stress in plate i may be expressed in terms of edge stresses:

$$\sigma_i = \frac{\sigma_k b_i + \sigma_{k+1} a_i}{a_i + b_i} + \frac{\sigma_{k+1} - \sigma_k}{a_i + b_i} y_i. \quad (12.22)$$

By means of the well-known substitutions

$$\int_{F_i} dF_i = F_i, \quad \int_{F_i} y_i dF_i = 0 \quad \text{and} \quad \int_{F_i} y_i y_i dF_i = I_i.$$

the right sides of Eqs. (12.21 a) and (12.21 b) become:

$$\frac{\sigma_k b_i + \sigma_{k+1} a_i}{a_i + b_i} F_i \quad \text{and} \quad \frac{\sigma_{k+1} - \sigma_k}{a_i + b_i} I_i, \quad \text{respectively,}$$

which lead to the following solutions for the system (12.21):

$$\left. \begin{aligned} F_k^* &= \frac{1}{(a_i + b_i)^2} \left[I_i + b_i^2 F_i + \frac{\sigma_{k+1}}{\sigma_k} (a_i b_i F_i - I_i) \right] \\ F_{k+1}^* &= \frac{1}{(a_i + b_i)^2} \left[I_i + a_i^2 F_i + \frac{\sigma_k}{\sigma_{k+1}} (a_i b_i F_i - I_i) \right] \end{aligned} \right\}. \quad (12.23)$$

In case of a symmetric cross section, an arbitrary load may be divided up into a symmetric and antisymmetric part. A plate which is orthogonal to the axis of symmetry shows a symmetric ($\sigma_k/\sigma_{k+1} = 1$) and an antisymmetric ($\sigma_k/\sigma_{k+1} = -1$) stress distribution also.

For the symmetrical case the ideal areas F^* become:

$$F_k^* = F_{k+1}^* = \frac{F_i}{2}, \quad (12.24)$$

and in the case of antisymmetry:

$$F_k^* = F_{k+1}^* = \frac{2 I_i}{c_i^2}. \quad (12.25a)$$

Note that I_i means the moment of inertia of plate i with respect to the axis of symmetry and $c_i = a_i + b_i$ the distance between the two hinges k and $k + 1$ (v. Fig. 12.6d). Eq. (12.25a) simplifies for plates connected at their longitudinal edges:

$$F_k^* = F_{k+1}^* = \frac{F_i}{6}. \quad (12.25b)$$

The cross section presented in Fig. 12.7a will be used to illustrate the procedure described above. This rectangular, closed, folded-plate cross section is doubly symmetric and the indicated load will cause a state of stress which is antisymmetric with respect to the horizontal axis of symmetry. The latter property may

be formulated as:

$$\frac{\sigma_1}{\sigma_3} = \frac{\sigma_5}{\sigma_7} = -1.$$

The cross section may thus be opened according to the considerations which led to Eq. (12.25b). The new cross section shown in Fig. 12.7b may now be treated by means of the recurrence relations (12.1) and (12.2) which lead to:

$$\frac{\sigma_7}{\sigma_1} = \frac{\sigma_5}{\sigma_3} = -\frac{\varrho}{1+2\varrho}$$

and

$$F_1^* = F_3^* = \frac{\varrho F_0}{6} \frac{2+3\varrho}{1+2\varrho}.$$

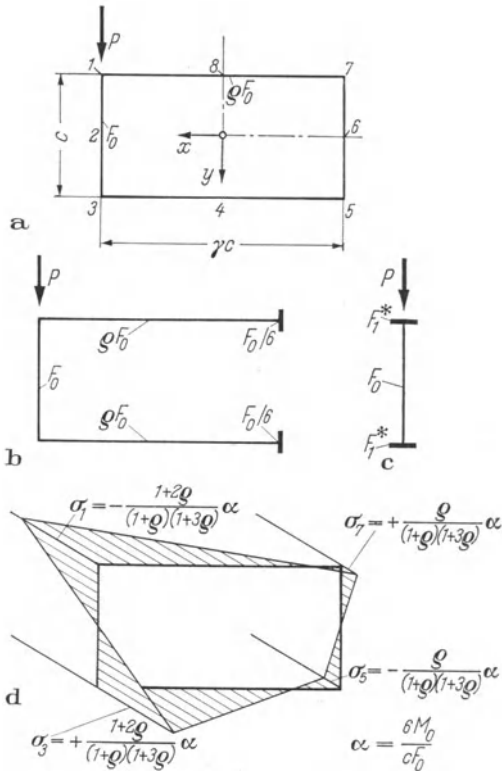


Fig. 12.7. Example for a Closed Folded-Plate Cross Section.

The remaining symmetric I -cross section has a moment of inertia

$$I_2^* = \frac{c^2 F_0}{12} \frac{(1+\varrho)(1+3\varrho)}{1+2\varrho}. \quad (12.26)$$

The moment of inertia provides immediate calculation of the stresses in the edges 1 and 3 and the edge-stress ratios thereby lead to the stresses in the edges 5

and 7. The following expressions refer to the moment in plate 2, $M_{20} = M_0$:

$$\left. \begin{aligned} \sigma_1 &= -6 \frac{1+2\varrho}{(1+\varrho)(1+3\varrho)} \frac{M_0}{c F_0}, \\ \sigma_3 &= +6 \frac{1+2\varrho}{(1+\varrho)(1+3\varrho)} \frac{M_0}{c F_0}, \\ \sigma_5 &= -6 \frac{\varrho}{(1+\varrho)(1+3\varrho)} \frac{M_0}{c F_0}, \\ \sigma_7 &= +6 \frac{\varrho}{(1+\varrho)(1+3\varrho)} \frac{M_0}{c F_0}. \end{aligned} \right\} \quad (12.27)$$

These results are plotted in Fig. 12.7d for an area ratio $\varrho = 2$.

If, on the other hand, one chooses to apply the three-stress equations (11.9) as another possible *means of analysis*, they result in the following system of equations:

$$\left. \begin{aligned} \sigma_1 &\quad \sigma_3 & \sigma_5 & \sigma_7 & \text{Gen. Displ.} \\ 2(1+\varrho)F_0 & \quad F_0 & & \varrho F_0 & = -6 \frac{M_0}{c} \\ F_0 & \quad 2(1+\varrho)F_0 & \varrho F_0 & & = +6 \frac{M_0}{c} \\ \varrho F_0 & \quad 2(1+\varrho)F_0 & F_0 & = 0 & \\ \varrho F_0 & \quad F_0 & & 2(1+\varrho)F_0 = 0 & \end{aligned} \right\} \quad (12.28)$$

The Eqs. (12.27) are in fact solutions of this system.

The *shear flows* are equal to the derivative of the edge forces with respect to z . Since the edge forces may be formulated immediately by means of Eq. (11.8), their derivatives with respect to z considering $dM_0/dz = Q_0$ are as follows:

$$\begin{aligned} q_1 = q_3 &= + \frac{\varrho(2+3\varrho)}{(1+\varrho)(1+3\varrho)} \frac{Q_0}{c}, \\ q_5 = q_7 &= - \frac{\varrho}{(1+\varrho)(1+3\varrho)} \frac{Q_0}{c}. \end{aligned} \quad (12.29a)$$

The shear flows at the centers of the plates follow from Eq. (11.21). The parameters α and λ appearing therein may readily be read from Eqs. (12.29a) respectively (12.27). According to the definitions (11.15) and (11.16) they are equal to the first factors in these expressions.

$$q_2 = + \frac{1}{2} \frac{6\varrho^2 + 10\varrho + 3}{(1+\varrho)(1+3\varrho)} \frac{Q_0}{c},$$

$$q_4 = q_8 = - \frac{\varrho}{4(1+\varrho)} \frac{Q_0}{c}, \quad (12.29b)$$

$$q_6 = + \frac{1}{2} \frac{\varrho}{(1+\varrho)(1+3\varrho)} \frac{Q_0}{c}.$$

The *plate deflections*, finally, are according to Section 11.4f a consequence of the differences in the edge stresses. In order to arrive at useful results, it will

further be specified that the load P is acting in the position $\alpha = a/l$ and $\beta = b/l$ of a simply supported, prismatic member of span l . The bending moment at $\alpha = a/l$ is $M_0 = Pl\alpha\beta$.

If the stresses (12.27) are successively introduced into Eq. (11.43a), one arrives at:

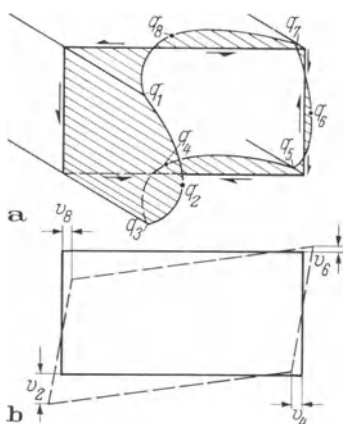


Fig. 12.8. Distribution of the Shear Flows $q = \tau t$ (a) and Deformations (b) of the Closed Folded Plate Defined in Fig. 12.7a.

The shear flows and deflections are plotted in Fig. 12.8 for the cross-sectional parameters $\varrho = 2$ and $\gamma = 2$.

$$v_2 = + \frac{4(1+2\varrho)}{(1+\varrho)(1+3\varrho)} \frac{Pl^3}{Ec^2 F_0} (\alpha\beta)^2,$$

$$v_4 = v_8 = - \frac{2}{\gamma(1+\varrho)} \frac{Pl^3}{Ec^2 F_0} (\alpha\beta)^2, \quad (12.30)$$

$$v_6 = + \frac{4\varrho}{(1+\varrho)(1+3\varrho)} \frac{Pl^3}{Ec^2 F_0} (\alpha\beta)^2.$$

13 Relations Between the Folded-Plate Theory and the Theory of Slender Members

It is the purpose of this chapter to examine the differences, similarities and possible equivalence of the folded-plate theory and the theory of slender members.

While the methods for the analysis of a slender member depend on the type of the load, the *folded-plate theory* does not make this distinction. Chapters 5 and 7 investigated the stresses in thin-walled cross sections due to torsional load alone. This analysis has to be supplemented by a flexural analysis if lateral loads also require consideration. A complete analysis of a *slender member* leads therefore to two types of stresses, torsional stresses and flexural stresses. The folded-plate theory, however, yields immediately one single set of stresses.

This chapter deals with the following subjects: Cases which may not be treated with the folded-plate theory and which therefore do not permit comparison are eliminated in Section 13.1. Section 13.1 excludes the cases for which both methods yield equivalent results. This section will nevertheless permit useful conclusions with respect to the suitability of a particular method for the analysis of such cases. The actual confrontation of both methods will be presented in Section 13.3. Section 13.4 finally, will consider the influence of cross girders and interior diaphragms, thus helping to gain a clearer picture of the approximations inherent in either of these analytical models.

13.1 Folded-Plate Theory Not Applicable

a) Several Plates Meeting at One Common Hinge

The methods for the analysis of folded plates implicitly assume that each plate is at most preceded and followed by one plate only. The methods are no longer applicable if one hinge belongs to more than two plates.

Such problems might be solved by use of concepts valid in the solution of statically indeterminate problems. Redundant plates are thought of as cut-off at the outset. The original continuity of the structure is thereafter reestablished by means of compatibility conditions.

If a profile consists of plates whose planes intersect along the same line or if a member may be reduced to such a structure by means of the core-point method, no formulation of compatibility conditions is necessary. It will be proved hereinafter that the strict application of the folded-plate theory to this type of profile would yield results which are equivalent to those of the slender-member theory.

The curvature v''_i of each individual plate i is defined by Eq. (11.38). The deflection v of the common line of intersection is related to the plate deflection v_i as defined by $v_i = v \cos \varphi_i$. The symbol φ_i means the angle between the plane of the deflection v and the plane of plate i . Since deflections may be differentiated at least twice $v''_i = v'' \cos \varphi_i$, and it follows from Eq. (11.38):

$$\frac{\sigma_{k+1} - \sigma_k}{c_i} \frac{1}{\cos \varphi_i} = E v''.$$

The right side of this expression is a constant which does not depend on plate i . The equation states therefore that the projection of the stress difference on the plane of the deflection v is constant. Since the strains and, (in case of a uniform modulus of elasticity) the stresses are equal at the common line of intersection, the stress distribution in the cross section may be described by a linear function. The latter, however, is a fundamental assumption for the slender-member theory whose results are unique.

b) Coinciding Planes of the Plates

The folded-plate theory excludes the limiting case of coinciding planes of the plates. While the theory of warping torsion assumes the floor slab of the bridge cross section in Fig. 6.3 to consist of three different plates (two sidewalks and one roadway), the folded-plate theory introduces the entire floor slab as a single plate of variable thickness. The bridge cross section of Fig. 6.3 constitutes therefore a three-plate cross section in the scope of the folded-plate theory.

If one assumes, regardless of this condition, consecutive plates in the same plane to represent a sequence of individual plates, the result of the subsequent analysis will no longer be unique. This shall be demonstrated hereinafter.

The admissible moment M_{zul} of an angle section with equal legs ($\varrho = 1$) may be derived from the first of the Eqs. (13.11). If the admissible stress is denoted by σ_{zul} , the corresponding moment follows from the relation:

$$M_{zul} = \frac{2}{9} c F \sigma_{zul}. \quad (13.1a)$$

The admissible moment is, as is proved in Section 13.2a, independent of the angular aperture φ . It may therefore be represented by a horizontal line in the coordinate system of Fig. 13.1.

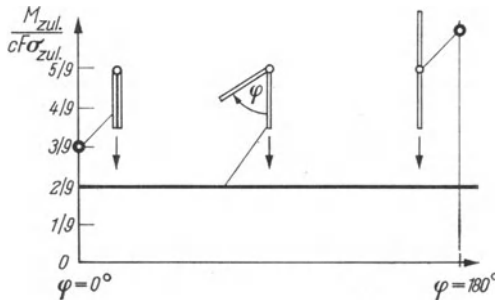


Fig. 13.1. The Admissible Bending Moment M_{zul} of an Angle Section with Equal Legs as a Function of the Aperture Angle φ .

The two limiting cases, the closed angle ($\varphi = 0$) and the stretched angle ($\varphi = 180^\circ$) have to be treated separately. The two different profiles have section moduli of $cF/3$ and $2cF/3$ resp. and therefore the following admissible bending moments:

$$\text{for } \varphi = 0^\circ: M_{zul} = \frac{1}{3} c F \sigma_{zul}, \quad (13.1b)$$

$$\text{for } \varphi = 180^\circ: M_{zul} = \frac{2}{3} c F \sigma_{zul}. \quad (13.1c)$$

These two values are entered into Fig. 13.1. This figure illustrates that no unique solution exists for the special cases $\varphi = 0^\circ$ and $\varphi = 180^\circ$, i.e. when the planes of the two plates coincide.

c) Large Changes in the Geometry of the Cross Section

It is a characteristic of the first order analysis of structural systems that the calculation of internal forces and stresses is based on the geometry of the unloaded structure. Such an assumption is no longer admissible whenever structures undergo large changes in geometry at the working load. This is the case for certain types of folded plates which will be investigated in this section.

Consider as an example the folded plate shown in Fig. 13.2. The load P acts at the edge of two plates which enclose an angle that deviates but little from the critical value $\varphi = 180^\circ$. This structure is an extreme case of the folded plate

shown in Fig. 11.1a for which a load-deformation diagram may be calculated under the assumption that the angle at the ridge is very obtuse to start with.

The slope of the plates 4 and 4' is denoted by α in the loaded state and by α_0 in the unloaded state (Fig. 13.2). The stresses in this structure were already calculated in relation to Fig. 12.5. Eqs. (12.20), however, have to be adapted to the notation used in Fig. 13.2, i.e. c has to be replaced by $c \sin \alpha$. The stresses yield according to Eq. (11.43b) the following expressions for the deflections:

$$\begin{aligned} v_2 &= \frac{\sigma_3 - \sigma_1}{c_2} \frac{l^2}{12E} = + \frac{9}{16} \frac{Pl}{F \frac{3}{5} c^2 \sin \alpha} \cdot \frac{l^2}{12E}, \\ v_4 &= \frac{\sigma_5 - \sigma_3}{c_4} \frac{l^2}{12E} = - \frac{15}{16} \frac{Pl}{Fc^2 \sin \alpha} \cdot \frac{l^2}{12E} = - v_2. \end{aligned} \quad (13.2)$$

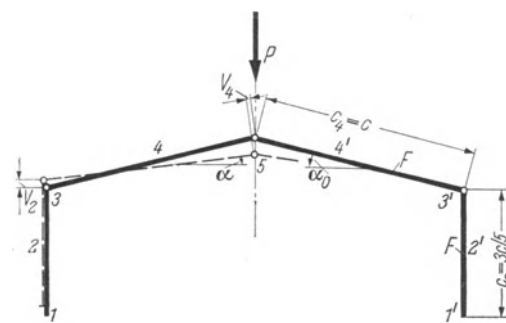


Fig. 13.2. Deformation of Plates Enclosing an Extremely Obtuse Angle.

If the slope of the plates 4 and 4' is small such as to permit the approximation $\operatorname{tg} \alpha \simeq \sin \alpha \simeq \alpha$, the change in the slope induced by the load may, in view of Fig. 13.2, be formulated as follows:

$$\alpha_0 - \alpha = \frac{-\frac{v_4}{\alpha} + v_2}{c_4}.$$

The deflections are given by Eq. (13.2). If they are introduced in the small-angle approximation, they lead to:

$$\alpha_0 - \alpha = \frac{5}{64} \frac{Pl^3}{EFc^3} \left(\frac{1}{\alpha^2} + \frac{1}{\alpha} \right).$$

This expression may also be written as:

$$\frac{P}{P_0} = \alpha^2 \frac{\alpha_0 - \alpha}{1 + \alpha} \quad (13.3)$$

introducing the reference load

$$P_0 = \frac{64}{5} EF \left(\frac{c}{l} \right)^3. \quad (13.4)$$

The functional relationship (13.3) is visualized in Fig. 13.3 with respect to the load intensity P/P_0 as ordinate and the angle α as the abscissa. This figure shows by a heavy, solid line the curve for the initial slope $\alpha_0 = 1/4$ (which is the slope of the cross section in Fig. 13.2) and by a thin and solid line the curve for $\alpha_0 = 1/8 (\sim 8^\circ)$.

It is readily apparent from Eq. (13.3) that P becomes zero for either $\alpha = 0$ or $\alpha = \alpha_0$. The first zero of the curves may be explained by means of a simple equilibrium consideration. It is impossible that a vertical load can be counteracted

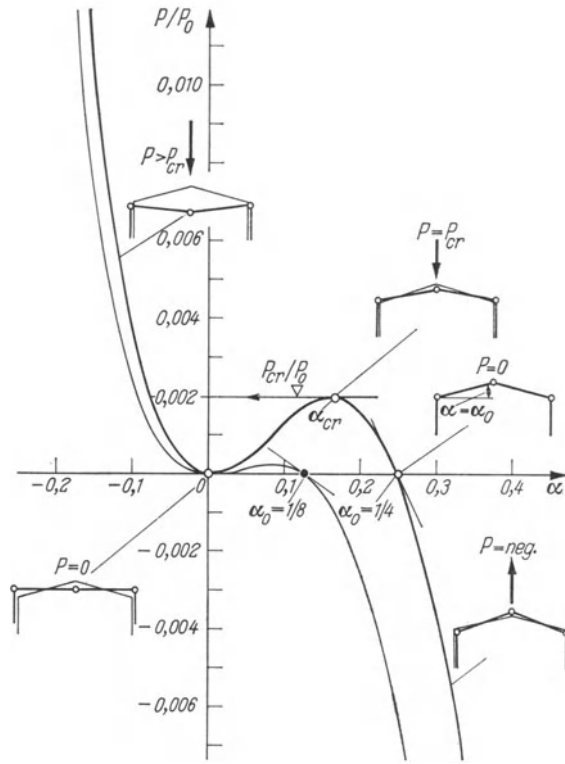


Fig. 13.3. The Snap-Through Problem of Folded Plates [Presentation of Function (13.3) for the Parameters $\alpha_0 = 1/4$ and $1/8$].

by plate forces acting in the same horizontal plane. The second zero simply confirms the assumption that the slope is α_0 in the unloaded state of the cross section.

The ratio P/P_0 is negative for $\alpha > \alpha_0$, i.e. the load has to act upwards in order to increase the slope of the roof. The load P is positive for all angles $\alpha < \alpha_0$. It is therefore for simple continuity reasons that the load P assumes a maximum for some positive value α_{cr} between the two zeros of the curve. Increasing load decreases the slope of the roof only down to α_{cr} . A further decrease of the slope requires less load. If, on the other hand, the maximum load P_{cr} is maintained, the roof will snap-through and assume the corresponding stable position with negative

slopes of the roof. Aside from the restrictions imposed by the strength of the material, increasing load decreases the slope thereafter within the range for which the small slope assumption is valid.

The large deformations of such structures are accompanied by a rearrangement of the stresses. The sign reversal which takes place at snap-through usually would result in the collapse of the structure. The best means to avoid this is an appropriate selection of the angle between the plates. It is the purpose of the subsequent considerations to devise recommendations for the selection of a safe angle.

The first derivative of the fundamental relation (13.3) is:

$$\frac{d}{d\alpha} \left(\frac{P}{P_0} \right) = \frac{\alpha}{(1 + \alpha)^2} (2\alpha_0 - 3\alpha + \alpha_0\alpha - 2\alpha^2). \quad (13.5)$$

This derivative has to become zero for the critical angle α_{cr} between zero and α_0 . The angle α_{cr} is therefore a root of the algebraic expression (13.5). Since this expression was derived for small angles α , $\alpha \ll 1$, one may as well neglect the products of such angles as opposed to the linear terms. The angle α_{cr} may thus be determined from the equation $2\alpha_0 - 3\alpha = 0$ and becomes:

$$\alpha_{cr} = \frac{2}{3} \alpha_0. \quad (13.6)$$

If this value is introduced into Eq. (13.3), one arrives at the following relation for the critical load P_{cr} of the structure:

$$\frac{P_{cr}}{P_0} = \frac{4}{9} \frac{\alpha_0^3}{3 + 2\alpha_0} \simeq \frac{4}{27} \alpha_0^3. \quad (13.7)$$

It is reasonable to require that the structure should not fail because of instability before the strength of the material is exhausted. If the maximum permissible stress for the material is denoted by σ_r , the corresponding ultimate load P_r follows from the first of Eqs. (12.20). The distance c in this expression needs to be replaced by $c \sin \alpha$ which for small angles α is approximately $c\alpha$. This leads to:

$$-\sigma_s = \sigma_r = \frac{9}{16} \frac{Pl}{Fc\alpha} \quad (13.8a)$$

which determines:

$$P_r = \frac{16}{9} \sigma_r F \frac{c}{l} \alpha, \quad (13.8b)$$

where α is restricted by the inequality $2\alpha_0/3 < \alpha < \alpha_0$. The condition that the structure does not become unstable before the strength of the material is fully utilized, $P_{cr} \geq P_r$, may according to Eqs. (13.7) and (13.8b) be formulated as follows:

$$\frac{4}{27} \alpha_0^3 P_0 \geq \frac{16}{9} \sigma_r F_0 \frac{c}{l} \frac{2}{3} \alpha_0.$$

Considering the definition of the reference load P_0 by Eq. (13.4), one arrives at:

$$\frac{4}{27} \alpha_0^3 \frac{64}{5} E F_0 \left(\frac{c}{l} \right)^3 \geq \frac{16}{9} \sigma_r F_0 \frac{c}{l} \frac{2}{3} \alpha_0$$

which reduces to:

$$\alpha_0^2 \geq \frac{5}{8} \frac{\sigma_r}{E} \left(\frac{l}{c} \right)^2,$$

and finally to:

$$\alpha_0 \geq \sqrt{\frac{5}{8} \varepsilon_r} \frac{l}{c}. \quad (13.9a)$$

There is some advantage in writing Eq. (13.9a) in terms of the ultimate permissible strain ε_r .

If the angle δ_k between two adjacent plates is defined as the deviation from the entire contained angle, Eq. (13.9a) may alternatively be formulated as:

$$\delta_k \geq 2 \sqrt{\frac{5}{8} \varepsilon_r} \frac{l}{c}. \quad (13.9b)$$

Reinforced concrete under axial compression exhibits an ultimate strain $\varepsilon_r \simeq 2\%$, a value which is more or less independent of the strength.

If this ultimate strain is introduced into Eq. (13.9b) and if the angle δ_k is expressed in degrees instead of in radians (π corresponds to 180°), the condition becomes:

$$\delta_k \geq 4 \frac{l}{c} [\text{degrees}]. \quad (13.10a)$$

This condition is quite conservative since it was derived for quite unfavourable conditions which rarely occur in practice, a concentrated load at mid-span and plates connected by longitudinal hinges.

The condition (13.10a), on the other hand, does not consider the fact that the ordinary folded plate theory, which determines the stresses for the undeformed shape of the cross section, overestimates the capacity of a folded-plate structure.

Since the effects of the nonlinear behavior become considerable both for extremely obtuse and acute angles, it is advisable to satisfy the following rule when selecting the angle α_k between adjacent plates:

$$4 \frac{l}{c} \leq \delta_k \leq 180 - 4 \frac{l}{c} [\text{degrees}]. \quad (13.10b)$$

If, for instance, the span l is five times as large as the average width c of the plates, the angle α_k is restricted by the following inequality:

$$20^\circ \leq \delta_k \leq 160^\circ.$$

Exercise 13.1. The Snap-Through Problem of a Folded Plate

- a) A model of the structure shown in Fig. 11.1 is to be built in order to verify experimentally the load-deformation curves of Fig. 13.3. Devise the conditions which ensure that these curves may be produced without exceeding the proportional limit ε_p of the model material.

(Hint.: Calculate the maximum stress in the region $0 < \alpha < \alpha_0$.)

b) Which region of α may be covered by the experiment if α_0 is selected such that the proportional limit ϵ_p is reached but not exceeded in the range $0 < \alpha < \alpha_0$?

Solutions:

a) The maximum stress is σ_5 as given by Eq. (13.8a). If the load is introduced as given by Eqs. (13.3) and (13.4), this expression becomes:

$$\sigma_5 = -\frac{36}{5} E \left(\frac{c}{l}\right)^2 \frac{\alpha(\alpha_0 - \alpha)}{1 + \alpha}. \quad (\text{a})$$

The stress σ_5 assumes the following extreme value at $\alpha \simeq \frac{\alpha_0}{2}$:

$$|\max \sigma_5| = \frac{9}{5} E \left(\frac{c}{l}\right)^2 \alpha_0^2. \quad (\text{b})$$

The given condition for the proportional limit ϵ_p imposes therefore the following restriction on the initial slope α_0 :

$$\alpha_0 \frac{c}{l} > \frac{\sqrt{5} \epsilon_p}{3}.$$

b) If the general stress formula (a) is set equal to its extreme value (b), one arrives at the following limits for the deformation α :

$$-\frac{\sqrt{2} - 1}{2} \alpha_0 < \alpha < +\frac{\sqrt{2} + 1}{2} \alpha_0.$$

13.2 Equivalence of Both Theories

a) The Two-Plate Profile

These two titles imply that the folded-plate theory and the slender-member theory yield equivalent results when applied to a structure consisting of two prismatic plates. The results of the slender-member theory will be considered first.

The shear center location for this open, thin-walled, two-plate cross section is predetermined. The shear stresses in such an angle-type cross section result in two force components, one in each leg. Since two forces may be in equilibrium with a third only if the line of action of the latter includes their point of intersection, the shear center is at the intersection of the middle lines of the two plates. Hence, the shearing force may be in equilibrium with the applied loads only if their line of action includes the line of intersection of the two plates.

The folded-plate theory imposes the same condition on the load. The load has to be applied at the common edge of the plates. A planar stress distribution, however, is only required for the individual plates and not for the entire cross section. But these two requirements are equivalent for the special case of a two-plate cross section since the two intersecting linear stress distributions of the two plates uniquely define the planar stress distribution of the entire cross section.

Since there is only one planar stress distribution which is in equilibrium with a given load, the results of the slender-member theory and the folded-plate theory are the same.

The only criterion for the preference of a particular method is therefore the ease of application and this depends on the symmetries and the loads. The use of the folded-plate theory, for instance, is easier whenever the load acts in the plane of one plate.

The angle section defined in Fig. 13.4a shall be treated as an example. The section, which might be looked at as a simple crane girder consists of a horizontal stiffening plate with cross-sectional area ϱF_0 which is attached to the vertical plate of the area F_0 . The plane of the latter coincides with the plane of the load. The core-point method transforms this section into the one of Fig. 13.4b which may be utilized for the calculation of stresses and vertical deflections (transformed flange: $F^* = \varrho \cdot F_0/4$, $\sigma_1/\sigma_3 = -1/2$). The fundamental relations for the analysis of the transformed section are listed in Table 12.1. If the bending moment caused by the load is denoted by M_0 , the following stress formulas are immediately arrived at:

$$\begin{aligned}\sigma_5 &= + \frac{M_0}{\frac{c F_0}{6} \frac{F_0 + \varrho F_0}{F_0 + \frac{\varrho F_0}{2}}} = + \frac{3(2 + \varrho)}{1 + \varrho} \frac{M_0}{c F_0}, \\ \sigma_3 &= - \frac{M_0}{\frac{c F_0}{6} + \frac{2}{3} c \frac{\varrho F_0}{4}} = - \frac{6}{1 + \varrho} \frac{M_0}{c F_0}, \\ \sigma_1 &= - \frac{\sigma_3}{2} = + \frac{3}{1 + \varrho} \frac{M_0}{c F_0}.\end{aligned}\quad (13.11)$$

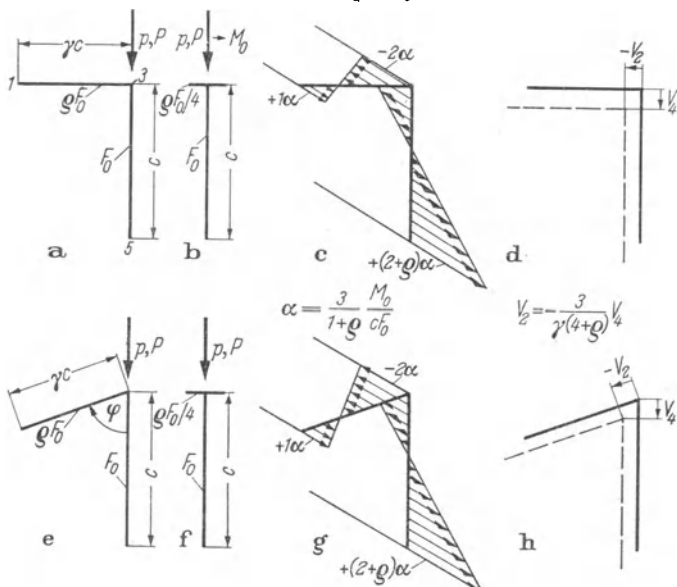


Fig. 13.4. Folded-Plate Theory Applied to an Angle Section.

The vertical deflection v_4 is calculated from the curvature $v_4'' = -M_0/(EI^*)$ under consideration of the given boundary conditions. By means of the formula for I^* listed in Table 12.1 this curvature may be expressed as follows:

$$v_4'' = -\frac{M_0}{E \frac{c^2 F_0}{12} \frac{F_0 + \varrho F_0}{F_0 + \frac{\varrho F_0}{4}}} = -\frac{3(4 + \varrho)}{1 + \varrho} \frac{M_0}{E c^2 F_0}. \quad (13.12)$$

According to Eq. (12.14) the horizontal deflection v_2 may be calculated from the vertical deflection v_4 :

$$v_2 = v_4 \frac{-6 - 3}{3(2 + \varrho) + 6} \frac{c}{\gamma c} = -\frac{3}{4 + \varrho} \frac{v_4}{\gamma}. \quad (13.13)$$

The stresses and the deflections are plotted in Figs. 13.4c and d for the geometrical assumptions $\varrho = 1$ and $\gamma = 3/4$.

The lower half of Fig. 13.4 shows the results for an angle section having legs that are no longer perpendicular to each other but which enclose the arbitrary angle φ . Since the ideal area F^* is independent of the plate angle φ , both stresses and deflections remain the same. Merely the direction of the deflection v_2 changes together with the position of the corresponding plate.

It would have been considerably more difficult to make these fundamental observations if the slender-member theory were used.

b) The Three-Plate Profile

The internal forces of a member must be in equilibrium with the applied loads. The internal forces again are the resultants of the stresses in the cross sections. Since the shear stresses in a three-plate profile may be added up to three forces, each having its line of action in the plane of a plate, their correspondence to the resultant shear force is unique.

The last statement makes use of the fundamental theorem of planar statics which says that an arbitrary force may uniquely be divided up into three forces with prescribed lines of action which do not meet in the same point. The exception of this theorem corresponds to the case of three plates with one common hinge, i. e. a case which was already excluded in Section 13.1. There remains therefore only the unique relation between the plate shears and the resulting shearing force. The stress distribution in the plates will be the same independent of the theory used since both assume according to Eq. (11.19) a linear distribution of the axial stresses in each plate and the same boundary conditions (no shear flow at free ends and continuity at common edges).

The shear flows, axial stresses and deformations of a three-plate profile do not therefore depend on whether they were derived by means of the slender-member theory or the folded-plate theory.

These considerations shall be illustrated by means of a cross section analyzed in Chapter 6 (refer to Fig. 6.1 for the dimensions and to Fig. 6.2 for the load).

The load p_y is divided up into three forces acting in the planes of the plates by means of a procedure first described by RITTER¹. The moment equilibrium is formulated for each corner of the triangle defined by the components p_2 , p_4 and p_6 (v. Fig. 13.5):

$$\begin{aligned} p_2 \cdot 4a &= -p_y \cdot 1,5a, \\ -p_4 \cdot 5,6a &= -p_y \cdot 5,5a, \\ -p_6 \cdot 4,95a &= +p_y \cdot 1,5a. \end{aligned}$$

Each of these conditions involves only one unknown component. The solutions are:

$$\begin{aligned} p_2 &= -0,375 p_y, \\ p_4 &= +0,982 p_y, \\ p_6 &= -0,303 p_y. \end{aligned} \quad (13.14)$$

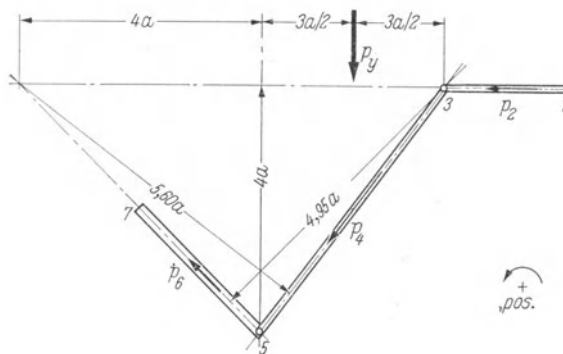


Fig. 13.5. Evaluation of the Plate Forces for the Three-Plate Profile of Fig. 6.1.

The expressions for M_{i0}/W_i , which will be used later for the formulation of the generalized displacements in the System (11.7) as well as for the calculation of edge stresses according to Eqs. (11.6), are as follows:

$$\begin{aligned} \frac{M_{20}}{W_2} &= -\frac{0,375 M_y}{\frac{1}{6} F_0 2a} = -1,125 \frac{M_y}{a F_0}, \\ \frac{M_{40}}{W_4} &= +\frac{0,982 M_y}{\frac{1}{6} 2 F_0 5a} = +0,589 \frac{M_y}{a F_0}, \\ \frac{M_{60}}{W_6} &= -\frac{0,303 M_y}{\frac{1}{6} 2 F_0 2 \sqrt{2}a} = -0,321 \frac{M_y}{a F_0}. \end{aligned} \quad (13.15)$$

M_y denotes the bending moment for the load p_y evaluated for a prismatic member whose boundary conditions are the same as those of the folded plate.

¹ RITTER, W.: Anwendungen der graphischen Statik, 4 Volumes, 1888, 1890, 1900, 1906.

The edge forces R_3 and R_5 result from the System (11.7) which by means of the auxiliary values (13.15) may be formulated as follows:

$$R_3 \frac{1}{2F_0} + R_5 \frac{1}{2F_0} = \frac{1}{2} (-1,125 + 0,589) \frac{M_y}{aF_0},$$

$$R_3 \frac{1}{2F_0} + R_5 \frac{2}{2F_0} = \frac{1}{2} (0,589 - 0,321) \frac{M_y}{aF_0}.$$

The solutions to this system of equations are:

$$\begin{aligned} R_3 &= -0,105 \frac{M_y}{a}, \\ R_5 &= +0,093 \frac{M_y}{a}. \end{aligned} \quad (13.16)$$

The derivative of these expressions with respect to z involves the substitution of M_y by Q_y and according to Eq. (11.17) is equal to the shear flow at the corresponding edges. Since these shear flows were calculated earlier by another means, the numerical factors of Eqs. (13.16) should be equal to the corresponding ones of Fig. 6.2 thus permitting a valuable check for the accuracy of the results.

If the values (3.16) and (3.15) are introduced into Eqs. (11.6), one arrives, aside from some rounding off error in the last decimal place, at the axial stresses plotted in Fig. 6.2.

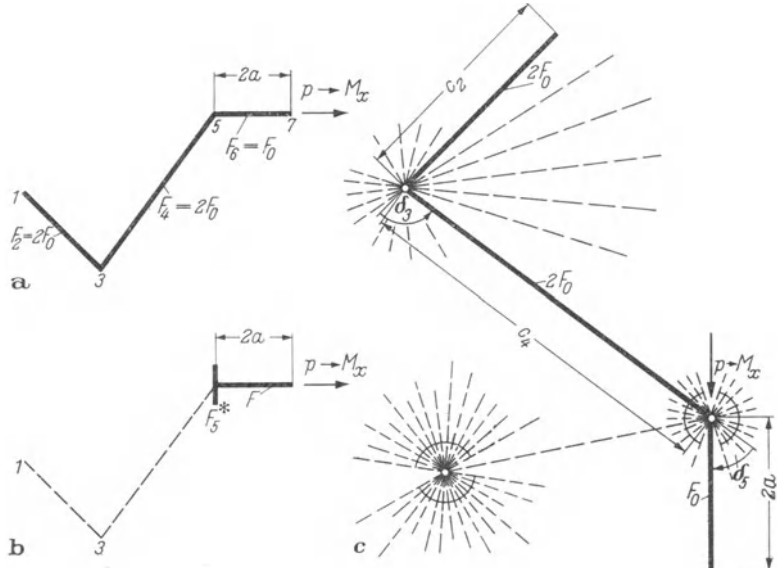


Fig. 13.6. Application of the Folded-Plate Theory for the Solution of the Problem in Exercise 6.1 (a, b). The Stresses are Independent of the Four Parameters δ_3 , δ_5 , c_2 and c_4 (c).

If one compares now the effort necessary for the application of the folded-plate theory and the slender-member theory, it may be concluded that the use of the folded-plate theory is simpler whenever the analysis of the three-plate

profile is required only once or whenever the load acts in the plane of one plate. The problem presented in Exercise 6.1 will be solved as an example for the second case.

The problem is presented again in Fig. 13.6a only with a reversed annotation of plates and hinges.

The ideal area F_5^* of the reduced cross section shown in Fig. 13.6b follows from the first of the Eqs. (12.19b):

$$F_5^* = 2 F_0 \frac{2 F_0 + 2 F_0}{6 F_0 + 8 F_0} = \frac{4}{7} F_0.$$

The section moduli of this cross section are:

$$W_5^* = \frac{23}{21} a F_0,$$

$$W_7^* = \frac{23}{45} a F_0.$$

The edge-stress ratios, finally, which follow from Eqs. (12.19) and amount to $\sigma_1/\sigma_3 = -1/2$ and $\sigma_3/\sigma_5 = -2/7$ yield the following edge stresses:

$$\begin{aligned} \sigma_7 &= + \frac{M_x}{W_7^*} = + \frac{45}{23} \frac{M_x}{a F_0}, \\ \sigma_5 &= - \frac{M_x}{W_5^*} = - \frac{21}{23} \frac{M_x}{a F_0}, \\ \sigma_3 &= - \frac{2}{7} \sigma_5 = + \frac{6}{23} \frac{M_x}{a F_0}, \\ \sigma_1 &= - \frac{1}{2} \sigma_3 = - \frac{3}{23} \frac{M_x}{a F_0}. \end{aligned} \quad (13.17)$$

The results are identical with those obtained by means of the slender-member theory in Exercise 6.1 (note the reversed annotation of plates and edges).

Aside from permitting a greatly simplified analysis, the folded-plate method permits the observation that the results do not depend on the shape and the plate widths of the unloaded portion of the folded plate. The stresses summarized in Eqs. (13.17) may therefore occur in infinitely many other profiles.

The parameters which may be selected arbitrarily within the limits set by Section 13.1 are δ_3 , δ_5 , c_2 and c_4 (v. Fig. 13.6c).

A symmetric, three-plate profile which is very often applied for bridges shall be treated next. It consists of a horizontal floor slab which rests on two main girders. An arbitrary vertical load may always be divided up into a symmetric and antisymmetric system of loads whose forces act in the planes of the plate girders only (v. Figs. 13.7b and c). The edge-stress ratios of the floor slab are an immediate consequence of the symmetries. They are +1 for the symmetric and -1 for the antisymmetric case. In every case, the cross section according to the core-point method may be separated into two independent plate girder cross sections (v. Figs. 13.7b and c). The areas F^* of the top flanges follow from Eq. (12.24) resp. Eq. (12.25). The axial stresses, shear stresses as well as the deflec-

tions may now be calculated for these substitute plate girders. The axial stresses are linearly distributed in the floor slab and the shear flow, finally, may be calculated by means of Eqs. (11.28).

The foregoing procedure had been proposed by a few authors^{1,2} and an observation by F. RESINGER³ made it even more suitable. He pointed out that the shear center of this bridge cross section is as much above the floor slab

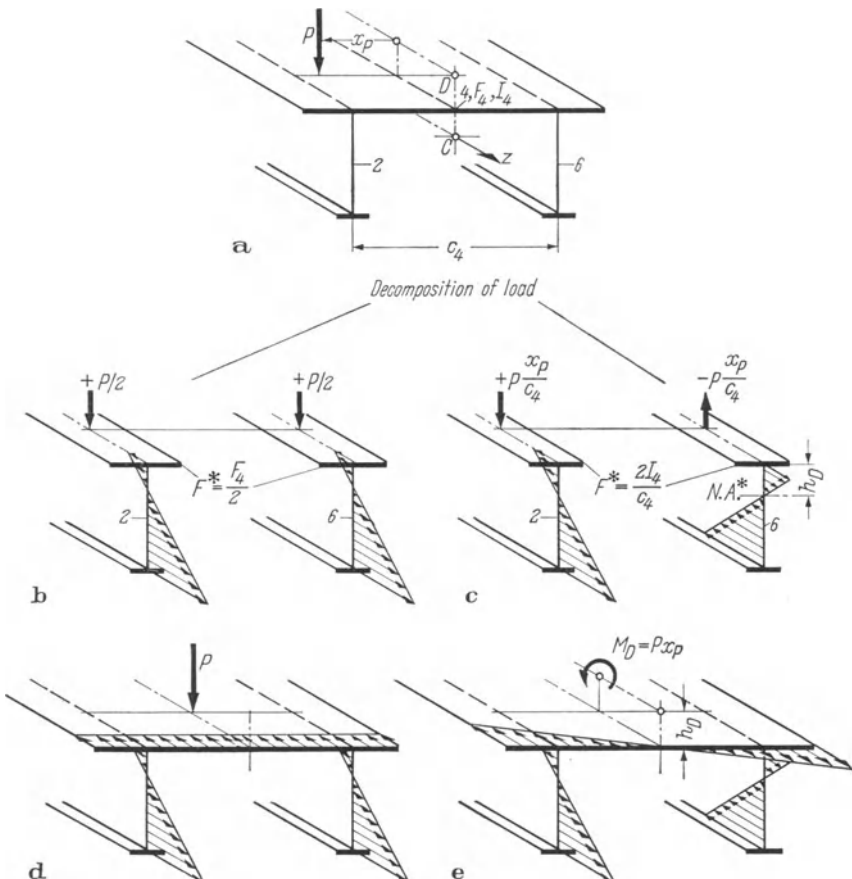


Fig. 13.7. Axial Stresses in a Symmetric Three-Plate Profile
Using the Folded-Plate Theory (b and c) and the Slender-Member Theory
(d and e).

(v. Fig. 13.7a) as the neutral axis of the substitute plate girder for antisymmetric load is below (v. Fig. 13.7c). The position of the shear center must be known whenever an analysis for arbitrarily directed loads (e.g. wind) is required. The shear center is not required, however; in the application of the general folded-plate theory described above (v. Fig. 13.5).

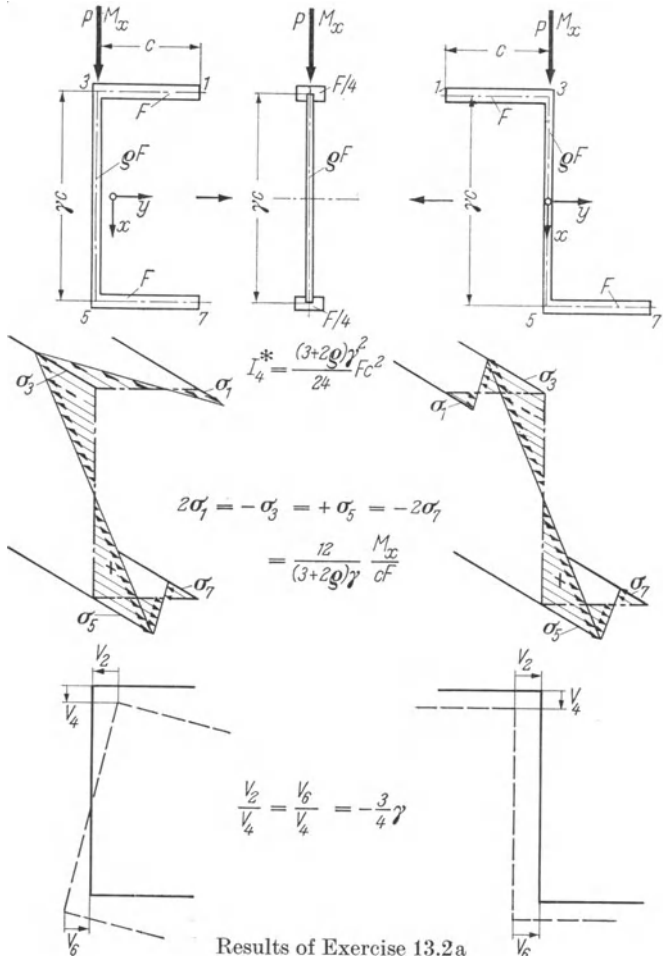
¹ BEUSCH, J., and G. PESTALOZZI: *Statische Berechnung der St. Albanbrücke*, Basel, 1953.

² BASLER, K.: *Diplomarbeit, ETH Zürich*, 1954.

³ RESINGER, F.: *Ermittlung der Wölbspannungen an einfach symmetrischen Profilen nach dem Drillträgerverfahren*. *Stahlbau* 26 (1957) 321.

For illustrative comparison of the fundamental differences between the two theories, the concept of the folded-plate theory (Figs. 13.7 b and c) and the slender-member theory (Figs. 13.7 d and e) are shown together. The latter replaces a lateral load with components at the shear center and considers bending and warping torsion separately.

It should be remembered that both theories are bound to yield the same results since the structural shape belongs to the class of three-plate profiles whose Saint-Venant torsional resistance is negligible.



Exercise 13.2. L and T Cross Sections. The axial stresses and deflections of parallel-flanged L and T cross sections shall be calculated by means of the folded-plate theory. The loads are either acting in the plane of the web or in the plane of the flanges.

Data:

Flange area F and flange width c , web area qF and depth of web γc .

Required Results:

Axial stresses, moment of inertia I^* for the evaluation of the deflection of the loaded plate and relative deflections of the remaining plates. The load shall be characterized:

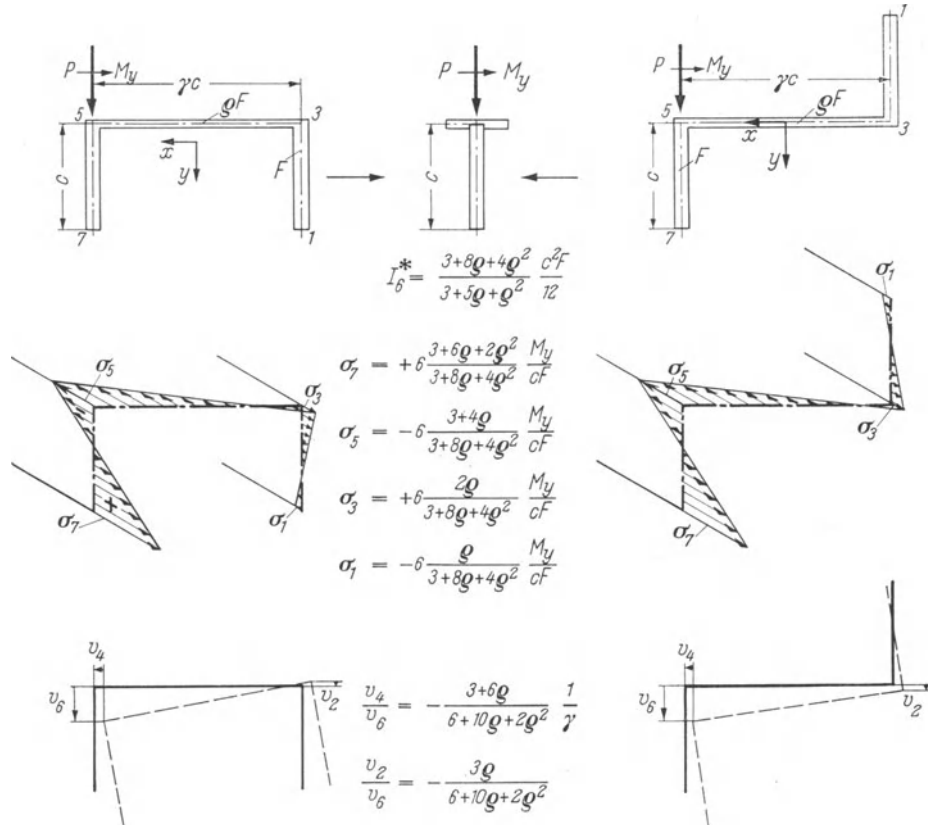
- a) by M_x if acting in the plane of the web,
- b) by M_y if acting in the plane of the flange.

Results:

a) The substitute profile for both the L and T section is a symmetric I section whose flange areas are one fourth of the actual ones. The moment of inertia I_6^* of this reduced cross section leads to the deflection v_4 and the remaining deflections follow from Eq. (11.40).

The results are summarized below. They are identical for both types of cross sections.

b) The substitute for both cross sections is the same T section. Its flange area follows from the relation (12.19).



Results of Exercise 13.2b

Exercise 13.3. Comparison. Verify that the results of Exercise 13.2 are equivalent to those determined in Section 10.1c and d if the slender-member theory used therein considers only bending and warping resistance, i. e. neglects the contribution of Saint-Venant torsion.

Hint: The stress distribution in an L section for load in the plane of the web only is according to Eq. 10.9a described by the following relation:

$$\sigma = \frac{M_x}{I_{xx}} x + \frac{M_\omega}{I_{\omega\omega}} \omega .$$

Without Saint-Venant torsion, the relation for the warping moment is $M_\omega = -e M_x$. With the eccentricity of the shear center e given by Eq. (10.11b) and the cross-sectional values listed in Table 10.1, one will arrive at the identical results of Exercise 13.2a.

13.3 The Essential Difference Between the Two Theories

a) General Remarks

a) Deformation. If the Saint-Venant torsional resistance is neglected, the differences between the folded plate theory and the slender-member theory arise from different assumptions for the deformations. These differences and their consequences shall therefore be discussed subsequently.

Aside from the common assumption of negligible shear deformations and linearly elastic material, the slender-member theory assumes the preservation of the entire cross section while the folded-plate theory subjects only each plate to this condition. This distinction may have significant consequences in some cases and may be meaningless in others.

The distance between two parallel edges of a plate, i.e. the width of a plate, does not change if a loaded member deforms. The affinitive plate deflections resulting from a folded-plate analysis therefore completely determine the displacement of interior edges or hinges between two adjacent plates but they do not impose restrictions for the position of end-plates. This uncertainty was in some cases simply suppressed in that the deformed positions of *end-plates* were assumed to be parallel to the original ones (v. Fig. 11.9 or Fig. 12.2c). But note that any other position could have been equally possible as long as these arbitrary rotations are of the same order of magnitude as those of the remaining plates. This restriction has to be imposed in order not to violate the assumption that the stresses may be determined for the undeformed geometry of the cross section. It is thus possible to have the end-plates undergo the rotation of the adjoining plates. This means that the shape may at least be preserved for portions of the cross section consisting of the first two and the last two plates.

Since the internal plate of a three-plate profile is common to both the first two and the last two plates, this cross section may preserve its shape even though the stresses are calculated by means of the folded-plate theory. These considerations were applied in the sketches of the deformed cross sections in Exercise 13.2. It may be recognized that there is no difference between the assumptions of the slender-member and the folded-plate theory in the case of a three-plate profile. Aside from the effect of Saint-Venant torsional resistance, the results of both theories are therefore identical.

The very same train of thought yields the conclusion that the differences in the deformations of a four-plate structure with the plates 2, 4, 6 and 8 must originate in angle 5 and, generalizing, those of an n -plate structure must be attributed to the changes of $n - 3$ plate angles. The general folded plate has therefore $n - 3$ possibilities or degrees of freedom to develop differences in the deformations.

b) Stresses. Since the complete set of stresses or internal forces has to be in equilibrium with the applied load independently of the method used for the analysis, the difference between the results of different methods will constitute a *residual state of stress*.

The residual shear stresses may likewise be added to resultant plate shears which may be thought of as introduced by loads at the edges (v. Fig. 13.8).

Such a group of three parallel edge loads may be defined by means of the distances between the lines of action and the reference load X . The latter quantity needs to be determined. Since according to the folded plate theory loads may only be introduced at interior edges and not at free plate boundaries, the first position of the group incorporates already the first three plate intersections. Another independent state of residual stress produced if the entire group of loads is shifted by one plate.

It is therefore possible to produce as many different states of residual stresses as there are degrees of freedom for differences in deformations. It may be immediately confirmed that a folded plate consisting of n plates offers $n - 3$ such possibilities. The three-plate profile which has only two plate intersections is therefore not able to exhibit residual stresses which might be the reason for differences in the results.

If the results of the folded-plate theory are to be converted into those of the slender-member theory, one applies $n - 3$ groups of load to the structure. The redundant quantities X_k may be determined from the conditions requiring constant angles between the plates.

b) The Roof Cross Section

A very simple example for a folded plate with more than three plates was presented in Fig. 11.1. The dimensions of its thin-walled, open cross section are given in Fig. 11.3.

This system was analyzed by means of the folded-plate theory in Section 12.4c and the results are presented in Eqs. (12.20). The corresponding results for an undeformed cross section are:

$$\sigma_5 = -\frac{3}{4} \frac{Pl}{4cF},$$

$$\sigma_3 = \sigma_7 = 0, \quad (13.18)$$

$$\sigma_1 = \sigma_9 = +\frac{3}{4} \frac{Pl}{4cF}.$$

Since the two different stress distributions are in equilibrium with the single load P , their difference [Eqs. (12.20) minus Eqs. (13.18)] yields the following residual stresses.

$$\sigma_5 = -\frac{3}{2} \frac{Pl}{4cF_0},$$

$$\sigma_3 = \sigma_7 = +\frac{3}{2} \frac{Pl}{4cF_0}, \quad (13.19)$$

$$\sigma_1 = \sigma_9 = -\frac{3}{2} \frac{Pl}{4cF_0}.$$

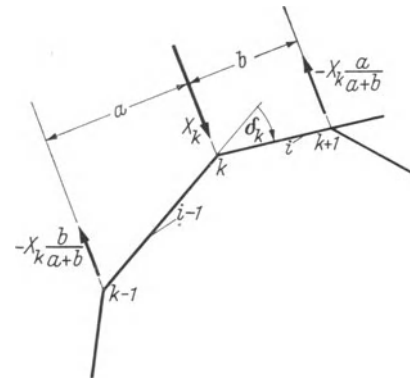


Fig. 13.8. Group of Forces Producing a Residual State of Stress.

The distribution of these residual stresses is shown in Fig. 13.9. The shape of this stress distribution will be the same for all possible loads since the differences in a four-plate profile have only one degree of freedom ($n = 4, n - 3 = 1$). The magnitude of the stresses depends of course on the load. In order to verify the truth of this statement, the residual stresses shall subsequently be calculated for the unsymmetric load of Fig. 11.3.

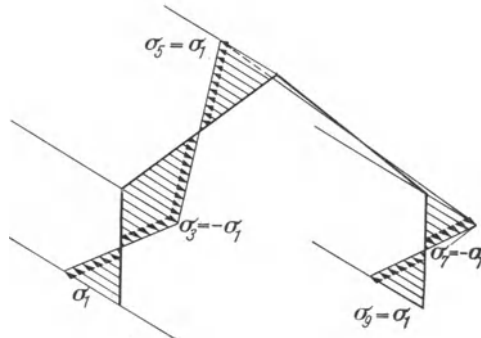


Fig. 13.9. The Distribution of Residual Stresses in the Four-Plate Profile of Fig. 11.3.

The axial stresses which result from the folded-plate theory were presented in Eqs. (11.11) while those according to the slender-member theory were calculated in Exercise 6.2 b. The difference between the two stress distributions is as follows:

Common multiplier	Eq. (11.11)	Exercise 6.2 b	Residual Stresses $\Delta\sigma$
	$\frac{M_{80}}{cF}$	$\frac{M_{80}}{cF}$	$\frac{M_{80}}{cF}$
σ_1 :	$+\frac{3}{28}$	$- \left(-\frac{39}{28} \right)$	$= +\frac{3}{2}$,
σ_3 :	$-\frac{3}{14}$	$- \left(+\frac{9}{7} \right)$	$= -\frac{3}{2}$,
σ_5 :	$+\frac{3}{4}$	$- \left(-\frac{3}{4} \right)$	$= +\frac{3}{2}$, (13.20)
σ_7 :	$-\frac{39}{14}$	$- \left(-\frac{9}{7} \right)$	$= -\frac{3}{2}$,
σ_9 :	$+\frac{123}{28}$	$- \left(+\frac{81}{28} \right)$	$= +\frac{3}{2}$.

The shape of the stress distributions (13.19) and (13.20) is in fact the same and equal to the distribution shown in Fig. 13.9. These two results give rise to further observation. Since the absolute values of both residual stresses are the same, it may be concluded that the symmetric load diminishes the angle δ_5 at the ridge by the same amount as this angle is increased by the eccentric load.

c) T-Beam Cross Sections

The open bridge cross sections encountered heretofore belonged to the class of three-plate profiles from the view-point of the folded-plate theory. The same member would have to be analyzed as a four-plate profile if the floor slab were made to rest on three plate girders instead of on two.

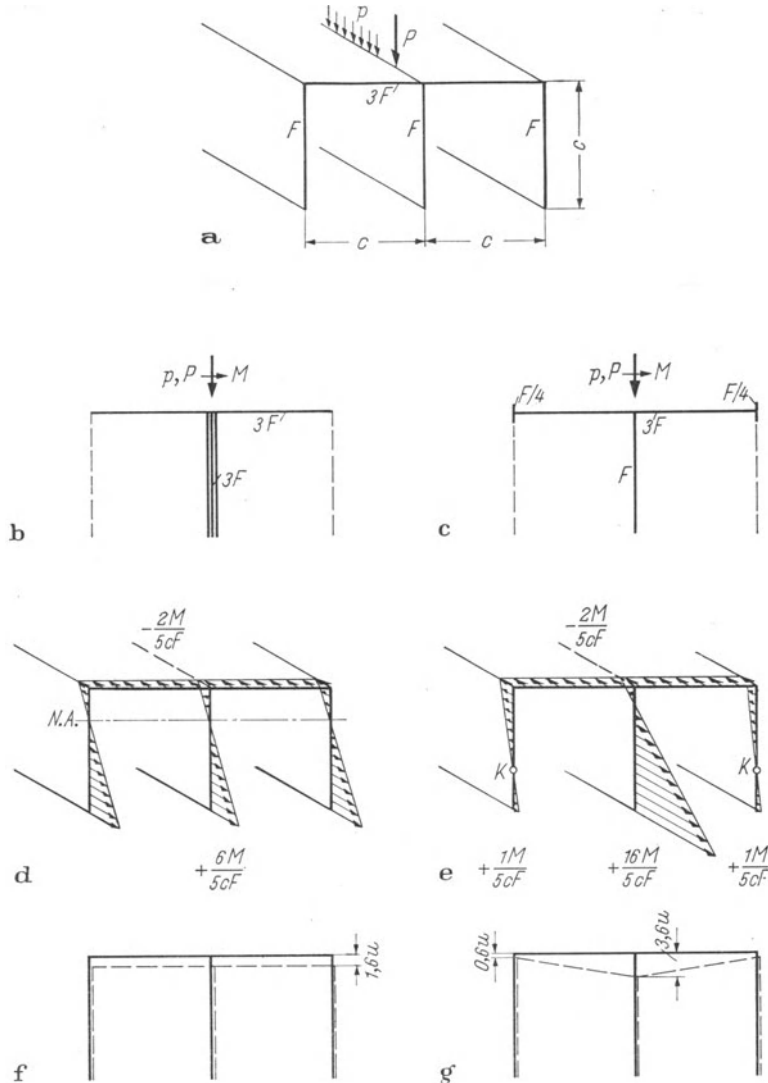


Fig. 13.10. Example of a T-Beam Cross Section. Application of the Slender-Member Theory (to the left) and the Folded-Plate Theory (to the Right) for a Load on the Central Girder.

Such a cross section, which is only too often analyzed as a girder grillage, will be the subject of the subsequent studies. In order to arrive at simple analytical results, the following considerations will be concerned with the cross section shown in Fig. 13.10a.

a) Load On the Central Girder. The bending theory may be applied to the modified cross section of Fig. 13.10b. It leads to the stress distribution shown in Fig. 13.10d.

The *folded-plate theory*, however, leads to a completely different state of stress. It assigns only the edge forces in the plane of the floor plate to the two outer girders. The core point K belonging to their point of action is therefore free of axial stresses. These outer girders may be replaced by the areas $F^* = F/4$ and the edge-stress ratio amounts to $-1/2$. The results of the folded-plate theory may therefore be calculated for the T -section of Fig. 13.10c. The resulting axial stresses are presented in Fig. 13.10e.

Fig. 13.10d and e illustrate drastically the difference between the two theories. The folded-plate theory yields a heavily non-uniform stress distribution. The bottom flange stresses of the outer girders are 6 times smaller and those of the central girder 2.7 times larger than the corresponding values of the bending theory.

It is only because of the simple proportions that both theories lead to the same axial stresses in the floor slab. This is only accidental and is in general not the case.

The plate deflections as given by Eq. (11.40) are plotted in Fig. 13.10f and g. In accordance with the assumption, the bending theory assumes preservation of the shape of the cross section while the folded-plate theory does not.

b) Load on an Outer Plate Girder (Fig. 13.11a). In accordance with the *theory of open, thin-walled cross sections*, the load is divided up into a symmetric and antisymmetric component. If the load in the longitudinal direction is arranged as in Fig. 13.10, the stresses caused by the symmetric component are those given by Fig. 13.10d. The antisymmetric component does not cause stresses in the central plate girder and may therefore be treated as in Fig. 13.7. The results for this simple problem may be obtained even more readily if the results of Exercise 13.2 are modified for $\varrho = 3$ and $\gamma = 2$. Fig. 13.11d shows the superposition of the flexural and torsional stress components.

The contribution of unloaded plate girders is according to the folded-plate concept considered by means of replacement areas [Eqs. (12.16)] and corresponding edge-stress ratios [Eq. (12.17)]. In the simple case considered herein, the latter are again $F/4$ resp. $-1/2$. Elimination of the two unloaded plate girders reduces therefore the cross section to the one shown in Fig. 13.11c. It may, by means of the recurrence relation (12.6), be even further reduced to a simple T -section with substituting flange area $F^* = 23 F/28$. Eq. (12.5) yields an edge-stress ratio of $-3/7$ in the floor slab. The resulting axial stresses are presented in Fig. 13.11e.

γ) Residual Stresses. According to the theory presented above, the difference between the folded-plate theory and the slender-member theory will in each case consist of a residual stress distribution of the same shape accompanied by a kink at the center of the floor slab which depends on the corresponding load.

For the case of centric loads, the state of residual stresses (folded-plate minus slender-member stresses) is given in Fig. 13.12a. The corresponding difference in the deflection of the plate girders is shown in Fig. 13.12b. The relative deflection

of the central plate girder with respect to the outer ones is $+3u$ thus defining a kink of the floor slab of $\Psi = 6u/c$.

If the same load stands on an outer plate girder, the relative deflection of the central girder is $-1.5 u$ and the resulting angle of the kink is $\Psi = -3u/c$.

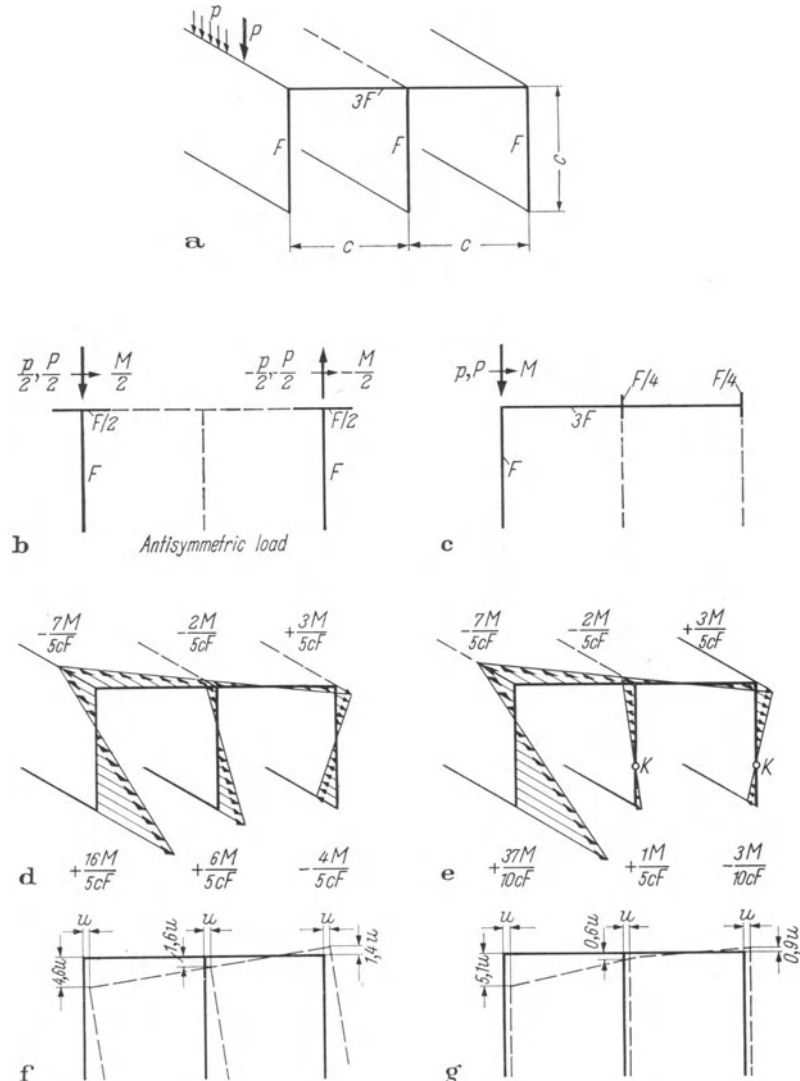


Fig. 13.11. Example of a *T*-Beam Cross Section. Application of the Slender-Member Theory (to the left) and the Folded-Plate Theory (to the right) for a Load on the Outer Girder.

If one therefore would like to obtain the stresses in the eccentrically loaded slender member without going through the warping analysis, the corresponding folded-plate stresses would have to be added to those resulting from half ($1,5u/(3u) = 0,5$) the equilibrium system of Fig. 13.12a. Such a procedure does in fact yield the stresses presented in Fig. 13.11d.

Exercise 13.4. Configuration of the Load

a) What must be the distribution of a symmetric load on the three main girders of the cross section shown in Fig. 13.10a so that both the folded-plate theory and the slender-member theory yield equivalent results?

b) What must be the position of an eccentric load on a secondary cross girder stretching from the outer to the central main girder so that again both theories lead to the same results?

Solution:

- One third of the total load on each girder.
- The distance $2c/3$ away from the axis of symmetry.

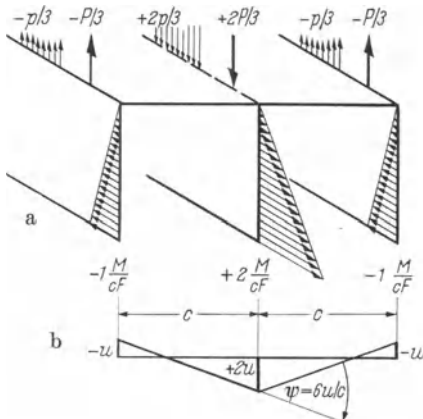


Fig. 13.12. Difference Between the Folded-Plate and Slender-Member Theory, a State of Residual Stresses.

13.4 The Approximation to the Actual Structural Behavior

a) The Influence of a Cross Beam

Since the differences between the folded-plate theory and the slender-member theory may be attributed solely to the different assumptions for the deformation of the member cross-section, it may be expected that any stiffeners, whether cross beams, ribs or transverse diaphragms, must have a marked influence on the stresses.

In order to have a basis for the subsequent discussions, the influence of a cross beam on the behavior of a T -beam bridge will be studied. It will again be referred to the schematic cross section of Fig. 13.10a. The bridge has a span of length l and the cross beam is placed at mid-span. It is acted upon by a concentrated single load P in the position z resp. z' ($\zeta = z/l$, $\zeta' = z'/l$) of the central girder (v. Fig. 13.13a).

The unit u for the deformations shown in Figs. 13.10g and 13.11g may be calculated from Eq. (11.42) in which $\Delta\sigma_i/c_i$ assumes the value $M/(c^2F) = (1/2)Pl\zeta/(c^2F)$.

The deflection at mid-span for the load in the first half of the bridge ($\zeta < 1/2$) amounts to:

$$u = \frac{1}{2} \frac{Pl\zeta}{c^2F} \frac{l^2}{6E} \left(\frac{3}{4} - \zeta^2 \right)$$

thus defining a kink $\Psi_0 = 6u/c$ in the floor slab at mid-span of:

$$\Psi_0 = \frac{P}{2EF} \frac{l^3}{c^3} \zeta \left(\frac{3}{4} - \zeta^2 \right). \quad (13.21)$$

This deformation of the cross section is resisted by the cross girder which consequently exerts a reaction on the folded plate in the form of the equilibrium system X shown in Fig. 13.13 b. The reactions induce again the same state of residual stresses as presented by Fig. 13.12.

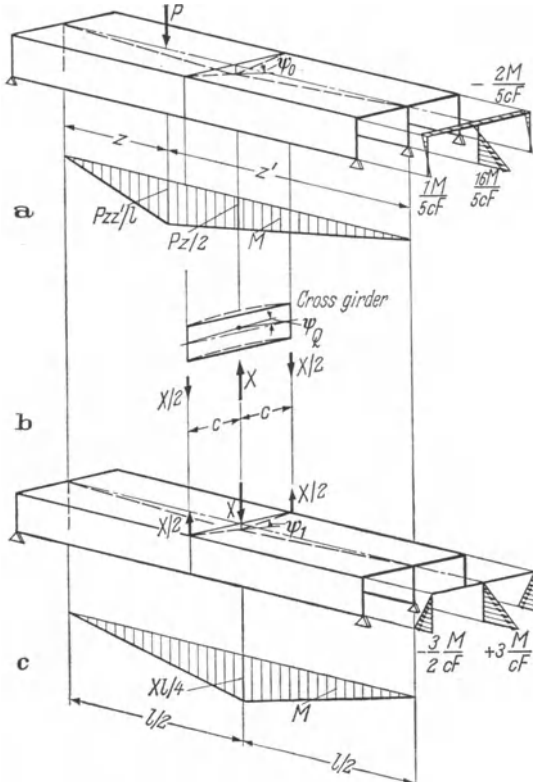


Fig. 13.13. The Influence of a Cross Beam.

If X is assumed to be unity and therefore $M = l/4$ at mid-span, both the residual stresses and the kink in the floor slab at mid-span are equal to $3/2$ times the values given by Fig. 13.12. The expression for the kink Ψ_1 is thus $3/2$ times the value of Eq. (13.21) for $\zeta = 1/2$ and $P = 1$:

$$\Psi_1 = \frac{3}{16} \frac{1}{EF} \frac{l^3}{c^3}. \quad (13.22)$$

The deflection of the cross beam itself when acted upon by the force system X is:

$$\Psi_Q = - \frac{c^2}{3EI_Q}. \quad (13.23)$$

The compatibility condition may be formulated as:

$$\Psi_0 + \Psi_1 X = \Psi_Q X$$

or as:

$$X = - \frac{\Psi_0}{\Psi_1 - \Psi_Q}. \quad (13.24a)$$

The different angles of the kink Ψ are expressed by Eqs. (13.21), (13.22) and (13.23). They transform Eq. (13.24a) into:

$$X = - \frac{8}{3} P \frac{\zeta \left(\frac{3}{4} - \zeta^2 \right)}{1 + \frac{16}{9} \frac{Fc^2}{I_Q} \frac{c^3}{l^3}} \quad (\zeta \leq 1/2). \quad (13.24b)$$

If the structure had such proportions that the second element in the denominator would become equal to one, the redundant X for a load at $\zeta = 1/3$ would become $X = -0,284 P$.

If the cross girder is missing, $I_Q = 0$, the redundant X becomes zero. If, on the other hand, the rigidity of the cross beam is infinite, $I_Q = \infty$, the resisting force X is:

$$X = - \frac{8}{3} P \zeta \left(\frac{3}{4} - \zeta^2 \right). \quad (13.25)$$

The resulting stresses are the superposition of the stresses in the folded plate (Fig. 13.13a) and the effect of the cross girder (Fig. 13.13c). The bottom-flange stresses as the result of such a superposition are presented in Fig. 13.14 assuming an infinitely rigid cross girder and the load at $\zeta = 0,2$ ($X = -0,38 P$).

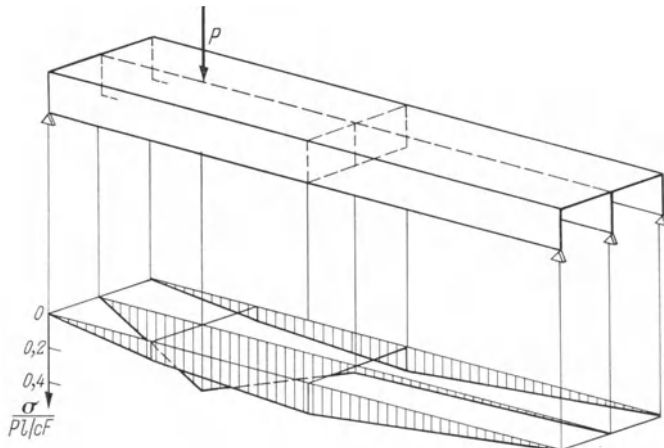


Fig. 13.14. Axial Stresses in the Bottom Flanges of the Structure Shown in Fig. 13.13a.
Cross Girder is Infinitely Rigid and the Load Stands at $\zeta = 0,2$.

Exercise 13.5. *Eccentric Load.* Calculate and sketch the axial stresses in the bottom flanges if the cross girder is still infinitely rigid ($I_Q = \infty$), the load is still at $\zeta = 0,2$ but is now standing on an outer girder (v. subsequent figure).

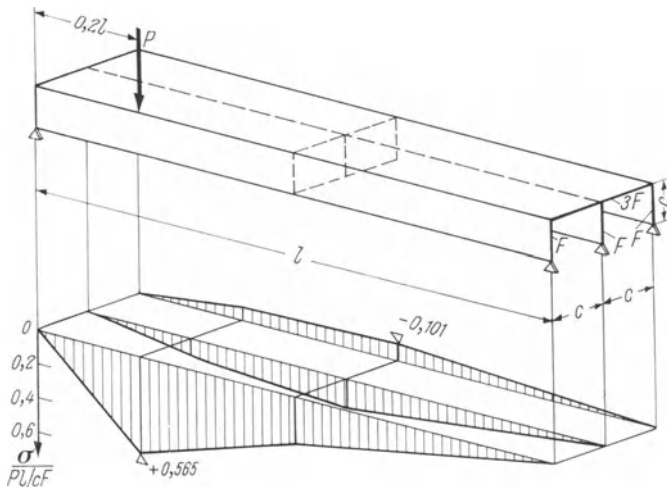
Solution:

The general expression for the redundant is:

$$X = + \frac{4}{3} P \frac{\zeta \left(\frac{3}{4} - \zeta^2 \right)}{1 + \frac{16 F c^2}{9 I_Q} \frac{c^3}{l^3}}.$$

The latter becomes $X = 0,19 P$ for $\zeta = 0,2$ and $I_Q = \infty$.

The resulting distribution of the axial stresses in the bottom flanges is presented in the following figure.



Solution to Exercise 13.5

b) Diaphragms as Infinitely Rigid Cross Girders

It was shown in the previous section that the influence of a flexible cross girder might be considered without taking refuge in the inadequate girder-grillage techniques. The procedure was demonstrated by means of a simple four-plate profile. However, it may be considerably simplified in most cases since the cross girders may usually be assumed to be completely rigid. Such infinitely rigid transverse stiffeners shall be denoted as *diaphragms*.

It shall first be numerically verified how small the influence of cross-girder deformations actually is. If the cross-sectional dimensions of a cross beam are assumed to be the same as those of the longitudinal girders, its rigidity is $I_Q = c^2 F / 12$ or more depending on whether the floor slab is made to participate or not. Since the ratio between the span l and the depth of the main girders c is certainly not less than 10, the denominator of Eq. (13.24b) will certainly not be larger than

$$1 + \frac{16}{9} \frac{12}{10^3} = 1 + 0,02.$$

This denominator is unity for an infinitely rigid cross girder. It appears therefore that the consideration of cross girder flexibility is not likely to change the redundant quantity X by more than 2%.

The redundant quantity X for the single load P at the rigid cross girder becomes according to Eq. (13.25) $X = -2P/3$. It appears from Fig. 13.12 that this is exactly the load which causes the differential residual stresses which

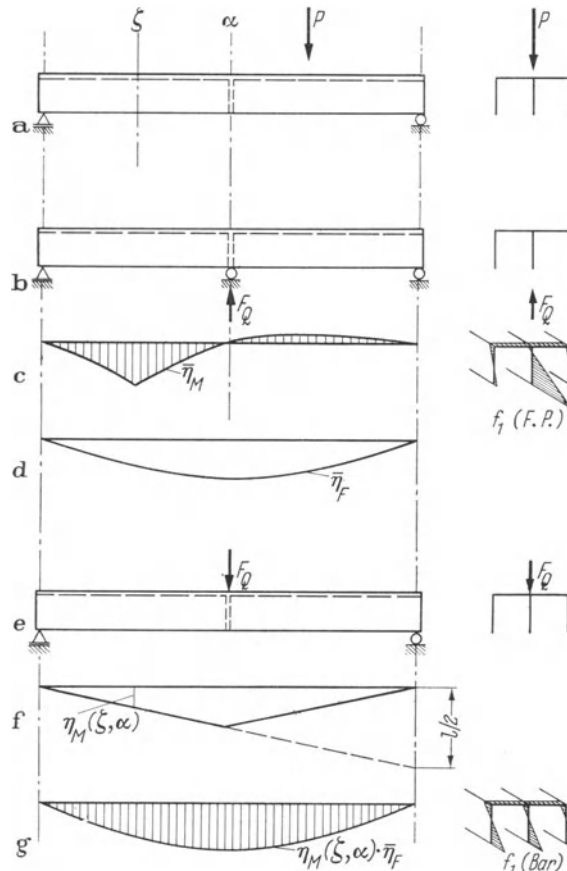


Fig. 13.15. Analysis of a Folded Plate with Diaphragm.

represent the difference between folded-plate theory and slender-member theory. If therefore the folded-plate stresses for the load P at the cross girder are added to those of the redundant X , one arrives exactly at the results of the ordinary beam theory. Since this is not a peculiarity of this simple four-plate structure, one may formulate the following fundamental theorem:

If a four or multiple-plate structure is acted upon by concentrated loads, it suffices to introduce diaphragms at each load in order to secure the assumptions of the slender-member theory.

Even though this theorem is not applicable for the case of moving loads, it may nevertheless be utilized in the analysis of a structure by influence lines. The following ideas will again be explained by means of a practical example. Consider for this purpose the structure shown in Fig. 13.13a which has the cross section of Fig. 13.10a. All the statements may arbitrarily be extrapolated to continuous, fixed-end or cantilever structures. The symbols f_1 and f_2 which were introduced in Section 11.2b for the application of influence lines shall again be used.

Imagine first that the structure (Fig. 13.15a) has one additional support at the interior diaphragm (Fig. 13.15b). The new system represents now an *unstiffened*, i.e. true folded plate structure which therefore may be analyzed accordingly. However, the new structure has more and considerably shorter spans.

The bending moments in the transformed structure may be determined from the influence lines $\bar{\eta}_M = \bar{f}_2$ and the stress distribution in the cross section follows from the folded-plate scheme f_1 (F. P.) (Fig. 13.15c).

The reaction F_Q at the support which is represented by the influence line $\bar{\eta}_F$ (Fig. 13.15d) is now assumed to act as a load on the structure. The above theorem states clearly that the stress distribution for this load follows from the slender-member theory, f_1 (Bar).

If the influence coefficient for the bending moment in ζ due to the load at the position α of the diaphragm is denoted by $\eta_M(\zeta, \alpha)$ (Fig. 13.15f), one may calculate therefrom the function $f_2(z)$ (Fig. 13.15g) which gives rise to the stress distribution from the slender-member theory.

The superposition of the two effects represented by Figs. 13.15c and g may be formulated as follows:

$$\sigma = f_1(\text{F.P.}) \cdot \bar{\eta}_M + f_1(\text{Bar}) \cdot \eta_M(\zeta, \alpha) \cdot \bar{\eta}_F. \quad (13.26)$$

It must be noted here that the distribution of the reactions is affinitive to the plate forces effected by the loads. Only in this example the central plate girder is therefore responsible for the reaction F_Q .

Exercise 13.6. *Alternate Way of Solving Exercise 13.4.*
Check the two numerical values that were introduced in the solution of Exercise 13.5 using the method described above.

e) The Number of Diaphragms

The information given in this section leads to the following limit functions for the axial stresses in the bottom flange of the central girder caused by the moving centric load P (Fig. 13.13a):

From slender-member theory:

$$\sigma = \frac{6}{5} \frac{Pl}{cF} \zeta (1 - \zeta). \quad (13.27a)$$

From folded-plate theory considering a diaphragm at mid-span:

$$\sigma = \frac{Pl}{cF} \zeta \left(\frac{16}{5} - \frac{31}{5} \zeta + 4\zeta^3 \right) \quad (\zeta \leq \frac{1}{2}). \quad (13.27b)$$

From folded-plate theory without diaphragm:

$$\sigma = \frac{16}{5} \frac{Pl}{cF} \zeta(1 - \zeta). \quad (13.27c)$$

The distribution of the stress limits (13.27) is presented in Fig. 13.16. These curves show clearly the significant effect of only one diaphragm at mid-span. They confirm the observation made earlier that the slender-member theory and the folded-plate theory are equivalent if the loads are positioned at diaphragms.

The extreme difference between the two theories occurs about halfway between the support and the diaphragm.

A very similar picture would be obtained if two equally spaced diaphragms were introduced. The limit curve would consist of three parts and the difference between both theories would, because of the reduced intermediate spans, be even smaller. This, however, is not necessarily an advantage since the maximum slender-member stresses would have to be added to the maximum deviation thus making the expense for an additional diaphragm of dubious value.

The effect of a division into four equal parts, however, would be considerable, but the stresses may not be reduced below those of the slender-member theory no matter how many interior diaphragms are provided.

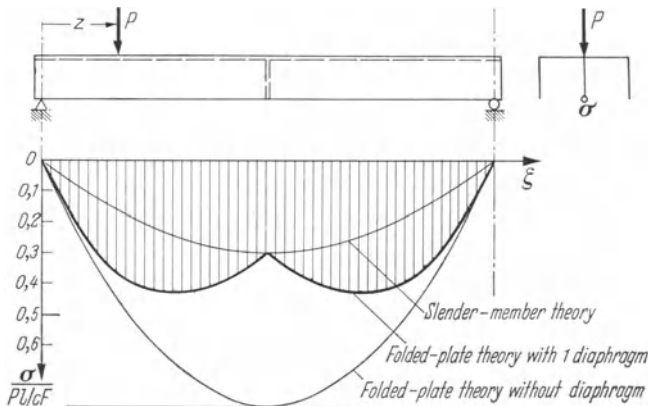


Fig. 13.16. Limit Curves for the Bottom-Flange Stresses of the Central Girder which is Acted Upon by a Moving Load P .

The curve representing the results of the slender-member theory in Fig. 13.16 might alternatively be denoted as the curve which presents the results of the folded-plate theory for a structure with infinitely many interior diaphragms. This gives rise to another possibility of achieving equivalence of both theories.

The extreme tensile stresses in the considered structure occur in the bottom flange of an outer girder for a load P acting in its plane. The same three limit curves are presented for this case in Fig. 13.17. It appears from these curves that after introducing one diaphragm at mid-span, the difference between the extreme stresses of both theories becomes almost negligible.

If one considers further that there is not any difference between the two theories if the three main girders carry equal load (dead load) or if the live load acts at certain positions between the central and outer girder (v. results to Exercise 13.3), one will find in most cases that the provision of only one diaphragm at the position of extreme positive moments constitutes the most economical solution.

This single diaphragm usually suffices to reasonably satisfy the assumptions of the slender-member theory. This does not mean that the influence of member rotation may altogether be neglected. Figs. 13.16 and 13.17 demonstrate clearly what the difference may be if the load moves from the central to an outer girder. It merely states that the condition of an undeformed cross section is sufficiently satisfied in most practical applications.

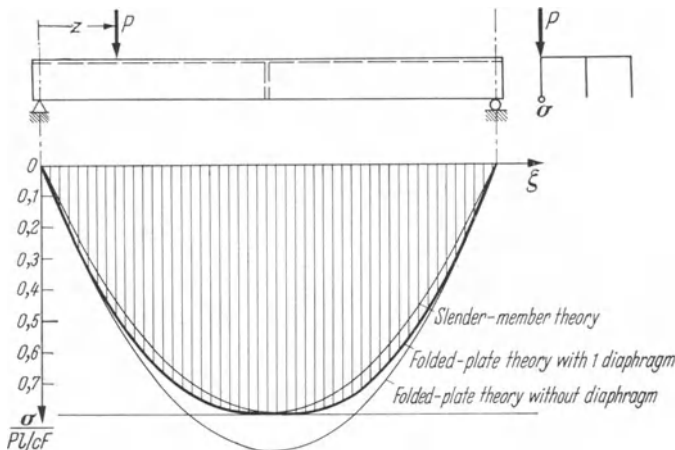


Fig. 13.17. Limit Curves for the Bottom-Flange Stresses of an Outer Girder which is Acted Upon by a Moving Load P .

Exercise 13.7. Eccentric Load. Calculate the limit curves for the axial stresses in the lower flange of an outer girder both by means of slender-member theory and folded-plate theory. The structure may or may not be stiffened by a diaphragm at mid-span.

The structure with the span l and a cross section as shown in Fig. 13.11 is acted upon by a moving load P on the outer girder.

Solution:

Slender-member theory, with or without diaphragm:

$$\sigma = \frac{16}{5} \frac{Pl}{cF} \zeta (1 - \zeta).$$

Folded-plate theory, without diaphragm:

$$\sigma = \frac{37}{10} \frac{Pl}{cF} \zeta (1 - \zeta).$$

Folded-plate theory, with diaphragm:

$$\sigma = \frac{Pl}{cF} \zeta \left(\frac{37}{10} - \frac{89}{20} \zeta + \zeta^3 \right), \quad (\zeta \leq \frac{1}{2}).$$

d) Summary

Even though the folded-plate theory as presented herein is based on assumptions that may not be exactly satisfied in practice, it is an important fact that it furnishes, together with the slender-member theory, limits for the actual behavior of a structure. The preservation of the cross-sectional shape which constitutes the main assumption of the slender-member theory is completely disregarded by the folded-plate theory.

The plates of an actual folded-plate structure are always rigidly connected along their longitudinal edges. Their transverse rigidity, however, is usually not large enough to guarantee the shape of the cross section. The deviations from the theoretical assumptions are usually not serious. It was demonstrated that the differences induced by the two extreme assumptions, — complete preservation of the cross section or none at all —, are usually so small that it is sufficient to calculate the bounds. The results even coincide for two- or three-plate profiles whose Saint-Venant torsional resistance is negligible. Extreme differences may be eliminated by means of diaphragms. In some cases it is even necessary to provide diaphragms in order to arrive at an economical design.

The bounds for the stresses in a structure whose cross sectional deformations are restrained by means of diaphragms may readily be found: the folded-plate stresses may be thought to be the superposition of two components. One is represented by the folded plate stresses in the structure with imaginary intermediate supports at the diaphragms and the second considers, by means of the slender-member theory, the effect of the imaginary reactions. The actual stresses are always between those of a folded-plate and a slender-member analysis.

It is always conservative to determine the stresses in a cross girder by means of the slender-member theory only.

Dimensions of a Few Newly Introduced Quantities

I_{xx}, I_{yy}, I_{xy} :	[Length] ⁴	M_x, M_y :	[Force] · [Length]
$I_{\omega\omega}$:	[Length] ⁶	M_ω :	[Force] · [Length] ²
$I_{\omega x}, I_{\omega y}$:	[Length] ⁵	q :	[Force] · [Length] ⁻¹
K :	[Length] ⁴	\tilde{S}_x, \tilde{S}_y :	[Length] ³
m_D :	[Force]	\tilde{S}_ω :	[Length] ⁴
M_D :	[Force] · [Length]	T, T_s, T_ω :	[Force] · [Length]
		ω, Ω :	[Length] ²

Appendix

By

BRUCE G. JOHNSTON

Rolled Structural Shapes

A. 1 Introduction

Accurate formulas have been developed for the calculation of the torsion constants for standard rolled shapes. They are not for direct use in design, but have made possible the preparation of tables in manuals for the torsion constants of rolled shapes based on nominal handbook dimensions. These formulas are summarized in this Appendix and additional information is provided regarding the shear stress resulting from Saint-Venant torsion of such shapes.

The torsion constant of a rolled shape of open cross section may be roughly approximated simply as the sum of the constants of its separate rectangular or trapezoidal components. For example, if the components consist of rectangles of breadth " b_i " and thickness " t_i ", the torsion constant is approximated by:

$$K = \sum_i \frac{b_i t_i^3}{3}. \quad (\text{A. 1})$$

The torsion constant is equal in magnitude to twice the volume under the stress function surface, divided by $G\theta$. The shape of the stress function may be visualized by a consideration of Prandtl's Membrane Analogy. The stress function is zero at the periphery of an open section. Away from the edges, a cross section through the stress function surface, normal to the broad side of the rectangle, acquires a nearly uniform parabolic shape. Eq. (A. 1) would be exact if the parabolic shape were maintained right to the edges. But, because it does not maintain this shape to the edges, there is an "edge loss" at each edge. On the other hand, if two or more rectangles are joined to form an angle, channel or wide flange shape, Eq. (A. 1) neglects the "hump" in the stress function surface at a filleted juncture between any two rectangular components. The negative edge loss effect may be evaluated accurately by means of Saint-Venant's exact solution. A correction for the positive juncture effect may be evaluated experimentally by use of Prandtl's membrane analogy or by an iterative numeric procedure with the basic differential equation replaced by a difference equation. Since corrections to

Eq. (A. 1) tend to counterbalance, it is better either not to use any, or, if a very accurate solution is desired, both the negative and positive corrections should be made.

In 1935 the writer reported on test procedures that made use of a soap film as a membrane to accurately evaluate the juncture correction for rolled wide flange and *I*-shaped cross sections¹. Torsion tests of rolled shapes agreed well with the results². Recently the results of the soap film tests were corroborated by the difference equation network analysis, using the electronic digital computer, and the work was extended to include the juncture effect of angle and channel sections³. The procedure for building up the formulas for the torsion constant of structural shapes follows the pattern that had been suggested by TRAYER and MARCH⁴ in their investigation of aircraft strut sections whereby the added correction to the torsion constant for a juncture of two rectangular component parts is denoted as αD^4 , in which D refers to the diameter of the largest circle that can be inscribed at the juncture and α is a dimensionless parameter, evaluated either by means of soap film tests or by use of difference equations.

A. 2 The Rectangular and Trapezoidal Sections

The Saint-Venant torsion constant for the rectangular cross-section may be expressed as follows:

$$K = \frac{bt^3}{3} - 2Vt^4 \quad (\text{A. 2})$$

in which t = the thickness and b = the breadth of a rectangular section. The maximum shearing stress, in the surface of sides b , away from the edges, is given by

$$\tau_m = \frac{M_z \gamma t}{J}. \quad (\text{A. 3})$$

V and γ are factors depending upon the ratio $\frac{b}{t}$ and are given by the following table.

It should be noted that when b/t is greater than 2, the value of $2V$ may be taken as a constant equal to 0,210 and γ may be taken as unity. V may be termed the "coefficient of edge loss" for a rectangular cross section.

The formula for the trapezoidal section, (Fig. A. 1 as developed in Reference A. 2) can be written:

$$K = (b/12)(t_1^2 + t_2^2)(t_1 + t_2) - V_L t_2^4 - V_S t_1^4. \quad (\text{A. 4})$$

¹ JOHNSTON, B. G.: Torsional Rigidity of Structural Sections. Civ. Engng. Mag. (1935) 698.

² LYSE, I., and B. G. JOHNSTON: Structural Beams in Torsion. Trans. Amer. Soc. civ. Engrs. 101 (1936).

³ EL DARWISH, I. A., and B. G. JOHNSTON: Torsion of Structural Shapes. Proc. Amer. Soc. civ. Engrs., Struct. Div. J. Vol. 91, No. STI, Feb. 1965.

⁴ TRAYER, G. W., and H. W. MARCH: The Torsion of Members Having Sections Common in Aircraft Construction. Technical Report of the Advisory Committee for Aeronautics, No. 334, 1930.

V_L and V_S are the edge constants V , for the thick edge and the thin edge, respectively, of the trapezoid.

Table A. 1

Ratio $\frac{b}{t}$	$2V$	γ
1,00	0,1928	0,6753
1,10	0,1973	0,7198
1,20	0,2006	0,7578
1,30	0,2031	0,7935
1,40	0,2050	0,8222
1,50	0,2064	0,8476
1,60	0,2074	0,8695
1,80	0,2086	0,9044
2,00	0,2093	0,9300
2,50	0,2099	0,9681
3,00	0,2101	0,9855
4,00	0,2101	0,9970
∞	0,2101	1,0000

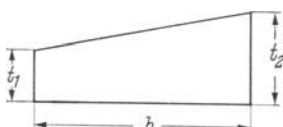


Fig. A. 1.

$$V_L = 0,10504 - 0,10000 S + 0,08480 S^2 - 0,06746 S^3 + 0,05153 S^4 \quad (\text{A. } 5)$$

and,

$$V_S = 0,10504 + 0,10000 S + 0,08480 S^2 + 0,06746 S^3 + 0,05153 S^4 \quad (\text{A. } 6)$$

in which S = the total slope of the section or tangent of the slope angle.

A. 3 Torsion Constants for Structural Shapes

Equations are presented below for nine different types of rolled structural shapes which may be classified according to four basic categories. These categories may be distinguished, as shown in Fig. A. 2, by the subscripts 1 through 4 that are indicated for the juncture coefficient “ α ” and the juncture diameter parameter “ D ”. The calculation of the torsion constant K for any one of the nine sections is summarized as follows:

1. Determine the appropriate D by means of Eqs. (A. 7) through (A. 12).
2. Determine the value of α by means of Eqs. (A. 13) through (A. 16).
3. Determine K by means of the applicable Eqs. (A. 17) through (A. 24).

The bulk of each evaluation of K is based on Saint-Venant's exact solution of the general torsion problem, as is the edge loss, but the juncture correction αD^4 is evaluated on the basis of a digital computer analysis of a difference equation network (A. 3).

Corresponding to the four categories in Fig. A. 2, formulas for D are as follows:
For Category 1, the parallel flange tee segment,

$$D_1 = \frac{(t+r)^2 + w \left(r + \frac{w}{4} \right)}{2r+t}. \quad (\text{A. } 7)$$

For Category 2, the *I*-section tee segment,

$$D_2 = \frac{(F + t_3)^2 + w \left(r + \frac{w}{4} \right)}{F + r + t_3}. \quad (\text{A. 8})$$

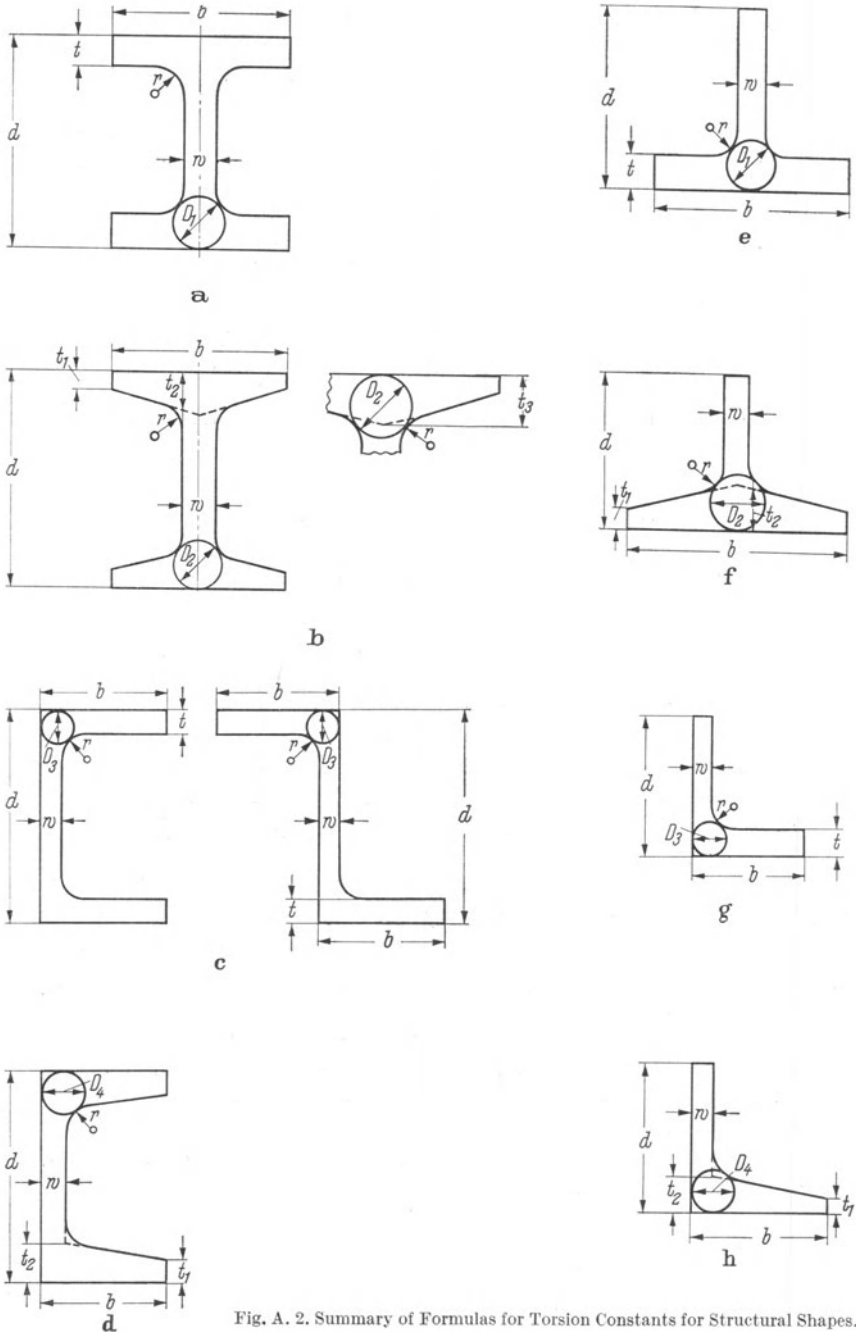


Fig. A. 2. Summary of Formulas for Torsion Constants for Structural Shapes.

in which

$$F = rS \left(\sqrt{\frac{1}{S^2} + 1} - 1 - \frac{w}{2r} \right) \quad (\text{A. 9})$$

in which S is the flange slope, i.e.; the tangent of the slope angle.

For Category 3, the angle segment,

$$D_3 = 2 \{ (3r + w + t) - \sqrt{2(2r + w)(2r + t)} \}. \quad (\text{A. 10})$$

For Category 4, the angle segment of a standard channel,

$$D_4 = 2 \{ (3r + w + M) - \sqrt{2(2r + w)(2r + M)} \} \quad (\text{A. 11})$$

in which

$$M = t_2 - r \left(S + 1 - \sqrt{1 + S^2} \right). \quad (\text{A. 12})$$

Reference A. 3 provides graphical plots of α values in terms of two dimensionless parameters, the ratio of web to flange thickness (w/t), and the ratio of fillet radius to flange thickness (r/t). However, for computer compiled tabulation of torsion constants, it is necessary to provide formulas that provide a close curve fit to the individual computer evaluations of α . These equations for α are as follows:

$$\alpha_1 = -0,0420 + 0,2204 \frac{w}{t} + 0,1355 \frac{r}{t} - 0,0865 \frac{wr}{t^2} - 0,0725 \left(\frac{w}{t} \right)^2, \quad (\text{A. 13})$$

$$\alpha_2 = -0,0836 + 0,2536 \frac{w}{t_2} + 0,1268 \frac{r}{t_2} - 0,0806 \frac{wr}{t_2^2} - 0,0858 \left(\frac{w}{t_2} \right)^2, \quad (\text{A. 14})$$

$$\alpha_3 = -0,0908 + 0,2621 \frac{w}{t} + 0,1231 \frac{r}{t} - 0,0752 \frac{wr}{t^2} - 0,0945 \left(\frac{w}{t} \right)^2, \quad (\text{A. 15})$$

$$\alpha_4 = -0,1325 + 0,3015 \frac{w}{t_2} + 0,1400 \frac{r}{t_2} - 0,1070 \frac{wr}{t_2^2} - 0,0956 \left(\frac{w}{t_2} \right)^2. \quad (\text{A. 16})$$

In each of the foregoing cases the pertinent empirical formula gives a good approximation for α in the range

$$0,2 < (r/t) < 1,0,$$

$$0,5 < (w/t) < 1,0.$$

The Saint-Venant torsion constant K for any one of the nine structural shape cross sections illustrated in Fig. A. 2 may now be evaluated by the appropriate formula provided by the following eight equations. (The same formula is applicable to both the zee and channel shapes.)

For Fig. A. 2a, *I*-shape, uniform flange thickness,

$$K = \frac{2}{3} b t^3 + \frac{1}{3} (d - 2t) w^3 + 2\alpha_1 D_1^4 - 0,420 t^4. \quad (\text{A. 17})$$

For Fig. A. 2b, *I*-shape, variable flange thickness,

$$K = \frac{(b-w)}{6} (t_1 + t_2) (t_1^2 + t_2^2) + \frac{2}{3} w t_2^3 + \frac{1}{3} (d - 2t_2) w^3 + 2\alpha_2 D_2^4 - 4 V_s t_1^4. \quad (\text{A. 18})$$

For Fig. A. 2c, Channel or zee shape, uniform flange thickness

$$K = \frac{2}{3} b t^3 + \frac{1}{3} (d - 2t) w^3 + 2\alpha_3 D_3^4 - 0,420 t^4. \quad (\text{A. 19})$$

For Fig. A. 2d, Channel or zee shape, variable flange thickness,

$$K = \frac{b-w}{6} (t_1 + t_2) (t_1^2 + t_2^2) + \frac{2}{3} w t_2^3 + \frac{1}{3} (d - 2t_2) w^3 + 2\alpha_4 D_4^4 - 2 V_s t_1^4 - 0,210 t_2^4. \quad (\text{A. 20})$$

For Fig. A. 2e, Tee shape, uniform flange thickness,

$$K = \frac{1}{3} b t^3 + \frac{(d-t)}{3} w^3 + \alpha_1 D_1^4 - 0,210 t^4 - 0,105 w^4. \quad (\text{A. 21})$$

For Fig. A. 2f, Tee shape, variable flange thickness,

$$K = \frac{b-w}{12} (t_1 + t_2) (t_1^2 + t_2^2) + \frac{1}{3} w t_2^3 + \frac{1}{3} (d - t_2) w^3 + \alpha_2 D_2^4 - 2 V_s t_1^4 - 0,105 w^4. \quad (\text{A. 22})$$

For Fig. A. 2g, Angle, leg thicknesses individually uniform,

$$K = \frac{1}{3} b t^3 + \frac{(d-t)}{3} w^3 + \alpha_3 D_3^4 - 0,210 t^4 - 0,105 w^4. \quad (\text{A. 23})$$

For Fig. A. 2h, Angle, one leg of variable thickness,

$$K = \frac{b-w}{12} (t_1 + t_2) (t_1^2 + t_2^2) + \frac{1}{3} w t_2^3 + \frac{1}{3} (d - t_2) w^3 + \alpha_4 D_4^4 - V_s t_1^4 - 0,105 t_2^4 - 0,105 w^4. \quad (\text{A. 24})$$

Further information on the development of the foregoing equations together with experimental confirmation will be found in Reference A. 3. The equations are approximately applicable to sections built up by means of fully continuous fillet and/or groove welds. Tables of torsion constants based on an application of these equations may be obtained from the major steel producers of hot rolled shapes in the United States and Great Britain. All currently rolled shapes are included and information on design applications is also provided. The forthcoming 1970 Edition of the Am. Inst. of Steel Construction Manual will also list the constants.

A. 4 Maximum Shear Stress due to Saint-Venant Torsion

In a rectangular bar, the maximum shear stress occurs in the outer fibers at the center of the broad sides. Saint-Venant's analysis for this stress has been presented herein by Table A. 1 and Eq. (A. 3). For the proportions of rectangles that comprise components of standard structural shapes, with b/t generally greater than 4, Eq. (A. 3) becomes simply

$$\tau_{\max} = \frac{M_z t}{K}. \quad (\text{A. 25})$$

When a rolled shape is made up of two or more rectangular or trapezoidal components joined together at an angle, (usually a right angle), fillets are provided at the reentry corners. These reduce the stress concentration effect but at the same time there is a thickening of the section at the fillet which has the dual effect of increasing K and (for a given unit twist) of increasing τ_{\max} , which may then be written:

$$\tau_{\max} = \frac{M_z \delta t}{K}. \quad (\text{A. 26})$$

In Eq. (A. 26), "t", for reference, is taken as the thickness of the thickest rectangular component entering the juncture. The modifying factor, " δ ", is usually greater than unity. For small fillet radii, δ reduces rapidly with increasing fillet radius, because of the decrease in the stress concentration effect, but δ , as in-

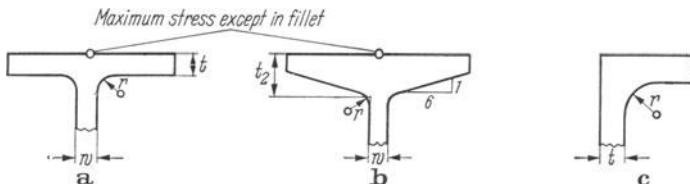


Fig. A. 3. Locations of Maximum Saint-Venant Shear Stress as Evaluated in Eqs. (A. 27), (A. 28) and (A. 29).

creasing thickness becomes the predominate factor, eventually passes through a minimum and then increases. However, even with no stress concentration effect, for a given M_z , the torsional shear stress will *decrease* with increasing fillet size of relatively large fillets because the juncture effect increases K in relation to the fourth power of the juncture diameter "D" as heretofore described.

In Reference A. 3, the stress function values were determined at closely spaced mesh intersection points over the entire cross section. It was thus possible to determine empirical polynomial functions representing the stress function values on lines normal to the boundary of a cross section, at a fillet or elsewhere. Thus the Saint-Venant shear stress parallel with the boundary could be determined as the maximum slope of the stress function surface at any boundary location. In this way, the maximum shear stress was evaluated at the center of the flat flange surface of wide flange and I shapes, and at the point of maximum stress in the angle section, as shown in Fig. A. 3a, Fig. A. 3b, and Fig. A. 3c.

Dr. I. A. EL DARWISH later extended these stress studies to include cases where symmetry (as in Fig. A. 3) did not simplify the problem¹. In this reference the boundary Saint-Venant shear stresses for both faces as well as in the fillets are determined for the angle and tee junctures.

For design purposes, when the *I* or wide flange section is used in combined bending and torsion, the Saint-Venant shear stress in the outer face of the flanges (Fig. A. 3a and Fig. A. 3b) are directly additive to the maximum shear that accompanies flange bending in warping torsion. Within prescribed limits, the following empirical formulas for δ in Eq. (A. 26) give a close approximation for these two cases and for the maximum stress in the fillet of the angle section (Fig. A. 3c).

(a) For the maximum stress in the outside face of the wide or tee shape with parallel sided flanges, for

$$0 < w/t < 1, \text{ and } 0,2 < r/t < 1,0$$

$$\delta = 1,0 + 0,02 (w/t) + 0,16 (w/t)^2 + 0,05 (r/t) \dots$$

$$\dots + 0,125 (r/t)^2 + 0,10 (w/t) (r/t). \quad (\text{A. 27})$$

(b) For the maximum stress in the outside face of the *I* or tee section with a 1–6 flange slope, for

$$0 < w/t_2 < 1 \text{ and } 0,2 < r/t_2 < 1,0$$

$$\delta = 0,93 + 0,058 (w/t_2) + 0,154 (w/t_2)^2 + 0,06 (r/t_2) \dots$$

$$\dots + 0,03 (r/t_2)^2 + 0,106 (r/t_2) (w/t_2). \quad (\text{A. 28})$$

(c) For the maximum stress in the fillet of an angle with equal thickness of each leg, combining the stress concentration effect with the effect of added thickness, for

$$0,2 < r/t < 1,0,$$

$$\delta = 2,25 - 2,16 (r/t) + 1,97 (r/t)^2 - 0,56 (r/t)^3. \quad (\text{A. 29})$$

A. 5 Acknowledgement

Acknowledgement should be made of the cooperation of the University of Michigan computing center in contributing computer time for the work reported upon in Reference 3, p. 268 which forms the basis for much of this Appendix.

¹ EL DARWISH, I. A.: Elastic Torsional Strength of Structural Shapes, Alexandria: University Press 1966.

A. 6 Notation for Appendix

D_1, D_2, D_3, D_4	Diameter of circle inscribed at a juncture
G	Shear modulus of elasticity
K	Saint-Venant torsion constant
M_z	Torsional moment
S	Slope of flange
V, V_S, V_L	Coefficient of edge loss
b	Breadth of rectangle or of flange
d	Overall depth of section
r	Fillet radius
t, t_1, t_2, t_3	Thickness of flange (see Fig. A. 2)
θ	Angle of twist per unit length
τ_m	Maximum shear stress
$\alpha_1, \alpha_2, \alpha_3, \alpha_4$	Coefficients of juncture correction to torsion constant
γ	Coefficient for maximum shear stress in a rectangular bar
δ	Coefficient for shear stress at a juncture

Author Index

- American Institute of Steel Construction** 272
Bach, C. von VII
Basler, K. VII, 65, 249
Beusch, J. 249
Bleich, F. VII
Bornscheuer, F. W. VII, 96, 172
Bredt, R. VII, 13, 41, 86
Chang, F. K. 10
Committee on Masonry and Reinforced Concrete 203
Ebner, H. 43
Eggenschwyler, A. VII, 106
El Darwisch, I. A. 268, 274
Föppl, A. & L. VII, 10
Goodey, W. J. 43
Goodier, J. N. VII
Günther, W. VII
Hajdin, N. 170
Heilig, R. VII, 99
Johnston, B. G. 10, 268
Kappus, R. VII
Karamuk, E. 90
Kollbrunner, C. F. VII, 170
Kuhn, P. VII, 32
Lyse, I. 268
Maillart, R. VII, 106
March, H. W. 268
Navier, C. L. 1
Pei, M. 221
Pestalozzi, G. 249
Pflüger, A. 43
Prandtl, L. VII, 2
Resinger, F. 249
Ritter, M. 221
Ritter, W. 246
Saint-Venant, B., de VII, 1, 8
Schwyzer, H. 203
Thürlimann, B. VII, 113, 221
Timoshenko, S. VII
Trayer, G. W. 268
Vlasov, V. Z. VII, 143
Wagner, H. VII
Wansleben, F. VII, 65
Weber, C. VII
Winter, G. 221
Wolf, J. P. 113
Zucker, O. 35

Subject Index

- accuracy
 - of approximation for torsion constant 8
 - of approximation to mixed torsion 194
- affinity of load 209
- analogy
 - Prandtl's (membrane) a. 2
 - hydrodynamic a. 12
 - between flexure and warping 99
 - between moment and stress distribution method 221
 - between core point and fixed-point method 221
- applicability
 - of methods for torsional analysis 196
 - of folded-plate analysis 237
- approximation
 - for torsion constant 7, 10
 - for behavior due to mixed torsion 187
- assumptions for analysis
 - of solid cross section 1
 - of closed, thin-walled cross section 10, 15
 - of skew supported member 58, 145
 - of open, thin-walled cross section 102
 - of folded plate 203, 209
- axial force, consideration in warping structures 143
- bending moment, devinition 97
- Bernoulli-Navier's hypothesis 103
- bicellular cross section 33
- boundary condition 47, 131, 163
 - theoretical vs. actual 90
- bounds
 - for torsion constant 32
 - for shear stress caused by skew supports 93
 - for axial stresses due to mixed torsion 189
 - for ideal area F^* in folfed plates 230
- bracketing
 - of torsion constant 32
 - of folded-plate behavior 230
- branching 124
- Bredt's formula
 - stipulation 12
 - for circular, hollow cross section 13
 - for composite, hollow cross section 17
- for hollow cross section with lattice walls 19
- built-up, open cross section 123
- built-up, solid cross section 9
- center of twist 109
 - identity with shear center 111
- circular, hollow cross section 13
 - in full plastic state 14
- circular, solid cross section 2, 3
 - Prandtl's analogy 3
 - shear stress 4
 - torsion constant 4
- classification of cross sections for torsion 196
- closed, folded-plate structure 232
- closed, thin-walled cross section
 - Saint-Venant torsion 10
 - Prandtl's analogy 11
 - torsion stress function 11
 - hydrodynamic analogy 12
 - monocellular 13
 - criterion for "thin-walled" 15
 - multicellular 21
 - shear center 45
- composite
 - closed, thin-walled cross section 17
 - open, thin-walled cross section 125
- computational scheme
 - for shear flow analysis 27
 - for calculation of cross-sectional constants 112, 182
- constants of integration 163
- continuous member
 - with Saint-Venant torsion 50
 - with warping torsion 138
 - with mixed torsion 170
- contour line of membrane
 - of solid cross section 2
 - of closed, thin-walled cross section 12
- convergence of iteration 65
- coordinate system, definition for warping torsion 96
- core point method 221
 - simplified version 223
 - general version 225

- correction at support 90
 cover plate, effect on torsion constant 10
 crane girder 53
 cross beam, influence of 258
deflection
 of skew supported member 70
 of folded plates 220
deformation
 of open vs. closed cross section 15
 of open, thin-walled cross section 101
 of skew supported member 149
 of folded plate structure 219
degree of freedom 253
diaphragms 202, 210, 261
 influence of number 263
difference between
 open and closed, hollow cross sections 13
 theoretical and actual boundary conditions 90
 folded-plate and slender-member theory 236
differential equation
 for Saint-Venant torsion 46
 for warping torsion 99
 for mixed torsion 158
displacement coefficient
 of Saint-Venant torsion
 regularly supported member 47
 skew supported member 60
 of warping torsion
 regularly supported member 138
 skew supported member 149
 of mixed torsion
 regularly supported member 171
 approximation for small α 74, 193
eccentric load 75, 79
edge forces 204
edge loss 267
edge stresses 204
elastic material 1
 elastically rotating support 50
equilibrium condition 3, 51, 77, 101, 112
 equivalence of folded-plate and slender-member theory 243
equivalent load system 208
error ratio 134
fictitious wall thickness, see “modified wall thickness”
fillets
 effect on torsion constant 10, 269
 effect on stress 273
finite differences 113
folded plates 202
 simple analysis 203
 general analysis 213
 relation to slender members 236
folded-plate vs. slender member theory 236
generalised displacement
 of Saint-Venant torsion
 shear flow analysis 28
 regularly supported member 47
 skew supported member 60
 of warping torsion
 regularly supported member 138
 skew supported member 149
 of mixed torsion
 regularly supported member 171
 approximation for small x 193
geometry of structure, influence of change in 238
hollows cross section
 see “closed, thin-walled cross section”
Hooke’s law 1, 2, 102
hydrodynamic analogy 12
 ideal area 222
identity
 of shear center and center of twist 111
 of folded plate and slender member theory 243
index for torsional behavior 187
influence coefficient 47, 59
influence function 82
influence line
 for Saint-Venant torsion quantities 57
 for warping quantities 132
 transverse i. l. 133
influence surface
 Saint-Venant torsion
 skew supported member 81
 warping torsion
 two-span continuous beam 141
 iterative procedure for skew supported member 63, 150, 200
lattice walls 19
limits, see “bounds”
matrix formulation
 of shear flow problem 25
 for analysis of skew supported member 66
 for torsion analysis of continuous member 50, 52, 55
membrane
 see “Prandtl’s analogy”
 plane lid 11
mixed torsion 158
 of simply supported member 164
 of skew supported member 198
 differential equation 158
modified wall thickness
 of composite cross sections 17
 of lattice walls 19

- moment of inertia
 relation to torsion constant 7
 definition 96
 properties 110
 calculation 112
 monocellular box section 11
 Prandtl's analogy 11
 shear flow 12, 42
 multicellular box section 21
 Prandtl's analogy 23
 shear flow 23, 42
 torsion constant 24
 computational scheme 27
 limiting cases 31
 narrow cross section 5
 notation
 general XIV
 Saint-Venant torsion
 regularly supported member 47
 skew supported member 58
 warping torsion
 stress analysis 96
 skew supported member 145
 numerical calculation
 of shear flows 27
 of cross sectional constants 112
 oblique, see "skew"
 particular solution 162
 plastic state of circular, hollow cross section 14
 Poisson's ratio 59, 85
 polar coordinates 3
 polar moment of inertia 1
 Prandtl's analogy
 stipulation 2
 for circular cross section 3
 for rectangular cross section 4
 for triangular cross section 5
 for monocellular box section 11
 for multicellular box section 23
 preservation of cross-sectional shape 102, 202
 prestressed folded plates 214
 rectangular cross section 4
 Prandtl's analogy 4
 torsion constant 5, 268
 shear stress 5
 recurrence relations 223, 228
 residual state of stress 252
 rolled sections
 stress analysis 176, 273
 torsion constant 267, 269
 Saint-Venant's principle 188
 Saint-Venant torsion
 of solid cross section 1
 of closed, thin-walled cross section 10
 of simple structural members 46
 of skew supported members 58
 differential equation 46
 notation 47, 58
 sectorial coordinate, definition 97
 sectorial monument of inertia
 definition 109
 properties 110
 calculation 112
 sectorial statical moment
 definition 108
 properties 110
 calculation 112
 separation of variables 208
 shear center
 definition 44
 of closed, hollow cross section 45
 of thin-walled, open cross section 106, 180, 186
 of three-plate cross section 249
 shear deformation 1, 47, 102, 188
 shear flow
 definition 12
 due to torsion
 in monocellular box section 12
 in multicellular box section 23
 due to shear
 in closed, hollow cross section 42
 sign convention 23
 matrix analysis 25
 in thin-walled open cross section 105, 181, 186
 in folded plates 210
 shear modulus 1, 17, 44, 46
 shear stress
 in solid cross section 1
 see "shear flow"
 sign convention
 for shear flows 23
 for stresses in warping structures 96
 general consideration 97
 for built-up, open cross section 123
 skew angle, influence on moments 74
 skew supported member
 with Saint-Venant torsion 58
 with warping torsion 145
 with mixed torsion 198
 snap-through problem 238
 soap film experiment 3, 268
 solid cross section
 Saint-Venant torsion 1
 torsion stress function 2
 spring constant 50
 stability of flat, folded-plate roof 238
 statical moment
 definition 97

- properties 110
- calculation 112
- stiffeners, longitudinal 35
- stress analysis
 - for Saint-Venant torsion 1
 - for warping torsion 96
 - for mixed torsion 158
 - of folded plates 202
 - of rolled sections 176, 273
- stress distribution method 221
- structural shapes, see „rolled sections“
- substitute area 222
- substitute plate girder 249
- substitute two-plate structure 231
- support conditions 86, 131, 147, 210
- symmetries in system and load, consideration of 55, 71, 124, 173, 194
- thin-walled, hollow cross section
 - see “closed, thin-walled c. s.”
- thin-walled, open cross section 100
 - bending 103
 - warping 103
 - shear center 106
 - twist 107
 - center of twist 109
- three-moment equation 66, 150
- three-plate profile 245
- three-rotation equation 50
- three-shear equation 203, 216
- three-stress equation 205, 216
- three-torsionel-moment equation 52
- three-warping-moment equation 141, 150, 170
 - approximation for small α 194
- torsion constant
 - definition 1
- calculation 2
- of circular cross section 4
- of rectangular cross section 5
- of triangular cross section 7
- relation to moments of inertia 7
- approximation 7, 10
- of built-up cross section 9
- effect of cover plate 10
- effect of fillets 10
- of monocellular box section 13
- of multicellular box section 24
- bounds 32
- bracketing 32
- of trapezoidal cross section 268
- of rolled section 269
- torsion stress function
 - of solid cross section 2
 - of closed, thin-walled cross section 11
- torsional rigidity 1, 7, 188
- transverse influence line 133
- transverse stiffeners 202
- trapezoidal cross section 268
- triangular cross section 5
 - Prandtl's analogy 5
 - shear stress 6
 - torsion constant 7
 - twist, center of 109
 - identity with shear center 111
 - two-plate profile (angle) 243
 - two-plate structure 231
- warping torsion 96
 - notation 96, 145
 - differential equation 99
 - of thin-walled cross section 100
 - of simple structural members 131
 - of skew supported members 145